

Native Vegetation Classification Using Remote Sensing Techniques: A Case Study of Dairy Flat Regrowth Bush by Using the AUT Unmanned Aerial Vehicle

ZhaoXuan Zhang (Hins)

School of Applied Science

AUT University

2014

**A thesis submitted to the Auckland University of Technology in
partial fulfilment of the requirements for the degree of Master of
Science (MSc)**

List of Contents

List of Figures	v
List of Tables	x
List of Abbreviations	xi
Attestation of Authorship.....	xii
Acknowledgements.....	xiii
Abstract.....	xiv
1 Introduction.....	1
1.1 Natural Heritage on New Zealand Private Land	1
1.2 New Zealand Private Land Conservation and Management	1
1.2.1 Legal protection.....	2
1.2.2 Active management.....	5
1.3 Remote Sensing for Private Land Conservation	6
1.3.1 Unmanned Aerial Vehicle remote sensing.....	6
1.3.2 UAV remote sensing for environmental application.....	7
1.4 Study Location and Research Area Importance	9
1.5 Research Questions and Objectives	10
1.6 Structure of the Thesis.....	11
2 Literature Review.....	12
2.1 Vegetation Classification	12
2.1.1 Traditional vegetation classification.....	12
2.1.2 Vegetation mapping and classification in New Zealand.....	12
2.2 History and Status of Remote Sensing in New Zealand	13
2.3 Unmanned Aerial Vehicles	15
2.3.1 History of UAV.....	15

2.3.2 Non-military UAVs.....	16
2.3.3 Modern use of UAVs.....	16
2.3.4 Main concerns in relation to use of UAVs.....	17
2.3.5 The future of UAVs.....	18
2.3.6 Unmanned Aerial Vehicles in New Zealand conservation planning.....	18
2.3.7 Unmanned Aerial Vehicle remote sensing.....	19
2.4 Vegetation Classification Using Remote Sensing.....	20
2.4.1 Satellite remote sensing for vegetation classification.....	20
2.4.2 Aerial remote sensing for vegetation classification.....	21
2.4.3 Unmanned Aerial Vehicle remote sensing for vegetation classification.....	21
2.5 Image Mosaic and Processing.....	22
2.5.1 Image processing using the Pix4UAV software.....	22
2.5.2 Normalized Difference Vegetation Index (NDVI).....	24
2.6 Vegetation Spectral Reflectance.....	24
2.6.1 Spectral response of vegetation.....	24
2.6.2 Spectral variation of vegetation.....	26
2.7 Vegetation Classification Methodologies.....	27
2.7.1 Unsupervised classification.....	27
2.7.2 Supervised classification.....	29
2.7.3 Advantages and disadvantages of unsupervised and supervised classification.....	30
2.7.4 Object-based image analysis classification.....	31
2.8 Accuracy Assessment.....	32
2.8.1 Confusion matrix of classification results.....	32
2.8.2 Evaluation of the confusion matrix.....	33
2.8.3 Important considerations for the confusion matrix.....	34
3 Materials and Method.....	37
3.1 Study Site.....	37

3.2 Hardware and Software Required for the UAV	37
3.2.1 Unmanned Aerial Vehicle (UAV) system description.	37
3.2.2 AUT Hawk and Swampfox UAV.....	38
3.2.3 DTA Ground Control Station.	41
3.3 UAV Work Flow	42
3.3.1 Mission planning.	43
3.3.2 UAV image acquisition.	44
3.3.3 UAV image pre-processing.	45
3.3.4 Image classification.	47
3.3.4a Ground truth data collection.	47
3.3.4b Vegetation classification.....	48
4 Results.....	53
4.1 Field Data GPS Location Map	53
4.2 UAV Images Mosaic Map.....	54
4.2.1 Mosaic maps of near-infrared images.	54
4.2.2 Mosaic map of vegetation stress camera images.....	59
4.2.3 Mosaic map of red edge images.	62
4.2.4 Mosaic map of true colour images.	64
4.3 Pixel-based Unsupervised and Supervised Classification.....	67
4.3.1 Unsupervised classification results.....	67
4.3.2 Supervised classification results.	70
4.4 Object-Based Unsupervised and Supervised Classification Results.....	74
4.4.1 Object-based unsupervised classification.	77
4.4.2 Object-based supervised classification.	80
4.5 Confusion Matrix	84
4.6 Normalised Difference Vegetation Index Classification	89
4.7 ENDVI and NDVI Processed Maps Using Vegetation Stress Images.....	93

4.8 Final Classification Map	96
5 Discussion	99
5.1 UAV Flight Planning	99
5.1.1 Wind conditions.....	99
5.1.2 Sun conditions.	99
5.1.3 Cloud conditions.....	99
5.2 UAV Image Acquisition.....	99
5.2.1 Camera.....	99
5.2.2 Flight route.	100
5.2.3 UAV control.	101
5.2.4 Landing.....	101
5.2.5 Observation during flight.....	101
5.3 UAV Images Mosaic Processing.....	101
5.3.1 Overlaps.....	101
5.3.2 Processing time.....	103
5.3.3 Potential factors affecting the mosaic quality.....	103
5.3.4 Mosaic Result Quality	103
5.4 Collection and Digitization of Training Data and Ground Truth Data	104
5.5 UAV Images Mosaic Classification.....	105
5.5.1 Mosaic quality.	105
5.5.2 Classification methods and results.	106
5.6 Normalized Difference Vegetation Index Value Calculation and Processing	107
5.6.1 NDVI and ENDVI Scripts	107
6 Conclusion	108
7 References.....	110
Appendix A. Object-based Classification.....	117
Appendix B. Mosaic Quality Report	146

List of Figures

<i>Figure 1.</i> Legally protected areas of North Island, New Zealand, 2009.	3
<i>Figure 2.</i> Research location map.	10
<i>Figure 3.</i> Typical spectral reflectance curve for vegetation.	26
<i>Figure 4.</i> The study site of re-growth bush area.	37
<i>Figure 5.</i> AUT Hawk UAV.	39
<i>Figure 6.</i> The Swampfox UAV.	39
<i>Figure 7.</i> Flow chart of the research procedure for using the Kahu and Swampfox UAVs to map vegetation at the Dairy Flat bush area.	42
<i>Figure 8.</i> UAV flight route on 8 August, 2013.	45
<i>Figure 9.</i> GPS location of field data collection points.	53
<i>Figure 10.</i> Mosaic map of near-infrared images acquired on 28 July, 2013.	54
<i>Figure 11.</i> Quality check of near-infrared Mosaic map on 28 July, 2013.	55
<i>Figure 12.</i> Overlapping level of near-infrared Mosaic map on 28 July, 2013.	55
<i>Figure 13.</i> Mosaic map of near-infrared images acquired on 8 August, 2013.	56
<i>Figure 14.</i> Quality check of near-infrared mosaic map on 8 August, 2013.	56
<i>Figure 15.</i> Overlapping level of near-infrared mosaic map on 8 August, 2013.	57
<i>Figure 16.</i> Mosaic map of near-infrared images acquired on 1 April, 2014 (Flight 2). ...	58
<i>Figure 17.</i> Quality check of near-infrared mosaic map on 1 April, 2014 (Flight 2).	58
<i>Figure 18.</i> Overlapping level of near-infrared mosaic map on 1 April, 2014 (Flight 2). ...	59
<i>Figure 19.</i> Mosaic map of vegetation stress camera images acquired in 2013.	59
<i>Figure 20.</i> Quality check of vegetation stress mosaic map in 2013.	60

<i>Figure 21.</i> Overlapping level of vegetation stress mosaic map in 2013.....	60
<i>Figure 22.</i> Mosaic map of vegetation stress camera images acquired in 2014.	61
<i>Figure 23.</i> Quality check of vegetation stress mosaic map in 2014.....	62
<i>Figure 24.</i> Overlapping level of vegetation stress mosaic map in 2014.....	62
<i>Figure 25.</i> Mosaic map of red edge images acquired on 8 August, 2013.	63
<i>Figure 26.</i> Quality check of red edge mosaic map on 8 August, 2013.....	63
<i>Figure 27.</i> Overlapping level of red edge mosaic map on 8 August, 2013.	64
<i>Figure 28.</i> Mosaic map of true colour images acquired on 1 April, 2014 (merge Flight 1 and Flight 2).....	65
<i>Figure 29.</i> Quality check of true colour mosaic map on 1 April, 2014 (merge Flight 1 and Flight 2).....	65
<i>Figure 30.</i> Overlapping level of true colour mosaic map on 1 April, 2014 (merge Flight 1 and Flight 2).....	66
<i>Figure 31.</i> Unsupervised classification of vegetation stress images mosaic in 2013. (A. Original mosaic. B. ISODATA. C. K-mean.).....	67
<i>Figure 32.</i> Unsupervised classification of vegetation stress images mosaic in 2014. (A. Original mosaic. B. ISODATA. C. K-mean.).....	67
<i>Figure 33.</i> Unsupervised classification of near-infrared images mosaic on 28 July, 2013. (A. Original mosaic. B. ISODATA. C. K-mean.).....	68
<i>Figure 34.</i> Unsupervised classification of near-infrared images mosaic on 8 August, 2013. (A. Original mosaic. B. ISODATA. C. K-mean.).....	68
<i>Figure 35.</i> Unsupervised classification of near-infrared images mosaic on 1 April, 2014 (Flight 2). (A. Original mosaic. B. ISODATA. C. K-mean.).	68
<i>Figure 36.</i> Unsupervised classification of red edge images mosaic on 8 August, 2013. (A. Original mosaic. B. ISODATA. C. K-mean.).....	69

<i>Figure 37.</i> Unsupervised classification of true colour images on 1 April, 2014 merge mosaic. (A. Original mosaic. B. ISODATA. C. K-mean.).....	69
<i>Figure 38.</i> Supervised classification of vegetation stress images mosaic in 2013. (A. Maximum likelihood. B. Minimum distance.).....	70
<i>Figure 39.</i> Supervised classification of vegetation stress images mosaic in 2014. (A. Maximum likelihood. B. Minimum distance.).....	71
<i>Figure 40.</i> Supervised classification of near-infrared images' mosaic on 28 July, 2013.(A. Maximum likelihood. B. Minimum distance.).....	72
<i>Figure 41.</i> Supervised classification of near-infrared images' mosaic on 8 August, 2013.(A. Maximum likelihood. B. Minimum distance.).....	72
<i>Figure 42.</i> Supervised classification of near-infrared images mosaic on 1 April, 2014 (Flight 2).(A. Maximum likelihood. B. Minimum distance.).....	73
<i>Figure 43.</i> Supervised classification of red edge images mosaic on 8 August, 2013. (A. Maximum likelihood. B. Minimum distance.).....	74
<i>Figure 44.</i> Supervised classification of true colour images on 1 April, 2014 merge mosaic. (A. Maximum likelihood. B. Minimum distance.).....	74
<i>Figure 45.</i> Comparison of true colour images before and after object segmentation. (A. Before. B. After.).....	75
<i>Figure 46.</i> Comparison of near-infrared images before and after object segmentation. (A. Before. B. After.).....	75
<i>Figure 47.</i> Comparison of red edge images before and after object segmentation.(A. Before. B. After.).....	76
<i>Figure 48.</i> Comparison of vegetation stress images before and after object segmentation. (A. Before. B. After.).....	76
<i>Figure 49.</i> Object-based unsupervised classification of vegetation stress images mosaic in 2013. (A. Original mosaic. B. ISODATA. C. K-mean.).....	77

<i>Figure 50.</i> Object-based unsupervised classification of vegetation stress images mosaic in 2014. (A. Original mosaic. B. ISODATA. C. K-mean.).....	77
<i>Figure 51.</i> Object-based unsupervised classification of near-infrared images mosaic on 28 July, 2013. (A. Original mosaic. B. ISODATA. C. K-mean.).....	78
<i>Figure 52.</i> Object-based unsupervised classification of near-infrared images mosaic on 8 August, 2013. (A. Original mosaic. B. ISODATA. C. K-mean.).....	78
<i>Figure 53.</i> Object-based unsupervised classification of near-infrared images mosaic on 1 April, 2014 (Flight 2).(A. Original mosaic. B. ISODATA. C. K-mean.).....	78
<i>Figure 54.</i> Object-based unsupervised classification of red edge images mosaic on 8 August, 2013. (A. Original mosaic. B. ISODATA. C. K-mean.).....	79
<i>Figure 55.</i> Object-based unsupervised classification of true colour images on 1 April, 2014 merge mosaic. (A. Original mosaic. B. ISODATA. C. K-mean.).....	79
<i>Figure 56.</i> Object-based supervised classification of vegetation stress images mosaic in 2013. (A. Maximum likelihood. B. Minimum distance.).....	80
<i>Figure 57.</i> Object-based supervised classification of vegetation stress images mosaic in 2014. (A. Maximum likelihood. B. Minimum distance.).....	81
<i>Figure 58.</i> Object-based supervised classification of near-infrared images mosaic on 28 July, 2013. (A. Maximum likelihood. B. Minimum distance.).....	81
<i>Figure 59.</i> Object-based supervised classification of near-infrared images mosaic on 8 August, 2013. (A. Maximum likelihood. B. Minimum distance.).....	82
<i>Figure 60.</i> Object-based supervised classification of near-infrared images mosaic on 1 April, 2014 (Flight 2). (A. Maximum likelihood. B. Minimum distance.).....	83
<i>Figure 61.</i> Object-based supervised classification of red edge images mosaic on 8 August, 2013. (A. Maximum likelihood. B. Minimum distance.).....	83
<i>Figure 62.</i> Object-based supervised classification of true colour images on 1 April, 2014 merged mosaic. (A. Maximum likelihood. B. Minimum distance.).....	84
<i>Figure 63.</i> Presentation of layer stacking result (2013).....	90

<i>Figure 64.</i> Normalized difference vegetation index (NDVI) value of layer stacking result (2013).....	90
<i>Figure 65.</i> Presentation of layer stacking result (2014).....	91
<i>Figure 66.</i> Normalized difference vegetation index (NDVI) value of layer stacking result (2014).....	91
<i>Figure 67.</i> Unsupervised classification of normalized difference vegetation index (NDVI) value image (2013) (A. NDVI value image. B. ISODATA. C. K-Mean.).....	92
<i>Figure 68.</i> Unsupervised classification of normalized difference vegetation index (NDVI) value image (2014) (A. NDVI value image. B. ISODATA. C. K-Mean.).....	92
<i>Figure 69.</i> Supervised classification of normalized difference vegetation index (NDVI) value image (2013) (A. NDVI value image. B. Maximum Likelihood. C. Minimum Distance.).....	93
<i>Figure 70.</i> Supervised classification of normalized difference vegetation index (NDVI) value image (2014) (A. NDVI value image. B. Maximum Likelihood. C. Minimum Distance.).....	93
<i>Figure 71.</i> Processed NDVI result of vegetation stress images mosaic (2013).....	94
<i>Figure 72.</i> Processed ENDVI result of vegetation stress images mosaic (2013).....	95
<i>Figure 73.</i> Final classification map of vegetation stress images mosaic (2013).....	97
<i>Figure 74.</i> Final classification map of true colour images mosaic (merge 1 April, 2014 flight 1 and flight 2).....	98
<i>Figure 75.</i> Presentation of overlapping images score.....	102
<i>Figure 76.</i> Presentation of mosaic result with different overlap score.....	102

List of Tables

Table 1. <i>Details of each UAV Flight Mission</i>	43
Table 2. <i>Confusion Matrix Results of Pixel-Based Supervised Classification</i>	85
Table 3. <i>Confusion Matrix Results of Object-Based Supervised Classification</i>	86

List of Abbreviations

ALS: Airborne Laser Scanning

ATC: Air Traffic Control System

CAA: New Zealand Civil Aviation Authority

DSM: Digital Surface Model

DTA: New Zealand Defence Technology Agency

ENDVI: Enhanced Normalised Difference Vegetation Index

FOV: Field of View

GIS: Geographic Information Systems

IDL: Interactive Data Language

ISODATA: Iterative Self-Organizing Data Technique Analysis

MLC: Maximum Likelihood Classification

MODIS: Moderate Resolution Imaging Spectroradiometer

NDVI: Normalised Difference Vegetation Index

NIR: Near-Infrared

NZLRI: New Zealand Land Resource Inventory

OBIA: Object-based Image Analysis

QEII: Queen Elizabeth II National Trust

ROI: Region of Interest

RPAS: Remote piloted Aircraft Systems

TM: Thematic Mapper

UAV: Unmanned Aerial Vehicle

Attestation of Authorship

I hereby declare that this submission is my own work and that, to the best of my knowledge and belief, it contains no material previously published or written by another person nor material which to a substantial extent has been accepted for the qualification of any other degree or diploma of a University or other institution of higher learning, except where due acknowledge is made in the acknowledgements.

Signed:  _____

ZhaoXuan Zhang (Hins)

20 May, 2014

Acknowledgements

I would like to thank the AUT unmanned aerial vehicle team that has helped me during the period of completing this thesis, especially my supervisors Dr Barbara Breen who has encouraged and supported my research throughout the thesis year. I really appreciate the time and effort she has generously given.

And special thanks to another two supervisors Dr John Robertson and Professor John Brooks for all the technical support and time that helped me on the UAV things. Without the generous help from them, there would have been no way to complete this thesis successfully.

Great thanks to my friends and other postgraduate students in WL including Choo Khoo, and Xiaolei Li; and especially Grant Lawrence who gave support to me without hesitation in terms of identifying vegetation species in the field data collection and discussed the technical difficulties with me.

Great thanks to the people and land owners who allow me to fly the drone. Special thanks to Dr Tim Brooks from Skycam Ltd for all the technical support. And thanks to the support team from Pix4D Company for the help with the Pix4UAV software technical back up. And special thanks to Jo Adams for proof reading of the thesis draft.

Finally, I would like to thank my family for supporting me to study and live in New Zealand, especially my lovely wife Lily, who gave up her career in China and came to Auckland to support me.

Abstract

Traditional field-based methods of habitat mapping to determine and classify vegetation on private land have been proven unsatisfying in terms of coverage, and time and cost-effectiveness. Remote sensing using Unmanned Aerial Vehicles (UAVs) is a new technology which is able to acquire land resources and environmental gradients as well as other spatial information. Although research using UAV techniques has been active since the beginning of the 21st century in New Zealand, it still has tremendous potential value for further and deeper exploration of UAV use. There has been, to date, little academic research based on UAVs' remote sensing apart from commercial and military use. The aim of this study was to develop effective UAV-based remote sensing methods to classify native New Zealand vegetation on private land using an easily accessible area of regenerating bush.

Results of this research provide a systematic method for UAV remote sensing classification. The object-based maximum likelihood supervised classification produced the most accurate classification result of approximately 80% using the true colour imagery mosaic. The results of this thesis suggest that the UAV remote sensing technique is capable of acquiring sufficiently high quality data from private land that can be used to mosaic and produce accurate vegetation classification at a species level.

1 Introduction

1.1 Natural Heritage on New Zealand Private Land

New Zealand (NZ) is rich in biodiversity, with an estimated 80,000 different species of native animals, plants and fungi. To date, 72 types of naturally occurring ecosystems have been identified in New Zealand which can be pooled into six categories including coastal, geothermal, inland and alpine, subterranean and semi-subterranean, wetlands and ecosystem induced by native vertebrates (Landcare Research, n.d.; Ministry for the Environment, 2010). All of the ecosystems, animals, and vegetation occur on NZ's both public and private land. Seventy per cent of New Zealand's land mass is privately owned (approximately 19 million hectares). Threatened habitats mainly occur on the lowlands on private land, where even small remnants are important (Queen Elizabeth II National Trust, n.d.).

In recent years, the natural habitats for native plants and animals have been dramatically decreasing or damaged as land has been developed to accommodate NZ's growing population. This is pronounced in the Auckland region. The influence of environmental disruption reminds local, regional and national governments of the significance of protecting the natural heritage. The protection and restoration of much of the region's biodiversity is dependent on landowner and community efforts and initiatives, especially on private land (Auckland Council, n.d.). There are a number of mechanisms which allow private land owners to conserve and manage the natural values of their property. Generally speaking, there are two ways to protect the natural heritage on private land including formal and informal ways. The formal way is legal protection (covenants) while the informal way is carried out through active management or partnership agreements between local people or owners.

1.2 New Zealand Private Land Conservation and Management

Interest in conservation and management of natural resources on private land has grown globally and a series of policies are designed to achieve this. However many of these policies rely on compensation for loss of property rights and are therefore expensive and not always feasible, owing to budgetary or other constraints particularly for privately owned land (Saunders, 1996). In addition to government policies, there are also policies and mechanisms that rely on voluntary principles with limited or even no compensation including advisory services and voluntary organizations offering assistance with practical conservation work. In

New Zealand, limited resources restrict the protection of private land in the interests of conservation due to land size, population, late development and ownership. It is estimated that only five per cent of New Zealand belongs to conservation organisations, for example the Department of Conservation (Government of New Zealand, n.d.). Thus policies for voluntary conservation and management on private land have focused on the use of formal legal protection particularly voluntary statutory covenants (Saunders, 1996). Besides formal legal protection, there are informal ways to protect conservation land by owners or local people, which is called ‘active management.’

1.2.1 Legal protection.

The main advantages of legal protection are the preservation of land areas and on-going management. Private land owners can ask for funding from agencies including the Nature Heritage Fund, the Queen Elizabeth II National Trust (QEII), the Department of Conservation, local authorities and Ngā Whenua Rāhui (for Māori land) to help with surveying, and legal and fencing costs according to different legal protection options (Davis & Meurk, 2001).

Legal protection includes the options of conservation covenants, management agreements, and protected private land agreements. Each of these is described below in the following subsections. As of July, 2009, 8,763,300 hectares of New Zealand’s land was legally protected for the primary purposes of conservation. Legally protected private land accounted for 238,300 hectares while public land accounted for 8,525,000 hectares. In 2009, legally protected areas represented 33.4% of New Zealand’s total land area. Simultaneously, NZ had the highest proportion of land area legally protected for conservation purposes out of all the 30 Organization for Economic Co-operation and Development (OECD) countries in 2009 (Ministry for the Environment, 2010).

However, less than 20% of the North Island land is legally protected (Figure 1). The Bay of Plenty region has the largest amount of its land legally protected. In the Auckland region, only 14% of the land is legally protected (Ministry for the Environment, 2010).

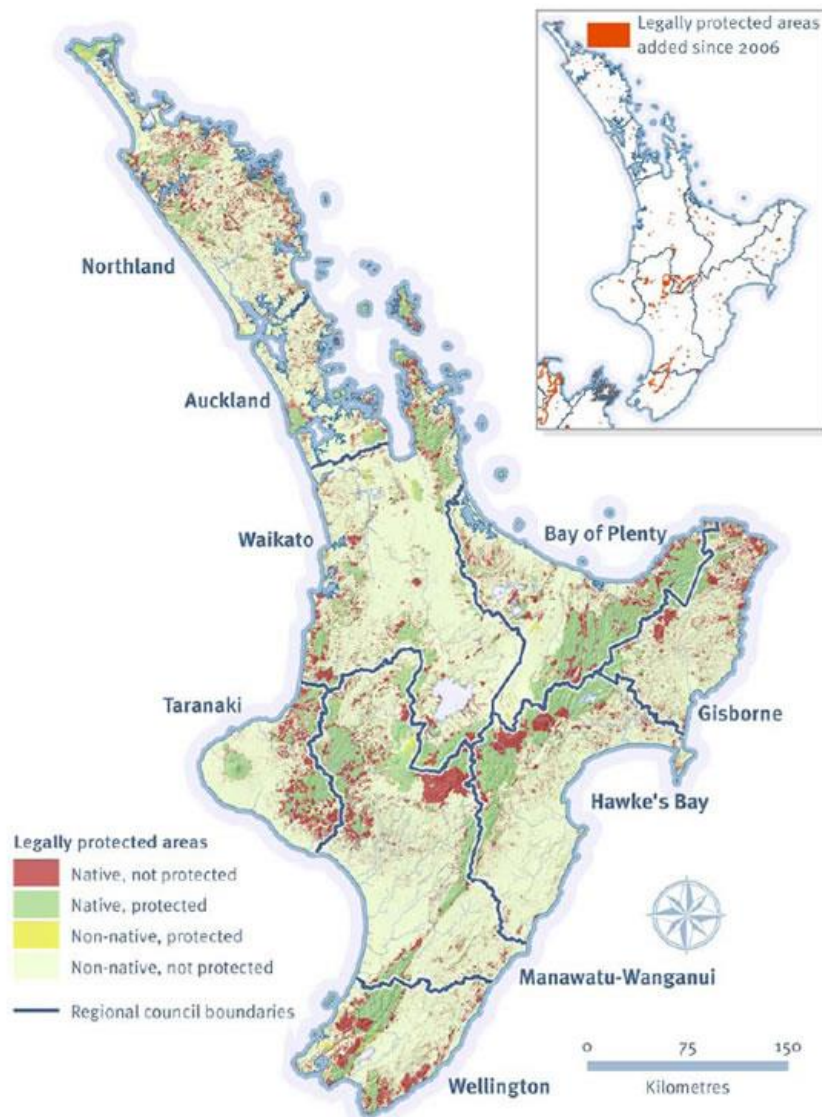


Figure 1. Legally protected areas of North Island, New Zealand, 2009.

Retrieved from <https://www.mfe.govt.nz/environmental-reporting/land/area-native-land-cover-indicator/legally-protected-conservation-land.html>. Copyright 2010 by Ministry for the Environment. Reprinted with permission.

Conservation covenants.

A covenant is a legal agreement between the land owner and the covenanting agency regarding the protection of the area's natural value and is the most common form of legal protection on private land in Auckland. When conservation covenants first started in New Zealand, powers to enter into covenants were given to the Department of Conservation under the Reserve Act 1977 and the Conservation Act 1987; and to the Queen Elizabeth II (QEII) National Trust, a voluntary organization established under the Queen Elizabeth the Second National Trust Act in 1977. The QEII National Trust is described in the next sub-section.

Covenants are usually in perpetuity, thus legally binding both the current and future landholders. Financial assistance and specialist advice are available to the landowner for surveying, legal and fencing costs. Monitoring is needed to assess the effectiveness of management actions and changes in protecting values. Either the landowner and covenant agency can do the monitoring according to each individual agreement (Auckland Council, n.d.; Davis & Meurk, 2001; Saunders, 1996).

The Queen Elizabeth II National Trust.

The Queen Elizabeth II National Trust, referred to here as QEII, is the main type of covenant protection used on private land in New Zealand. An open space QEII covenant is a legally binding protection agreement registered on the title of the land. The landholders still retain the ownership and management of the covenanted land, while the QEII helps the landowners with conservation and management advice and support. A management plan is prepared for the landowners once the QEII covenant is established, which determines, suggests and provides on-going conservation and management objectives and guidance on aspects including species management, pest control and restoration methods (Queen Elizabeth II National Trust, n.d.).

The benefits of conservation covenants are many, and include helping to protect the unique natural and cultural heritage of New Zealand. Many landowners are motivated to protect natural heritage because it makes good land management sense. In addition, a covenant within a community often inspires other landowners to follow suit and collectively protect special values in their area. In terms of region councils, covenants help local authorities to fulfil their responsibilities under the Resource Management Act (Queen Elizabeth II National Trust, n.d.).

To establish an open space QEII conservation covenant, a few steps are required to implement it, including enquiry, evaluation, approval, fencing, surveying, registration and funding assistance. The QEII regional representative evaluates a range of criteria such as ecological and biodiversity value, naturalness, existing or potential value as an ecological corridor, wildlife, geological features, cultural and heritage values, and sustainability of the land (amongst other factors). A survey plan and aerial photo-diagram of the covenanted area is prepared and the area fenced as well if required. Finally, the QEII pays the survey cost, and landholders are eligible for other funding assistance including fencing costs, weed and pest control, rates relief and restoration planning. The QEII regional representative visits each

conservation covenanted area every two years to monitor the condition and trends, identify and address any threats and advise the landowner how to meet the covenant objectives of the land (Queen Elizabeth II National Trust, n.d.).

The QEII open space covenant has been a successful mechanism for the protection of private land in most areas. A total of 3,803 covenants have been registered and 410 covenants have been approved, while 33 covenants are in the phase of formal agreements. Thus, the QEII covenants are protecting a total of 104,393.90 hectares of New Zealand land (Queen Elizabeth II National Trust, 2013).

Management agreements.

The management agreement between the Department of Conservation and landowner under section 29 of the Conservation Act is not registered against the title and does not bind future owners. It is a temporary agreement to keep the management options open until the landholder reach a final agreement for improved protection (Davis & Meurk, 2001).

Protected private land agreements.

A protected private land agreement is made between the Department of Conservation and landowner. The landowner retains the ownership and the agreement is recorded on the title by a gazette notice (Davis & Meurk, 2001).

1.2.2 Active management.

Private lands which aren't protected by legal covenants or agreements are more likely to be protected by landowners using an active management approach. Natural areas such as forest fragments and wetlands are vulnerable to pest animal damage, weed invasion, livestock grazing and trampling, and wind exposure. Active management can improve plant establishment and growth, reduce wind damage and reduce the effects of introduced pests on native plants, birds, bats, lizards and invertebrates (Auckland Council, n.d.).

Active management includes fencing off the area from stock, eradicating or controlling pest plants and animals, planting native vegetation, and reconnecting isolated remnants (Auckland Council, n.d.). Active management is personal voluntary operation for landowners, which may include extensive costs. Considering that an area of high natural heritage value could be owned by several people, landholders can create private partnership agreements to protect their land. Although some funding for the active management might be available from regional councils, it is not guaranteed. The on-going monitoring and maintenance of the area

may also exceed the budgets of the landowners and lead to a failure of the protection measures.

1.3 Remote Sensing for Private Land Conservation

Remote sensing of private land for conservation purposes provides landowners with a cost effective way of mapping and monitoring the natural environment. Combining remote sensing with Geographic Information Systems (GIS) would help landowners manage, analyse and model the remotely sensed data for better natural heritage protection, conservation and management.

There are three main methods of collecting remotely sensed images including by satellite, unmanned aerial vehicle (UAV) and aerial photography from fixed wing aircraft. For environment conservation, satellite remote sensing is the most widely used method by managing agencies. However, the limitations of satellite remote sensing restrict its use for private land conservation. Specifically, data from satellite remote sensing may not be available and free online data may not be current; and data may not have been collected at a resolution relevant to small covenanted areas. In addition, it may be prohibitively expensive for private landowners to purchase the higher resolution satellite data.

In the past decade, UAVs have developed dramatically. Characteristics such as flexibility, low cost, high resolution and repeatability of UAV remote sensing address the restrictions of satellite remote sensing, while providing a new and practical tool for private land conservation and management. This low cost and convenient technology enables landholders to effectively monitor the condition of their land.

1.3.1 Unmanned Aerial Vehicle remote sensing.

UAV remote sensing is a new technology which has the capability to map land resources and other spatial entities automatically, intelligently and quickly to complete remote sensing data processing, modelling and analysis.

With technology development, improvement of navigation and operation systems as well as the decreasing cost, the operation of UAVs has increased dramatically worldwide over the last few years. Opportunities for UAV activity include military operations, policing duties, traffic monitoring, fisheries protection, pipeline surveys, sports events film coverage, border patrol, agricultural operation, power line surveys and aerial photography (Civil Aviation Authority of New Zealand, 2007). However, apart from some commercial and military

operators in New Zealand, most of the UAV use is recreational. The industry is developing so rapidly that the New Zealand Civil Aviation Authority (CAA) has serious concerns about public safety and privacy due to the lack of robust regulation and standards. Meanwhile, the true extent of UAVs' use in New Zealand is not clear either (Jones, 2013). To date, eight organizations had been authorized to operate UAVs in New Zealand (reference March 14, 2013). To authorize, the CAA had to be satisfied that the operators of UAVs did not endanger any person or property under the Civil Aviation Act as well not operating in restricted airport areas (Migone, 2012). All of the authorized organizations are commercial companies, although three of them have links to military use. For commercial usage in New Zealand, business activities range from 3D imaging and photography, inspecting power pylons, movie making, and real estate photography. Simultaneously, the Defence Force applies UAV technology in military areas as a targeting system with a Phoenix drone system (Civil Aviation Authority of New Zealand, 2007, 2013). A Skycam Kahu UAV is now used in a "limited interim capability for military tasks" (Jones, 2013). The New Zealand Police also introduced UAV technology in two criminal investigations in 2012, and purchased a helicopter-style UAV to see how it could be applied in police detection (Fisher, 2013). However, UAV remote sensing is still new to New Zealand, and has had limited academic research based on its use. Auckland University of Technology is the first university in New Zealand to make attempts in using the innovative UAV techniques to a series of conservation research such as vegetation classification, mapping and biology monitoring (Auckland University of Technology, 2012).

1.3.2 UAV remote sensing for environmental application.

The military roles of UAVs are being replaced by the scientific ones especially in the environmental sciences. At the International Society for Photogrammetry and Remote Sensing congress, UAVs were mentioned and defined as giving a new and controllable platform for data acquisition processes without effects on, or harm to, the environment; nor human life (Samad, Kamarulzaman, Hamdani, Mastor, & Hashim, 2013). There are environmentally friendly UAVs and normal UAVs. The difference is defined by the types of fuel used and the amount of noise produced. Environmental friendly UAVs use electricity instead of gasoline as their fuel, which does not generate any carbon dioxide. Furthermore, electrical UAVs produce much less noise compared to normal UAVs; noise may scare off animals when undertaking an animal monitoring mission. Also important to note is the feature of UAVs being able to go through dangerous areas in order to conduct examinations,

including of volcanic activities, toxic spills and other similar situations, for use in environmental science.

Due to the advantages of cost-effectiveness, safety, high resolution and flexibility, UAVs are particularly suitable for use in environmental and conservation science. UAVs can acquire first-time data and update the data without waiting for long term information such as from satellite imagery, which enables UAVs to provide strong and powerful technical assistance and support in several respects, such as the environmental conservation management of construction projects, environment assessment, environment monitoring, meeting emergencies of environmental incidents, and wildlife and vegetation conservation (Everaerts, 2008). The last aspect is addressed in the next sub-section.

Wildlife and vegetation conservation.

Protection of wildlife and vegetation is a predominant theme of the world currently, which is also a common application of UAV technology. Generally speaking, the main difficulties of wildlife and vegetation protection rise from the large areas involved, rural locations, and inconvenient transportation. All of the features above make the protection hard to carry out. However, by applying UAV techniques, government departments responsible for conservation and the environment can acquire real time remotely sensed images of conservation areas when required, then compare and calculate the time-series UAV images for monitoring vegetation change. Thus, the ecological environment as well as the dynamic evolution of a region can be understood clearly. The high resolution imagery generated by UAVs can even identify the mutual substitution of different vegetation types within that region, which can play a reference role for the ecological study within the area. Moreover, the UAV system is a good tool to monitor wildlife and illegal activities. For instance, a successful test of two conservation drones was carried out on 12 June, 2012 in Nepal. The two UAVs were used for monitoring tigers and rhinos as well as illegal activities within the protected area. The UAVs were two meters in width and flew up to two hundred meters so they were capable of covering a distance of up to 25 kilometres within 45 minutes. UAVs are the latest addition to new scientific techniques and technologies are being introduced to aid conservation purposes in the world, and conservation (WWF, 2012). Most importantly, when nature reserves and protection areas are being illegally occupied, the UAV system can be the first detection mechanism. Remotely sensed images can also be used as supporting evidence for ecological conservation enforcement.

1.4 Study Location and Research Area Importance

Dairy Flat is a rural area within the Rodney District of the Auckland region in the North Island of New Zealand and it is around 28 kilometres north of the centre of Auckland. Most of the area was dairy farms until the early 1990s; with the development of Auckland city and the extension of the Northern Motorway in this area, Dairy Flat was subdivided into several living and lifestyle areas, which still contain large areas of vegetation. According to a report by the Auckland City Council (2013), 65% of the land cover of Dairy Flat is pastoral vegetation, while 22% of the land cover is native and 10% exotic (Auckland Council, 2013). Because of its close proximity to Auckland, its natural heritage value and diversity of native tree species, as well as its proximity to a model airfield where a UAV can be safely operated, it was chosen as the study site for this research programme. And most importantly, the research region is private land which has not yet been listed on any legal protection menu or put under any other form of legal protection. The bush area has been protected by the active management of fencing off. The research bush area is a very typical example of countless private lands with natural and conservation values in New Zealand, providing a chance to determine if the UAV remote sensing technique could be applied to such private land for conservation and management purposes.

Furthermore, the accessible regrowth bush area is near the model airfield, which meant the whole procedure of UAV missions could be observed and safety issues are addressed. It is illegal to fly a UAV without the approval of the CAA; therefore we had flight approval from the CAA first to fly over the Dairy Flat regrowth area.

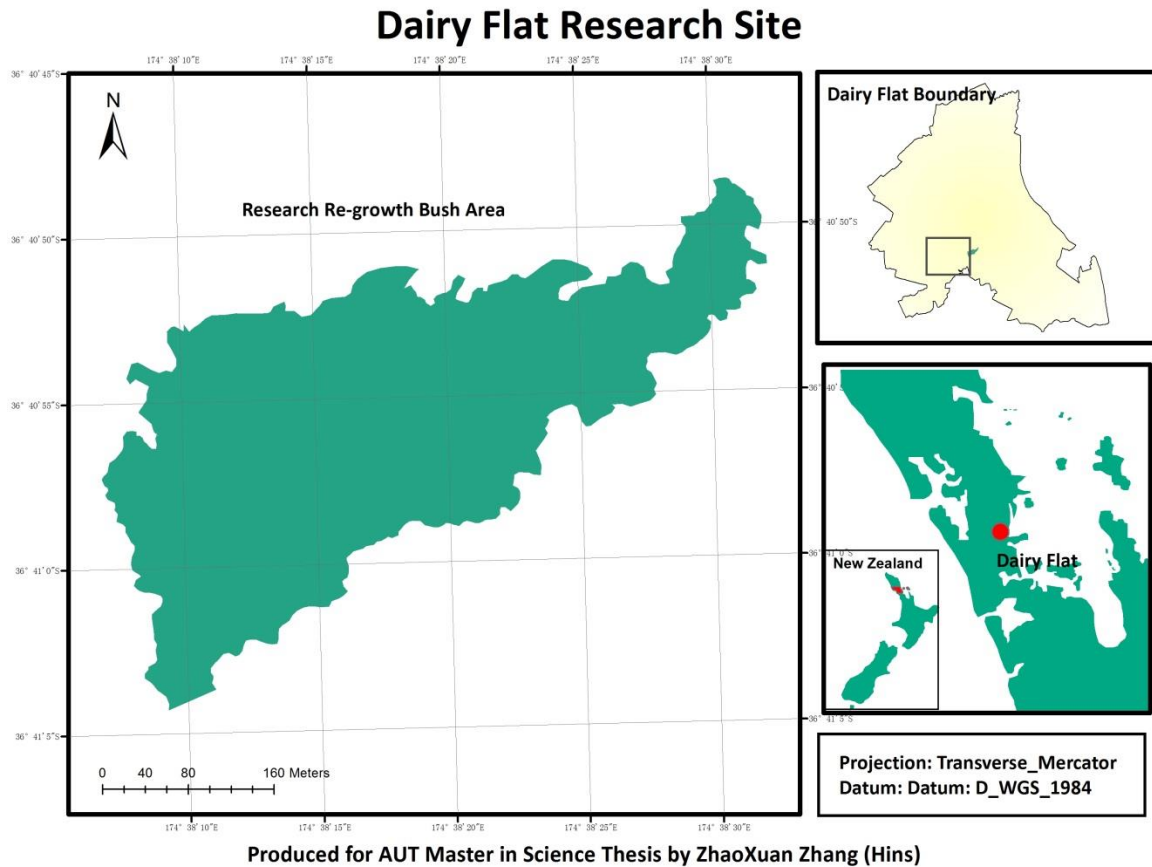


Figure 2. Research location map.

1.5 Research Questions and Objectives

This master’s research was designed to answer the question: “Can small, inexpensive, autonomous UAVs acquire sufficiently high quality data that can be used to mosaic and produce accurate vegetation classification on an area of small private land at a species level?”

The five objectives were:

Objective 1: To critically examine the capability of Hawk and Swampfox UAVs and unsupervised classification algorithms to identify vegetation at the species level.

Objective 2: To use the field data to perform a supervised classification of the Hawk and Swampfox UAV imagery at the species level.

Objective 3: To examine the performance of pixel-based and object-based classification using UAV mosaic imagery.

Objective 4: To use the Hawk and Swampfox UAV mosaic imagery to perform normalized difference vegetation index value calculations.

Objective 5: To examine whether the UAV data could be used for Normalized Difference Vegetation Index (NDVI) value calculations, then the NDVI value used for vegetation classification.

1.6 Structure of the Thesis

The intention of this study was to address the research question by developing a set of UAV imagery classification methods including the use of pre-processed data, creation of imagery mosaics, and classification and accuracy assessments within the bush area on private land at Dairy Flat.

Chapter 2 presents a review of the relevant literature. It briefly outlines the background, and describes the development, and latest techniques and studies of remote sensing, UAV remote sensing and vegetation classification.

Chapter 3 describes the equipment and methods I used to acquire the UAV images and how these images were used to create a mosaic. I then outline how I applied pixel-based and object-based classification (supervised and unsupervised) techniques to UAV imagery mosaics, evaluated the accuracy of the classification results and ran the post-classification processing in ArcGIS software.

In chapter 4, I present all the UAV image mosaics, and the classification results of pixel-based and object-based methods. Following that, all the accuracy assessments of the supervised classifications are presented using a confusion matrix, along with the results of the NDVI value calculations as well as the NDVI and Enhanced Normalised Difference Vegetation Index (ENDVI) scripts' processed results.

In chapter 5 I discuss the study as a whole, from the beginning of the UAV flight planning, UAV images processing, UAV mosaic classification to the accuracy assessment of the classification results.

2 Literature Review

2.1 Vegetation Classification

The aim of vegetation classification is to obtain groups of plant communities that are understood as similar internally and distinct from other groups of vegetation in a given geographical area (Wildi & Otto, 2010). Vegetation classification not only provides a meaningful way for us to develop the understanding of vegetation patterns, but also becomes a convenient and useful tool for conservation science, land mapping and land use planning (International Association for Vegetation Scientists (IAVS), n.d.).

2.1.1 Traditional vegetation classification.

Before the appearance of remote sensing vegetation classification, traditional classification was extremely time-consuming and required a lot of labour. Traditional vegetation classification involves establishing a set of quadrats over an area. The location of quadrats depends on the sampling method employed by the researchers and approaches to sampling distributions including random, stratified and systematic; or, for example, where a large number of species needs to be recorded in a large vegetation research project. It is always necessary to employ various multivariate statistical techniques to measure the similarity between observations. Cluster analysis is a method that considers the formation of groups of vegetation depending on the species' composition similarity; while ordination is about reducing the multitude of the data into a few indices to represent the majority of variability of the data (Bean, n.d.).

2.1.2 Vegetation mapping and classification in New Zealand.

Since 1973, a major survey of New Zealand physical land resources, named the New Zealand Land Resource Inventory (NZLRI), has been undertaken by the (then) Ministry of Works and Development. The information presented in this survey initially contained five key physical factors, including rock type, soil, slope, erosion and vegetation. However, all of the information was recorded at a scale of 1:63360. Vegetation was the secondary inventory factor and thus recorded within a map unit boundary predetermined by the primary inventory factors. Moreover, the vegetation information recorded in this inventory was acquired from 1973 to 1979 by combining the data and information from stereoscopic aerial photograph interpretations and extensive fieldwork, along with existing information. The vegetation cover was assessed by using a classification of 45 components arranged into five groupings

including grassland, cropland, scrub and fernland, forest, as well as miscellaneous. In 1981, Blaschke et al. (1981) proposed a research project which used the vegetation information within the NZLRI to present an analysis of New Zealand vegetation. This research confirmed the dynamic and complex nature of New Zealand's present vegetation cover; however, it is a very brief analysis of the vegetation cover due to the information restriction at that time, and species classification has not been carried out (Blaschke et al., 1981).

In the 1990s, twenty years after the establishment of the NZLRI, (which is still useful for people in New Zealand to study vegetation), the data collection methods and information generated changed dramatically. Satellite information became available, and vegetation mapping or classification using the satellite was possible. At the beginning of the 1990s, several scientists demonstrated that satellite imagery is ideal for providing quick vegetation information over a large area. Dymond et al. (1996) produced a vegetation map for the Gisborne district of New Zealand by using the Landsat Thematic Mapper (TM) imagery with an accuracy of over eighty per cent. The classified imagery was compared with the NZLRI to identify gross errors. Nevertheless, there still were many technical limitations and restrictions at that stage of development of vegetation mapping, such as varying illumination of topography, and variable atmospheric conditions, which hamper the classification process (Dymond et al., 1996). Recently, Ashraf et al. (2010) conducted research using remotely sensed data to map vegetation in New Zealand freshwater environments. They commented that a variety of problems associated with access, scale and distribution can be overcome by using satellite remote sensing; however, there is a need for more accessible, high resolution images with appropriate spectral characteristics (Ashraf, 2010).

2.2 History and Status of Remote Sensing in New Zealand

Remote sensing is a powerful and convenient tool for efficient, non-destructive mapping of vegetation over broad spatial scales. Satellite and aircraft remote sensing are widely used in obtaining distribution maps according to vegetation classification (DeFries & Ruth, 2008; Hill, Wilson, George, & Hinsley, 2010; Xie, Sha, & Yu, 2008).

Remote sensing was introduced to New Zealand in 1926, when the first aerial surveys were conducted by flying over Christchurch, and systematic photographic coverage of the whole of New Zealand had commenced by 1936 (Belliss, 1984; Vassilaros, n.d.). The first satellite remote sensing imagery was available from Landsat-1 in 1973. By 1977, NZ scientists had already used Landsat data to map the regional and seasonal sediment discharges along the

New Zealand coast (Cochrane & Male, 1977). With the development of the National Aeronautics and Space Administration (NASA) of the United States of America (US) Landsat-2 programme, NZ investigators had access to satellite remotely sensed data, and they used them in various application projects during the 1980s, including agricultural and forest monitoring, snowfield assessment, sedimentation modelling, structural and geomorphic studies and cartography. The satellite data were mainly used by the New Zealand Physics and Engineering Laboratory, but also by other government departments, especially the Department of Lands and Surveys (Belliss, 1984).

In the 1980s, scientists conducted remote sensing research using Landsat and multispectral aircraft scanner data to examine the land cover classification accuracies. Simultaneously, a project was carried out to measure sea surface temperatures and chlorophyll levels using remote sensing technique (Belliss, 1984).

Israel and Fyfe (1996) examined the ability of SPOT XS (satellite) multispectral data to detect different intertidal and shallow subtidal habitats by classifying coastal vegetation using eelgrass as a case study (Israel & Fyfe, 1996). Gao (1999) also used satellite data to classify and map mangrove forests in the Auckland western Waitemata Harbour using a maximum likelihood method (Gao, 1999) and used the methods to map vegetation damage caused by animals. Other studies in New Zealand used remote sensing technology, including the estimation of biomass for NZ pasture, through the application of optical remote sensing techniques (Hanna, Steyn-Ross, & Steyn-Ross, 1999).

Despite the recent development in remote sensing, more sophisticated observing systems are needed, which require increased resolution in the spatial, spectral, radiometric and temporal domains for the further development of research (Hartley, 2003). Entering the 21st century, satellite remotely sensed data became more accessible. As a result, most studies in New Zealand related to remote sensing have used satellite imagery as their main data sources. Allan et al. (2011) investigated the ability of Landsat Enhanced Thematic Mapper imagery to quantify the chlorophyll α concentrations in New Zealand's central North Island lakes. They found that remote sensing provides a potential and valuable tool to measure the temporal and spatial distribution of chlorophyll α (Allan, Hamilton, Hicks, & Brabyn, 2011). Moreover, the remote sensing technique was also applied in a land-use/cover changes detection study in New Zealand's grassland using four different methods. They concluded that visual interpretation resulted in the best classification with 98% accuracy and suggested that this is

why visual interpretation of high resolution imagery is still needed (Weeks, Ausseil, Shepherd, & Dymond, 2013).

2.3 Unmanned Aerial Vehicles

Remotely Piloted Aircraft Systems (RPAS) commonly known as ‘unmanned aerial vehicle systems’ or ‘drones’, are aircraft which are controlled remotely by wireless signals from the ground or operated by its own program. Each UAV can be different in terms of shape, size, safety consideration, cost, purpose, configuration and relevant equipment. Historically, the majority of UAVs have been regarded as remotely controlled aerial vehicles. With the development of miniature electronics technology, an increasing emphasis on autonomous control has occurred (Hexmoor, Rahimi, & Little, 2009). Over the last decade, UAVs have been widely used in the military because the aircraft can safely conduct dangerous missions which are beyond the physical limitations of pilots. The success of military usage has encouraged efforts to establish UAV in non-military roles (Fahlstrom & Gleason, 2012).

2.3.1 History of UAV.

The development of UAV technology was initially driven by the military applications. According to Fahlstrom and Gleason (2012), in 1887, Douglas Archibald attached cameras to a kite which was regarded as the world's first reconnaissance UAV. When William Eddy took hundreds of images from the kite during the Spanish-American war, it was the first implementation of UAVs on the battle field. However, the first remotely controlled UAV was designed and created by Archibald Montgomery Low, who developed data links. Professor Low's first UAV crashed, but later on 3 September, 1921, he made the world's first successful radio controlled flight. In the early 1930s, the British flew three UAVs from a ship and though two of them crashed, the third one flew successfully. The British intended to use it as a gunnery target, but failed to shoot it down. The mobility of the UAV caused the British to recognise and appreciate its value. In 1937, a group of people developed a series of UAVs named RP-1, RP-2, RP-3 and RP-4, and they established a company called the Radioplane Company which built thousands of drones during World War II (Fahlstrom & Gleason, 2012). The de Havilland DH.82B Queen Bee was a full size remote-controlled target drone. They were first produced in 1935, as an inexpensive, expendable radio-controlled target drone for anti-aircraft gunnery practice (Braithwaite, 2012). However, it was not until the Vietnam War that the potential of the UAV for reconnaissance was explored and used

successfully (Bryson, Reid, Ramos, & Sukkarieh, 2010; Nikolos, Zografos, & Brintaki, 2007; Xiang & Tian, 2011).

2.3.2 Non-military UAVs.

During the last decade, an increasing number of UAVs have been developed for civilian application, ranging from military-style surveillance, search and rescue missions, climate and atmospheric study, environmental and conservation science, wildlife protection and agricultural purposes, to even 3D geographic mapping (Baker & Stuart, 2009; Carroll, n.d.).

The application of a UAV in aerial measurement can be an enhancement of the satellite remote sensing technique. Satellite imagery is the main source of remote sensing mapping. However, due to the limitations of the period of satellite's position, cloud cover, as well as the supply methods to customers, high resolution remotely sensed data purchased by customers may be unsatisfactory in terms of coverage, timeliness and cost. Data from a UAV can supplement satellite remote sensing because of its flexibility and high image resolution. The combination of both is able to form a comprehensive measurement system. However, UAVs have not so far been broadly used in civilian applications, owing to the immature technology.

2.3.3 Modern use of UAVs.

Some of the most well-known UAVs were put utilised and provided great service in the last few decades of the 20th century, such as the Hewitt-Sperry Automatic Airplane (1936), the Teledyn Ryan Firebee I (1951), the Model 1001 (1955), the Israel Pioneer UAV (1982) and the General Atomics MQ-1 Raptor (2011), a highly intensive surveillance, heavily armed, modern unmanned combat aerial vehicle.

The technology has been serving well in other fields, such as remote sensing, commercial aerial surveillance, natural resources exploration, environmental monitoring, environment conservation as well as production evaluation, transportation, scientific research and possibly search and rescue. Bryson et al. (2010) have used UAV technology to map and identify the land cover over a large farmland area, which is contributing to the conservation of the terrestrial environment (Bryson et al., 2010). As for remote sensing, UAV techniques have been widely used, for example, Xiang and Tian (2011) used a UAV equipped with an autonomous flying route and GPS guided coordinates to accurately circle and patrol an area to provide long term autopilot surveillance of agricultural land. It has proved effective in regions without many weather anomalies and is cost effective (Xiang & Tian, 2011). The fields of archaeology and geology have also adopted this technology in an area with possible

artefacts sites and around highly inaccessible areas. Remote sensing for plant or animal taxonomy and long term monitoring are also possible if the UAV is equipped with a spectral radiometer for various wavelengths spectral detection. Long distance weather surveillance and monitoring work are also effective, provided the UAV can report real-time data in a hurricane or help towards a weather forecast (Hexmoor et al., 2009; Kim et al., 2010).

2.3.4 Main concerns in relation to use of UAVs.

As UAV systems are becoming more widely available, a number of issues are arising that may restrict their use. The US probably has more military UAVs than any other country and there are many requests to use them in law enforcement, emergency response, forest fire monitoring, weather research and scientific data collection. However, the Federal Aviation Administration has restricted the use of UAVs in the US due to the following concerns (Longley, 2013), which are described in the next sub-sections.

Safety concerns.

The main concern is that without ‘see and avoid’ capability, UAVs may pose a safety threat in terms of potential air collisions and danger to those on the ground. In the US (and every other developed country), UAV operation within the air traffic control system (ATC) differs from the manned flight system in that unmanned vehicle control and traffic avoidance are functionally different (Baldwin, n.d.). For traditional, manned aircraft, the ATC will send a command to the pilot to avoid air collision. As always, avoidance of a collision is the responsibility of the pilot, but there is also an electronic system, the Traffic Collision and Avoidance System, fitted to most aircraft (Harley, 2012; Weibel & Hansman, 2006).

Security concerns.

Another concern is the vulnerabilities in the command and control of UAV operations, which include GPS-jamming, hacking and the potential for cyber-terrorism (Longley, 2013). In 2011, a drone belonging to the Department of Homeland Security was hacked by a university’s research team. This case led to a wave of debate about the security of UAV systems within the US. Security of the Ground Control Station and data link infrastructure is a critical requirement for Unmanned Aircraft Systems integration (Baldwin, n.d.). To address this grave issue and produce ‘spoof-proof’ UAVs, new technologies need to be included on-board which allow the UAVs to detect modified GPS data. It is also important to ensure the security of the common data link (CDL) which connects the aircraft to the ground control system and the operator (Baldwin, n.d.).

Privacy concerns.

Although safety and security issues can be fixed by technical improvements of UAV systems, privacy concerns are not easy to manage. The public pay much more attention to privacy issues than safety issues. It is possible to purchase an inexpensive camera and install it on a UAV, which can be used for any purpose by the public. As the development of UAVs continues, more advanced, smaller drones are coming to the market. The public has expressed concerns for those extremely small UAVs which, equipped with video camera and tracking devices, hover silently in residential neighbourhoods largely unnoticed, especially at night; thus everyone's privacy may be exposed and violated (Longley, 2013). To protect the privacy of US citizens, a bill "The Drone Aircraft Privacy and Transparency Act of 2013" has been proposed (RD Collins & Associates, n.d.).

2.3.5 The future of UAVs.

Putting aside the future military use of UAVs, their potential in scientific studies is huge. In addition to technical development including new designs and advanced hardware, the UAV will become more automated, as well as becoming safe enough to avoid accident or loss. Those enhancements of UAV systems enable them to be applied in many fields, such as search and rescue, exploration, crop pollination, surveillance, and traffic monitoring. Researchers in Switzerland even proposed recently that the UAV could be used as a local communication network for emergency workers in disaster regions. These ideas are already in production or are currently in the experiment and testing phases (Frink, n.d.).

2.3.6 Unmanned Aerial Vehicles in New Zealand conservation planning.

Up to the time of writing, the application of UAVs in scientific research has been limited. It appears that the use of UAVs could address the limitations of those projects which are inconvenient, unsafe, high cost, and time consuming. It is therefore timely to seek to make UAVs more accessible, easier to operate, and cheaper for New Zealand scientists. The issues that need to be addressed are described in the following sub-sections.

Necessary regulations and laws.

Considering the safety issues, UAV operator certification appears to be the best method to regulate UAV activities. The Civil Aviation Authority of New Zealand released the UAV Issue Paper in January, 2007 (one of the very first documents about UAVs in New Zealand), and presented the relevant UAV regulations and operation issues identified by the CAA, New Zealand Defence Force, Airways Corporation and industry at a seminar in Wellington on

25th October, 2006 (Civil Aviation Authority of New Zealand, 2007; National Aeronautics and Space Administration, 2013). On 1st April, 2014, the CAA released the latest consolidation document of operating rules for remote piloted aircraft systems (Civil Aviation Authority of New Zealand, 2014). This is a continuing process, as there are a number of interested parties and many opposed opinions.

Cost.

Research funding is always a limitation for research institutes. A UAV system, including other hardware and cameras may cost a few hundred thousand dollars, though this is significantly less than the capital cost of manned aircraft or satellites. The actual cost of satellite images ranges from \$44 to \$3,980 US dollars according to the satellite type, suppliers, image size, resolution and land area per image (IntraSearch, n.d.).

Operation.

In order to use UAVs in conservation research, there is a need for skilled operators. The more reputable UAV suppliers will provide training and it is most likely that CAA will require operators to have knowledge of radio procedures and air law as a minimum qualification. However, possession of a commercial pilot's license is, at this time, thought to be unnecessary. An experienced UAV operator is more likely to produce good quality data in a safe manner, and the CAA will require all operations to be supervised by a qualified operator. Simplification of the UAV operating systems and automation will reduce the workload of operators, but will not remove the requirement for suitable training and certification.

2.3.7 Unmanned Aerial Vehicle remote sensing.

In recent years, the potential of UAVs for remote sensing has been highlighted because of their flexible flight activation and re-flight capability (Skoglar, Orguner, Törnqvist, & Gustafsson, 2012). The UAV remote sensing technique has already been used in vegetation mapping, monitoring and classification. Lucieer et al. (2012) were the first to use a UAV for mapping moss beds in Antarctica. Their UAV system, with ultra-high resolution cameras, allowed them to map the different environmental characteristics of the moss beds. This study used Structure from Motion techniques to generate a detailed 3D point cloud of the terrain from overlapping UAV photography (Lucieer, Robinson, Turner, Harwin, & Keleey, 2012). UAV remote sensing is also significant in monitoring. A project was conducted by Gay et al. (2009) in the United Kingdom (UK) to establish whether a small UAV could be operated in the UK airspace to collect high resolution images over agricultural field trials. This was the

first report of UAV-based NDVI mapping in the UK, and it illustrated that it is feasible to monitor crops and that images of sufficient resolution can be obtained (Gay et al., 2009). In another study conducted by Hunt et al. (2010), they acquired near-infrared, green and blue images by UAV for crop monitoring over two winter wheat fields. They found a good correlation between leaf area index and the green normalized difference vegetation index, and concluded that the low cost and high resolution advantages of a UAV camera system is prominent in site specific agriculture by providing important information (Hunt et al., 2010). Oleire-Oltmanns et al. (2012) presented a study of soil erosion in Morocco, using remote sensing by UAV. They used the collected data to quantify gully and badland erosion in 2D and 3D in order to analyse the surrounding areas and landscape development (Oleire-Oltmanns, Marzloff, Peter, & Ries, 2012).

2.4 Vegetation Classification Using Remote Sensing

2.4.1 Satellite remote sensing for vegetation classification.

The history of satellite imagery remote sensing usage can be traced back to the 1970s when the first earth observation satellite was launched (Hamilton, 1977). Satellite image have been one of the main data sources for identification and classification of all kinds of vegetation in recent years. Traditional methods of satellite remote sensing have some limitations, such as low resolution, lack of cloud free days, mass area coverage, time consumption and cost effectiveness. One main constraint of lower resolution satellite data, such as Landsat TM is the limitation on capturing tree demographic information when doing classification for some heterogeneous landscapes (Gibbes, Adhikari, Rostant, Southworth, & Qiu, 2010). The use of high resolution, multispectral and hyperspectral imagery may bridge this gap. Although there is an inevitable conflict between the resolution and observation speed, the application of high resolution remote sensing systems should outweigh the reduced speed (Ishihama, Watabe, & Oguma, 2012). One study differentiated tree canopies by exploring the utility of IKONOS (a satellite) data in order to help classify woodland savannah, shrub and grasslands (Gibbes et al., 2010); while Yu (2005) has conducted an objective-based vegetation classification using high resolution remote sensing imagery. Both examples show applications of high resolution remotely sensed data to classify vegetation, and have contributed to the understanding of the potential of vegetation information extracted from satellite imagery (Yu, 2005). The limitation of cloud cover can also be addressed by IKONOS (a high resolution earth

observation satellite) imagery, which includes sufficient information to remove all non-vegetated classes from vegetated classes (Andersen, 2006).

2.4.2 Aerial remote sensing for vegetation classification.

Aerial remote sensing also plays a significant role in vegetation monitoring, mapping and classification. Airborne remote sensing supports species identification of tree crowns by generating spatial and spectral resolution remote sensing data. Using sophisticated classification methods, aerial remote sensing has successfully mapped 16 African savannah species classes with almost 70% accuracy (Baldeck & Asner, 2013; Colgan, Baldeck, F  ret, & Asner, 2012). Different aerial remote sensing techniques are contingent on the sensors used. Oldeland et al. (2010) used images which were taken by the airborne imaging spectrometer HyMap in different seasons to map a spatial distribution of two bush encroacher species. Another aerial remote sensing technique, airborne laser scanning (ALS), is a potential tool, as it can be used to quantify 3-Dimensional vegetation structure. ALS was applied to an area of mature boreal forest in Finland; scientists concluded that the ALS technique is a useful technology for site type identification and provides excellent 3D information on landscapes (Vehmas, Eerik   nen, Peuhkurinen, Packal   n, & Maltamo, 2011). Moreover, Zlinszky et al. (2012) produced a study that categorized wetland vegetation using ALS, and concluded that the data acquisition parameters are similar to some national surveys, which suggests that these datasets could be used for further vegetation mapping and monitoring.

Unfortunately, remote sensing from piloted aircraft is limited by cost and safety concerns. Such limitations often make it difficult to develop research in certain seasons (Ishihama et al., 2012).

2.4.3 Unmanned Aerial Vehicle remote sensing for vegetation classification.

Although satellite and aerial remote sensing are effective for environmental observations, they are limited to relatively large target or rough vegetation classification because their low resolution (Ishihama et al., 2012). For vegetation classification or mapping in detail which requires a remote sensing technique with a resolution of ≤ 1 cm, UAV imagery meets the requirements of higher resolution, flexible timing for data acquisition, low cost and safety.

A project carried out by Dunford et al (2009) used UAVs for the characterization of riparian vegetation and standing dead wood in France. They used a paraglider UAV to develop this research, while pixel-based and object-oriented classification approaches were used at the

scale of a single image. However, constraints including illumination conditions and sensor movement during flight, which will create variations in spatial resolution and radiometry, need to be addressed in order to improve the methodology. They also concluded that UAV remote sensing technology can provide the flexibility to rapidly produce very high resolution map products to aid riparian management.

Some satellite sensors have high spatial resolution; however, the lack of some spectral resolution makes it hard to apply in some specific areas of research because they allow only a limited number of vegetation indices and remote sensing calculations. One study described the method of combining high spatial resolution and the UAV remote sensing techniques for vegetation use. Ishihama et al. (2012) used a high resolution remote sensing system based on a radio-controlled helicopter to obtain data in order to classify two herbaceous species. The images obtained were at a high resolution (1 cm) with accurate position detection. This lightweight system can be applied to research in places that are hard to access. They concluded that aerial observation is possible on cloudy days, hence all season observation is practical (Ishihama et al., 2012). However, hyperspectral remote sensing based on UAVs is also available, which was developed by the Idaho National Lab and Idaho State University, US. Mitchell et al. (2012) successfully acquired usable data supporting different classification approaches and supervised and unsupervised classifications were applied to their hyperspectral data.

UAV remote sensing imagery may offer less spectral discrimination than traditional hyperspectral satellite imagery, but this limitation can be addressed, because the UAV is able to fly at very low altitude, so it provides very high spatial resolution, which may solve the unmixed colour information issues.

Although there are various remote sensing technologies available, high resolution imagery can be collected by UAVs more cheaply and hence more frequently than satellite image acquisition or aerial surveys from fixed wing aircraft (Dunford et al., 2009).

2.5 Image Mosaic and Processing

2.5.1 Image processing using the Pix4UAV software.

Once the images have been collected from the UAVs in RAW format, they need to be manipulated and converted into a full view imagery of the research site, which may contain different band information from a separated view or band images, in order to develop the

investigation further. Pix4UAV (Pix4D, Lausanne, Switzerland) is a powerful and unique, automatic and fast speed UAV data processing software. This program can deal with thousands of images obtained from the UAV camera, and produces professional and accurate 2D maps as well as 3D models.

Pix4UAV has been used in many fields such as mining and quarry surveys, emergency response, and vegetation classification. Mosini et Caviezel SA is a certified Swiss survey company that used Pix4UAV to process images acquired by a Sense fly Swinglet (a drone developed by senseFly Ltd) for gravel pits and quarries (Pix4D, n.d.-b). Their report concluded that the processing time with this program took only a few hours compared with four days previously; and that the accuracy was much better than traditional surveys as well as having an increase of productivity and reduction of cost achievable with this software (Laurent, 2012). In 2010, when the earthquake occurred in Haiti, Pix4UAV was used by the International Organization for Migration and United Nations Operational Satellite Applications programme to produce the overview mosaic and elevation model for topographical and hydrographical studies. They operated the swinglet CAM to obtain near-infrared (NIR) and visible image mosaics of various regions, which provided more specific aerial information about this area than before. Using Pix4UAV, it is easy to generate data maps and share them with other GIS or remote sensing programs. For vegetation usage, Strecha and his colleagues demonstrated the capability of UAVs with the Pix4UAV software to develop species-specific vegetation maps in Australia in 2012. This study shows that image sets of different wavelengths (NIR and visible) can be automatically combined to generate a 4 band orthoimage by using Pix4UAV. This research also examined a novel methodology to combine numerous sets of images from a UAVs with traditional image location and orientation uncertainties, in order to develop raster datasets capable of assessing complex vegetation communities at spatial resolutions appropriate to the features of interest (Strecha, Fletcher, Lechner, Erskine, & Fua, 2012). This paper presents the computation of the vegetation index and methods to achieve classification or mapping goals with difficult photogrammetric target material.

Strecha et al. (2011) also estimated the accuracy of several sets of UAV data using the Pix4UAV program. This study shows that the accuracy is highly dependent on the ground resolution of the input image. They concluded that the result is robust and the process is fully automatic. The software can deal with inaccurate position and orientation information which are typically problematic with traditional techniques (Strecha, 2011).

2.5.2 Normalized Difference Vegetation Index (NDVI).

Remote sensing technology is capable of monitoring the change of vegetation and mainly expressed as vegetation index. The Normalized Difference Vegetation Index (NDVI) is currently the most widely used index, serving to calculate the mean difference between reflectance in the red band and the reflectance of near-infrared and mid-infrared bands (Bannari, Morin, Bonn, & Huete, 1995).

NDVI has been used for years and applied in thousands of vegetation studies. In the early 1990s, scientists used NDVI to classify land cover at continental scales. Defries and Townshend (1994) used a low resolution spatial data set of monthly NDVI values for 1987 to explore the capabilities of the NDVI. Results demonstrated the feasibility of using a maximum likelihood, supervised classification method of eleven cover types to increase the accuracy of global land cover information, using satellite sensor data (Defries & Townshend, 1994). They concluded that finer spatial resolution, which would include other bands in addition to the NDVI would increase the accuracy of the classification. In addition to vegetation classification, scientists have also used the NDVI for monitoring sparse vegetation coverage. Ruiliang et al. (2008) assessed a vegetation change using classification and NDVI differencing change detection methods. They found that the use of the NDVI differencing images improved the accuracy of change detection compared with a traditional method. They recommended the use of NDVI differencing method if a suitable spectral normalization between multi-temporal images could be carried out before performing image differencing (Ruiliang et al., 2008). The NDVI can also be applied in vegetation mapping. A group of Chinese scientists used the Time-series Moderate Resolution Imaging Spectroradiometer (MODIS) (a payload scientific instrument on board the Aqua satellite) NDVI data combined with a denoising method for crop mapping in Hebei province, China. Previously, temporal crop signatures generated from the MODIS NDVI data were always accompanied by noise. The denoised time-series MODIS NDVI data were classified and they concluded that the denoising approach improved the MODIS NDVI product significantly in several periods, which may affect the accuracy of classification (Zhang, Lei, Wang, Li, & Zhao, 2011).

2.6 Vegetation Spectral Reflectance

2.6.1 Spectral response of vegetation.

The reflectance of electromagnetic energy by vegetation is determined by its chemical and morphological characteristics. These characteristics are related to the growth, health and

living conditions of the vegetation. The absorption and reflection of energy depend on the incident wavelengths and the vegetation properties that influence the scattering of photons and consequently control the leaf spectral response (Cochrane, 2000).

Within the visible wavelengths region, which range from 400 to 700 nm, leaf pigment is the dominant factor affecting the reflection, especially the effect of chlorophyll. The spectral response curve of healthy vegetation is always appears as continuous peaks and troughs, and the peaks within the visible wavelength are due to the influence of pigments in the leaves. Specifically, the absorption of chlorophyll shows peaks at 450 nm and 670 nm (blue and red), while the chlorophyll dominates the reflectance in green (500 – 560 nm). In addition to this, other pigments including the carotenoids and xanthophyll also influence the spectral response by reflecting primarily yellows and browns.

Within the near-infrared region from 700 nm to 1200 nm approximately, the vegetation spectral characteristics are mainly affected by the cell structure and arrangement within the leaves. In the region of middle-infrared, the spectral response of vegetation is dominated by water at 1400 nm, 1900 nm and 2700 nm due to the molecular qualities of water in the vegetation (Fyfe, 2003).

In summary, the three main factors of leaf pigment, cell structure and water content, generate the unique spectral signatures of vegetation, which enable identification in the near-infrared region.

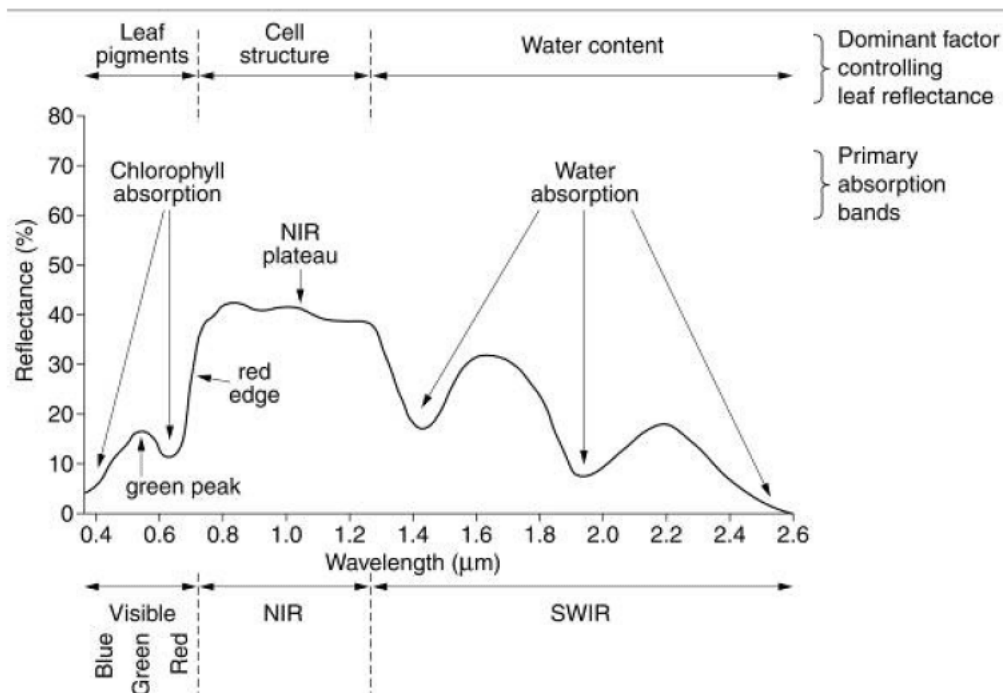


Figure 3. Typical spectral reflectance curve for vegetation.

Retrieved from <http://www.scotland.gov.uk/Publications/2009/11/06110108/6>. Copyright 2009 by the Scottish Government. Reprinted with permission.

2.6.2 Spectral variation of vegetation.

We know that different species of vegetation have different spectral responses, however it is noticeable that the response is variable even within the same individual tree. A number of factors influence spectral variation in vegetation such as vegetation properties, season, and spatial area, amongst others. These factors are outlined in the next sub-sections; namely biophysical, temporal and spatial variations.

Biophysical variation.

The reflectance features from different parts of the same plant vary from each other owing to their different biochemical composition which will lead to the spectral variation within an individual plant, a species or even a community (Fyfe, 2003). Because spectral variation can occur in a single plant, it is therefore possible that several species of vegetation may have spectral overlaps and hence the spectral response is not unique. This situation indicates that the understanding of intra-species spectral response is particularly important when classifying spectral responses between species (Hestir et al., 2008; Price, 1994). Apart from the internal biochemical factors, the external conditions such as the changes of environment or disease will affect the spectral response of plant too.

Temporal variation.

Temporal variation is the result of vegetation changes during a period of time. Within this period, vegetation undergoes a cycle including the phases of flowering, fruiting, seeding, growth and senescence which will lead to changes of the spectral features of vegetation. Apart from the biochemical cycle of vegetation, the changes of environmental conditions such as annual rainfall, sunlight and nutrient availability also affect the spectral reflectance. Vegetation response to the changes of environment and the differences of spectral from time to time decrease the spectral uniqueness to some extent. Förster and Kleinschmit (2009) discovered that vegetation produced various spectral reflectance and they recognized the dates of highest differentiation of the vegetation. In the case of temporal variation, each spectral response should be collected in different conditions based on a specific time, environment and biophysical states. In order to determine the most accurate spectral reflectance, all the variation of spectral reflectance should be collected to cover all conditions, and then the average calculated of the spectral response.

Spatial variation.

Spatial variation of spectral reflectance can be summarized as the changes of reflectance at different areas of the vegetation, such as the canopy, leaves or branches. When it comes to the remote sensing, the key factor concerns the relation of the distance of the target from the sensors and the field of view (FOV). For instance, when people try to determine the spectral response of an individual plant at the leaf level, it will produce a limited variation of spectral reflectance due to the single leaf containing only photosynthetic or non-photosynthetic tissues. However, when you acquire the spectral response of the plant at the canopy level, which includes all the photosynthetic and non-photosynthetic tissues, the variety of spectral reflectance can be collected thus producing more accurate and comprehensive spectral data for the species. However, the spectral acquisition by the FOV at leaf level can be achieved as well if enough individual spectral profiles are collected in addition to the increase in sample size (Cho, Sobhan, Skidmoreb, & de Leeuw, 2008).

2.7 Vegetation Classification Methodologies

2.7.1 Unsupervised classification.

If there is no map information or ground truth data of the research area, unsupervised classification is a good choice to carry out identification. Unsupervised clustering methods are particularly important in unsupervised classification. Unsupervised clustering is a

fundamental tool in image processing for geoscience and remote sensing applications (Richards & Jia, 2006). Two techniques are described in the next sub-sections: the use of Iterative Self-Organizing Data Technique of Analysis, and K-mean.

ISODATA.

Iterative Self-Organizing Data Technique of Analysis, known as ISODATA, is one of the most popular and widely used clustering methods of the remote sensing technique. Long and Giri (2011) used the ISODATA clustering technique to analyse 61 Landsat imageries from the Global Land Survey to map the spatial distribution and aerial extent of Philippines' mangroves as part of a global assessment of mangrove dynamics. The report analysing the statistics indicates that the total area of mangrove forests covered approximately 256,185 hectares (Long & Giri, 2011). Although the accuracy is quite satisfying, the ability to classify between specific vegetation types still needs to be tested. However, ISODATA and network classification methods were applied in another project that used airborne sensor data to map the shallow *Posidoniaoceanica* meadows in coastal areas of Italy. Scientists found that ISODATA classification of airborne images was generally more accurate (81-85%) than that of the aero photogrammetric image (79%) (Calvo, Ciruolo, & Loggia, 2003). Additionally, they indicated that apart from the classification method, the quality of data and the condition of the research site are other key points to affecting classification accuracy. Shen et al. (2009) proposed a study in the area using innovative methodology. They generated a vegetation map for pixels corresponding to vegetative areas, using the ISODATA classification method. Then they applied morphological operations to the clustered images to smooth the boundaries between clusters and fill the holes inside clusters. Finally they classified the resulting clusters as vegetation and non-vegetation types (Shen, Li, Mantena, & Jakkula, 2009). This paper introduces a novel method that alters vegetation colours in the satellite imagery to simulate seasonal changes. It also indicates that ISODATA, as basic classification algorithms, can be combined with other techniques to build a new, practical, remote sensing method.

K-mean.

K-mean is another widely used and simple unsupervised classification algorithm. In this algorithm, all the subjects need to be represented as a set of numerical features. The K-mean algorithm is different from the ISODATA algorithms. To be specific, ISODATA dynamically adjusts cluster numbers, while K-mean assumes that the number of clusters is fixed and is known *a priori* (Shen et al., 2009).

A study conducted by Baldeck and Asner (2013) estimated the vegetation beta diversity by using airborne imagery and a method based on K-mean clustering of crown spectra. The researchers indicated that this proposed unsupervised method can be used to estimate the spatial structure of species' turnover in a landscape when training data are unavailable, providing structured information for scientists, and conservation and ecosystem management applications (Baldeck & Asner, 2013).

Using the K-mean classification algorithms, if a large number of variables need to be analysed, the K-mean will be computationally faster and provide tighter clusters than small number of variables. However, K-mean has problems when clusters are of differing sizes, densities and non-regular shapes. Problems also arise with outliers and empty clusters.

2.7.2 Supervised classification.

Maximum likelihood.

The maximum likelihood classification (MLC) is one of the most widely used remote sensing classification algorithms. MLC calculates a probability function from the inputs for classes established from training sites based on statistics. Lewis et al. (2013) evaluated the cost-effectiveness of seven approaches, including the maximum likelihood method, to map vegetation communities in a north Australian tropical savannah environment. In their paper, two MLC methods, pixel-based image classification and pixel-based integrated classification, were examined and applied to the Landsat5 TM and SPOT5 image datasets using the ENVI software. Finally the classification results were smoothed using a majority filter. The overall accuracy shows that the image only pixel-based approach applied to Landsat5 TM, has the lowest accuracy of 28% when used without ground truth data (Lewis, Phinn, & Arroyo, 2013). Another study conducted by Alatorre et al. (2011) used the maximum likelihood algorithm to acquire a spectral distance map of vegetation signature characteristics of mangrove areas to identify the mangrove and non-mangrove regions in the Gulf of California in north western Mexico. In this paper, field observations and training samples were used to establish thematic categories, as well as to select training areas for each category. The MLC algorithm analyses the average characteristics of the spectral signature of each category and the covariance among all categories, hence allowing for identification of the categories (Alatorre, Sánchez-Andrés, Cirujano, Beguerá, & Sánchez-Carrillo, 2011).

The obvious advantage of maximum likelihood classification is that it takes the variability of the classes into account by using the covariance matrix. However, the classification will over

classify classes with large spectral variability, and the MLC is very processing intensive, and hence extremely slow (Mackay, n.d.).

Minimum distance.

Minimum distance is another widely used supervised classification algorithm which classifies an unknown pixel to a class depending on its proximity to a class mean vector, which minimizes the distance between the image data and the class.

In 1992, scientists had already conducted satellite remote sensing classification study using the minimum distance method. Imageries acquired from the Indian Remote Sensing Satellite were analysed and the green band, in addition to the infrared band, was used for classification. The remotely sensed data were segmented into six classes by using the minimum distance method, where the centres are chosen on the basis of spectral knowledge of the corresponding classes (Murthy, Chatterjee, Shankar, & Majumder, 1992).

The advantage of the minimum distance algorithm is that every pixel is assigned to a specific class and it takes little time to compute. However, the disadvantage of this approach is that it does not account for class variability (Mackay, n.d.). The pixels of classes such as urban land cover, which has high variance, perhaps inadequately classified.

2.7.3 Advantages and disadvantages of unsupervised and supervised classification.

The main difference of supervised and unsupervised classification is the understanding and knowledge of the research theme. In other words, which classification will be used is determined by whether you have sufficient and accurate information about the classification theme.

The first advantage of unsupervised classification is that no extensive or specific knowledge is required of the study region. Secondly, most of the analysis is done by the classification algorithm itself, human errors and bias can be minimized. Thirdly, unsupervised classification produces more informed classes, as well as some distinct spectral classes which are present in the data but may not have initially been apparent to the analyst. However, existing disadvantages include: limited control over the menu of classes, together with changes in spectral properties of specific classes over time; and spectral groupings may not correspond to information classes of interest to the analyst (Universiti Kebangsaan Malaysia, n.d.).

For supervised classification, knowledge of the study site is needed for the training data. The advantages are various. Firstly, the analyst has the control of the classification, and processing is tied to specific areas of known identity. Secondly, the problem of matching categories on the final map with field information will not occur either, as the operator can detect errors and often remedy them. However, even though supervised classification is supposed to produce results with higher accuracy, disadvantages also exist. Firstly, the training data and classes are generally based on field identification rather than spectral properties. In addition, training data selected by the analyst may not be representative of the whole condition encountered throughout the image. Also, the collection of training data can be labour intensive and time consuming. Last but not least, the supervised algorithm may constrain the operator to recognize and represent special or unique categories which are not represented in the training data (Universiti Kebangsaan Malaysia, n.d.).

2.7.4 Object-based image analysis classification.

A digital image is constituted of pixels that that couldn't be seen by unaided human eye. Traditional pixel-based analysis relies on the information in each pixel, while object-oriented analysis is based on the information from a group of similar and contiguous pixels, which called object, according to the measurement of spectral properties, colour, size, shape, texture and tone. Relationships among objects are important to object classification and identification. Object-based classification, termed 'object-based image analysis' (OBIA), is thought to be more effective than pixel-based methods when handling high resolution imagery, as the increase of spatial resolution that lead to more variability in the spectral content of individual pixels belonging to the same class. Thus, the issues of increasing complexity of a high resolution scene owing to shadow, changes in vegetation density, and similar spectral signatures of dissimilar features can be addressed by considering groups of pixels as objects (Penn State University, n.d.).

OBIA usually has two main procedures including segmentation and classification. More specifically, groups of pixels that have similar geographical features, such as shade, length as well as topological entities, will be segmented as an object before classifying (Baatz et al., 2004). There are already some existing studies comparing object-oriented classification and pixel-based classification methods; and most of those papers have illustrated that object-oriented techniques have promising and greater potential for high resolution classification than the pixel-based methods (Oruc, Marangoz, & Buyuksalih, 2004; Whiteside & Ahmad, 2005; Willhauck, 2000). Whiteside and Ahmad (2005) aimed to compare the classification

results of an object-oriented classification and a supervised pixel-based classification method for mapping the land coverage in northern Australia. First of all, image data were segmented into two scale level objects by using the software eCognition, according to three parameters including scale, colour and form. Then some specific objects were selected as ground truth data representing different land cover classes. Class rules such as spectral signatures, shape, location and the contextual relationships of objects were developed and used as a basis to classify the image. For accuracy assessment, both object-oriented classification and supervised pixel-based classification were undertaken by using confusion matrices and Kappa statistics (Congalton, 2009). The results indicated that better and more acceptable overall accuracy was provided by object-oriented classification, which has great potential for analysing land cover information from high resolution satellite images (Whiteside & Ahmad, 2005).

2.8 Accuracy Assessment

Effective studies including measurement, mapping, classification and identification, and decision making by using maps always require accurate maps or at least maps of known accuracy. Maps provide much valuable and important information, helping interested parties to measure, manage, monitor the resources, analyse and identify suitable sites for specific use and even plan for future events. In this case, the accuracy of maps has to be known if decisions rely on the maps' information. Reasons for performing accuracy assessments are numerous. Some Geographic Information Systems (GIS) projects are, about decision making based on the information of remote sensing data. In this case, it is critical to know the accuracy of that data, and normally the accuracy is included in the requirement of those mapping projects (Congalton, 2009). When carrying out vegetation classification, accuracy assessments will help the analyst to know which classification algorithm is more accurate, and which classification assessment is most reliable when using reference data collected on the ground or from aerial photographs at, or near the time of, satellite overpass.

Accuracy assessments measure the quality of maps produced from remotely sensed data. The assessment can be cheap or expensive, quick or time consuming, qualitative or quantitative. The final goal is the identification and determination of errors in maps (Congalton, 2009).

2.8.1 Confusion matrix of classification results.

The development of remote sensing accuracy assessment has advanced from qualitative confidence-building assessment to the quantitative evaluation of results dependants on

statistical models (Congalton, 2009; Kyriakidis & Dungan, 2001; Mowrer, 2000). Class-by-class comparisons between the classification images and ground truth information are accomplished through the use of a confusion matrix or an error matrix. Nowadays, the confusion matrix is widely used in evaluation of remote sensing results and has become the best practice standard of evaluation methods. A confusion matrix is used to calculate the accuracy of a classification result by comparing the classification with ground truth or reference data, which can identify the nature of classification errors and their quantities. The ground truth information includes ground truth imagery, which can include higher resolution satellite image, or maps derived from aerial photo interpretation and ground truth of the region of interest (ROI). ENVI software can calculate the confusion matrix with either ground truth images or ROI, and comprehensive results are reported.

2.8.2 Evaluation of the confusion matrix.

Actually, the measure of overall classification accuracy derived from the confusion matrix table does not show the quality of the individual. So, in addition the full assessment will report some other information which is calculated for the confusion matrix, including the overall accuracy, kappa coefficient, confusion matrix, producer accuracy and user accuracy. This additional information is described in the following sub-sections.

Overall accuracy.

The overall accuracy is the summing all the correctly classified pixels and dividing by the total number of pixels. The pixels of each class will be analysed and defined by the ground truth information and the number of them will be listed in the confusion matrix table. Finally, the total number of pixels is the sum of all the pixels in all ground truth classes (Exelis Visual Information Solutions, n.d.).

Kappa coefficient.

The kappa coefficient is another algorithm to calculate the accuracy of the classification. It measures the proportional improvement by the classifier over random assignment of classes (Exelis Visual Information Solutions, 2009).

Confusion matrix.

The confusion matrix is calculated by comparing the location and class of the pixels on the classification image with the pixels on the ground truth image. Each confusion matrix column means one class and the values in the column represent the labelling of the ground truth pixels (Exelis Visual Information Solutions, n.d.).

Producer accuracy and user accuracy.

The drawback of the overall accuracy measurement is that it doesn't indicate how well individual classes are classified. So the use of producer and user accuracy is to determine the class accuracy. The producer accuracy represents the probability that the classification algorithm identifies the land-cover type of an area correctly, while the user accuracy refers to the probability that a pixel which is labelled as a members of a specific class in the image is really in this class.

The results of the above accuracy evaluation provide information on how accurate the overall classification is and how correct the classification of each individual class is, on the basis of using the confusion matrix table.

2.8.3 Important considerations for the confusion matrix.

When applying a confusion matrix for accuracy assessment, it is inevitable to have some interferences and bias within the whole assessment. The bias of the confusion matrix can be both conservative and optimistic; the magnitude and direction of bias depends on the methods of classification and ground truth data sampling. It is impossible to measure the true class of each pixel perfectly, which means that the accuracy of classification cannot be one hundred per cent correct.

Conservative bias.

There are three main sources of conservative bias; namely errors in ground truth data, positional errors, and minimum mapping units for the reference grids.

When importing the ground truth data to the classification and accuracy assessment, we always assume that the ground truth data are perfectly correct. But things are different if there are any errors within the ground truth data such as incorrect class identification, change in land cover from time to time, and factual mistakes in data recording or processing, amongst others. As a result, some of the correctly classified pixels may be incorrectly assessed as being misclassified. Another concern is about the positional errors. It is impossible to ensure the correct geo-location of any pixels, because the rectification of images always causes positional errors, which are inherent features of any rectified image. Thus, some correctly classified pixels may not be correctly located during the field sampling while using the GPS device. The problem of positional errors will result in a conservative measurement of classification accuracy. Aerial imagery can be interpreted as a substitute for field collection of reference data and can be visually interpreted as polygons; while the minimum mapping

unit area used in the interpretation can lead to conservative results of accuracy assessment. It was illustrated by Verbyla and Hammond (1995) that if a large minimum mapping unit is used or the image is spatially heterogeneous in terms of classes, the conservative bias of a minimum mapping unit area can be greater than 50% and even more (Verbyla & Hammond, n.d.; Verbyla & Hammond, 1995).

Optimistic bias.

At least three optimistic biases will result in high classification accuracy even though the classification result is poor, including the use of training data for accuracy assessment, independent sampling of training data and reference data, along with sampling from homogeneous groups of pixels.

Due to limited research time, field trip opportunities and funding, it is tempting for researchers to use the training data as ground truth data to minimize the possible cost. This will lead to an optimistic result because the pixels selected for training data are usually from a homogenous area where the surroundings are relatively simple, pure, large and easy for correct classification. Nevertheless, if the image of the actual classification area is a heterogeneous mixture of vegetation types, the classification is probably particularly accurate. Simultaneously, it is optimistically biased and imprecise to use the training data for both model development and model validation (Verbyla & Hammond, n.d.). For instance, Verbyla (1986) developed a classifier on the basis of nonsense random numbers data, which unexpectedly had a 95% accuracy classification result. Furthermore, if the reference data are not independent of the training data, it will result in an optimistic estimate of classification accuracy, but some researchers carry out these two things simultaneously. The choice of the area for training data is often that the site is spectrally pure and therefore relatively easy to classify. The area of reference data will be correctly and easily classified if it is close to the area of the training data. Moreover, if the sample site of the reference data is restricted around the centre of homogeneous groups of pixels, the classification accuracy could be much higher than the actual accuracy achievable with real experimental data (Verbyla & Hammond, n.d.).

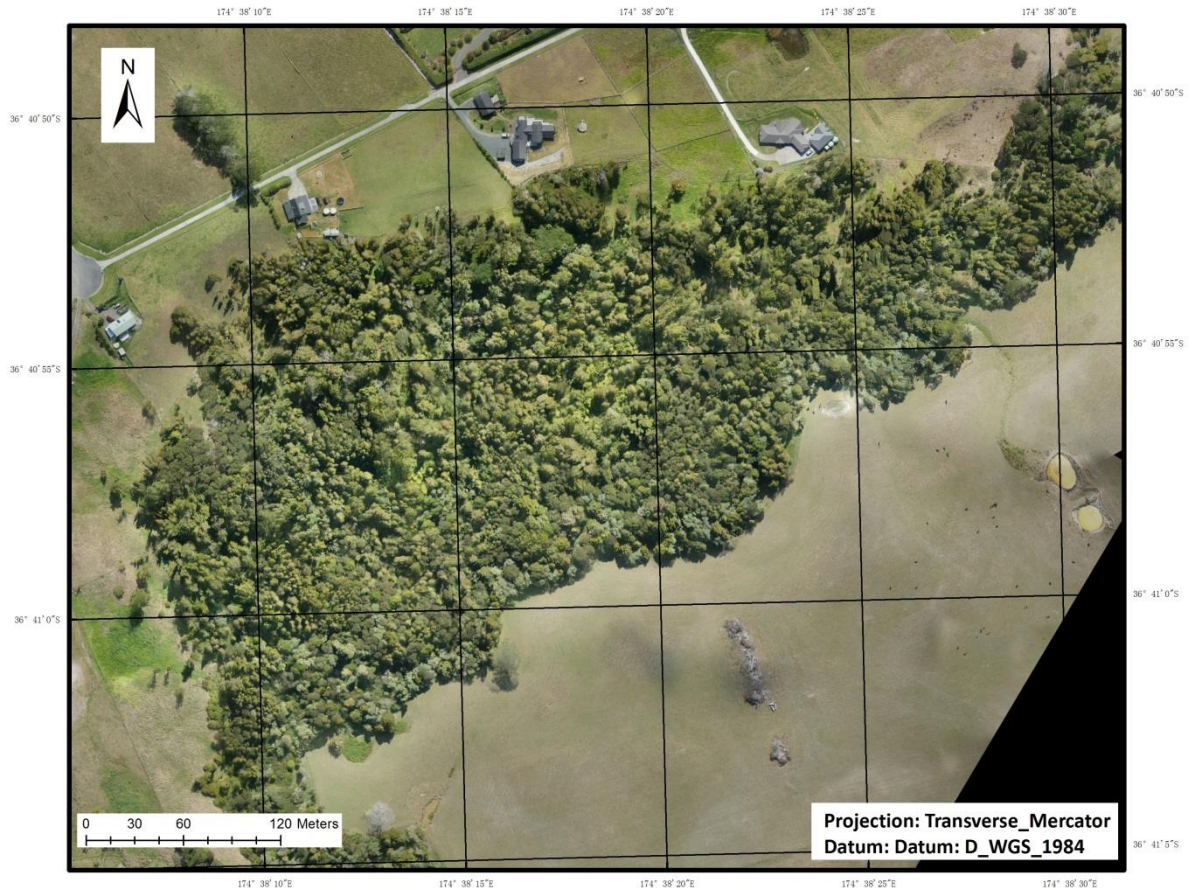
Good assessment of the accuracy of a project could result in several justifications for not doing it, including that it is time consuming, cost and requires more human resource. However, simply reporting the accuracy and confusion matrix results is not enough. The confusion matrix is practically meaningless unless methods are reported in sufficient detail to

enable readers to assess the potential for bias in the classification accuracy measurement (Verbyla & Hammond, n.d.).

3 Materials and Method

3.1 Study Site

The study area was a regrowth bush area at Dairy Flat, which is approximately 0.1 km². Specifically, the centre location of the study on GPS coordinates was -36.682472S, 174.637559E; and an area within a 1 km radius was classified.



Produced for AUT Master in Science Thesis by ZhaoXuan Zhang (Hins)

Figure 4. The study site of re-growth bush area.

3.2 Hardware and Software Required for the UAV

3.2.1 Unmanned Aerial Vehicle (UAV) system description.

To complete an UAV flight mission, the relevant equipment is as important as the aircraft. In order to complete complex and multi-purpose UAV flight missions and acquire data or imagery, advanced equipment communicating with the UAV aircraft is required. The aircraft plus the associated equipment comprise the unmanned aerial vehicle system. In my research, the UAV System was designed and developed by the New Zealand Defence Technology Agency (DTA) and Skycam Ltd.

3.2.2 AUT Hawk and Swampfox UAV.

The AUT Hawk and Swampfox UAV were designed as high performance, aerodynamically efficient unmanned aerial vehicles to take advantage of the DTA autopilot system. The Hawk is able to carry a range of high performance still, motion video and FLIR camera sensors (SKYCAM UAV, n.d.-b). For my research, these UAVs carried the Sony NEX5N14Mp camera with NIR, red-edge filters, Sony true colour camera, and Canon vegetation stress camera. Both aircraft used are described in the next sub-sections.

Aircraft.

The Hawk UAV.

The AUT Hawk UAV is 2.2 metres long with a composite materials airframe. The frame's composite materials were carefully selected and laminated using E glass, S glass and Carbon fibre, which is specially designed to decrease drag and improve the performance of aircraft endurance as well as the environmental operating envelope. The airframe is constructed from the DTA-designed production aluminium moulds and the materials are layered and positioned properly to provide maximum strength with minimal weight. Moreover, the Lithium-Ion Polymer battery can provide up to two hours' flight duration; while the speed is up to 100 kph and maximum flight altitude 16,500 feet. The aircraft incorporates a 1200 W electric motor and novel cooling mount as well as the DTA pilot static sensor for measurement of air data which make it possible to fly even in light rain. Positioning of the UAV is achieved by using a combination of GPS and biometric height and distance plotting undertaken by the autopilot. Communication between the Hawk UAV and the Ground Control Station is provided by wireless radio link (Titus, 2007). Some convenient designs and features of the aircraft also make it an excellent UAV; more specifically, the large camera port with the custom moulded transparent cover provides enough space and area for a range of cameras with a clear view. The full span ailerons are applied as flaps to assist the aircraft in take-off, flight and landing. The full tails of the aircraft are also easily removed for transportation and replacement (SKYCAM UAV, n.d.-b).



Figure 5. AUT Hawk UAV.



Figure 6. The Swampfox UAV.

The Swampfox UAV.

The second UAV aircraft, called the Swampfox UAV, was developed by Skycam Ltd., and was also deployed in this study. Using the same autopilot system of the AUT Hawk UAV, the Swampfox UAV is a fully autonomous platform for gathering aerial images which can be easily and safely operated by two people. The aircraft and Ground Control Station can be broken down quickly and stored in two cases. The main difference between the Swampfox UAV and Hawk UAV is that the former has the capability to carry two sensors simultaneously when undertaking flight missions. By using the Swampfox UAV, multiple-spectral imagery without the temporal variance can be acquired by the two sensors that are equipped in the Swampfox's large sensor bay (SKYCAM UAV, n.d.-c). In this study, the Canon vegetation stress camera and Sony near-infrared camera, along with the Sony true colour camera were equipped at different flights to acquire imagery for the purpose of calculating the normalised difference vegetation index value. AUT did not acquire the Swampfox UAV until the end of my thesis study (February 2014), therefore only one mission was flown with multiple sensors.

Sensors.

Sony NEX-5 Near-infrared and True Colour Camera.

Two Sony NEX series cameras were used in this research as the CMOS sensors to capture UAV imagery because of its high quality and outstanding performance as well as the ability and convenience to be customised. More importantly, this camera can be separated into several components including battery, viewing screen and other non-crucial components unnecessary for undertaking the imagery acquisition mission. Being able to remove non-crucial components is extremely important because the space within the airframe and the weight is very limited. The cameras were modified by Skycam Ltd. to allow direct trigger access via the autopilot software, log capture rates' change as low as 1.30 fps, and provide a 100% reliable capture of every frame taken, ensuring perfect synchronisation (SKYCAM UAV, n.d.-b).

The HOYA R72 Infrared filter was deployed on the Sony NEX5 in this research. The HOYA R72 filter was designed and mainly used for photography with infrared film, because infrared film is sensitive to ultraviolet rays and the shorter wavelengths of the visible spectrum. It is necessary to filter out all but the infrared rays and this filter passes only infrared rays above 720 nm.

Canon ELPH 300 NDVI vegetation stress camera.

The Canon NDVI vegetation stress camera is a conversion from the original Canon PowerShot ELPHG 300HS 12.1 megapixel digital camera, modified by the LDP LLC Company. It is a 3-Band vegetation stress camera which allows for accurate analysis. Furthermore, it is suitable for remote sensing of vegetation for monitoring and identification. Specifically, the three bands are comprised of the blue channel, which responds to visible blue light from 450 nm to 495 nm; the green channel, which responds to visible green light from 495 nm to 570 nm; and the red channel, which responds to near-infrared from 670 nm to 770 nm. The near-infrared has wavelengths ranging from 750 nm to 1400 nm. Healthy plants have a strong and obvious infrared reflection in the near-infrared region called the 'Red Edge', while the less healthy plants have a decrease in near-infrared reflection. The spectral sensitivity of the Canon vegetation stress camera allows the red channel to precisely capture the near-infrared wavelengths in the specific region that changes the most for plants. If a picture is taken by this camera, healthy plants will appear to have a red tint while the other colours will look fairly normal. Furthermore, the ratio of the near-infrared reflectivity to the visible reflectivity will give information on the plants' health; and discern bodies of water,

barren land, shrubbery, rainforest, mineral locations and more by evaluating the red versus the blue and green channels (LDP LLC, n.d.-b).

For vegetation identification, the information from the three channels can be used in the vegetation index to identify vegetation.

Using the Canon vegetation stress camera, the red channel responds to near infrared wavelengths while the green and blue channels respond to the visible light. The LDP LLC Company improved the original NDVI formula and created the ENDVI for better results. The ENDVI uses the green and red as the reflective channel while the blue is used as the absorption channel, because healthy plants will always respond to both visible green light and near-infrared light. The improved NDVI formula is:

$$ENDVI = \frac{((NIR + GREEN) - (2 * BLUE))}{((NIR + GREEN) + (2 * BLUE))}$$

The ENDVI formula sums the NIR and green channels together for the reflective channel; the blue channel is multiplied by two to compensate for the NIR and green channels being summed together (LDP LLC, n.d.-a).

3.2.3 DTA Ground Control Station.

The DTA Ground Control System is another important part of the unmanned aerial vehicle systems that were used in this study. The Ground Control System used in the study consisted of the hardware, including a tripod with top cross mount to place the case or aircraft on, as well as a portable case, which contained a Panasonic Toughbook CF-31 laptop computer, a free wave data link radio, data link antennae and cables, video receiver and cables, video recorder and video patch panel antenna. (All of the data link equipment were Freewave MM2 series). In case of emergency, a hand held controller was required, along with DTA flight planning software.

Being an advanced and highly integrated system, the Ground Control Station enables people to plan missions, control and command the aircraft in flight and automate or manually control sensors. As a bridge to help people communicate and control the aircraft, the Ground Control Station makes the UAV operations safe and convenient.

The DTA software aims to make the process of controlling and commanding the aircraft simple as well as practical. All UAVs equipped with the DTA autopilot system are

compatible with the software. From the preparation to the termination and landing, the DTA software is an indispensable tool for planning missions, communicating with the host networks and operating the UAV. However, the specific procedure depends on operators' needs. There are several different modes that can be chosen for operating the UAV flight mission including start mode, take off mode, navigation stabilised mode, return mode, partial control mode, and landing mode which makes the flight fully autonomous. During the flight, operators can use point-and-click navigation tool on the map window to control the UAV, or use keystrokes to get specific transects of an area with geo-referenced photos (SKYCAM UAV, n.d.-a). The advanced Ground Control Station allows opportunistic changes during the flight.

3.3 UAV Work Flow

This section describes the work flow that I used to classify vegetation at the Dairy Flat bush area using the UAV. The work flow is illustrated in Figure 7 and shows details from the stage of mission planning, to that of image acquisition, image pre-processing to the end stages of classification and final vegetation maps.

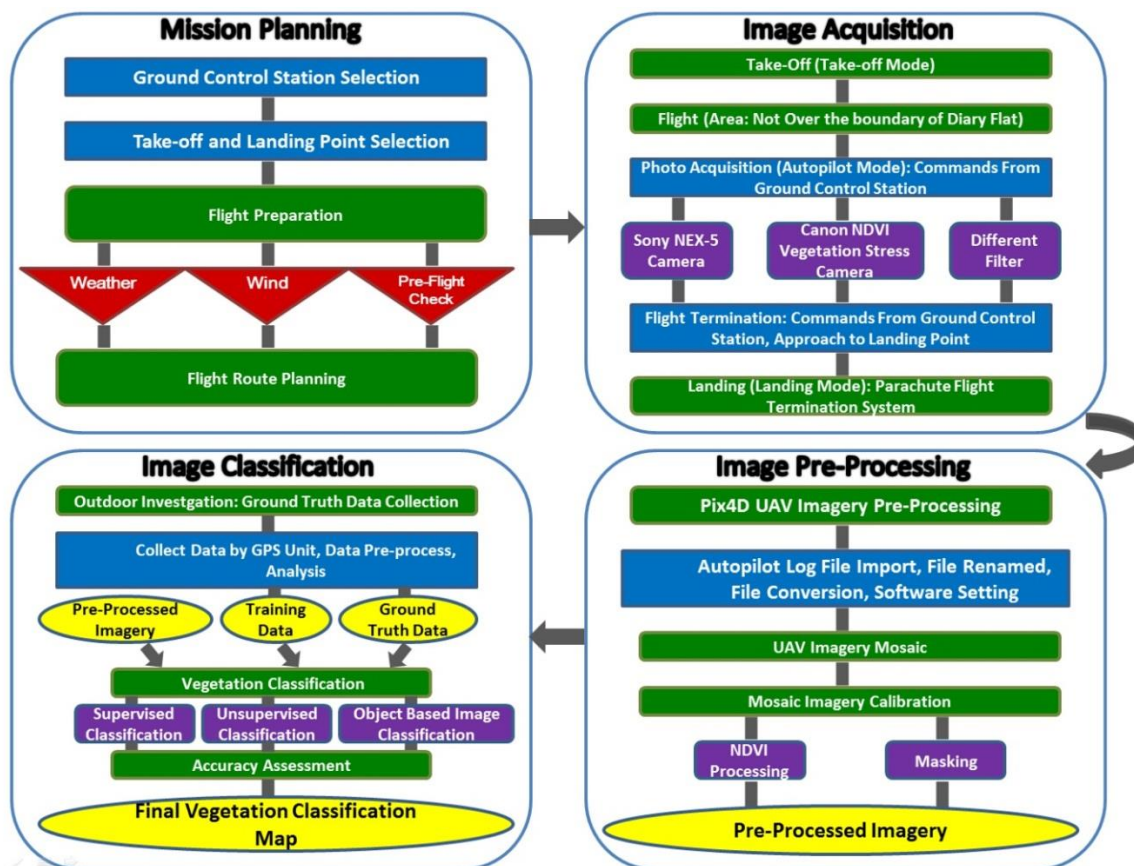


Figure 7. Flow chart of the research procedure for using the Kahu and Swampfox UAVs to map vegetation at the Dairy Flat bush area.

3.3.1 Mission planning.

The flight missions were planned using the DTA software.

Table 1. Details of each UAV Flight Mission

Time	Season	Weather	UAV	Sensors	Image Quantity	Area Coverage
28 July, 2013	Summer	Sunny	AUT Hawk UAV	Sony near-infrared camera	159	35.33 hectares
8 August, 2013	Summer	Cloudy	AUT Hawk UAV	Sony near-infrared camera	470	30.75 hectares
1 April, 2014 (Flight 1)	Winter	Sunny	Swampfox UAV	Sony near-infrared camera	528	27.46 hectares
1 April, 2014 (Flight 2)	Winter	Cloudy	Swampfox UAV	Sony near-infrared camera	668	32.91 hectares
2013	Summer	Sunny	AUT Hawk UAV	Canon Vegetation Stress camera	620	15.67 hectares
2014	Winter	Sunny	Swampfox UAV	Canon Vegetation Stress camera	445	46.48 hectares
8 August, 2013	Summer	Cloudy	AUT Hawk UAV	Sony red edge camera	535	23.24 hectares
1 April, 2014 (Flight 1)	Winter	Cloudy	Swampfox UAV	Sony true colour camera	528	59.68 hectares
1 April, 2014 (Flight 2)	Winter	Sunny	Swampfox UAV	Sony true colour camera	668	67.32 hectares

Mission Time: All of the 7 UAV flights started from 11 am to 2pm; approximately 45 minutes each flight
 UAV: Swampfox equipped with Sony near-infrared and true colour cameras simultaneously on 1 April, 2014 (flight 1 and 2).

Route planning.

According to the flight approval we had from CAA, the flight area of our UAV had to be controlled strictly around the bush area in Diary Flat and could not cross over the nearby motorway. In addition, the post processing software required extensive overlapping of images, therefore flights were planned to take boundaries and image overlap into consideration.

Weather.

Although the Hawk UAV is capable of flying in slight rain, it was not done due to high risk to the sensors and aircraft performance. A Turnigy Mini Anemometer (wind meter) was used to measure wind speed. Wind speed from 0 to 20 km/h was within the safe operation procedures. This standard was strictly followed due to the concerns that strong wind would blow the aircraft from operation area and poor imagery would be taken, thus resulting post

processing mosaics would be compromised. Furthermore, strong winds made the landing much more complicated and uncertain and could lead to equipment damage. All of the weather conditions are presented in Table 1.

Selecting the ground control, take-off and landing points.

Before each flight, the operators set up a take-off / landing point that avoided trees and was on open and flat terrain. In addition, taking-off the UAV required a clear runway so that the take-off point was least 25 meters away from the Ground Control Station.

3.3.2 UAV image acquisition.

Initially, the operator launched the UAV with the Ground Control Station application. Then we navigated the aircraft to the transect using the DTA software and manual point entry. When the entire study area was covered with greater than 85% frontal overlaps and 60% side overlaps of images, the aircraft was recalled to the landing site. For my study site, the entire flight took approximately 45 minutes (see Table 1). In order to acquire images with sufficient overlap (85% frontal overlaps and 60% side overlaps) in a limited time, the time gap between taking each photo was set to 1.5 seconds.

In this project, to acquire the data cover both in winter and summer, the UAV flew four times in summer and three in winter (see Table 1). Imagery was collected between 11am and 2pm on each flight to minimise the influence of shadow on imagery (see Table 1). A total of 9 sets of imagery including the near-infrared, red edge, vegetation stress and true colour were acquired. Due to the conditions of the wind and battery charge length in each flight, roughly 250 to 1100 single images were collected for each flight. Figure 8 shows a typical flight plan and each red dot refers to a photograph taken along the transect.



Figure 8. UAV flight route on 8 August, 2013.

3.3.3 UAV image pre-processing.

The images acquired by the Sony NEX-5N and Canon Vegetation Stress camera were downloaded to a computer for mosaicking. Simultaneously, the flight log file recorded by the UAV was also exported to computer. However, before using the Pix4UAV software to process these files, the log file was transformed and edited due to the requirements of this application. Specifically, the Pix4UAV application can only recognise imagery as a .JPEG file, which means the images from Sony NEX-5N camera need to be transformed from an .ARW file to a .JPEG file. The photos from the Canon vegetation stress camera were generated as a .JPEG file, so these images could be imported to Pix4UAV directly. Additionally, the flight log file, which recorded the flight parameters and geographic information, needed to be edited to a specific layout which is required by the Pix4UAV application.

Pix4UAV image processing.

Mosaic.

The pre-processed data were loaded by the Pix4UAV application for imagery mosaicking. There are three main steps for the whole Pix4UAV mosaic processing; namely data and parameter input, mosaic processing and mosaic image scene edition. Specifically, image names and log files were modified to the format that can only be read by the Pix4UAV software. Images required for mosaicking were selected and the image type was chosen. To

continue, some image properties essential for analysis were edited such as the image coordinate system type, image geo-location and orientation and image camera model. Actually, most of these parameters or information was already recorded in the images' properties by the DTA software and the camera. However, some key information needed to be input manually; for example, the image geo-location and orientation. Such information was extremely important because it decided the position of the each image on the map. If the geo-location information was wrongly matched to each image, the final mosaic image would be incomprehensible.

Image mosaic processing was the second and core step of the whole analysis and it contains three procedures: the initial processing, point cloud densification, and orthomosaic and Digital Surface Model (DSM) generation. The initial processing step computed the true location and parameters of the original images by using the software's advanced Automatic Aerial Triangulation and Bundle Block Adjustment. An initial cloud of 3D points was computed and a low resolution DSM and orthomosaic were generated (Pix4D, n.d.-a). On the processing panel of the software interface, the two options, "Full" and "Rapid" process, were available. The full processing generates the most accurate results while the rapid one reduces the resolution of the images, resulting in lower accuracy and incomplete results. It is a good choice to do a rapid processing before the full processing, because it can provide users with a quick preview of the project reconstruction and serve as an indicator of the validity of the dataset. It allows the users to ensure the quality of the data immediately after its acquisition, to pre-empt avoidable errors being found in the full processing.

The following step was the point cloud densification which increased the density of 3D points of the 3D model and leads to a higher accuracy for both the DSM and the orthomosaic (Pix4D, n.d.-a). In this step, two options were available, the 3D Point Density and High Tolerance option. In addition, there were "High," "Optimal" and "Low" options for the 3D Point Density. Specifically, the "High" option means that a 3D point is computed for every pixel of the original images. The "Optimal" one means a 3D point is computed for every four pixels, while a 3D point will be computed for every 16 pixels of the images for the "Low" option. Computing time and RAM for mosaicking were different depending on the selection of the 3D Point Density option. The "High" option requires four times the time duration and RAM compared to "Optimal"; while the "Low" one computes four times faster and requires less RAM than the "Optimal" option. Given that this research was about vegetation, the "High" tolerance option was selected to process each image mosaic.

The next step was to generate the orthomosaic and DSM. The resolution of the orthomosaic was set to "Auto", thus the default resolution corresponded to the mean Ground Sampling Distance after the initial processing step (Pix4D, n.d.-a).

After the mosaic processing, the scene editor tool was employed because the quality of the mosaic was not satisfactory enough. There were two view modes in the scene editor function, one was the orthoimage view and the other was the elevation view. The former mode showed the mosaic meshes which could be edited. The modifications were displayed immediately after editing. In comparison, the elevation view presented the DSM in grey scale or RGB colour using the altitude values. This was helpful to provide measurement of geometric objects such as point altitudes, height profiles, path lengths, area and volumes (Pix4D, n.d.-a). Sometimes parts of pixels were twisted or distorted after the automatic mosaic procedure due to the lack of image overlaps. This issue was overcome by using the mosaic editing. In this mode, the selected image was edited by changing the projection or adjusting the brightness and contrast of the assigned image. At the same time, it was replaced by all available images appearing on the list. All the changes described above were updated to the scene view and editing panel in real time.

A quality report of the mosaic and the generated files were available in the project file after completing the whole mosaic procedure.

Masking.

Before the classification step, the masking of the bush area mosaic map was created in order to separate the classification area and non-considered area. As the area outside the bush region were mainly grass, farming cows and ponds in the winter data set, it was necessary to separate them from the classification area to ensure the accuracy and quality of the identification. By applying the ArcGIS, a polygon shaped file was created to circle the boundary of the bush area. Then by using the ENVI programme, the shaped file was adopted in creating the masking of the bush area mosaic to distinguish the bush area.

3.3.4 Image classification.

3.3.4a Ground truth data collection.

Ground truth data collecting.

The ground truth data contains two types of information including the GPS point of each individual tree, and the photo of the tree. Considering the accessibility of the whole study

area and safety issues, the collection of GPS data was carried out along the boundary of the bush area. As a result, the ground data were mainly focused on the south part of the bush area along the boundary. Simultaneously, photos of the tree and its leaves or fruits were taken for future identification use.

Training data and ground truth data digitizing and processing.

The field data was divided into training data and ground truth data. Training data was used for supervised classification while the ground truth data was used for accuracy assessment.

The GPS location data was imported to the ArcGIS software and digitized to be the training data. The rest of the field data were digitized to be the ground truth data. Finally, the training data was saved as a .SHAPEFILE file while the ground truth data was save as a .ROI file.

3.3.4b Vegetation classification.

Software.

ENVI.

ENVI is a powerful remotely sensed data processing software developed by Exelis Visual Information Solutions Company using interactive data language (IDL), which is ideal for visualization, analysis and presentation of types of image. This software includes spectral tools, geometric correction, terrain analysis, radar analysis, and raster and vector GIS capabilities. Essential tools required for image processing across multiple disciplines are available in ENVI, which also has the flexibility to allow implementation of customized analysis strategies (Exelis Visual Information Solutions, 2010). The advantages of ENVI have been widely recognized by users as the following: firstly, ENVI is an advanced and reliable imagery analyse tool, which provides a set of intelligent imagery information extraction tools and enhance the value of imagery; secondly, ENVI contains professional spectral analysis. The hyperspectral analysis of ENVI has been in the leading position in the world for years. Thirdly, the basic developed language of IDL enables users to add and expand the function of ENVI in a simple way, even to develop or customize their own professional remote sensing platform. Furthermore, the software includes approaches and algorithms which are the main and popular imagery process procedures. These approaches and algorithms are integrated as workflow tools that help in processing of imagery from the beginning to the end. Since 2007, ENVI has been collaborating with the Environmental Science Research Institute, developed the ArcGIS software. Their cooperation provides the

best solution for the integration of GIS and remote sensing, which also supports a wide range of images from a diverse array of sources (Exelis Visual Information Solutions, 2010).

ArcGIS 10.2.

ArcGIS is a geographic information system software capable of compiling, managing and expanding geographic information developed by Esri. Specifically, ArcGIS includes several tools and functions for Geographical Information Systems (GIS) professionals, location analytics and developers. It can be used for creating maps, geographic data compilation, map information analysis, data management and sharing geographic information; as well as applying geographic information in a range of fields. During the past few years, the cooperation of GIS and remote sensing software has provided new methods and solutions for remote sensing data extraction, analysis, and application. The post treatment and processing of remotely sensed data by ArcGIS after the analysis procedure by remote sensing software enable users to fully understand and apply those data for different purposes.

Pix4UAV.

Pix4UAV is a powerful and unique, automatic, fast speed UAV and aerial data processing software package. This programme can process a large amount of imagery acquired from UAVs, and produce professional and accurate 2D maps and 3D models, as well as DSM. Traditional imagery processing packages require hours of specialized manual labour for UAV data, while Pix4UAV take the UAV remote sensing to the next level by carrying out the whole procedure automatically and simply, achieving centimetre precision and excellent accuracy, which enables the UAV to become the next generation professional surveying tool (UAVPEOPLE, n.d.). Pix4UAV produces orthomosaic and DSM which are readable by GIS software from the raw imagery, and generates a specific quality and accuracy report.

Classification Techniques and Processing.

The ENVI program unsupervised and supervised classification algorithms were employed to identify and classify bush species on the UAV imagery. Unsupervised classification was carried out by using the cluster pixels in a dataset with its original statistical information, while the supervised classification was carried out by selecting regions of interest and using the training data to produce the classification results. The unsupervised and supervised classification techniques are described in the next sub-sections.

Unsupervised Classification.

ISODATA Classification

ISODATA unsupervised classification calculates class means evenly distributed in the data space then iteratively clusters the remaining pixels using minimum distance techniques. This process continues until the number of pixels in each class changes by less than the selected pixel change threshold or the maximum number of iterations is reached (Exelis Visual Information Solutions, 2009). Using this method, the iterative classes are processed and analysed with a threshold setting, which was set to 5% in this project.

K-means Classification

Similar to ISODATA classification, K-means algorithms run in the same way but clusters pixels into nearest class using the minimum distance technique. All the pixels are classified to the nearest class unless a standard deviation or distance threshold is specified (Exelis Visual Information Solutions, 2009). In this research, the number of classes was set to 10 or 11 according to the mosaic map; 10 iterations; and a threshold of 5% in the ENVI program.

Supervised Classification.

Maximum Likelihood Classification

The maximum likelihood algorithm assumes that the statistics for each class in each band are normally distributed and calculates the probability that a given pixel belongs to a specific class. Unless a probability threshold is selected, all pixels are classified and each pixel is assigned to the class that has the highest probability (Exelis Visual Information Solutions, 2009).

Minimum Distance Classification

The minimum distance classification uses the main vectors of each region of interest and calculates the Euclidean distance from each unknown pixel to the mean vector of each class. Some pixels will be unclassified if they are outside of the specified range (Exelis Visual Information Solutions, 2009).

Object-based classification.

The object-based classification is regarded as more suitable for medium to high resolution imagery, which provides an alternative to the traditional pixel-based classification method. The whole procedure of object-based classification can be split into image segmentation and image classification. Once the image data was segmented into objects, these objects were assigned to different classes by running supervised or unsupervised classification, or

according to the users' class rule such as spectrum, shape, colour and contextual relationships. Then these rules would be used as classification criteria (Whiteside & Ahmad, 2005).

Classification processing.

All of the UAV images mosaics were classified with pixel-based and object-based methods using supervised and unsupervised classification. Specifically, the processed mosaic from Pix4UAV software was analysed by pixel-based classification of supervised and unsupervised classification respectively. Supervised classification included the algorithms of maximum likelihood and minimum distance while unsupervised classification included ISODATA and K-mean techniques. Then the UAV images mosaics were processed by the object segmentation tool in ENVI, which generated the object segmentation map. Finally, the object-based map was analysed by the classification methods which are exactly the same with pixel-based classification.

NDVI Value Calculation.

As the images of near-infrared, red edge and true colour sensors contain the band information of near-infrared band and red band, the NDVI value can be calculated by using the equation mentioned in chapter 2. Firstly, the near-infrared and red band was extracted from the original imagery, and then the extracted bands were stacked together to become one individual layer file. Thus, the NDVI value could be calculated from this layer file using the NDVI tool in ENVI. Finally, each pixel of the imagery was assigned to a specific NDVI value to represent the vegetation stress condition. In this case, the NDVI value was applied in classification algorithms to carry out the vegetation classification.

Accuracy assessment.

Classification accuracy was assessed by using the standard confusion matrix approach, which indicates the percentage of correctly and incorrectly mapped observations in binary form. Using the confusion matrix tool from the ENVI programme, the classification results' accuracy was assessed by comparing the results and reference data, including the ground truth data acquired from the research field. Producer and user accuracies of each class were calculated by applying the overall accuracy and Kappa statistics (Congalton, 1991).

Post-classification processing.

Majority analysis.

Classification results were run through the majority analysis for post classification processing. By applying the majority analysis to classification results, any spurious pixels were changed

and replaced with large groupings of classes. More specifically, setting the kernel size as 3 by 3, the centre pixel in the kernel was replaced with the class value of the majority pixels in the kernel. The purpose of the majority analysis is to create smoother classifications for GIS analysis.

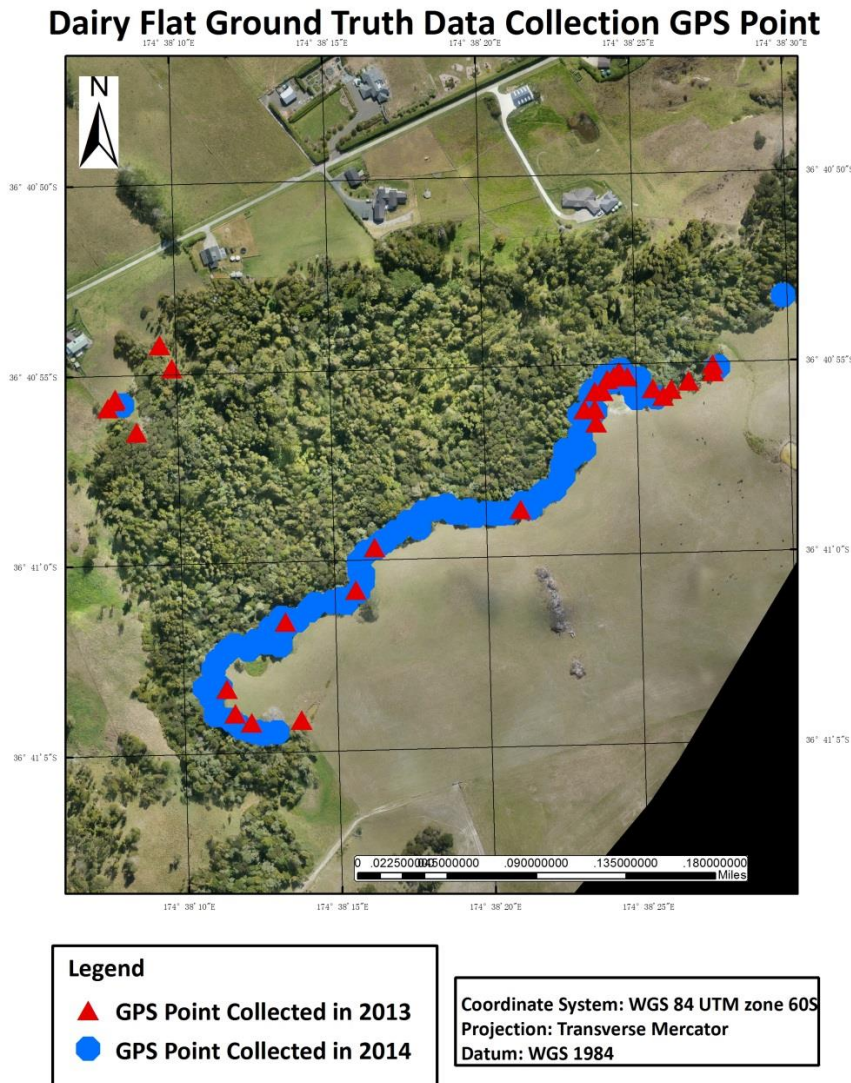
ArcGIS Processing

Once all the classification results were processed by the majority analysis, the data was imported into the ArcGIS software for further processing. Using the map export function, the layout of the results was edited, including the modification of size, style and the presentation of colour style. Finally, the final classification map was produced by the program.

4 Results

4.1 Field Data GPS Location Map

Figure 9 shows the GPS location of all field data collected in 2013 and 2014 respectively.



Produced by ZhaoXuan Zhang (Hins) for AUT Master in Applied Science Thesis

Figure 9. GPS location of field data collection points.

Six field surveys were conducted of this research. The species' names and spatial location data of trees along the boundary of the research area were collected in 2013 and 2014 respectively. While there were many species of trees within this area, only nine species had canopies that were tall enough to be captured by the UAV sensors while in flight. The field data of nine common tree species including Chinese Privet (*Ligustrum sinense*), Totara (*Podocarpus totara*), Kowhai (*Sophora microphylla*), Weeping Mapou (*Myrsine divaricata*),

Kahikatea (*Dacrycarpus dacrydioides*), Kānuka (*Kunzea ericoides*), Rimu (*Dacrydium cupressinum*), Miro (*Prumnopitys ferruginea*), and Kauri (*Agathis australis*) were acquired by using the Garmin Etrex GPS units and digital camera.

4.2 UAV Images Mosaic Map

4.2.1 Mosaic maps of near-infrared images.

One hundred and fifty nine near-infrared images were acquired on 28 July, 2013 and processed by Pix4D software. This image set covered an area of 0.35 km² (35.33 ha) over the bush area. As Figure 10 shows, there were two main problems in this mosaic map.



Produced by ZhaoXuan Zhang (Hins) for AUT Master in Applied Science Thesis

Figure 10. Mosaic map of near-infrared images acquired on 28 July, 2013.

Firstly, the area in the centre of the bush could not be processed and resulted in a blank area because the lack of enough overlaps. Secondly, images acquired from the UAV did not fully cover the bush area, ending with failure to mosaic the north-west boundary.

The quality report from the Pix4UAV software indicated that the average ground sampling distance of this mosaic was 10.74 cm, while the median of 1159 matches per calibrated image

showed good matching quality. The overlapping score indicated that the blank area in Figure 10 has only one overlap and even none.

Quality Check

Images:	median of 4874 keypoints per image	⚠
Dataset:	151 out of 159 images calibrated (94%) and 2 blocks	⚠
Camera optimization quality:	95.92% relative difference between initial and final focal length	⚠
Matching quality:	median of 1159 matches per calibrated image	✓
Georeferencing:	no GCP	⚠

Figure 11. Quality check of near-infrared Mosaic map on 28 July, 2013.

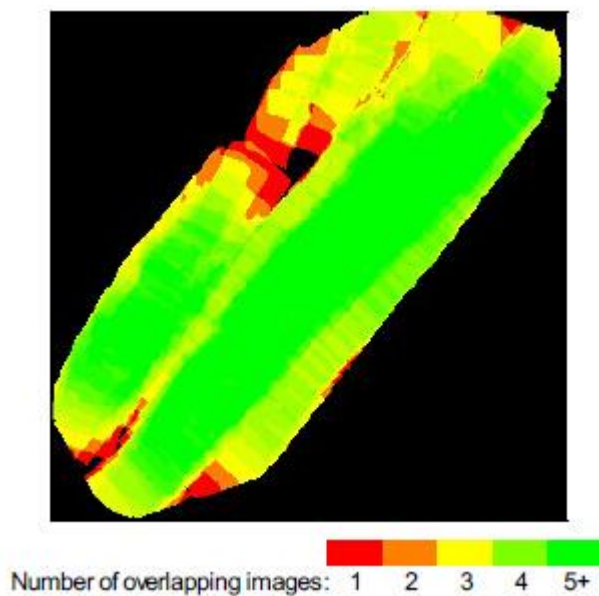
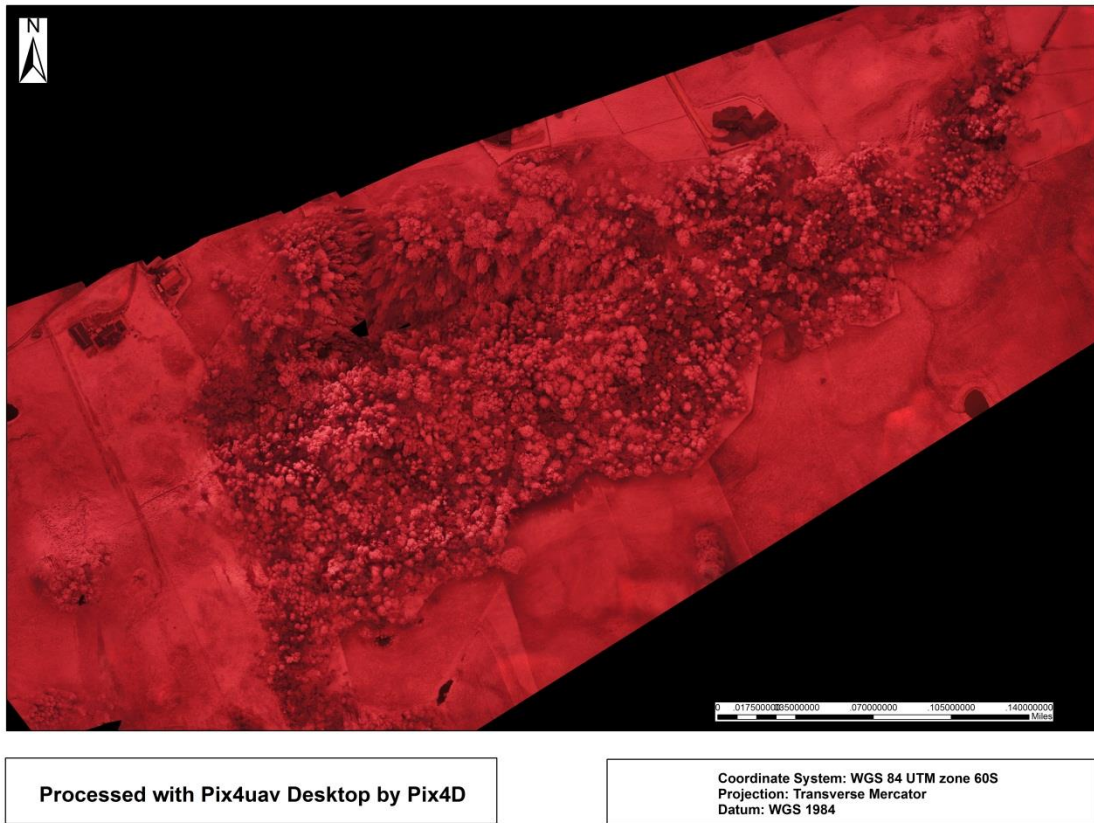


Figure 12. Overlapping level of near-infrared Mosaic map on 28 July, 2013.

On 8 August, 2013, the UAV equipped with the near-infrared camera collected 470 images and covered an area of 0.31 km² (30.75 ha) (refer Figure 13). The ground sampling distance of the mosaic was 9.76 cm.



Produced by ZhaoXuan Zhang (Hins) for AUT Master in Applied Science Thesis

Figure 13. Mosaic map of near-infrared images acquired on 8 August, 2013.

The bush area was fully covered in this flight mission, but the mosaic quality of the north part was not satisfactory. Magnifying, discontinuous and blurry mosaicking occurred because of overlap issues. Moreover, it was a cloudy day on 8 August, 2013, resulting in some small brighter and darker regions due to shadow.

The quality report shown in Figure 14 displays that the mosaic quality is not good enough. All the five quality factors have the second and third evaluated level.

Quality Check

Images:	median of 1355 keypoints per image	⚠
Dataset:	412 out of 470 images calibrated (87%) and 2 blocks	⚠
Camera optimization quality:	92.6% relative difference between initial and final focal length	⚠
Matching quality:	median of 402 matches per calibrated image	⚠
Georeferencing:	no GCP	⚠

Figure 14. Quality check of near-infrared mosaic map on 8 August, 2013.

The overlapping score also indicates that only one to two images overlap in the northern part, which resulted in the final magnifying, discontinuous and blurry mosaic.

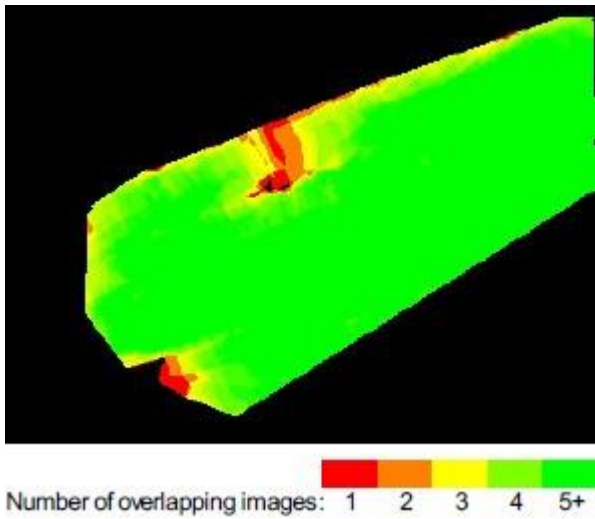
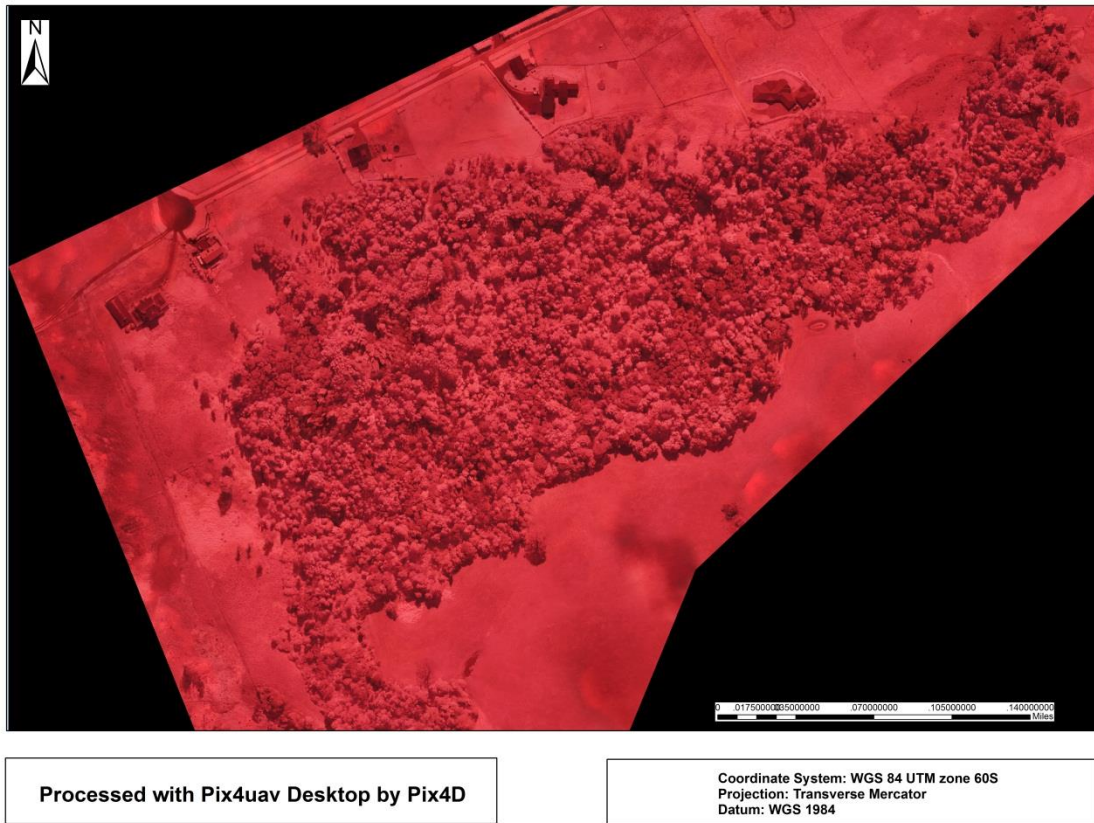


Figure 15. Overlapping level of near-infrared mosaic map on 8 August, 2013.

The second run of data acquisition collected 668 images on 1 April, 2014, and as shown in Figure 16, this is the one with the best quality among all near-infrared mosaicking projects. This mosaic map keeps the integrity of the whole bush region without obvious shadow or blurry or distorted mosaic with a 9.09 cm ground sampling distance. The flight route of the UAV was mainly focused the forest above, therefore we did not get many images of the location near the bush area.



Produced by ZhaoXuan Zhang (Hins) for AUT Master in Applied Science Thesis

Figure 16. Mosaic map of near-infrared images acquired on 1 April, 2014 (Flight 2).

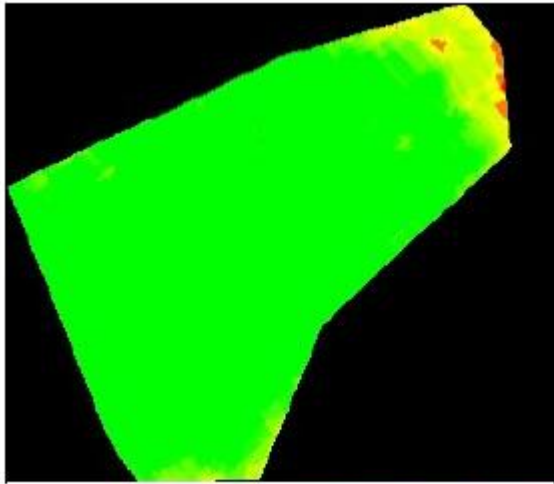
The quality report shown in Figure 17 shows that the mosaic has excellent quality in factors of dataset and matching quality. The differences between focal lengths can be explained as being due to the changing flight altitude because of strong wind.

Quality Check

Images:	median of 4152 keypoints per image	!
Dataset:	665 out of 668 images calibrated (99%)	✓
Camera optimization quality:	104.25% relative difference between initial and final focal length	!
Matching quality:	median of 1012 matches per calibrated image	✓
Georeferencing:	no GCP	!

Figure 17. Quality check of near-infrared mosaic map on 1 April, 2014 (Flight 2).

Moreover, as can be seen from the overlapping score, the mosaic has more than five overlaps of the whole bush area apart from the eastern part.

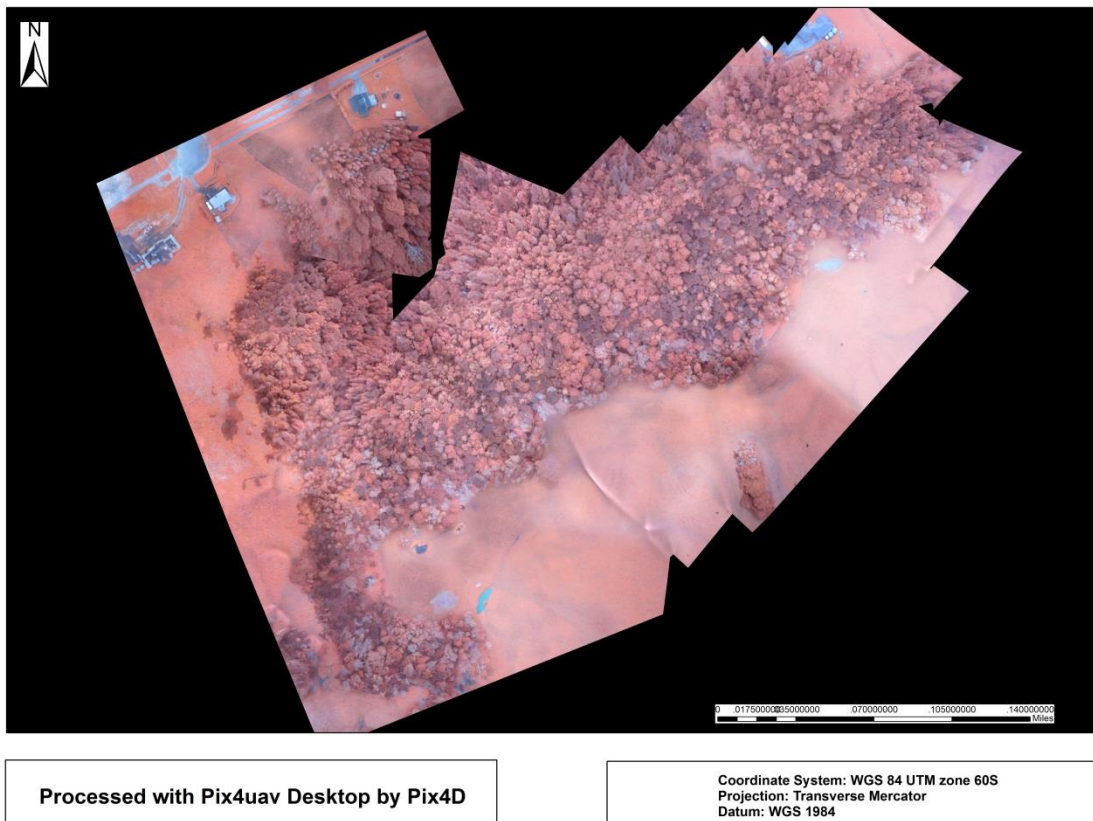


Number of overlapping images: 1 2 3 4 5+

Figure 18. Overlapping level of near-infrared mosaic map on 1 April, 2014 (Flight 2).

4.2.2 Mosaic map of vegetation stress camera images.

Vegetation stress images were generated by the Canon Vegetation Stress Camera in the winter of 2013 by using the AUT Hawk UAV. A total of 620 images were collected, covering an area of 0.16 km² (15.67 ha) (Figure 19) with a 3.9 cm ground sampling distance.



Produced by ZhaoXuan Zhang (Hins) for AUT Master in Applied Science Thesis
 Figure 19. Mosaic map of vegetation stress camera images acquired in 2013.

Although we gained similar quantity of images for this mosaic project to the near-infrared mosaic project on 1 April, 2014, the result wasn't good. Owing to the flight route of the UAV focusing on the centre of the bush area, we didn't get enough overlap images of the north part. This circumstance caused the blank, blurry, magnifying and distorted mosaic of that part.

As shown in Figure 20, the mosaic of vegetation stress images in 2013 has good quality in images and matching quality according to the report. However, only 36% of the images have been calibrated for the mosaic processing.

Quality Check

Images:	median of 1347 keypoints per image	✓
Dataset:	224 out of 620 images calibrated (36%)	⚠
Camera optimization quality:	6.73% relative difference between initial and final focal length	⚠
Matching quality:	median of 120 matches per calibrated image	✓
Georeferencing:	no GCP	⚠

Figure 20. Quality check of vegetation stress mosaic map in 2013.

The overlapping score (Figure 21) shows the blank area in Figure 19 has only one or even no overlap image.

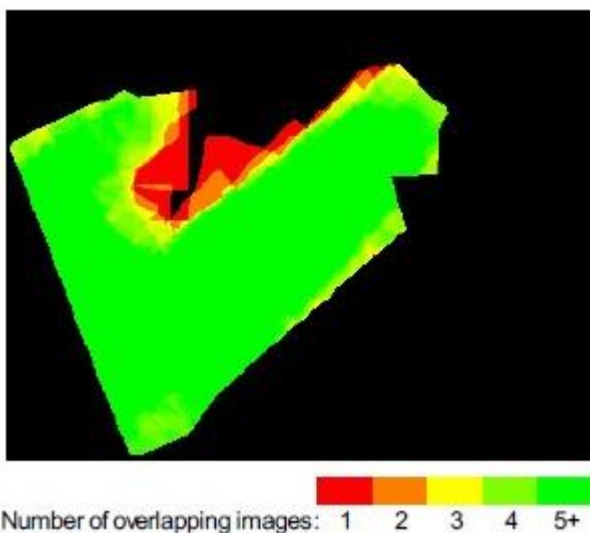
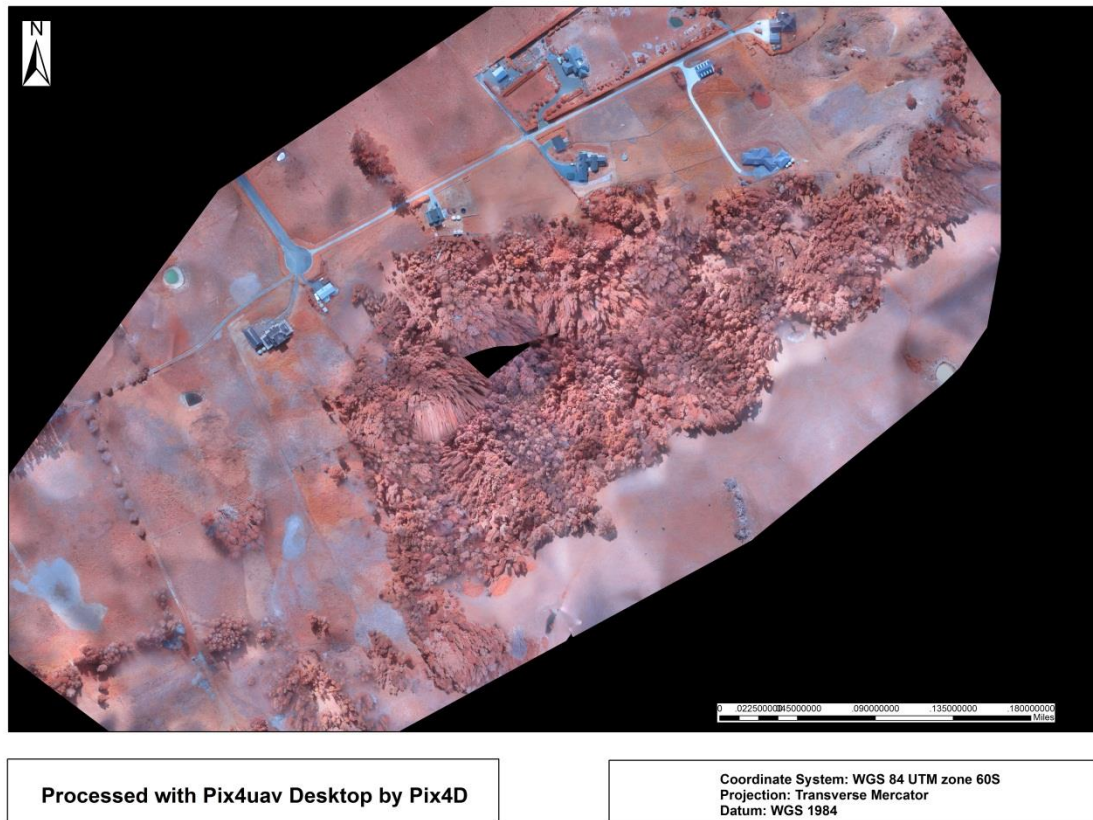


Figure 21. Overlapping level of vegetation stress mosaic map in 2013.

A total of 445 vegetation stress images were collected during February 2014 by the Canon ELPH 300 NDVI Vegetation Stress Camera on board the Swampfox UAV. Between the winter sample in August 2013 and the summer sample in 2014, the three small ponds at the northern boundary of the bush had dried out and were replaced by other plants. Four hundred

and forty five images were acquired for this mosaic project, covering an area of 0.46 km² (46.48 ha) (as shown in Figure 22) with a 3.61 cm ground sampling distance.



Produced by ZhaoXuan Zhang (Hins) for AUT Master in Applied Science Thesis

Figure 22. Mosaic map of vegetation stress camera images acquired in 2014.

The mosaic quality was acceptable except for a small area at the middle of the bush region which was blank, distorted and blurry. Despite the UAV autopilot indicating on the Ground Control Station that we had acceptable overlapping images in the central section, the strong wind (30 kms/hr) pushed the drone from its intended route, and decreased the actual amount of overlap. This resulted in the distortions that are seen in Figure 22.

The quality report (Figure 23) demonstrates that the acquired images are excellent, which have a median of 24,574 key points per image and the matching quality was good.

Quality Check

Images:	median of 24574 keypoints per image	✓
Dataset:	358 out of 445 images calibrated (80%) and 3 blocks	!
Camera optimization quality:	17.94% relative difference between initial and final focal length	!
Matching quality:	median of 1360 matches per calibrated image	✓
Georeferencing:	no GCP	!

Figure 23. Quality check of vegetation stress mosaic map in 2014.

Showing in the overlapping score, the blank, distorted and blurry mosaic in Figure 22 has too few overlaps.

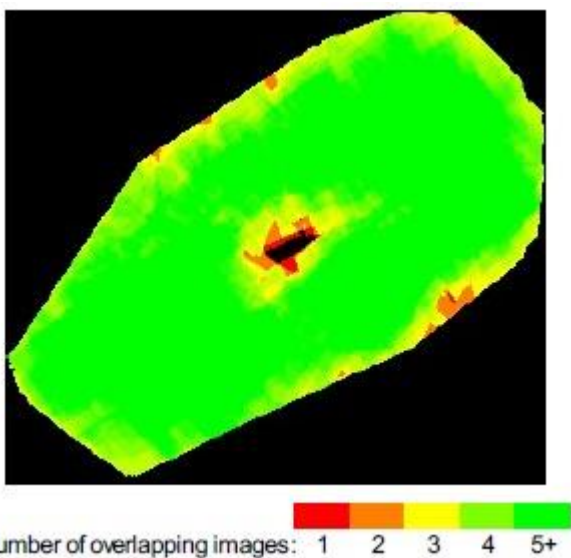
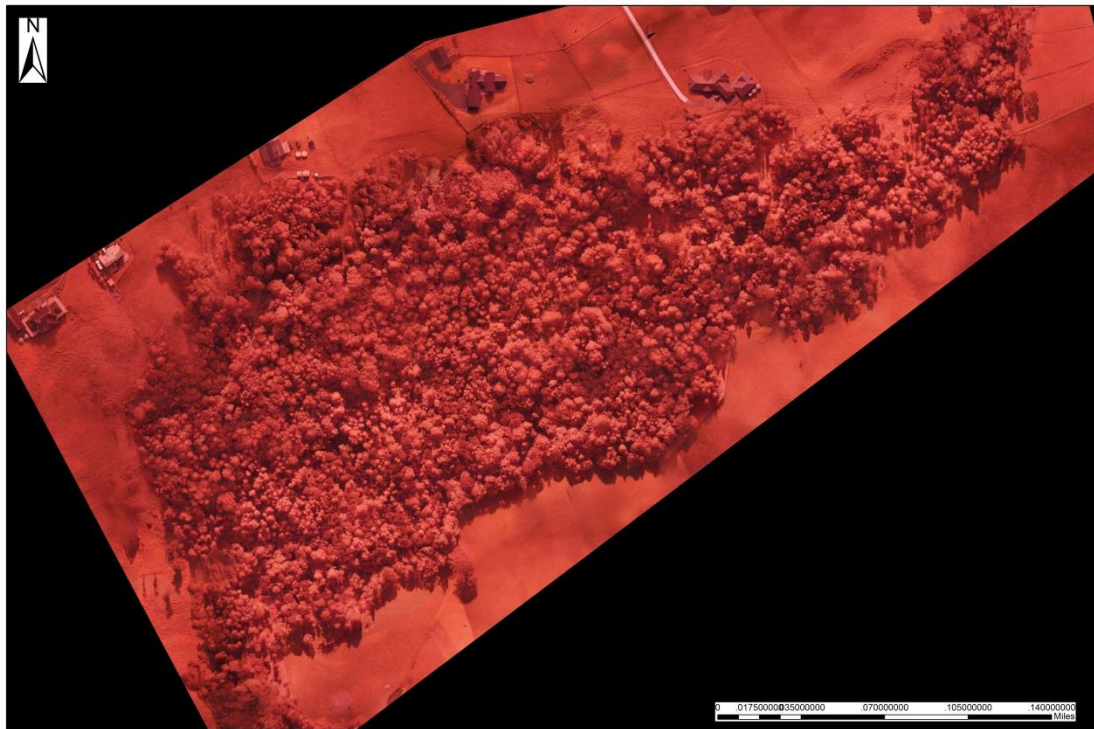


Figure 24. Overlapping level of vegetation stress mosaic map in 2014.

4.2.3 Mosaic map of red edge images.

On 8 August, 2013, two UAV flights equipped with two different sensors including the near-infrared camera and the red edge camera were completed by using the AUT Hawk UAV. Figure 25 is a mosaic of the red edge images and was processed from 535 photos, and covered an area of 0.23 km² (23.24 ha). The photographs had enough overlap and the mosaic quality was satisfied; the mosaic had a 9.59 cm ground sampling distance.



Processed with Pix4uav Desktop by Pix4D

Coordinate System: WGS 84 UTM zone 60S
 Projection: Transverse Mercator
 Datum: WGS 1984

Produced by ZhaoXuan Zhang (Hins) for AUT Master in Applied Science Thesis

Figure 25. Mosaic map of red edge images acquired on 8 August, 2013.

The integrity of the bush area was maintained by the mosaic. However, as shown in Figure 26, this mosaic had only one good performance in the quality check which was the matching quality; while there was a 93.44% relative difference between the initial and final focal length.

Quality Check

Images:	median of 5149 keypoints per image	!
Dataset:	499 out of 535 images calibrated (93%) and 2 blocks	!
Camera optimization quality:	93.44% relative difference between initial and final focal length	!
Matching quality:	median of 1331 matches per calibrated image	✓
Georeferencing:	no GCP	!

Figure 26. Quality check of red edge mosaic map on 8 August, 2013.

The whole bush area had more than five overlapping images from the overlap score (Figure 27), explaining why the integrity of the research site had been maintained.

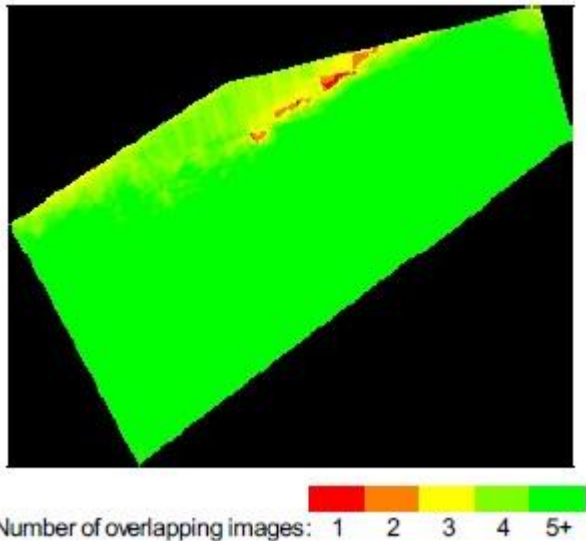


Figure 27. Overlapping level of red edge mosaic map on 8 August, 2013.

4.2.4 Mosaic map of true colour images.

The AUT Swampfox UAV equipped with the Sony NEX5 true colour sensor was used on two flights on 1 April, 2014. As the second flight was started just 15 minutes after the first flight, the weather and sun conditions didn't vary significantly, and as a result didn't affect the mosaic quality. The imagery set of these two flights was merged into one set for the mosaic. A total of 1196 images were used to process this merged true colour mosaic project. The merged mosaic maintained the integrity of the bush area well which covered an area of 0.73 km² (73.03 ha) (as shown in Figure 28) with a 9.58 cm ground sampling distance.



Produced by ZhaoXuan Zhang (Hins) for AUT Master in Applied Science Thesis

Figure 28. Mosaic map of true colour images acquired on 1 April, 2014 (merge Flight 1 and Flight 2).

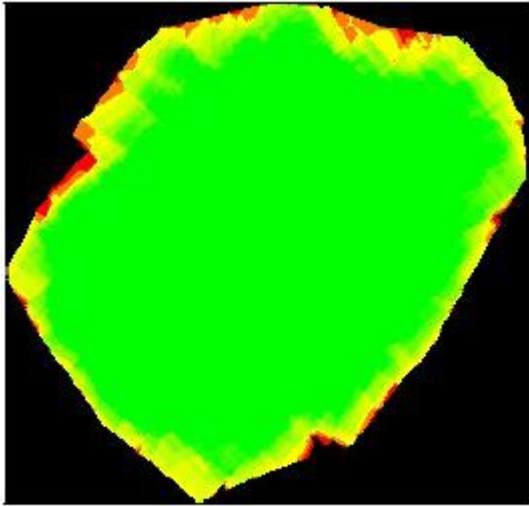
As can be seen from the quality report (Figure 29), the true colour images mosaic had good quality in the dataset and matching factors. But it had a 108.87% relative difference between initial and final focal length due to the combination of two dataset. The flight altitudes of the first and second flight were different, so the focal lengths of the images were different as well.

Quality Check

Images:	median of 6092 keypoints per image	⚠
Dataset:	1195 out of 1196 images calibrated (99%)	✓
Camera optimization quality:	108.87% relative difference between initial and final focal length	⚠
Matching quality:	median of 1797 matches per calibrated image	✓
Georeferencing:	no GCP	⚠

Figure 29. Quality check of true colour mosaic map on 1 April, 2014 (merge Flight 1 and Flight 2).

The whole research site had more than five overlapping images according to the overlaps' evaluation (shown in Figure 30). So the integrity of the bush area was maintained properly.



Number of overlapping images: 1 2 3 4 5+

Figure 30. Overlapping level of true colour mosaic map on 1 April, 2014 (merge Flight 1 and Flight 2).

Additionally, the original quality reports of each mosaic maps are display in Appendix B.

4.3 Pixel-based Unsupervised and Supervised Classification

Pixel-based classification consists of two main steps. The first step is to have a pre-knowledge about the research site and the second step is to run the classification algorithm. For this study, the first step was carried out during the field trips, UAV flights and GPS data collection. During field data collection trips, nine species of trees were targeted within the research area. Together with the class of shadow in the mosaic map, a total of ten classes of ground truth materials were used as training data for the supervised classification. In addition, when doing the unsupervised classification, 10 was the input number of the required classes for the unsupervised classification algorithm.

4.3.1 Unsupervised classification results.

Figures 31 to 37 show the results of the ISODATA and K-mean unsupervised classifications, as well as the comparisons of them to the original mosaic map.

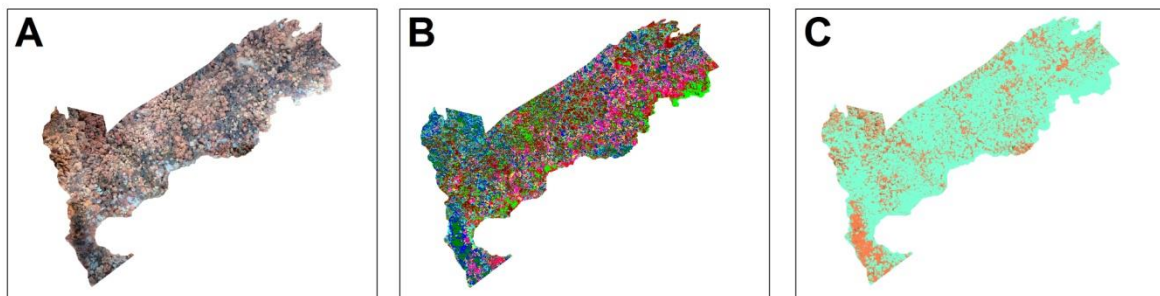


Figure 31. Unsupervised classification of vegetation stress images mosaic in 2013. (A. Original mosaic. B. ISODATA. C. K-mean.).

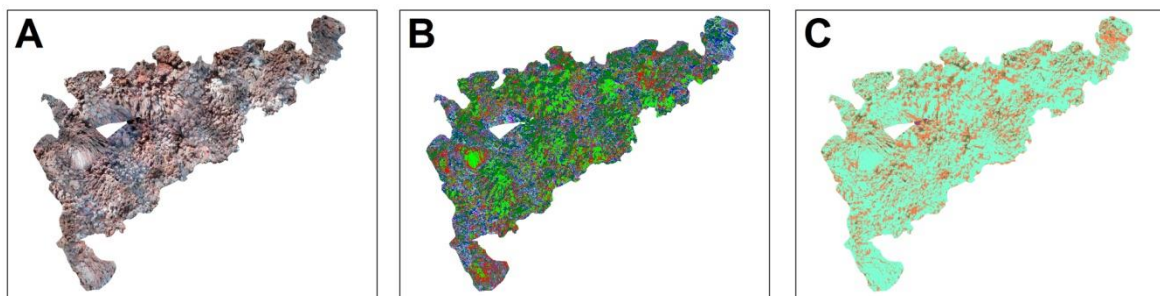


Figure 32. Unsupervised classification of vegetation stress images mosaic in 2014. (A. Original mosaic. B. ISODATA. C. K-mean.).

The two classification maps (Figure 31 and 32) are the results of the vegetation stress images mosaics in 2013 and 2014 respectively. The K-mean algorithm generated very little usable data for further study. The K-mean algorithm classified all the vegetation into three classes,

which turned out to be an unsuitable method for the UAV vegetation stress images classification. In terms of the ISODATA algorithm, nine species were classified in the vegetation stress mosaic in 2013, but the classification split a single tree into several classes. The vegetation stress map of 2014 was mainly classified as four classes by the method.

As seen from the four classification results of near-infrared images mosaic in Figures 33 to 35, the K-mean algorithm failed to classify the vegetation region.

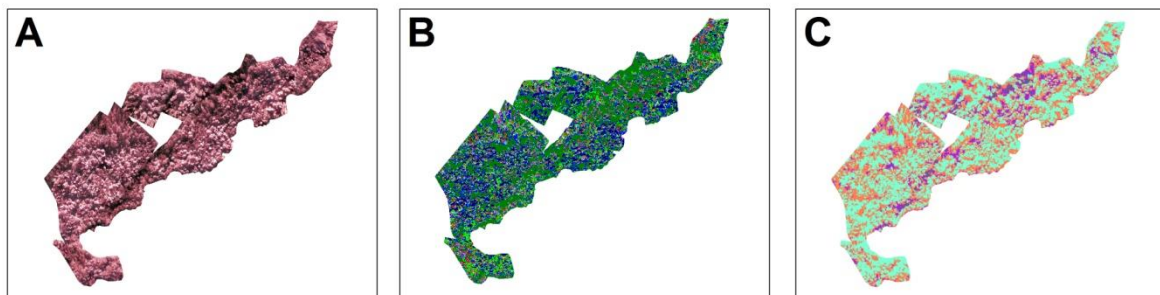


Figure 33. Unsupervised classification of near-infrared images mosaic on 28 July, 2013. (A. Original mosaic. B. ISODATA. C. K-mean.).

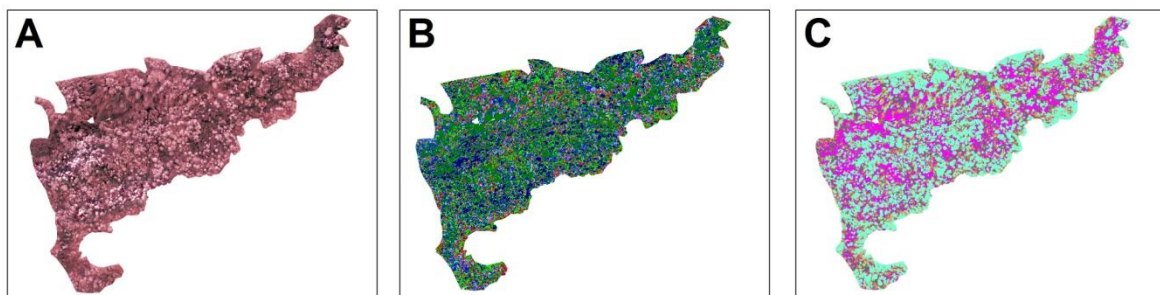


Figure 34. Unsupervised classification of near-infrared images mosaic on 8 August, 2013. (A. Original mosaic. B. ISODATA. C. K-mean.).

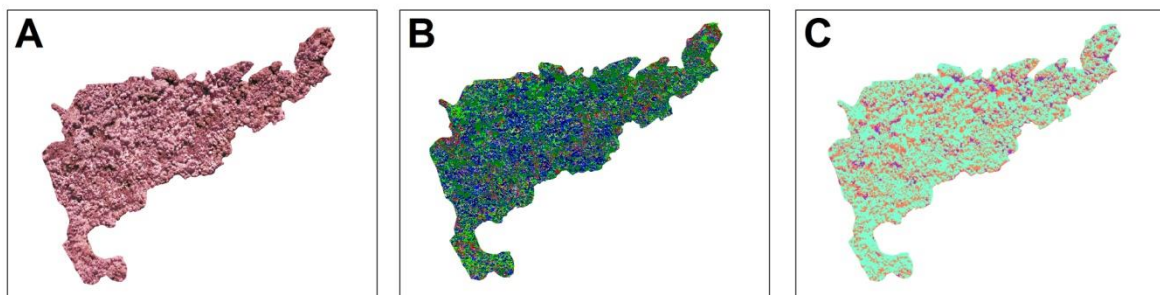


Figure 35. Unsupervised classification of near-infrared images mosaic on 1 April, 2014 (Flight 2). (A. Original mosaic. B. ISODATA. C. K-mean.).

Although ten classes were required during the input, the results produced three main classes. However, the ISODATA algorithm provided slightly better results with green and blue colour standing for shadow and Kowhai (*Sophora microphyll*) respectively, but other classes were presented in concentrated distributions at different sites within the bush area, which failed to reflect the real vegetation distribution.

Figure 36 illustrates the classification result of the red edge images mosaic.

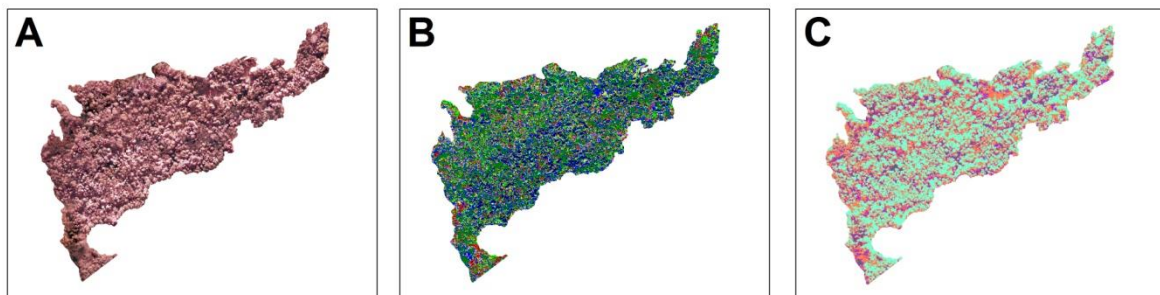


Figure 36. Unsupervised classification of red edge images mosaic on 8 August, 2013. (A. Original mosaic. B. ISODATA. C. K-mean.)

The K-mean algorithm could only distinguish the difference between shadow and vegetation as well as the difference between dark colour vegetation and light colour vegetation. The ISODATA method generated similar classification results as the three near-infrared classification (Figure 33, 34, 35). Furthermore, comparing the red edge classification with Figure 34 (the near-infrared mosaic classification of 8 August, 2013), they produced similar results.

As seen from the classification result of the true colour images mosaic (Figure 37), the ISODATA and K-mean classification produced different results.

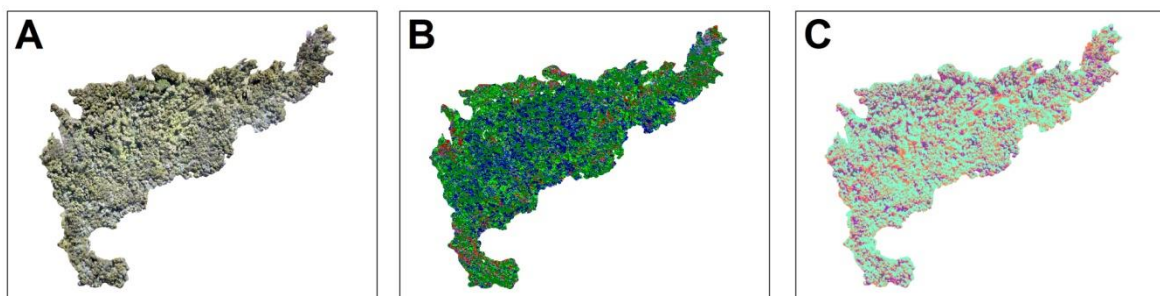


Figure 37. Unsupervised classification of true colour images on 1 April, 2014 merge mosaic. (A. Original mosaic. B. ISODATA. C. K-mean.)

The K-mean algorithm produced similar classifications compared with the results of the near-infrared and vegetation stress images. In comparison, the ISODATA classified the research area mainly as two classes.

4.3.2 Supervised classification results.

The supervised classification involved the digitizing of training data and the subsequent classification. Nine species of trees and the class of shadow areas were selected to represent each input classes.

The species identification of each tree geo-referenced in the training area was then used to classify which class each of the pixels belongs to. In this study, two widely used algorithms of supervised classification were used to process the classification including the maximum likelihood and minimum distance algorithms.

Figures 38 and 39 present the classification results of the vegetation stress images showing significant differences.

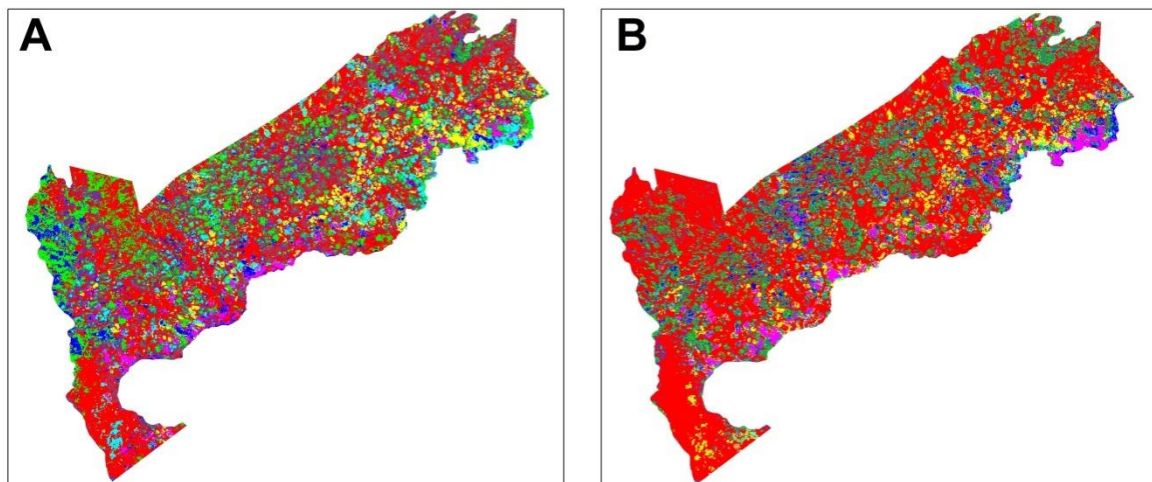


Figure 38. Supervised classification of vegetation stress images mosaic in 2013. (A. Maximum likelihood. B. Minimum distance.).

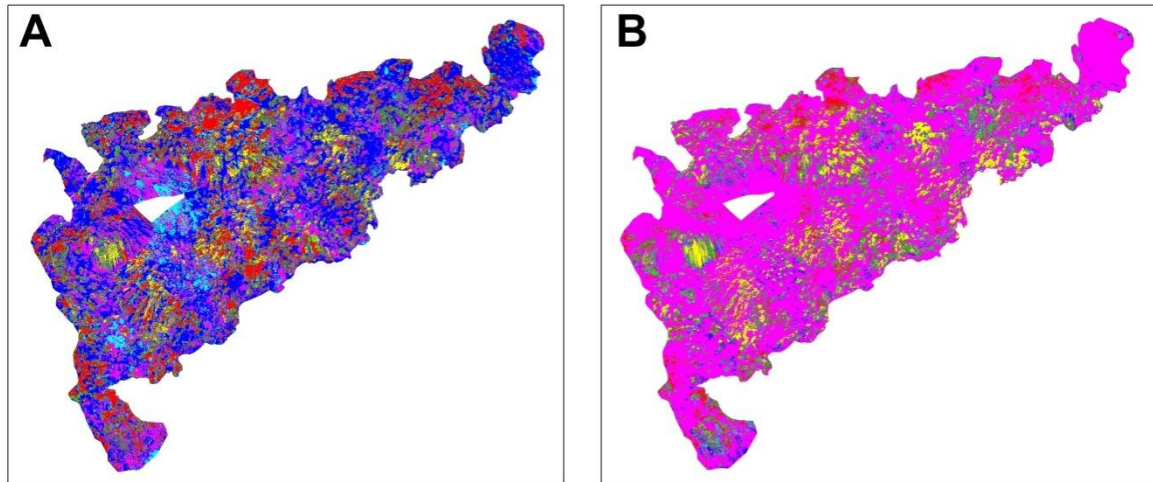


Figure 39. Supervised classification of vegetation stress images mosaic in 2014. (A. Maximum likelihood. B. Minimum distance.).

Specifically, the maximum likelihood algorithm and minimum distance algorithm generated proximate results of the vegetation stress mosaic in 2013. Comparing to maximum likelihood, the minimum distance classified more areas as a red colour, as shown in Figure 38. For vegetation stress images supervised classification, I input nine species of trees as training data, except for the shadow because there was not any obvious shadow that could be identified on the mosaic map. As the red colour stands for Chinese Privet (*Ligustrum sinense*), the minimum distance algorithm misclassified other trees (which were affected by shadow) as the class of Chinese Privet.

In terms of the vegetation stress images' mosaic in 2014, the yellow colour standing for Weeping Mapou (*Myrsine divaricata*) was classified at the same location of both algorithms. However, the minimum distance method classified the rest of the bush area as Kauri (*Agathis australis*) (coloured in pink) while the maximum likelihood method classified the map mainly as the class of Kowhai (blue colour). These two maps show the two supervised classification algorithms produced very different results using the same vegetation stress images' mosaic. Even using the same method, the results of different seasons' vegetation stress mosaics are different as well (the data collection dates were in the winter of 2013 and summer of 2014 respectively).

Figures 40 and 41 display the classification results of near-infrared images acquired in 2013.

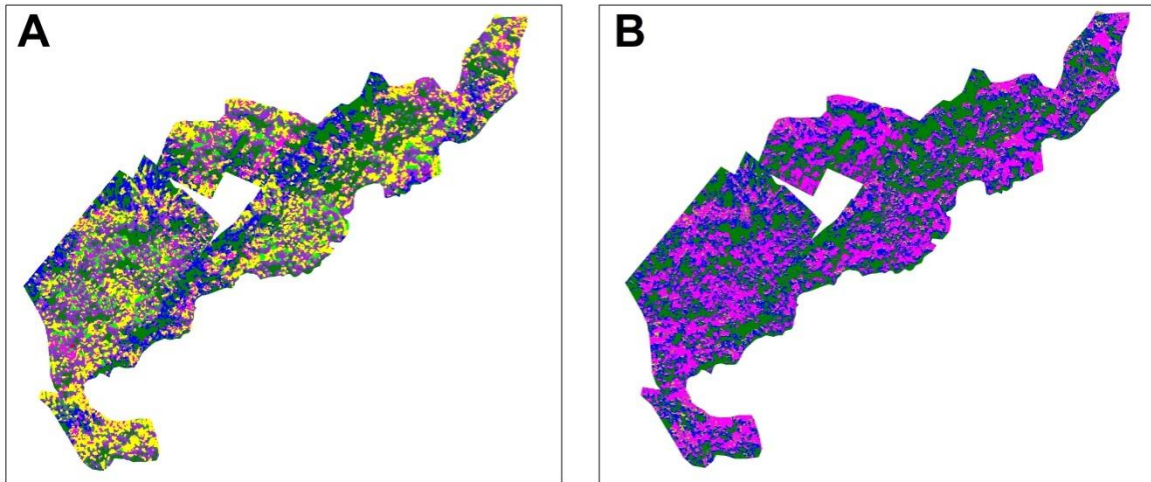


Figure 40. Supervised classification of near-infrared images' mosaic on 28 July, 2013.(A. Maximum likelihood. B. Minimum distance.).

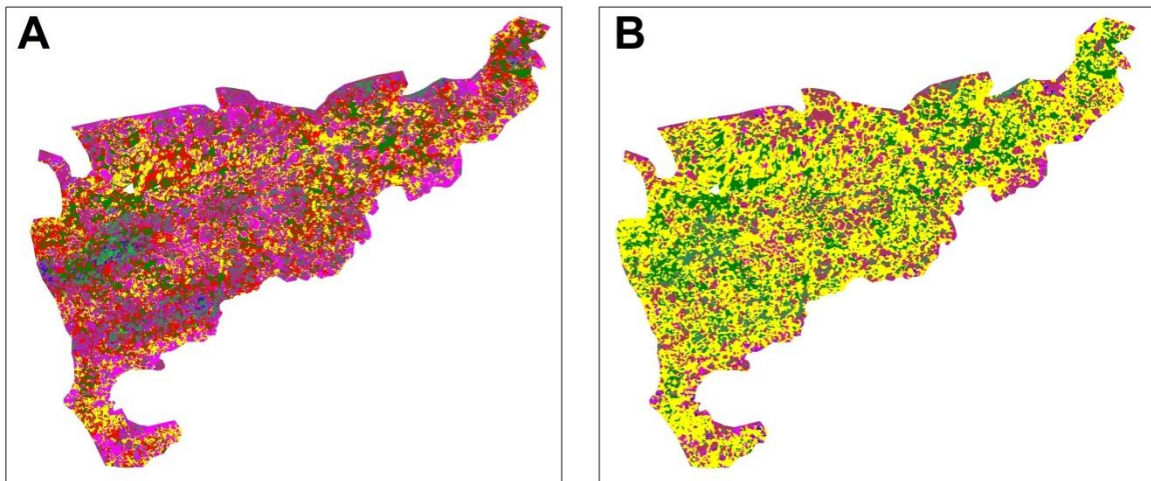


Figure 41. Supervised classification of near-infrared images' mosaic on 8 August, 2013.(A. Maximum likelihood. B. Minimum distance.).

The whole bush area was mainly classified as Weeping Mapou, Kowhai and shadow (yellow, blue and green colour) by the maximum likelihood algorithm as shown in Figure 40, which was unsuccessful in classifying the other vegetation species. Similar to the results of the maximum likelihood technique, the minimum distance classified the whole region into two classes.

The maximum likelihood misclassified most of the trees as Weeping Mapou, Kauri and Chinese Privet (yellow, pink and red), as shown in Figure 41. According to observations from several instances of field data collection, most of the trees along the south boundary are Totara, Kahikatea as well as Kowhai, which means the maximum likelihood produced very low accuracy of classifications. This low accuracy also was echoed in the results of the

minimum distance technique which merely classified the research site as Weeping Mapou and shadow.

Figure 42 presents the supervised classification results of near-infrared images acquired on 1 April, 2014 (flight 2).

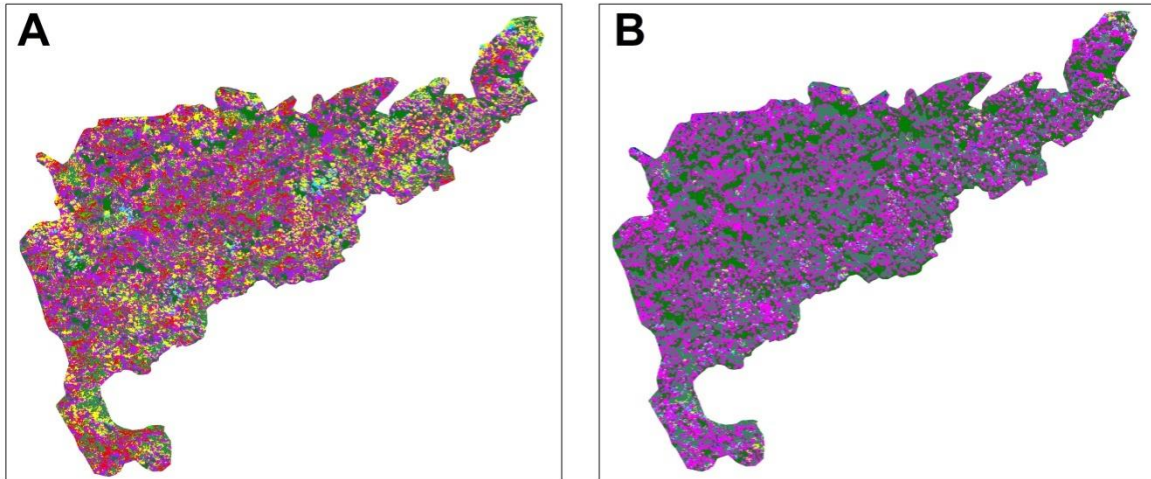


Figure 42. Supervised classification of near-infrared images mosaic on 1 April, 2014 (Flight 2).(A. Maximum likelihood. B. Minimum distance.).

The whole research area was classified as Kauri, Chinese Privet, Weeping Mapou and shadow (purple, red, yellow and green) by the using maximum likelihood algorithm. The result was very different from the classifications of near-infrared images acquired in 2013. However, the result of the minimum distance algorithm was similar to the results shown in Figure 40B.

Figure 43 presents the classification results of the red edge images mosaic.

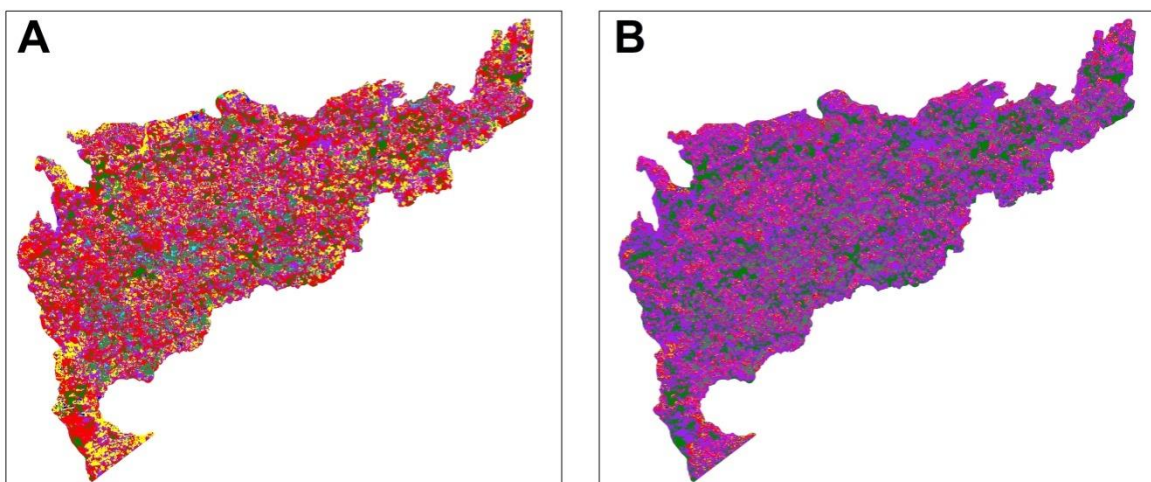


Figure 43. Supervised classification of red edge images mosaic on 8 August, 2013. (A. Maximum likelihood. B. Minimum distance.).

The mosaics shown in Figure 43 provided little usable information for further study, especially those of the minimum distance algorithm. And most of the trees' species were classified as Chinese Privet (red) by the maximum likelihood algorithm.

Figure 44 shows the results of the true colour images acquired on 1 April, 2014.

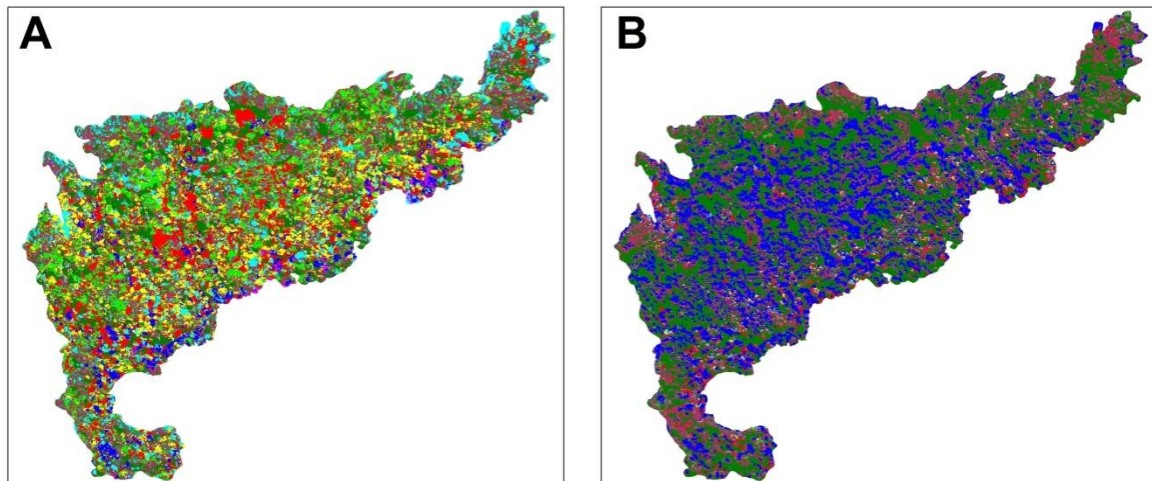


Figure 44. Supervised classification of true colour images on 1 April, 2014 merge mosaic. (A. Maximum likelihood. B. Minimum distance.).

The maximum likelihood technique was excellent in classifying true colour images (shown in Figure 44), which represented the tree species' distribution close to the reality. Especially the classification results of the south part, which were mainly Totara, Kahikatea and Kowhai (light green, light blue and blue). But the results of the minimum distance algorithm failed to classify the vegetation properly.

Overall, from the above seven supervised classifications, we can find that the minimum distance algorithm is not a good choice for creating UAV images mosaics to process pixel-based supervised classification.

4.4 Object-Based Unsupervised and Supervised Classification Results

The first step of object-based classification is to run the object segmentation. Different parameters and algorithms were given and tested in the segmentation procedure including the scale level of segment setting and merge level of merge setting. An appropriate combination of input number was selected to produce excellent segmentation. As expected, the larger scale number of segment setting divides the object into more sub-objects; the larger merge

level setting increases the combinations of adjacent segments with similar spectral attributes. In this research, the value 45 was selected as the segment scale level and 98 was used as the merge level for the object segmentation procedure after numerous attempts.

Figures 45 to 48 show the comparison of before and after the object segmentation of true colour, near-infrared, red edge and vegetation stress images.

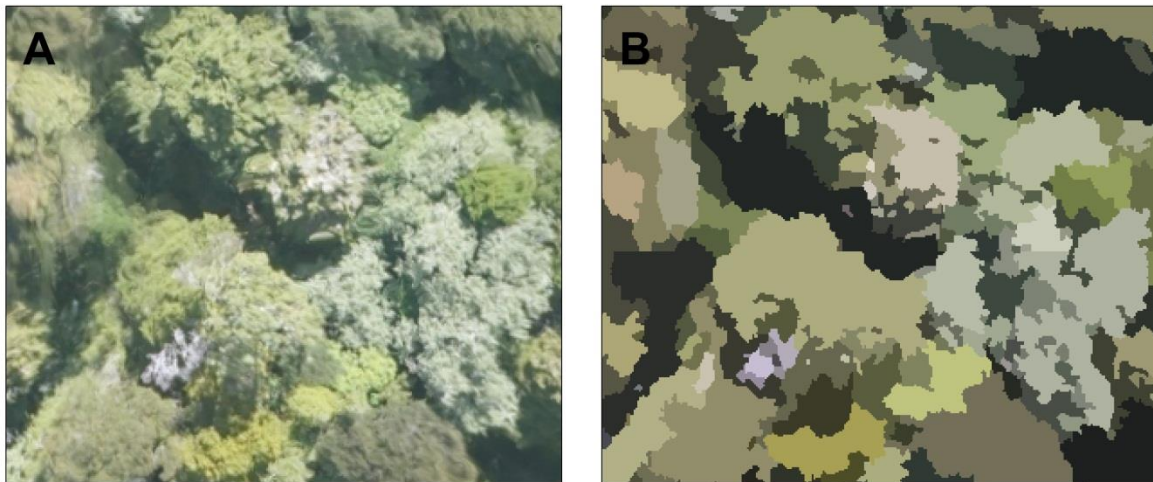


Figure 45. Comparison of true colour images before and after object segmentation. (A. Before. B. After.).

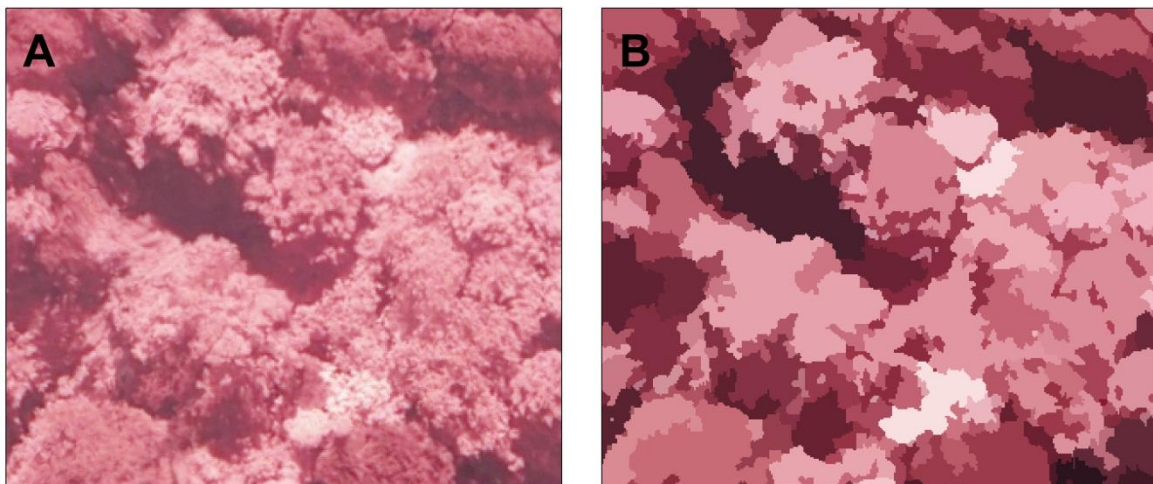


Figure 46. Comparison of near-infrared images before and after object segmentation. (A. Before. B. After.).

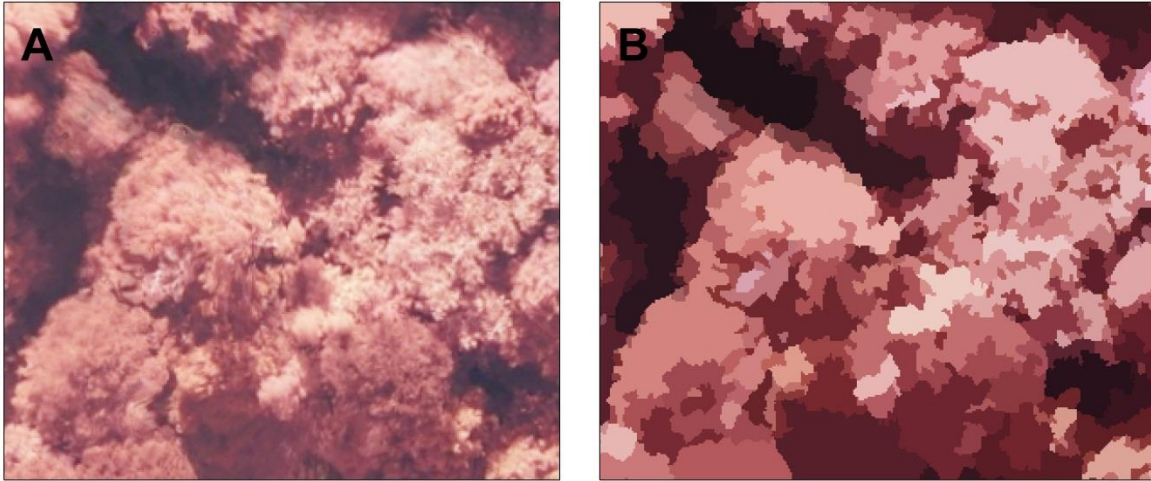


Figure 47. Comparison of red edge images before and after object segmentation.(A. Before. B. After.).

We can see that the majority of trees were accurately segmented as a single object, as shown in Figures 45 to 47. However, some trees which were covered by shadow were segmented as several objects. By processing the object segmentation, the pixels of one single tree would be calculated and assigned the mean value of them, which eliminates the possibility of classifying one species as several classes and increases the classification accuracy. The misclassification frequently occurred at most pixel-based unsupervised classification.

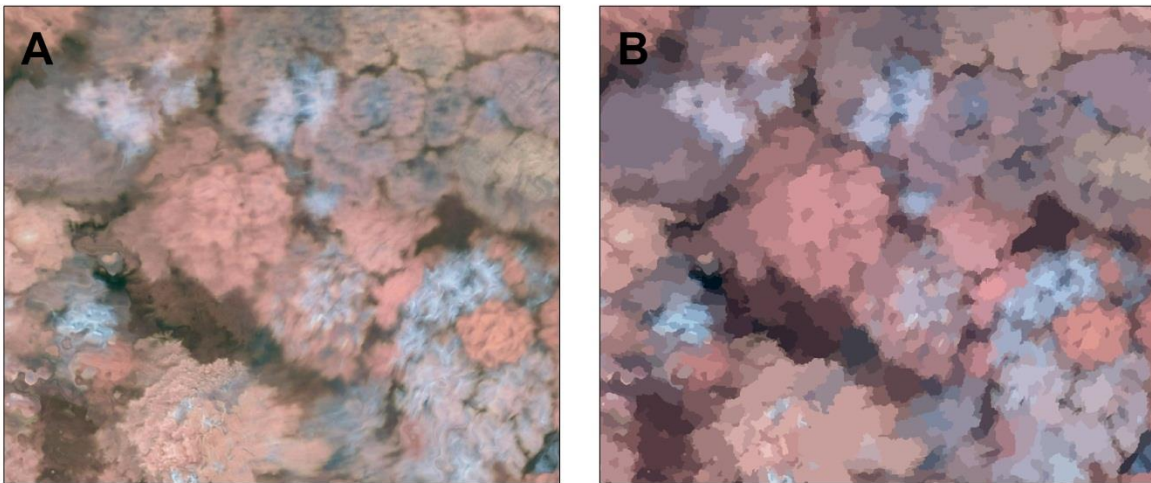


Figure 48. Comparison of vegetation stress images before and after object segmentation. (A. Before. B. After.).

However, the results of the vegetation stress images segmentation was not as good as the other three types of images. As shown in Figure 48, one single tree was segmented as two to three objects, which means a single tree could be possibly distinguished as two to three classes.

4.4.1 Object-based unsupervised classification.

Figures 49 to 55 are the presentations of the results of the object-based unsupervised classification, using the same setting as pixel-based unsupervised classification (Figure 31-37) of each mosaic.

Figures 49 and 50 display the object-based unsupervised classification results of the vegetation stress images in 2013 and 2014 respectively.

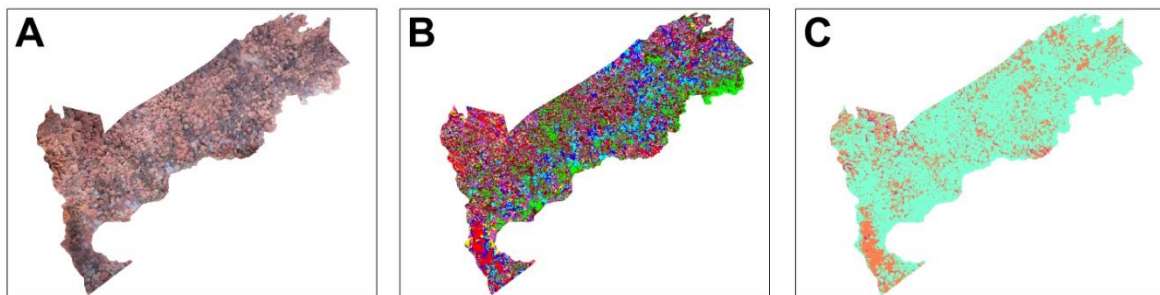


Figure 49. Object-based unsupervised classification of vegetation stress images mosaic in 2013. (A. Original mosaic. B. ISODATA. C. K-mean.).

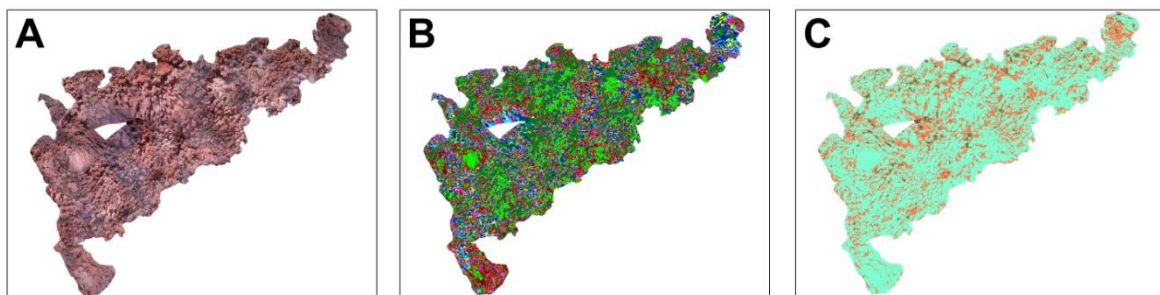


Figure 50. Object-based unsupervised classification of vegetation stress images mosaic in 2014. (A. Original mosaic. B. ISODATA. C. K-mean.).

The K-mean unsupervised classification showed poor results for the vegetation stress mosaic both in 2013 and 2014. In terms of the ISODATA technique, the result of the 2013 mosaic was improved upon in 2014. To be specific, the ISODATA classification results shown in Figure 49 shows each class as a larger object; while the results of the pixel-based classification shown in Figure 31 display small objects, even to a few pixels. Figure 49B shows that the species of Kahikatea (light blue) was well determined at the south part of the bush area, compared to the pixel-based classification. Figure 50 indicates that the results didn't improve greatly. Different classes were displayed as larger groups and were smoother than the pixel-based classification.

The classification results of the near-infrared images are shown in Figures 51 to 53. The results of object-based classification didn't change substantially, compared to the pixel-based classification (Figure 33-35).

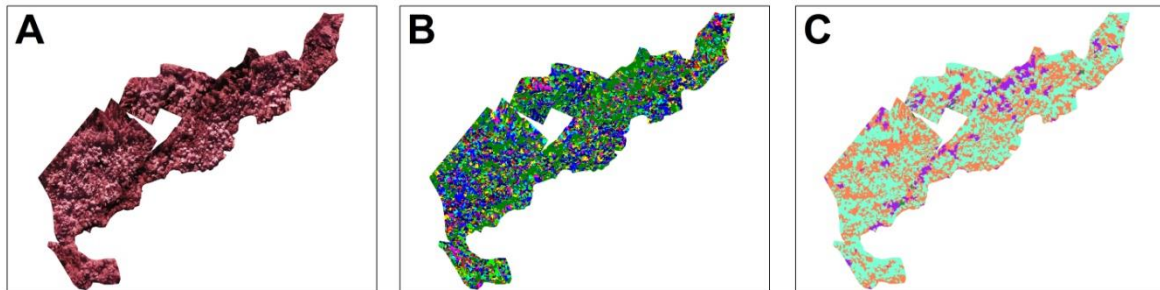


Figure 51. Object-based unsupervised classification of near-infrared images mosaic on 28 July, 2013. (A. Original mosaic. B. ISODATA. C. K-mean.).

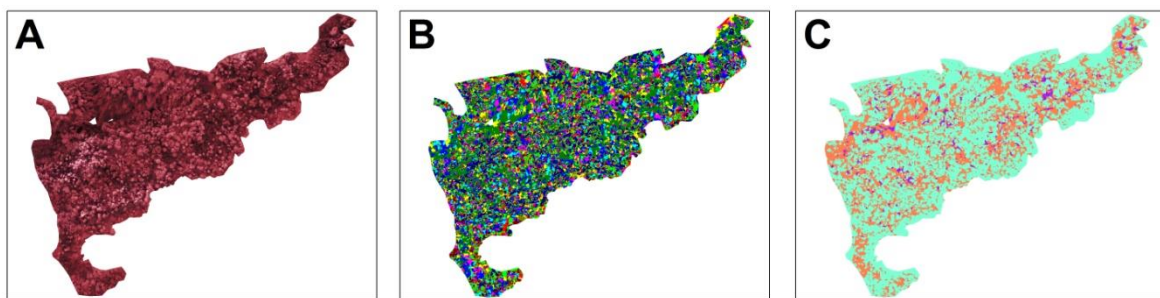


Figure 52. Object-based unsupervised classification of near-infrared images mosaic on 8 August, 2013. (A. Original mosaic. B. ISODATA. C. K-mean.).

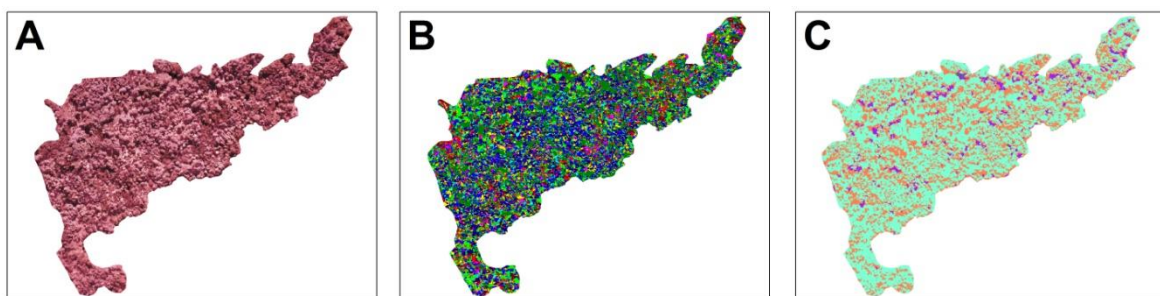


Figure 53. Object-based unsupervised classification of near-infrared images mosaic on 1 April, 2014 (Flight 2).(A. Original mosaic. B. ISODATA. C. K-mean.).

Pixels became smoother, as shown in Figures 51 to 53. The vegetation distributions were the same as the pixel-based classification results seen in Figures 33 to 35.

Figure 54 illustrates the unsupervised classification of red edge images.

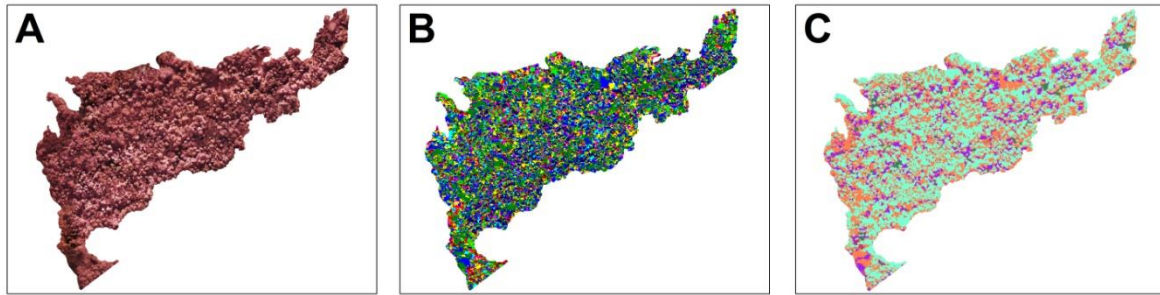


Figure 54. Object-based unsupervised classification of red edge images mosaic on 8 August, 2013. (A. Original mosaic. B. ISODATA. C. K-mean.).

The K-mean algorithm still failed to determine the vegetation species properly to resemble the pixel-based classification (Figure 36). Using the ISODATA technique, more bush areas were determined as the class of Kahikatea (light blue) as seen in Figure 54. while the pixel-based classification classified most of the bush region as Kowhai, Chinese Privet and Totara (seen in Figure 36).

The results of object-based unsupervised classification of the merge true colour mosaic is shown in Figure 55, which demonstrates better results using the ISODATA method; while the K-mean classification technique fails to classify the vegetation.

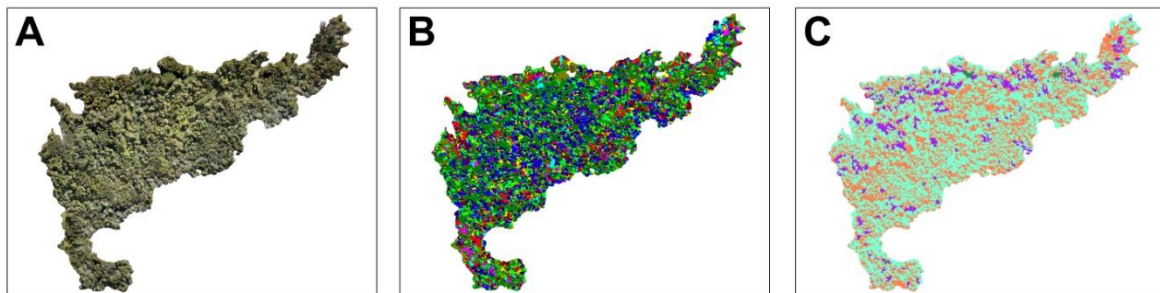


Figure 55. Object-based unsupervised classification of true colour images on 1 April, 2014 merge mosaic. (A. Original mosaic. B. ISODATA. C. K-mean.).

Specifically, the ISODATA classified a lesser area as shadow (green), while more areas were determined as Weeping Mapou (yellow). Simultaneously, the portion classified as Kahikatea (light blue) increased gently. The centre of the bush area was distinguished as several species rather than Kowhai (blue), solely in the pixel-based classification (Figure 37).

4.4.2 Object-based supervised classification.

In order to minimize the interference of inconsistent setting of the supervised classification, especially in the training data, the object-based supervised classification used the same training data set of the corresponding pixel-based supervised classification.

The classification of the vegetation stress images mosaic in 2013 showed good results (Figure 56), which was classified as a feasible nine classes.

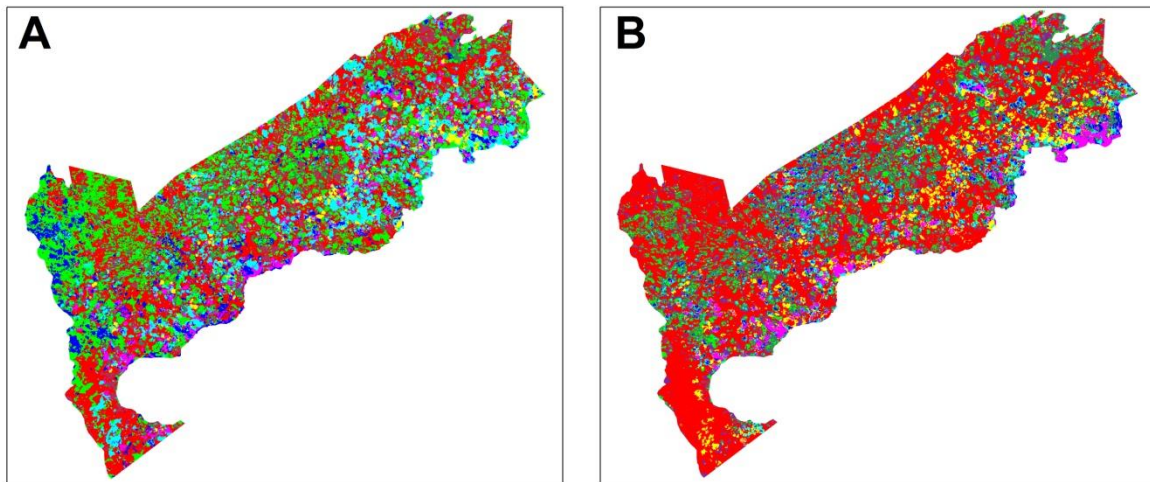


Figure 56. Object-based supervised classification of vegetation stress images mosaic in 2013. (A. Maximum likelihood. B. Minimum distance.).

According to the field investigation observations, the classifications of Totara (light green) and Kahikatea (light blue) were very close to the actual distribution, as seen in Figure 56A. However, the minimum distance results shown in Figure 56B provided approximate results comparing to the maximum likelihood technique. However, most areas classified as Totara and Kahikatea species in the maximum likelihood method were classified as Chinese Privet and Kauri (red and pink).

Figure 57 displays the object-based classification results of the vegetation stress images mosaic in 2014.

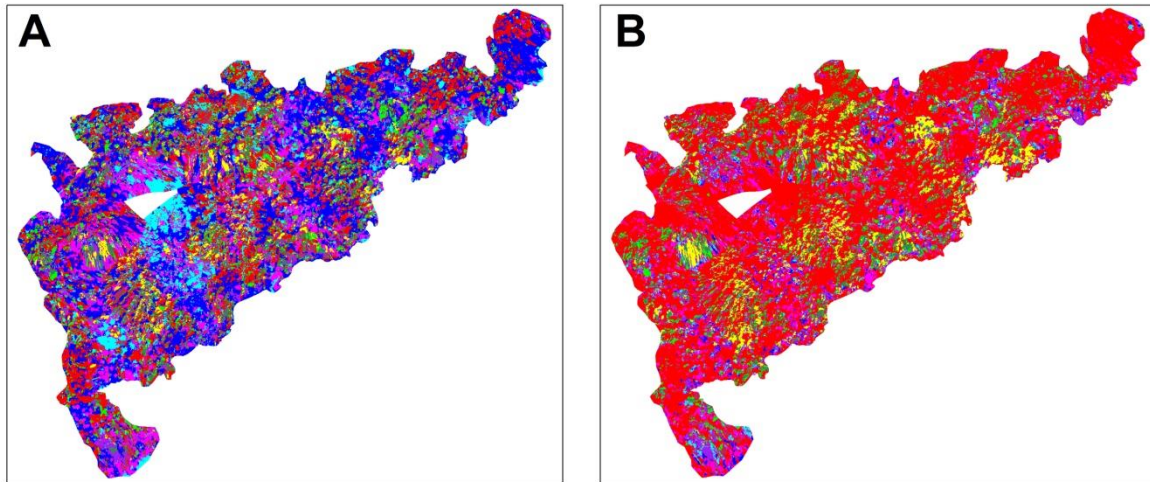


Figure 57. Object-based supervised classification of vegetation stress images mosaic in 2014. (A. Maximum likelihood. B. Minimum distance.).

The maximum likelihood technique did not show much improvement compared to the pixel-based classification of the vegetation stress images mosaic in 2014. Most of the bush areas were determined as Kowhai (coloured in blue); while the minimum distance algorithm classified them as Chinese Privet (coloured in red).

Figure 58 shows the classification results of near the infrared images mosaic on 28 July, 2013.

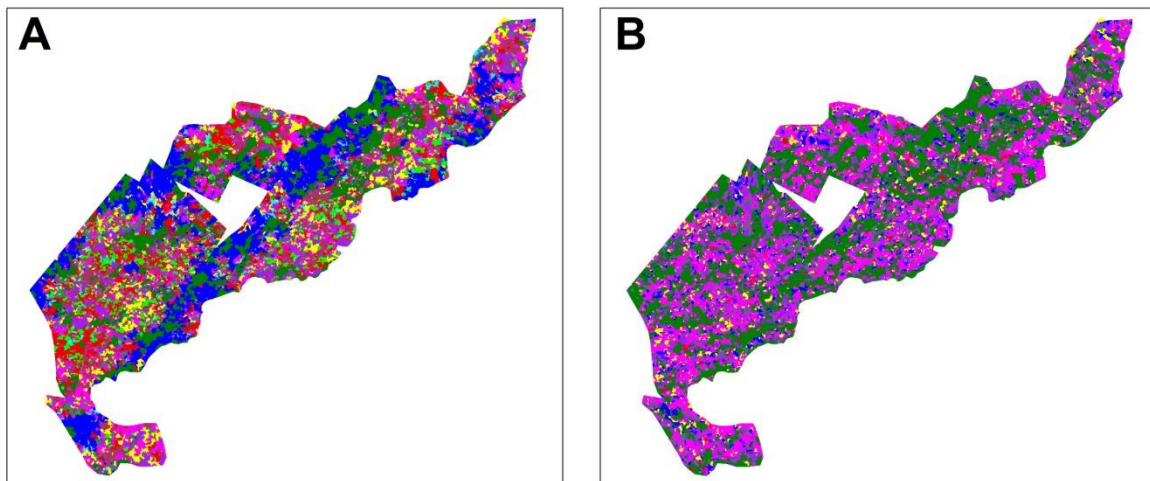


Figure 58. Object-based supervised classification of near-infrared images mosaic on 28 July, 2013. (A. Maximum likelihood. B. Minimum distance.).

The results of the minimum distance method provided little useful information for further analysis. The maximum likelihood technique generated a better result for the class of Chinese Privet (red); while the same technique failed to determine this species in pixel-based classification (Figure 40). However, both the pixel-based and object-based classifications

using the maximum likelihood algorithm were unsuccessful in identifying the species of Kahikatea (light blue).

Figure 59 illustrates the results of the near-infrared images mosaic on 8 August, 2013.

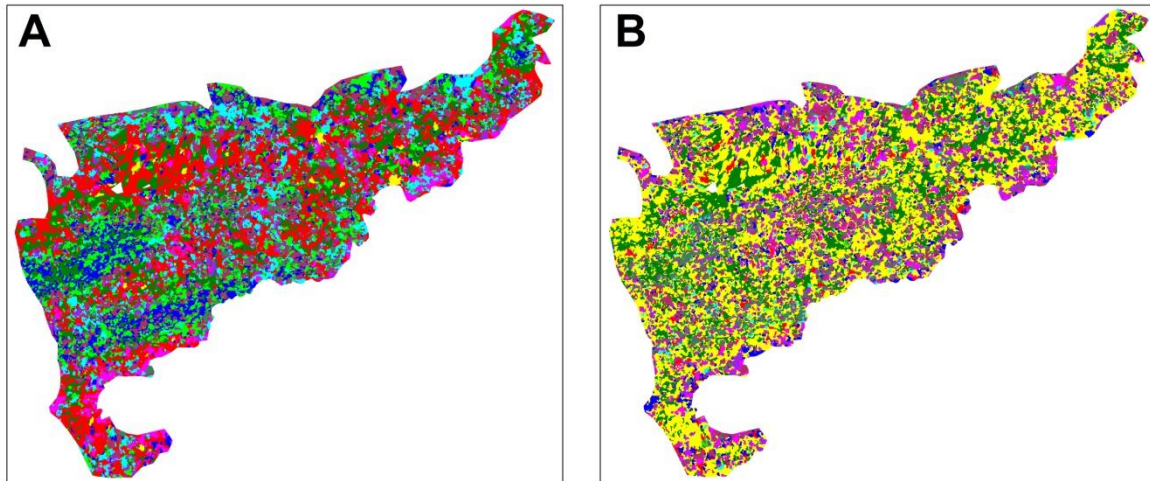


Figure 59. Object-based supervised classification of near-infrared images mosaic on 8 August, 2013. (A. Maximum likelihood. B. Minimum distance.).

As seen in Figure 41, few pixels were classified as Totara or Kahikatea (light green and light blue). However, the object-based classification successfully determined these two species and other tree species as well (Figure 59A). The minimum distance algorithm failed to classify the vegetation, and only classified the bush area mainly as Weeping Mapou, Kauri and Rimu (coloured in yellow, purple and green in Figure 59B).

Figure 60 demonstrates the supervised classification results of near-infrared images acquired on 1 April, 2014 (flight 2).

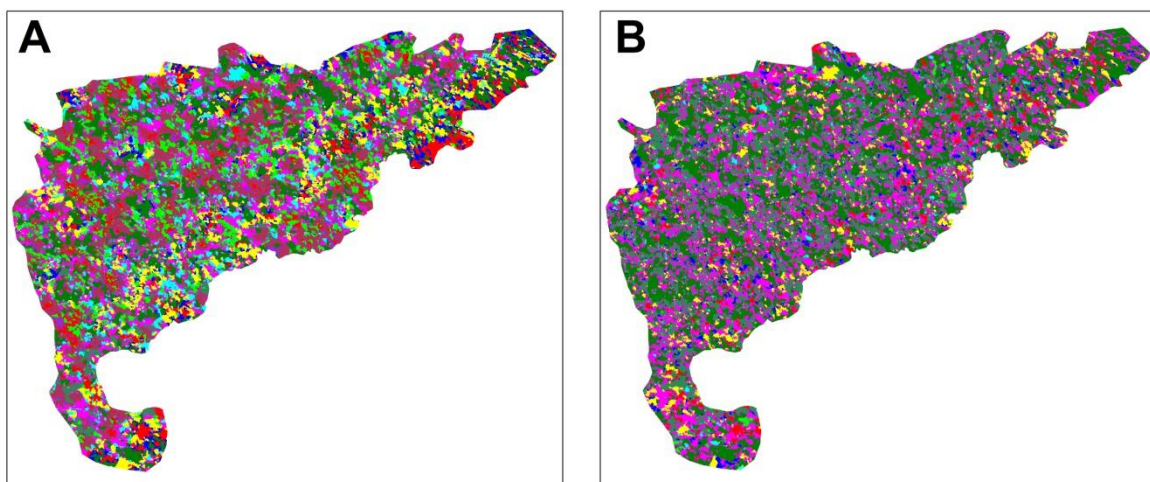


Figure 60. Object-based supervised classification of near-infrared images mosaic on 1 April, 2014 (Flight 2). (A. Maximum likelihood. B. Minimum distance.).

The classification results seen in Figure 60 showed certain improvements, contrasting with the pixel-based classification (Figure 42). Only three species of vegetation, including shadow, were determined in the pixel-based classification, while all ten classes were assigned to specific classes in the object-based maximum likelihood classification (Figure 60A). However, most of the Totara trees were misclassified as Rimu.

Figure 61 shows the classification of the red edge images mosaic on 8 August, 2013.

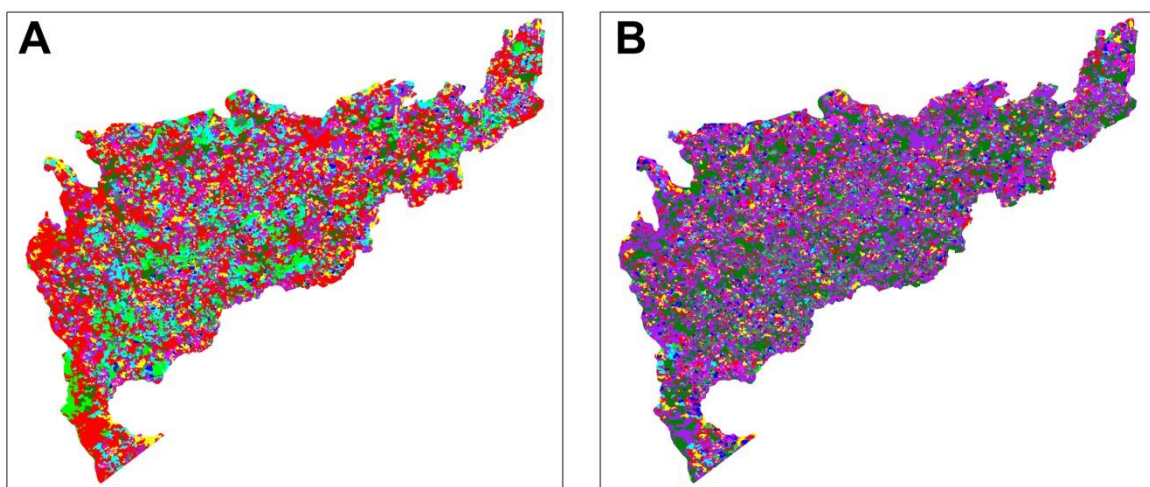


Figure 61. Object-based supervised classification of red edge images mosaic on 8 August, 2013. (A. Maximum likelihood. B. Minimum distance.).

The minimum distance algorithm provided few useful results for the whole bush area vegetation classification by using the red edge mosaic (Figure 61B). Totara and Kahikatea (light green and light blue) were successfully classified in Figure 61A, while the pixel-based classification failed to determine them in Figure 43.

Figure 62 shows the object-based supervised classification results of the true colour images (the merged one which combines the images of flights 1 and 2).

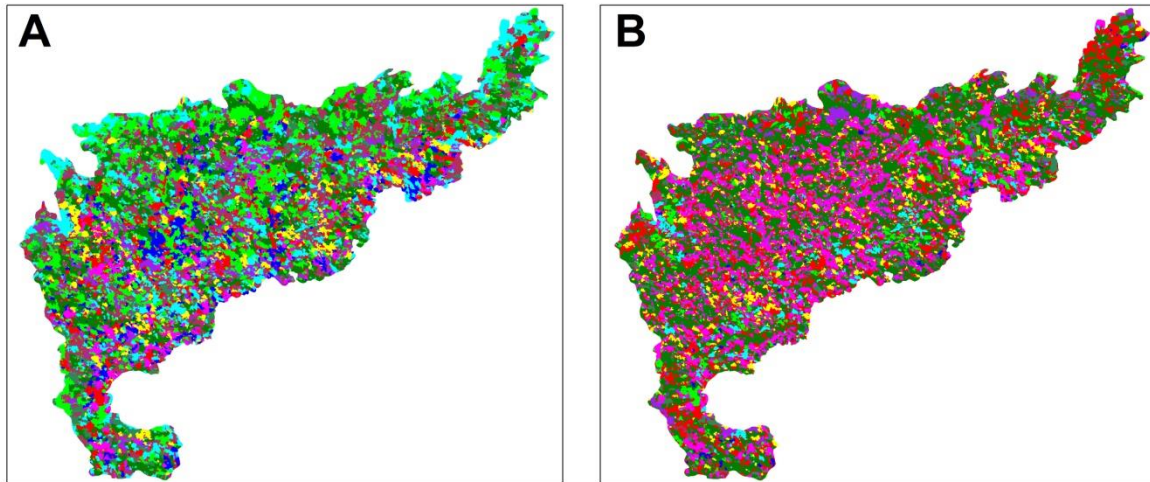


Figure 62. Object-based supervised classification of true colour images on 1 April, 2014 merged mosaic. (A. Maximum likelihood. B. Minimum distance.).

The object-based supervised classification showed reasonably good results using the maximum likelihood technique (shown in Figure 62A). Concurrently, the minimum distance algorithm produced very different results compared to the maximum likelihood method.

In terms of the maximum likelihood algorithm, the result shown in Figure 62A shows that the middle part of the bush area was reasonably accurately determined as containing different classes including Totara, Kowhai, Kauri and shadow (light green, blue, purple and green). In addition to the middle part, the quantities of other species were within reasonable expectations and distributed on the map in way that closely matched the reality according to the field trip observations. However, the minimum distance method (result shown in Figure 62B) classified the middle part as Kauri, Chinese Privet and shadow (purple, red, green).

Concluding from all the results of minimum distance pixel-based classification and object-based classifications, shadow could be easily distinguished in the map. However, the maximum likelihood technique is capable of providing more accurate classification. All of the classification results in section 4.4 of bigger scale and higher resolution are shown in Appendix A.

4.5 Confusion Matrix

Accuracy assessments of all pixel-based supervised classification and object-based supervised classification were undertaken by using a confusion matrix. All the field data were divided into training data for classification processing and ground truth data for accuracy assessment. Using the classification results and ground truth data, confusion matrices results

were generated and are provided in Tables 2 to 3. Considering the low accuracy of unsupervised classification and the unusable results of that as shown earlier, the classification results of the unsupervised classification are not evaluated here.

Table 2. Confusion Matrix Results of Pixel-Based Supervised Classification

Classification Method	Tree Species	Producer Accuracy (%)							User Accuracy (%)						
		1	2	3	4	5	6	7	1	2	3	4	5	6	7
Maximum Likelihood Classification	Chinese Privet (<i>Ligustrum sinense</i>)	60.96	60.96	0.37	5.02	13.06	49.63	51.90	29.67	39.78	35.95	13.33	22.21	35.10	66.55
	Totara (<i>Podocarpus totara</i>)	35.77	35.77	18.39	0.38	2.74	0.38	59.72	84.85	89.06	71.21	44.30	67.54	33.45	95.38
	Kowhai (<i>Sophora microphylla</i>)	88.12	88.12	21.71	0.00	0.49	0.91	84.08	82.03	70.34	44.43	0.00	44.42	12.85	80.62
	Weeping Mapou (<i>Myrsine divaricata</i>)	77.37	77.37	76.05	92.46	17.87	78.22	83.90	68.21	56.97	9.49	21.19	3.88	14.06	34.69
	Kahikatea (<i>Dacrycarpus dacrydioides</i>)	53.43	53.43	0.00	0.00	7.95	3.53	70.89	85.37	90.48	0.00	0.00	54.96	41.46	92.68
	Kānuka (<i>Kunzea ericoides</i>)	74.94	74.94	18.90	82.70	15.98	6.51	100.0	70.22	31.48	6.60	12.98	8.26	3.77	39.03
	Rimu (<i>Dacrydium cupressinum</i>)	59.32	59.32	0.00	46.07	10.26	0.00	76.23	79.83	47.21	0.00	7.02	7.28	0.00	12.81
	Miro (<i>Prumnopitys ferruginea</i>)	59.34	59.34	33.26	68.72	89.07	91.77	81.98	43.53	16.23	5.17	8.20	3.09	6.27	18.74
	Kauri (<i>Agathis australis</i>)	89.64	89.64	74.66	83.41	36.76	63.39	77.13	27.56	36.00	2.81	3.11	0.83	2.02	84.11
	Shadow	N/A	N/A	89.21	96.28	65.55	83.81	99.26	N/A	N/A	66.47	76.76	89.50	93.53	95.03
Overall Classification Accuracy		70.5269		61.8344		20.5278		13.8369		20.3472		17.2308		73.6683	
Kappa Coefficient		0.6560		0.5372		0.1399		0.1024		0.1509		0.1253		0.6886	
Classification Method	Tree Species	Producer Accuracy (%)							User Accuracy (%)						
		1	2	3	4	5	6	7	1	2	3	4	5	6	7
Minimum Distance Classification	Chinese Privet (<i>Ligustrum sinense</i>)	50.86	44.17	0.00	7.08	0.15	23.83	17.13	14.10	62.23	0.00	19.70	6.53	18.01	24.54
	Totara (<i>Podocarpus totara</i>)	10.66	14.04	0.01	0.00	0.00	0.00	1.64	40.65	62.92	0.92	0.00	0.00	0.00	4.93
	Kowhai (<i>Sophora microphylla</i>)	2.67	3.97	31.38	4.63	0.78	2.58	6.71	4.90	26.00	23.80	34.08	27.03	11.64	79.47
	Weeping Mapou (<i>Myrsine divaricata</i>)	63.76	71.35	7.46	91.12	8.56	6.41	0.00	48.63	36.40	7.14	13.12	10.78	7.26	0.00
	Kahikatea (<i>Dacrycarpus dacrydioides</i>)	2.88	0.36	0.00	0.00	6.86	0.14	80.56	11.30	7.57	0.00	0.00	26.57	76.47	27.11
	Kānuka (<i>Kunzea ericoides</i>)	72.02	57.45	89.20	34.49	38.03	30.26	16.39	31.86	4.54	7.55	14.07	5.04	6.34	3.80
	Rimu (<i>Dacrydium cupressinum</i>)	20.21	6.03	0.00	37.49	0.00	0.00	22.53	50.17	5.32	0.00	3.02	0.00	0.00	1.94
	Miro (<i>Prumnopitys ferruginea</i>)	45.09	42.73	4.14	67.73	85.84	80.02	0.52	11.08	13.87	2.49	8.11	2.57	5.48	42.96
	Kauri (<i>Agathis australis</i>)	25.58	18.91	0.00	8.05	0.00	70.38	0.00	5.09	5.83	0.00	0.86	0.00	1.31	0.00
	Shadow	N/A	N/A	91.55	96.60	87.95	92.30	99.90	N/A	N/A	36.01	60.78	70.20	71.76	66.52

	1	2	3	4	5	6	7
Overall Classification Accuracy (%)	22.8004	15.3212	15.1782	11.8958	22.9825	10.8195	33.3580
Kappa Coefficient	0.1445	0.0894	0.0807	0.0799	0.1613	0.0658	0.2433

1. Vegetation Stress Images Mosaic (2013); 2. Vegetation Stress Images Mosaic (2014); 3. Near-Infrared Images Mosaic (28 July, 2013); 4. Near-Infrared Images Mosaic (8 August, 2013); 5. Near-Infrared Images Mosaic (1 April, 2014 (flight 2)); 6. Red Edge Images Mosaic (8 August, 2013); 7. True Colour Images Mosaic (merge);

Table 3. Confusion Matrix Results of Object-Based Supervised Classification

Classification Method	Tree Species	Producer Accuracy (%)							User Accuracy (%)						
		1	2	3	4	5	6	7	1	2	3	4	5	6	7
Maximum Likelihood Classification	Chinese Privet (<i>Ligustrum sinense</i>)	79.90	62.12	0.90	66.04	50.95	63.21	85.96	46.60	30.31	1.43	34.42	62.22	32.73	81.42
	Totara (<i>Podocarpus totara</i>)	82.19	57.10	18.43	15.94	19.40	16.22	67.84	80.24	92.73	69.59	74.00	78.68	62.99	94.49
	Kowhai (<i>Sophora microphylla</i>)	63.47	78.38	58.90	2.67	7.85	6.40	80.94	75.07	76.05	48.00	22.06	39.66	21.43	90.83
	Weeping Mapou (<i>Myrsine divaricata</i>)	54.95	79.94	70.89	99.00	79.56	71.85	85.15	87.16	73.58	18.47	99.01	14.90	22.86	62.32
	Kahikatea (<i>Dacrycarpus dacrydioides</i>)	74.40	64.27	0.09	18.80	12.82	18.72	78.68	75.24	90.94	1.34	33.60	25.45	37.31	91.13
	Kānuka (<i>Kunzea ericoides</i>)	79.55	78.87	13.55	82.10	21.15	68.65	75.23	71.36	42.05	5.35	18.15	8.32	26.26	46.77
	Rimu (<i>Dacrydium cupressinum</i>)	73.98	80.87	51.31	34.15	56.56	0.00	48.82	85.60	48.19	7.57	5.98	10.93	0.00	16.81
	Miro (<i>Prumnopitys ferruginea</i>)	54.47	73.07	74.39	62.82	91.08	78.62	83.68	54.80	35.61	15.88	11.26	10.89	11.92	49.71
	Kauri (<i>Agathis australis</i>)	76.90	60.93	100.0	89.02	94.03	63.03	83.53	75.64	24.42	7.56	24.77	24.32	3.11	9.57
Shadow	N/A	N/A	88.21	97.24	99.01	86.08	95.91	N/A	N/A	80.77	72.94	90.14	99.66	90.90	
Overall Classification Accuracy		73.2668	68.2427	28.2064	31.7852	38.7205	30.0571	80.3443							
Kappa Coefficient		0.6812	0.6125	0.2040	0.2376	0.3202	0.2184	0.7661							
Classification Method	Tree Species	Producer Accuracy (%)							User Accuracy (%)						
		1	2	3	4	5	6	7	1	2	3	4	5	6	7
Minimum Distance Classification	Chinese Privet (<i>Ligustrum sinense</i>)	86.85	54.15	0.00	0.72	7.68	21.80	22.60	22.73	7.87	0.00	4.21	12.52	21.13	18.51
	Totara (<i>Podocarpus totara</i>)	14.23	22.28	0.06	0.15	1.03	5.94	9.58	45.23	61.43	5.32	19.30	46.00	34.07	22.22
	Kowhai (<i>Sophora microphylla</i>)	3.26	4.83	11.26	18.32	0.20	3.83	2.11	7.58	25.12	33.71	30.49	0.72	4.98	36.64
	Weeping Mapou (<i>Myrsine divaricata</i>)	61.85	76.13	11.58	99.27	20.17	12.63	0.00	49.90	43.53	11.09	20.21	6.56	15.28	0.00
	Kahikatea (<i>Dacrycarpus dacrydioides</i>)	4.18	0.82	0.00	0.10	0.00	2.61	7.13	11.46	11.00	0.00	2.45	0.00	26.34	22.50
	Kānuka (<i>Kunzea ericoides</i>)	67.22	29.09	88.31	36.56	16.65	17.60	61.37	31.16	12.01	7.93	11.60	3.45	4.98	8.67
	Rimu (<i>Dacrydium cupressinum</i>)	19.96	6.41	0.00	6.12	0.00	0.00	0.00	33.57	2.25	0.00	0.67	0.00	0.00	0.00
	Miro (<i>Prumnopitys ferruginea</i>)	31.46	71.74	6.58	69.09	83.47	78.94	0.00	9.53	22.30	2.08	9.52	3.27	5.54	0.00

Kauri (<i>Agathis australis</i>)	29.09	16.43	14.09	89.02	1.24	69.67	3.20	7.10	2.93	0.44	3.59	100.0	1.78	0.39
Shadow	N/A	N/A	91.67	97.10	99.69	96.35	99.88	N/A	N/A	32.98	49.14	70.68	70.55	60.51
	1	2	3	4	5	6	7							
Overall Classification Accuracy (%)	25.3486	17.7005	11.9535	13.8064	21.1210	13.1503	29.3430							
Kappa Coefficient	0.1673	0.1002	0.0735	0.0906	0.1450	0.0624	0.1845							
1. Vegetation Stress Images Mosaic (2013); 2. Vegetation Stress Images Mosaic (2014); 3. Near-Infrared Images Mosaic (28 July, 2013); 4. Near-Infrared Images Mosaic (8 August, 2013); 5. Near-Infrared Images Mosaic (1 April, 2014 (flight 2)); 6. Red Edge Images Mosaic (8 August, 2013); 7. True Colour Images Mosaic (merge);														

Vegetation Stress Images Mosaic (2013)

Looking at Table 2, the pixel-based maximum likelihood classification of vegetation stress images mosaic was more accurate than the minimum distance classification; the former having an overall accuracy of 70.52% and the latter only 22.80%. The classification results of the minimum distance technique showed very low accuracy, which was not used for further ArcGIS analysis.

Moreover, using the same classification algorithm, the object-based classification produced more accurate classifications than the pixel-based classification. As shown in Table 3, the overall accuracy of the object-based maximum likelihood classification was slightly higher than the results of the pixel-based maximum likelihood classification with an accuracy of 73.26%. Similarly, although the overall accuracy of the object-based minimum distance was lower than the maximum likelihood classification, it was still little higher than the results of same algorithm in the pixel-based classification (Table 2).

Specifically, as shown in Table 2, the classification accuracies for some tree species are slightly higher than others including the Rimu (*Dacrydium cupressinum*) and Miro (*Prumnopitys ferruginea*). The reason for this is the unavailability of sufficient training and ground truth data for these classes.

Vegetation Stress Images Mosaic (2014)

The accuracy of the classification results in portrayed Figures 39 and 57 were shown in Tables 2 and 3 as well. The maximum likelihood results were more accurate than minimum distance algorithm both in pixel-based and object-based classifications. The performance of the maximum likelihood classification increased from 61.83% to 68.24% after processing the object segmentation. However, the accuracy of the minimum distance technique didn't show

any striking difference following the object segmentation, while the kappa statistic had a very low agreement between producer and user accuracy.

Near-Infrared Images Mosaic (28 July, 2013; 8 August, 2013; 1 April, 2014(flight2))

The confusion matrices of all the near-infrared images mosaic pixel-based and object-based supervised classification were are shown in Tables 2 and 3.

In terms of the maximum likelihood classification, the overall classification accuracy of each near-infrared images mosaic showed different trends of growth after applying the object-based classification. The maximum likelihood accuracy of each near-infrared mosaic increased from 20.52% to 28.20% (28 July, 2013); 13.83% to 31.78% (8 August, 2013); and 20.34% to 38.72% (1 April, 2014 (flight2)). The increasing accuracy demonstrated that object-based maximum likelihood classification produced better classification results than the pixel-based maximum likelihood classification by using the near-infrared images mosaic. As for the minimum distance classification, all three near-infrared mosaics have very low classification accuracy using either pixel-based or object-based classification.

Red Edge Image Mosaic (8 August, 2013)

The confusion matrix results of red edge mosaic classification are shown in Table 2 and 3. A substantial increase in accuracy was witnessed in the object-based maximum likelihood classification, which increased to 30.05% of overall classification accuracy when compared with the pixel-based classification of 17.23%.

However, comparing to the accuracy of around 70% of the vegetation stress mosaic, the red edge images mosaic supervised classification failed to provide usable information. Similarly, the accuracy of the minimum distance algorithm had an increase of only 3% using the object-based classification, which was still very low in overall accuracy and kappa coefficient.

True Colour Images Mosaic (merge)

Tables 2 and 3 also present the confusion matrix results of the true colour images mosaic, the displayed data illustrating the idea that object-based supervised classification can produce more accurate classification than the pixel-based supervised classification.

The overall accuracy of maximum likelihood algorithm pixel-based classification was 73.66%, which means the merged mosaic had the most accurate result amongst all the pixel-based supervised classifications. From the object-based results of the maximum likelihood

technique, the overall accuracy of the merged mosaics increased to 80.34%. In terms of minimum distance classification, both pixel-based and object-based classification generated low accuracy results of around 30%, compared to maximum likelihood classification.

True colour images mosaics and vegetation stress images mosaics produced the most accurate classification. The object-based supervised classification produced more accurate results than the pixel-based supervised classification using the maximum likelihood algorithm. The accuracies of the minimum distance technique classification were higher or lower after applying the object segmentation, but still failed to provide usable information due to low overall accuracy. The best results of the true colour images mosaics and vegetation stress images mosaics (maximum likelihood object-based classification of true colour images mosaic (merged flights 1 and flight 2) and maximum likelihood object-based classification of vegetation stress images mosaic in 2013) were used for further analysis in ArcGIS.

4.6 Normalised Difference Vegetation Index Classification

The normalised difference vegetation index value could be calculated using the near-infrared band and red band from an image (see chapter 2). The reason for flying the AUT UAV with near-infrared, red-edge and true colour sensors was to acquire near-infrared band and red band data to see whether the NDVI value could be calculated using the UAV images mosaic. In order to do this, the near-infrared band of the near-infrared images mosaic generated on 8 August, 2013, and the red band of red edge images mosaic generated on 8 August were selected and processed by the layer stacking tool in ENVI software. A subset area of the map produced from both the 2013 and 2014 flights was chosen using same geo-location for further study.

Figures 63 and 64 display the layer stacking result and the NDVI value of it respectively using the images acquired in 2013.

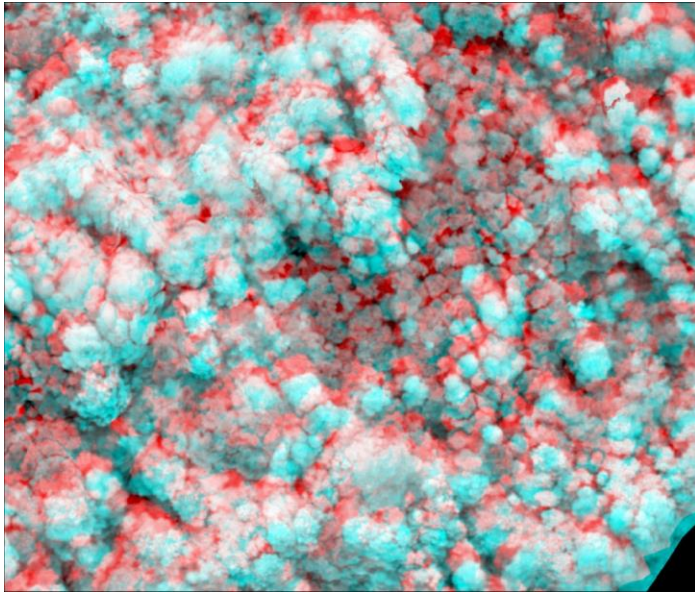


Figure 63. Presentation of layer stacking result (2013).

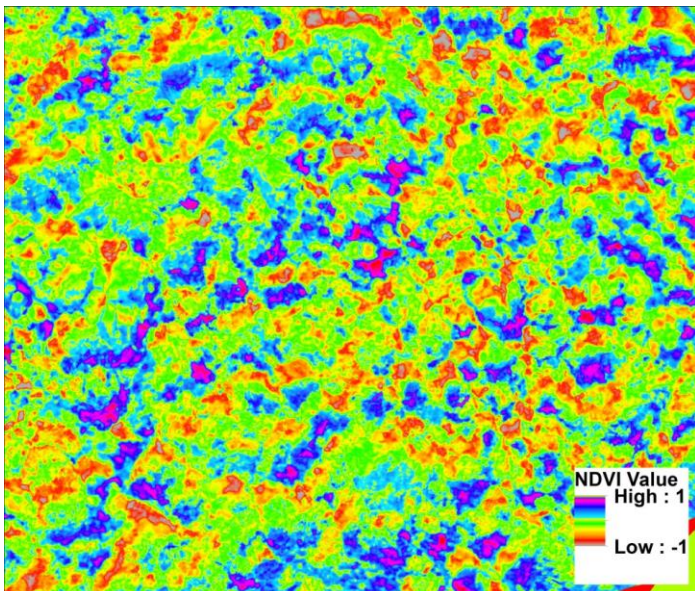


Figure 64. Normalized difference vegetation index (NDVI) value of layer stacking result (2013).

The red colour and light blue colour in Figure 63 represent the two bands respectively, but these two bands were not perfectly matched with each other. As a result, the calculation of the NDVI value generated an interferential result which is shown in Figure 64. Apparently, the red colour areas shown in Figure 64 were the gaps of the layer stacking between the two bands, which were not the real NDVI values of the vegetation in this subset.

In order to avoid the discrepancies between two mosaics and acquire more applicable data, the Swampfox UAV equipped with near-infrared and true colour sensors was employed in 2014. The near-infrared camera and true colour camera were equipped on the Swampfox

UAV simultaneously to acquire data at the same parameters and environmental conditions. In the same way, the near-infrared band of near-infrared image mosaic on 1 April, 2014 (flight 2) and red band of true colour images mosaic on 1 April, 2014 (flight 2) were selected and processed using the layer stacking tool in ENVI. The same subset area shown in Figure 63 was applied to produce the results shown in Figure 65 as well.

The layer stacking and NDVI value calculation results of images acquired in 2014 are shown in Figure 65 and 66 respectively.

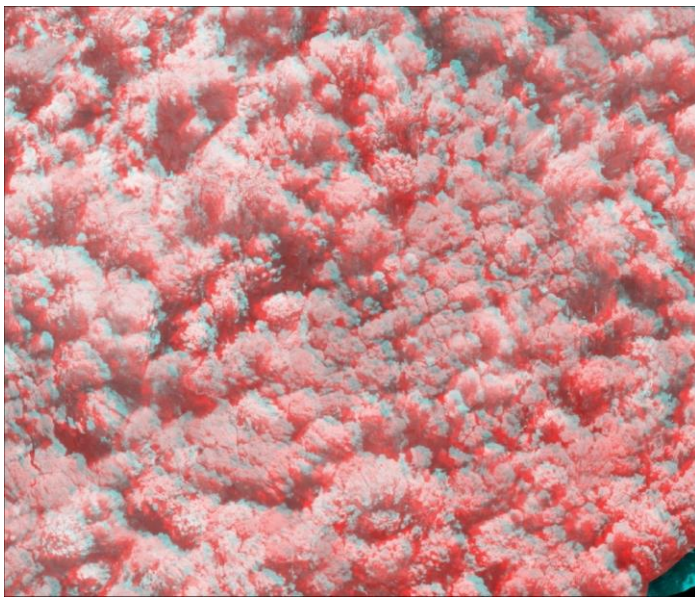


Figure 65. Presentation of layer stacking result (2014).

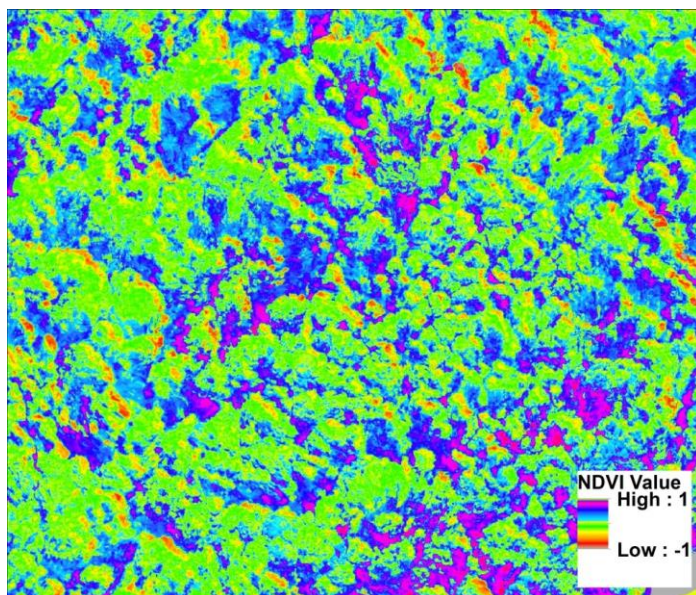


Figure 66. Normalized difference vegetation index (NDVI) value of layer stacking result (2014).

The influence after layer stacking was eliminated, as shown in Figure 65 when compared to Figure 63, is due to the lesser differences between the two mosaics. Although the gaps still existed, the overlap result of the two bands hugely improved. Most of the vegetation was shown as green while the shadow was shown as blue, as shown in Figure 66. Only some canopies on the maps were presented as a red colour due to the asymmetric problem of layer stacking.

The results of the unsupervised classification using the NDVI value images of 2013 and 2014 are shown in Figures 67 and 68.

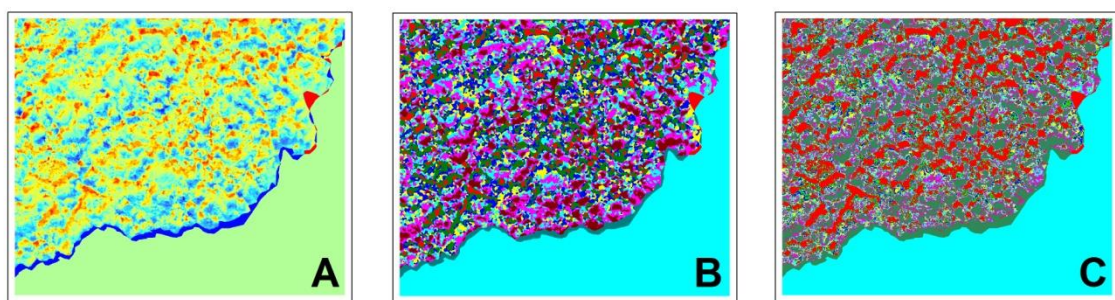


Figure 67. Unsupervised classification of normalized difference vegetation index (NDVI) value image (2013) (A. NDVI value image. B. ISODATA. C. K-Mean.).

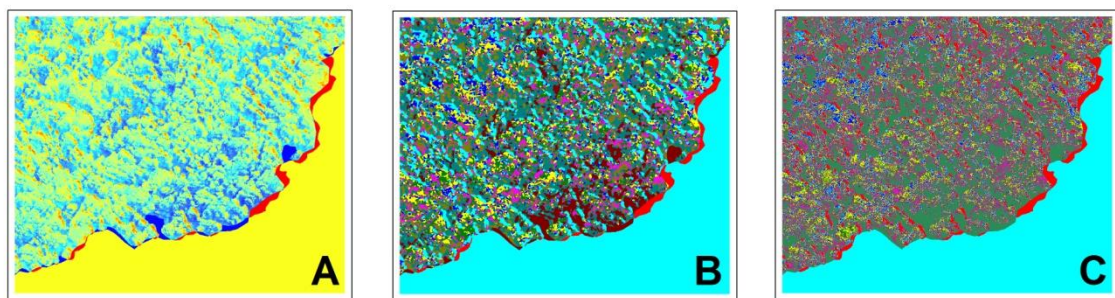


Figure 68. Unsupervised classification of normalized difference vegetation index (NDVI) value image (2014) (A. NDVI value image. B. ISODATA. C. K-Mean.).

According to the field data and digitized training data, there were seven species of trees as well as shadow within the subset area. The result of the 2013 NDVI value map was not good enough, because the gaps between the layers were classified by both the ISODATA and K-Mean techniques.

Figures 69 and 70 display the supervised classifications using the NDVI value images from 2013 and 2014.

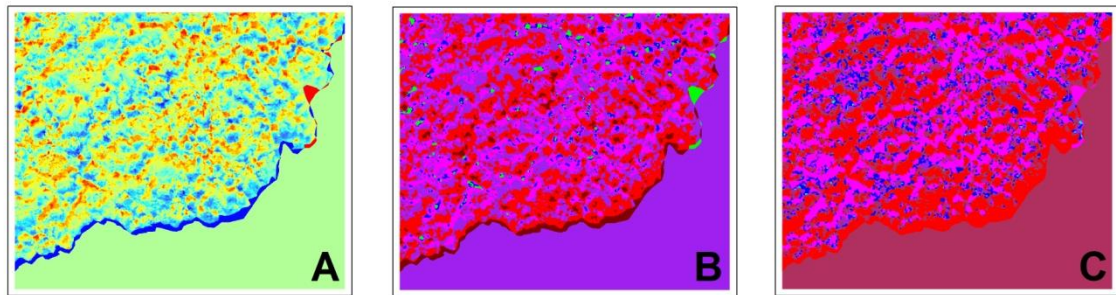


Figure 69. Supervised classification of normalized difference vegetation index (NDVI) value image (2013) (A. NDVI value image. B. Maximum Likelihood. C. Minimum Distance.).

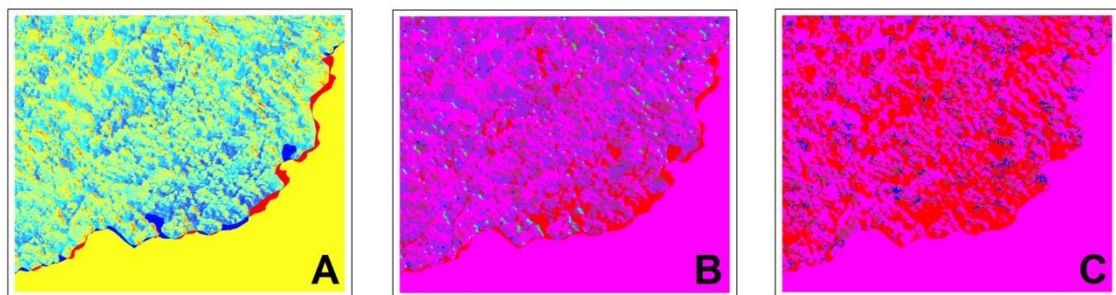


Figure 70. Supervised classification of normalized difference vegetation index (NDVI) value image (2014) (A. NDVI value image. B. Maximum Likelihood. C. Minimum Distance.).

The results of the supervised classification failed to present the vegetation species correctly in both the 2013 and 2014 NDVI value images. Both the maximum likelihood and minimum distance algorithms, which had excellent performances in former pixel- and object-based classification, failed to classify the vegetation. The subset area was classified simply as vegetation and shadow by supervised classification. Considering the unusable results of both supervised and unsupervised classification, accuracy assessment will not be presented for these results.

4.7 ENDVI and NDVI Processed Maps Using Vegetation Stress Images

The vegetation stress camera is capable of providing a method for quick and easy chlorophyll measurements of plants, which means the vegetation stress images mosaic can be used for a quick determination of the vegetation's health condition by using another piece of software called ImagesJ. The plants' health condition can be evaluated by comparing the near-infrared reflection to the visible green or blue in a non-destructive way, because chlorophyll is reflective in the near-infrared region and the concentration of chlorophyll of an unhealthy plant would decrease (LDP LLC, n.d.-b). Moreover, one of the designed purposes of the

vegetation stress camera is to make it capable of monitoring the growth and health status of the vegetation. By using the NDVI script, the pictures assign different colours to represent different health status. Furthermore, another script called ENDVI presents the results in a different ‘enhanced’ way. However, all of the theories above were based on single vegetation stress images; nobody had ever tried to process the NDVI and ENDVI scripts using mosaics of UAV vegetation stress images. To process the NDVI and ENDVI maps, two scripts were run by ImagesJ software.

The result of NDVI processing is shown in Figure 71. Different objects on the map were assigned to specific NDVI values and colour. Healthy plants with high NDVI values were assigned the green colour, while stressed plants with low NDVI value were assigned the red colour. Purple and black were assigned to negative NDVI values. From the map, the majority of vegetation within the bush area is in a healthy condition, while some trees at the north boundary are in a stressed condition.

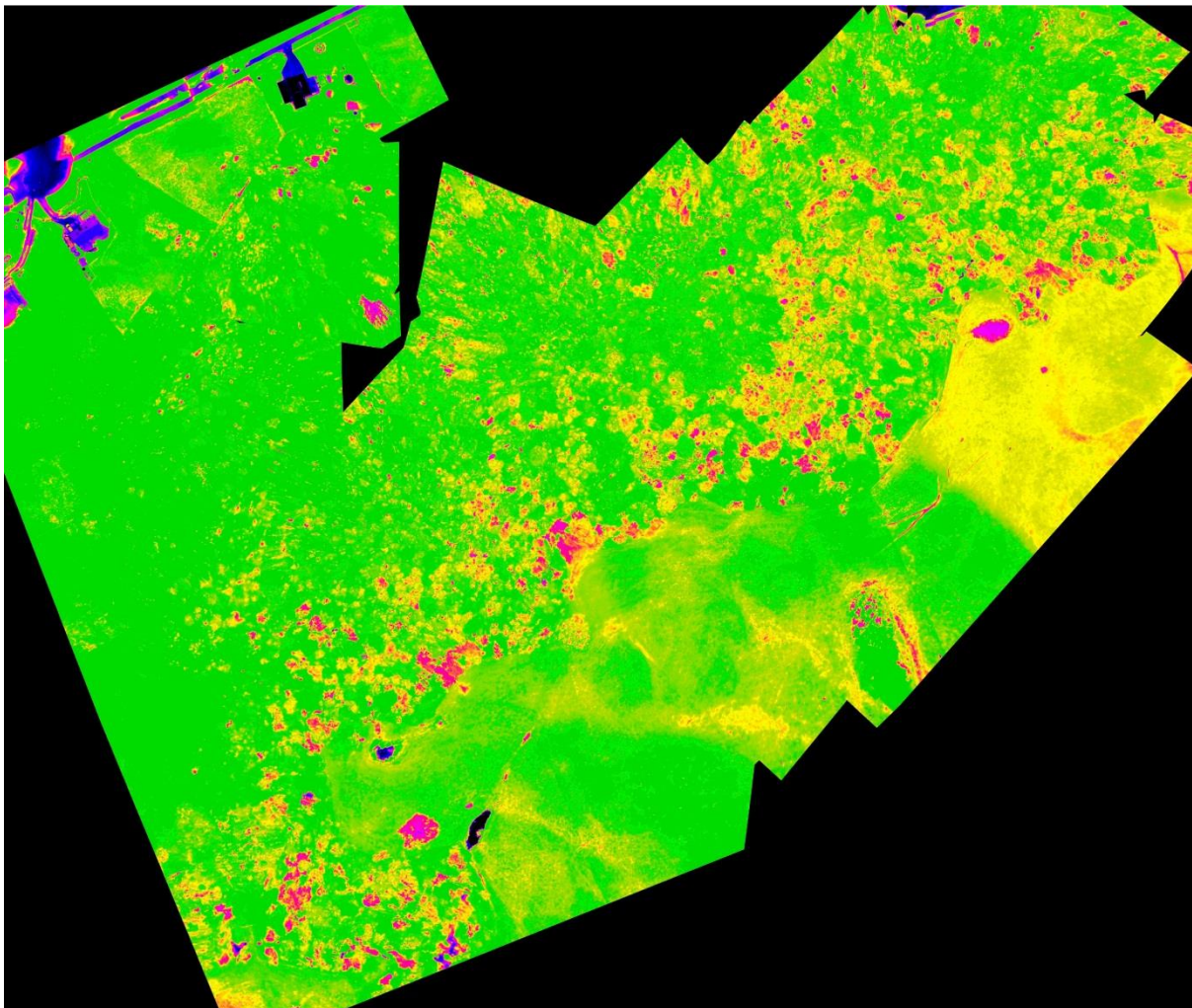


Figure 71. Processed NDVI result of vegetation stress images mosaic (2013).

Subsequently, the vegetation stress images mosaic was processed by another script called ENDVI. The calculation formula was changed slightly which enhances the presentation and quality of the NDVI map.

Figure 72 shows the processed result by using the ENDVI script. The presentation of colour has been modified, as yellow means healthy while red means a stressed condition.

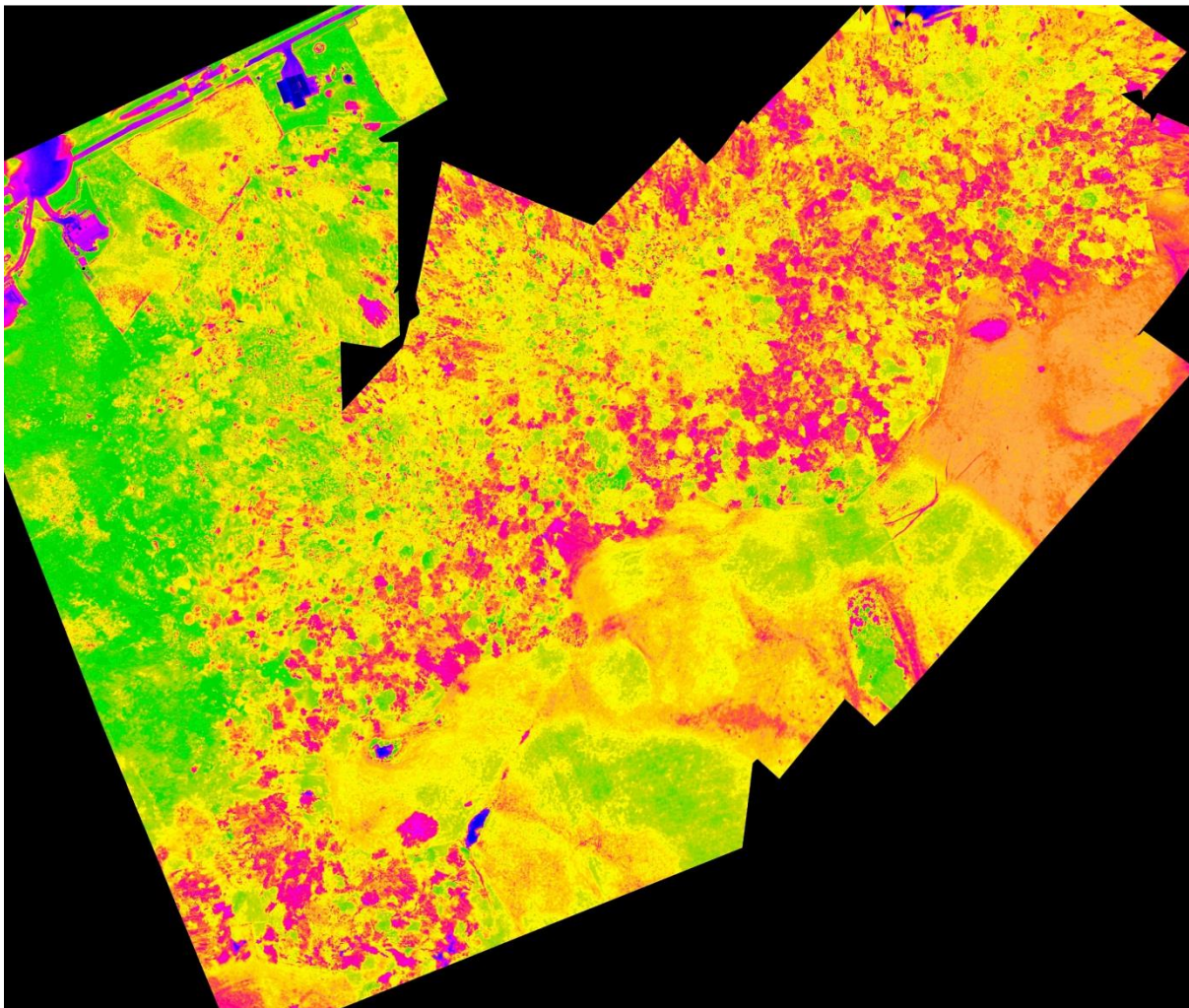


Figure 72. Processed ENDVI result of vegetation stress images mosaic (2013).

The results of the NDVI and ENDVI scripts were very similar, but in the presentation of the ENDVI map it was easier to distinguish the difference between healthy and stressed vegetation.

The application of the UAV mosaic for the NDVI and ENDVI scripts was successful. It provided an idea that the quick determination of the health condition of a large area of vegetation is becoming accessible. In this case, the traditional way of field investigation can

be replaced by the new technique of first time, fast speed, high accuracy and low cost vegetation health assessment.

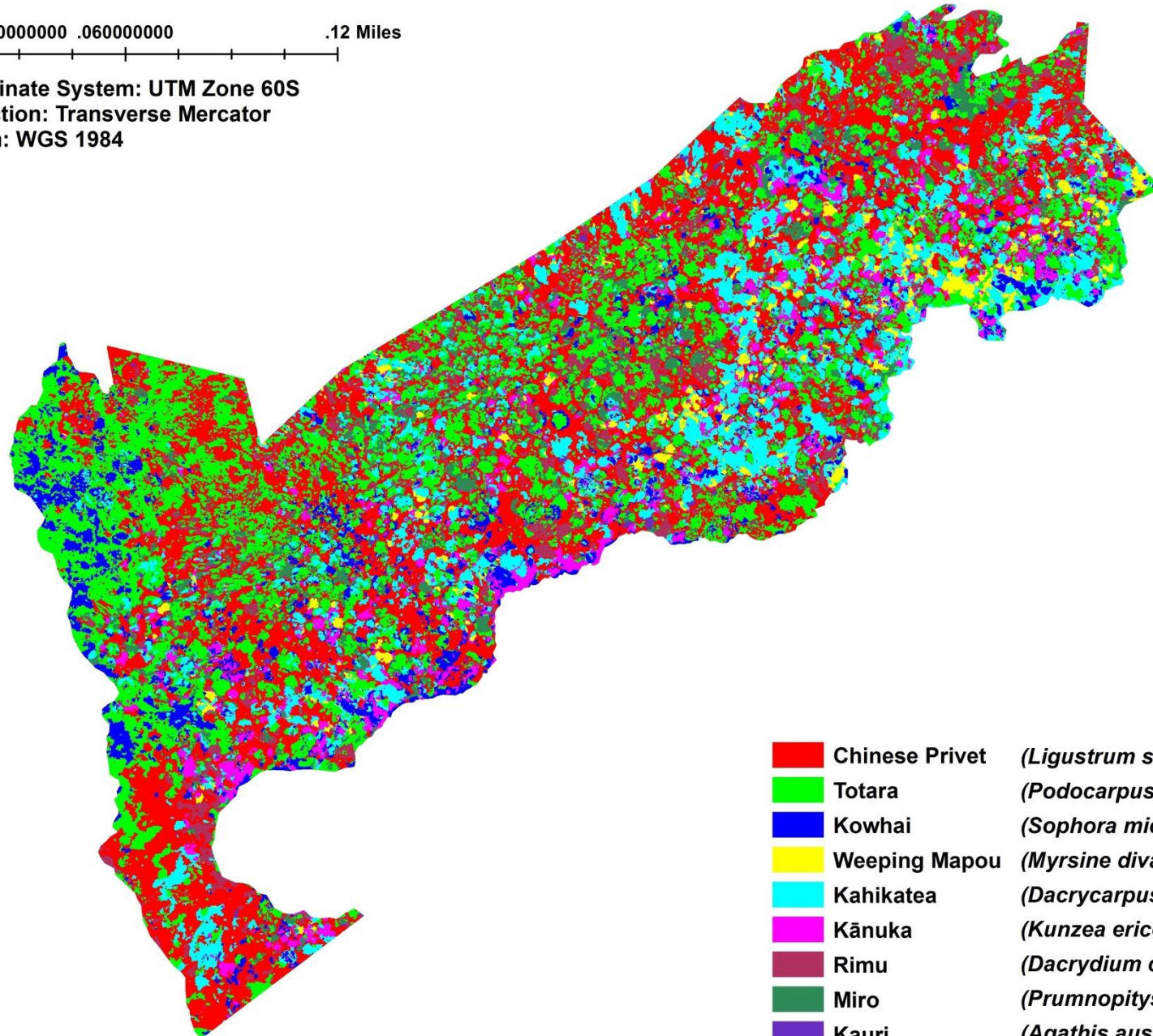
4.8 Final Classification Map

Figures 73 and 74 demonstrate the final vegetation classification of the bush area at Dairy Flat using a vegetation stress images mosaic and true colour images mosaic respectively. A total of nine classes of tree species were classified with an accuracy of 73.26% using object-based maximum likelihood supervised classification, as shown in Figure 73. Furthermore, a total of ten classes of tree species, including shadow, were classified with an accuracy of 80.34% using object-based maximum likelihood supervised classification, as shown in Figure 74.



0 .030000000 .060000000 .12 Miles

Coordinate System: UTM Zone 60S
Projection: Transverse Mercator
Datum: WGS 1984



- | | | |
|---------------------------------------------------------------------------------------|----------------|-------------------------------------|
|  | Chinese Privet | (<i>Ligustrum sinense</i>) |
|  | Totara | (<i>Podocarpus totara</i>) |
|  | Kowhai | (<i>Sophora microphylla</i>) |
|  | Weeping Mapou | (<i>Myrsine divaricata</i>) |
|  | Kahikatea | (<i>Dacrycarpus dacrydioides</i>) |
|  | Kānuka | (<i>Kunzea ericoides</i>) |
|  | Rimu | (<i>Dacrydium cupressinum</i>) |
|  | Miro | (<i>Prumnopitys ferruginea</i>) |
|  | Kauri | (<i>Agathis australis</i>) |

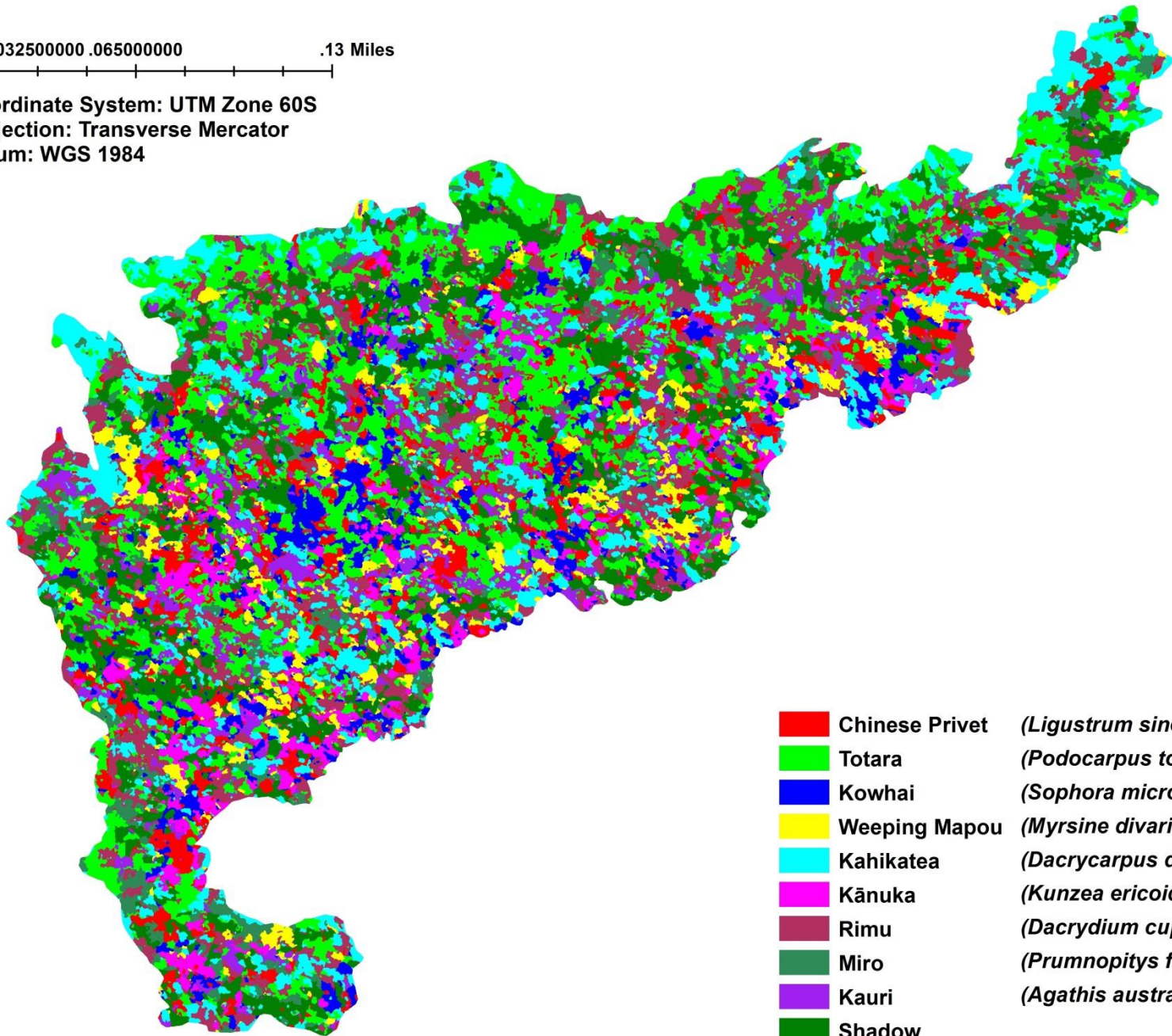
Produced by ZhaoXuan Zhang (Hins) for AUT Master in Applied Science Thesis

Figure 73. Final classification map of vegetation stress images mosaic (2013).



0 .032500000 .065000000 .13 Miles

Coordinate System: UTM Zone 60S
Projection: Transverse Mercator
Datum: WGS 1984



- | | | |
|---------------------------------------------------------------------------------------|----------------|-----------------------------------|
|  | Chinese Privet | <i>(Ligustrum sinense)</i> |
|  | Totara | <i>(Podocarpus totara)</i> |
|  | Kowhai | <i>(Sophora microphylla)</i> |
|  | Weeping Mapou | <i>(Myrsine divaricata)</i> |
|  | Kahikatea | <i>(Dacrycarpus dacrydioides)</i> |
|  | Kānuka | <i>(Kunzea ericoides)</i> |
|  | Rimu | <i>(Dacrydium cupressinum)</i> |
|  | Miro | <i>(Prumnopitys ferruginea)</i> |
|  | Kauri | <i>(Agathis australis)</i> |
|  | Shadow | |

Produced by ZhaoXuan Zhang (Hins) for AUT Master in Applied Science Thesis

Figure 74. Final classification map of true colour images mosaic (merge 1 April, 2014 flight 1 and flight 2).

5 Discussion

In this section, I discussed the research methods and materials from the UAV flight planning to final vegetation classification. All the current problems, potential problems, influential factors, results analysis and solutions were covered in the following sub-sections.

5.1 UAV Flight Planning

5.1.1 Wind conditions.

Wind is the main decisive factor of a successful UAV flight. The wind speed needs to be measured to ensure the conditions are consistent with the required standard before the UAV takes off. From the experience of more than ten UAV flights in this project, strong winds will not only generate safety concerns, but also affect the final mosaic quality. Moreover, strong winds will affect the stability of the UAV when undertaking the mission, resulting in vibration and tilt, as well as dramatic altitude increases or decreases. The consequences of the above factors would influence the photo quality due to the resultant blurry and distorted images and the change of focal length of the sensor.

5.1.2 Sun conditions.

The spectral reflection of vegetation would change slightly in different sun conditions, such as the altitude and angle of the sun. It is important to keep the sun conditions consistent in each UAV flight mission and avoid the shadows. It was decided to start the mission time from 11:00 AM till 2:00 PM to keep the sunlight vertical to the ground.

5.1.3 Cloud conditions.

Cloud is another influential factor influencing mosaic quality. Assuming that the sun is in good condition, but it is cloudy over the research site, the sunlight would be blocked by the cloud resulting in sunlight refraction which affects the spectral reflection of vegetation as a result. Furthermore, clouds over the research site would lead to shadow over the vegetation.

5.2 UAV Image Acquisition

Three cameras and two filters were employed in this study, and in order to gain consistent results, it was important to pay attention to the settings and way of using these devices.

5.2.1 Camera.

Cannon vegetation stress camera.

The images of the vegetation stress camera provided reasonable results and accuracy in this study; however the optimal method of use for this camera remains to be explored. As the vegetation stress camera was made by Canon Company and modified by the LDP LLC Company, some key features of it were different from the other two cameras which were made by the Sony Company. Specifically, this project encountered a problem whereby we obtained lesser images from the vegetation stress camera compared to the flight log file records after the UAV flight mission. Each time the Ground Control Station sent the signal to trigger the shutter, the information including the current altitude, location and pitch of the photo was recorded as a flight log file by the Ground Control Station software. As a result, we would have expected to have the same quantity of photos from the camera as the quantity of records on the log file. In fact, we had fewer images every time we used this sensor. The data recorded in the log file and the number of images did not match. The reason behind this problem is that the Canon vegetation stress camera needs more time to respond to the trigger signal or to write the data onto the memory card, resulting in a situation that the Ground Control Station sends the trigger signal and records the information, but the camera does not take any photo at all. To seek a solution, our team attempted to change the setting of the time gap between each trigger signal from two seconds to four seconds in order to give more time to the camera to respond to the signal and record the data. The problem was somewhat relieved but still remains to be thoroughly solved. However, we had substantially fewer images, as the time gap between each photo was shifted from two to four seconds. Additionally, the battery life could not support a longer mission and the sun and weather conditions were different if we were to have another flight after changing the battery. However, by using the AUT Swampfox UAV, which can be equipped with two sensors at the same time, the matching problem of images and log file was finally solved by comparing the images of the vegetation stress camera to the Sony camera (the Sony camera worked perfectly for each trigger signal).

5.2.2 Flight route.

A mission comprises a series of waypoints which the aircraft will follow out to a target and back. The plan of flight route needs to consider a series of conditions, such as the flight area, number of missions and camera specifications. The main considerations concern the width and length of the flight area, and the desired overlaps of the area. Furthermore, it is better to cover the same route more than once in order to have enough overlaps. It is recommended by the Pix4UAV software that the flight route plan should be conducted in a grid pattern

consisting of multiple lines. The frontal overlap should be at least 60%, while the side overlap should be at least 40%. According to the mosaic results, the middle part of the bush area always comes out with blank spots, magnifying the area results due to the lack of overlaps. As a solution to increase the mosaic quality, the UAV flight route should focus on the middle part of the bush area.

5.2.3 UAV control.

The control of the UAV is another potential reason for an inappropriate flight route. Considering the narrow space for the UAV to fly over the research site (not over the boundary) and the necessity to keep the flight route straight for better photo quality, it was very difficult to control the UAV to turn around and start another straight line flight path from the point we planned. At the same time, the camera needs to keep taking photos from the start point to the end point of each straight flight line. In the case of this study, some areas of the research site were not covered properly, while some areas had too much overlap.

5.2.4 Landing.

When the UAV is landing in "Parachute Landing Mode," the aircraft will head upwind on the planned landing position and deploy a parachute within 250ft, allowing the wind to carry the aircraft to the desired landing location. It is very important to ensure the wind speed and the parachute decent rate is correct in the setting window of the Ground Control Station for a safe landing.

5.2.5 Observation during flight.

As the research site was close to the model aircraft club where we located the Ground Control Station and made the take-offs and landings of the UAV, it is inevitable that we had to consider the possibility of crashing with another model aircraft. Actually, the UAV employed in this study is different from those aircraft models since it flies at a higher altitude and faster speed. So the possibility of crashing is very low. However, it is recommended that the operators "always keep an eye on the UAV" to observe the conditions at all times, especially when the UAV is landing.

5.3 UAV Images Mosaic Processing

5.3.1 Overlaps.

As the raw data in this study was further processed by Pix4UAV, enough overlaps played a particular important role in the final mosaic quality. More overlaps mean more data for the

software to compute and analyse. Pix4UAV assigns the overlap level a different value for each pixel on the mosaic, ranging from 1 to 5+.

Figure 75 portrays one example of an overlap condition from the mosaic quality report.

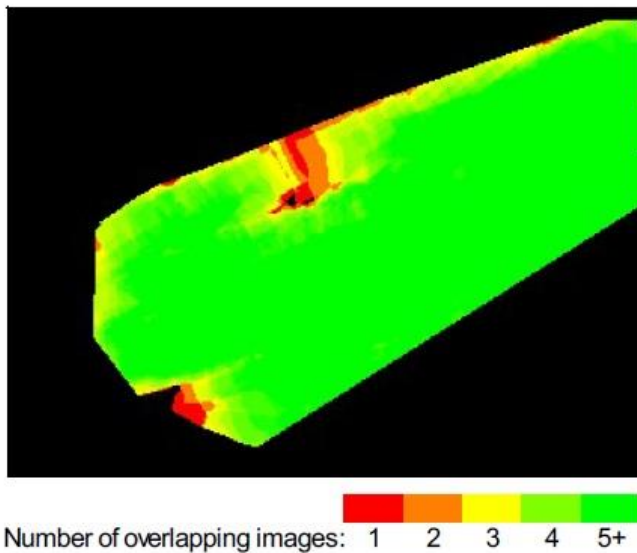


Figure 75. Presentation of overlapping images score.

Overlap scores were computed for each pixel on the mosaic map; red illustrates areas where the overlap between images was insufficient and could lead to poor mosaic results; while an overlap score of good mosaic results should be over five images (green) for each pixel of the mosaic.

The mosaics of different overlap scores are shown in Figure 76, including blank and magnifying results comparing to good results. In order to have accurate final classification results, enough overlap is required.



Figure 76. Presentation of mosaic result with different overlap score.

5.3.2 Processing time.

The first few UAV images mosaic projects took a considerable time to complete; the whole mosaicking procedure lasting up to approximately seven hours. The reason for the long processing time was because of the images which were taken when the UAV was turning. Photos taken when the UAV is turning have different angled view from normal images. In this case, the Pix4UAV has to spend a substantial amount of time on computing and analysing these data. To eliminate this problem, all photos taken mistakenly when the UAV was turning should not be used for mosaicking.

5.3.3 Potential factors affecting the mosaic quality.

The factors of poor mosaic quality are various, but the main reason is the image quality. For example, the influence on quality if the sun is blocked by clouds for several times when the UAV is undertaking missions. Obviously, we might have some over or under exposed images which are brighter or darker than normal images. In response to this phenomenon, the final mosaic will have unbalanced brightness in it. In addition, the spectral reflectance of vegetation would also be influenced under different sunlight conditions. Another factor could be described as blurry or distorted images. Some of the images acquired from the UAV are blurry or distorted inevitably due to various flying status factors and vibrations during the flight. As a result, these blurry and distorted images would lead to blurry or distorted mosaics, and poor quality mosaics would seriously affect the classification accuracy.

5.3.4 Mosaic Result Quality

After the process of creating the mosaic, a quality report was generated by the Pix4UAV after the initial processing step. From the quality report, we could have a general understanding and preview of our dataset and the final mosaic. Five contents were checked and evaluated at three levels in the quality report including images, dataset, camera optimization quality, matching quality and georeferencing.

Specifically, the dataset was checked to see whether the images have enough visual content to be processed. More than 10,000 key points means enough visual content could be computed; while more than 2,000 points indicates that not much visual information could be extracted from images. Consequently, the lack of visual content may lead to a low number of matches in images and incomplete reconstruction or poor quality results. Flying at a different altitude, adjusting the camera parameter or increasing the overlaps might be solutions to enhance the mosaic quality.

The second item on the list is to check how many images have been calibrated in a single block. If fewer than 95% of images are calibrated or there are multiple blocks, the uncalibrated images will not be used to generate the mosaic and digital surface model. Several methods are provided by Pix4UAV to solve this problem. For repetitive or complex datasets such as trees, forests or fields, the overlap might need to be increased to a higher number. Flying at a higher altitude often reduces visual complexity and improves the results, especially in forest and tree environments. Moreover, if the dataset contains images from multiple flights, it is necessary to process each flight individually due to different conditions such as capture time, temperature, moving objects and different lenses before combining them. Thirdly, images taken from the take-off and landing phase should be removed, and a higher level of overlap and more comprehensive flight route plan need to be carried out.

As for the camera optimization quality, if the optimized focal length is more than 5% of the initial, as was the case with some of the mosaic projects in this study, and the dataset completeness is above 50%, it is suggested to optimize the initial parameters again by using the optimized parameters as the initial parameters, in order to improve the quality and increase the processing speed. If the completeness is low, this may indicate either a problem in the project such as low overlap, poor image quality or wrong geo-tags, or that the initial camera model is not set properly. In that case, it is recommended to check whether the camera model corresponds to the physical camera, and edit the focal length parameter when creating the project.

In terms of the matching issue, if the number of matches is lower than 1,000 in each calibrated image, it may indicate that the results are not very reliable. A low number of matches are often related to low overlap between the images. Thus, a few changes in the initial camera model parameters or in the set of images may result in large changes in the results.

The last step is to check whether the mosaic project deploys the ground control points to geo-reference the mosaic images. Five well distributed and identified ground control points would result in excellent accuracy.

5.4 Collection and Digitization of Training Data and Ground Truth Data

The field data collected in this study were divided into half training data and half ground truth data. Some errors or interferences might be generated as a result of the procedure of converting this information to digital files that can be read by the ArcGIS and ENVI software

respectively. A few factors including human error, equipment, the digitizing procedure as well as the sampling method are important influences of the accuracy of field data, and therefore affect the final accuracy of classification.

Specifically, human errors are most likely to occur when determining tree species. In this research, the species of trees were identified by another group member who is experienced in New Zealand native vegetation identification. It is possible that the tree species might be misclassified due to factors such as different sunlight, colour (especially in different seasons) and visibility conditions.

Secondly, the errors could be generated from the field data collection equipment. On the one hand, the accuracy of the GPS unit is highly dependent on the signal from the satellite and the error of location accuracy could be more than ten metres or within two metres. In this case, the GPS location record of one tree may shift to another tree when I exported the data to software because the distance between samples was so close. As a consequence, one tree might be identified as another species even the species identification in the record was correct.

Simultaneously, errors might occur in the digitizing process of the field data. Ten final mosaics of different sensors are slightly different in geo-location although they use the same projection and datum system, which means the same digitized field data could not be applied in all of them and needed to be modified. Furthermore, the mosaic quality is different amongst the ten maps. Blurry or distorted mosaic results would lead to changes of the shape of some trees. So the polygons of field data need to be digitized again according to the shape changes of trees.

Finally, and very importantly, it is about the errors of sampling method. For better training data and ground truth data, the sampling points should be distributed around the whole bush area. But considering the safety and privacy issues, the field data along the south boundary of the bush area were collected since it was the only accessible area. The bias of field data collection might affect the accuracy and representativeness of the final training and ground truth data.

5.5 UAV Images Mosaic Classification

5.5.1 Mosaic quality.

The quality of mosaic plays a particularly important role in the accuracy of classification. Whether the integrity of the bush area and vegetation spectral information is maintained by

the mosaic is the critical factor of successful classification. First of all, the mosaic problems listed earlier including blurry, distorted and magnifying images would affect the mean spectral value of individual trees and then affect the classification result.

Another concern about the mosaic quality is the negative influence of shadow. Shadow on UAV images includes the shadow of cloud and shadow of taller trees on short trees. In this study, shadow was classified and listed as one class because the vegetation influenced by the shadow could not be identified. So how to eliminate the influence of shadow and how to address the affected mosaic is another important topic of UAV technique remote sensing in future studies.

5.5.2 Classification methods and results.

Overall, from the results presented in chapter 4 we can conclude that object-based classification is more suitable for UAV images' mosaic classification, while the maximum likelihood algorithm provides the most accurate results rather than other techniques.

Supervised and unsupervised classification.

Undoubtedly, the supervised classification produces better results. The unsupervised classification might perform well in the classification of different objects such as the sea, vegetation, rock and buildings and so forth, but for species-level classification, the results could not fulfil the demand for accuracy. In terms of supervised classification, the overall classification accuracy of the maximum likelihood algorithm is higher than the minimum distance technique regardless of near-infrared, vegetation stress, red edge or true colour mosaic. It indicates that the maximum likelihood supervised classification is capable to classify vegetation using UAV images mosaics.

Pixel-based and object-based classification.

The object-based classification is more suitable in this study considering the attribute of high resolution for all UAV images mosaics. Leaves at different heights of an individual tree might have slightly different spectral responses to sensors even though they are the same species. According to the spectral data, a classification technique is more likely to classify the individual tree as being of several classes. Applying the object-based classification idea, an individual tree would be segmented as one object and assigned with the mean spectral value. Through this method, one individual tree would no longer be misclassified as several species, resulting in higher accuracy.

However, the procedure of object segmentation is important for the final result. How to balance the values of segmentation with merge level is the critical point. Similarly, the quality of mosaic would affect the result of object segmentation as well.

Classification results.

The final results of this thesis illustrate a few interesting points regarding the different types of mosaic. Firstly, the true colour images mosaics and vegetation stress images mosaics produced better results. Secondly, seasons did not have a strong impact on the classification results since the results of the vegetation stress mosaic in winter is more accurate than summer; while the result of the near-infrared mosaic in winter is more accurate than in summer.

Finally, it is necessary to mention that only nine species of vegetation were determined along the south boundary of the research bush site. There might be trees belonging to other species beyond the reach of the field data collection.

5.6 Normalized Difference Vegetation Index Value Calculation and Processing

5.6.1 NDVI and ENDVI Scripts

There are two potential ways to acquire the NDVI and ENDVI maps of the mosaic by running the ImageJ software. The first one is to run the NDVI and ENDVI scripts directly using the mosaic of the vegetation stress images. The other option is to run the original and individual images from the camera with the scripts; then the NDVI and ENDVI processed images could be used for mosaic processing. However, after the attempts of both methods, it was proven that the second method is unsuccessful. In fact, when they were processed with the ImageJ software, the UAV images could not be computed by the Pix4UAV any more thus it was difficult to acquire the full view mosaic. So it is recommended to process the mosaic firstly and then compute it using the ImageJ software with the NDVI and ENDVI scripts.

6 Conclusion

The study set out to develop a method of using images from unmanned aerial vehicles to classify vegetation on private land at species level and has successfully produced the final classification of the research bush site by using the object-based supervised classification method. This thesis has also sought to find out whether the limitations of traditional satellite imagery remote sensing on private land could be addressed by high resolution, low cost and fast speed UAV remote sensing, particularly whether the UAV imagery could be successfully mosaicked and which classification techniques could provide the most accurate vegetation classification. The general theoretical and methodological literature on this subject, and especially in the field of species-level classification using UAV imagery, is uncomprehensive in respect of answering several questions. This project sought to answer the question of “Can small, inexpensive, autonomous UAVs acquire sufficiently high quality data that can be used to mosaic and produce accurate vegetation classification on small areas of private land at species level?” by completing several objectives.

The results of this project provide some ideas about the best methods to use and advantages as well as limitations of vegetation classification by using UAV imagery. All the methods which were applied in this thesis and the results from them built a framework for a systematic methodology of UAV imagery classification from the stages of imagery acquisition, imagery mosaic, vegetation classification to that of accuracy assessment. A significant finding to emerge from this thesis is that the mosaic processed from vegetation stress and true colour sensors images acquired in good weather conditions provide the most accurate classification results with object-based maximum likelihood supervised classification.

The findings of this thesis suggest several important considerations and points of note from the whole research procedure which are summarise here. In the UAV imagery acquisition step, the flight plan has to take the weather and environment conditions into consideration, as they are influential to the success of a project. During the flight, it is always preferable to collect as much overlap imagery as possible for better mosaic results. The flight route should cover the whole research region to maintain the integrity of the area. When conducting the field experiment, the field data sampling area should be sufficiently large. When using the Pix4UAV software, the setting needs to be adjusted according to the types of data and mosaic purpose for better result. A good quality UAV imagery mosaic is the fundamental requirement of a successful classification. Furthermore, the setting of the classification

algorithm is particularly important as a different setting would result in various inaccurate results. It is also very important to calculate a suitable value of image segmentation of object-based classification. In the accuracy assessment, try to use comprehensive and consistent ground truth data for all classification results. Finally, in order to calculate the NDVI value by using the UAV imagery mosaic, it is important to ensure that the data acquisition time, shooting angle, sunlight, temperature and environmental conditions of the UAV images are consistent.

The present study makes several noteworthy contributions to UAV remote sensing use in New Zealand as it is the first academic project aiming at using UAV techniques to classify vegetation at the species level. Additionally, this project also fills the gap in the literature by developing a set of systematic methods of UAV techniques for vegetation classification which combines the methodology of UAV imagery and imagery classification from the existing literature. The empirical findings in this study also provide new understandings of the pros and cons of pixel-based and object-based classification using UAV imagery mosaics. This research also explores and confirms the utility of the UAV imagery mosaic software Pix4UAV, verifying the potential contributions of this fast speed, high accuracy and automatic software to UAV remote sensing techniques.

Nevertheless, the generalizability of the results in this thesis is subject to certain limitations. For example, the restricted sampling size of the training data and ground truth data inevitably affect the final accuracy to some extent. Also, there are limitations in terms of the classification methods used; some other classification such as the rule-based classification and other algorithms of supervised classification might produce more accurate results, but have not been tested in this project.

This research has thrown up many questions in need of further study. A greater variety of sensors should be tested such as the hyper-spectral or multi-spectral camera to verify whether these more advanced sensors are capable and suitable for UAV imagery vegetation classification.

7 References

- Alatorre, L. C., Sánchez-Andrés, R., Cirujano, S., Beguerá, S., & Sánchez-Carrillo, S. (2011). Identification of Mangrove Areas by Remote Sensing: The ROC Curve Technique Applied to the Northwestern Mexico Coastal Zone Using Landsat Imagery. *Remote Sensing*, 3(8), 1568-1583.
- Allan, M. G., Hamilton, D. P., Hicks, B. J., & Brabyn, L. (2011). Landsat remote sensing of chlorophyll a concentrations in central North Island lakes of New Zealand. *International Journal of Remote Sensing*, 32(7), 2037-2055. doi:10.1080/01431161003645840
- Andersen, J. K. (2006). *Comparison of two classification methods for vegetation mapping in palau*. Available from ProQuest Dissertations & Theses Global. (304905165). Retrieved from <http://ezproxy.aut.ac.nz/login?url=http://search.proquest.com/docview/304905165?accountid=8440>
- Ashraf, S. L. B. J. C. K. (2010). Satellite remote sensing for mapping vegetation in New Zealand freshwater environments: A review [Article]. *New Zealand Geographer*, 66(1), 33-43. doi:10.1111/j.1745-7939.2010.01168.x
- Auckland Council. (2013). *2013 Freshwater Report Card Dairy Flat Reporting Area*. Retrieved from <http://stateofauckland.aucklandcouncil.govt.nz/freshwater-report-card/dairy-flat-reporting-area-2013/>
- Auckland Council. (n.d.). *Voluntary protection of natural area on private land*. Retrieved from <http://www.aucklandcouncil.govt.nz/EN/environmentwaste/naturalenvironment/Documents/voluntaryprotectionofnaturalareasonprivateland.pdf>
- Auckland University of Technology. (2012). *Big brother keeps an eye on NZ environment*. Retrieved from <http://www.aut.ac.nz/news/aut-news/2012/july/big-brother-keeps-an-eye-on-nz-environment>
- Baatz, M., Benz, U., Dehghani, S., Heynen, M., Holtje, A., Hofmann, P., . . . Weber, M. (2004). *eCognition Professional User Guide 4*. Retrieved from <http://www.gis.unbc.ca/help/software/ecognition4/ELUserguide.pdf>
- Baker, B., & Stuart, N. (2009). CIVILIAN UAVS: Eye in the sky. *The Engineer*, 18-22.
- Baldeck, C., & Asner, G. (2013). Estimating Vegetation Beta Diversity from Airborne Imaging Spectroscopy and Unsupervised Clustering. *Remote Sensing*, 5(5), 2057-2071.
- Baldwin, C., Evan. (n.d.). *Unmanned Aerial Vehicles: Examining the Safety, Security, Privacy and Regulatory*. Retrieved from www.ncpa.org/pdfs/sp-Drones-long-paper.pdf
- Bannari, A., Morin, D., Bonn, F., & Huete, A. R. (1995). A review of vegetation indices. *Remote Sensing Reviews*, 13(1-2), 95-120. doi:10.1080/02757259509532298
- Bean, D. (n.d.). *Classifying Vegetation Using Remote Sensing*. Retrieved from http://www.geog.ubc.ca/courses/geog570/talks_2000/classifyingvegetation.htm
- Belliss, S. E. (1984). Remote sensing in New Zealand A status report†. *International Journal of Remote Sensing*, 5(6), 877-881. doi:10.1080/01431168408948874
- Blaschke, P. M., Hunter, G. G., Eyles, G. O., & Van Berkel, P. R. (1981). *Analysis of New Zealand's Vegetation Cover Using Land Resource Inventory Data*. Retrieved from http://newzealandecology.org/nzje/free_issues/NZJEcol4_1.pdf
- Braithwaite, R. (2012). The queen of bees. *Light Aviation*, 50-53.

- Bryson, M., Reid, A., Ramos, F., & Sukkarieh, S. (2010). Airborne vision-based mapping and classification of large farmland environments. *Journal of Field Robotics*, 27(5), 632-655. doi:10.1002/rob.20343
- Calvo, S., Ciralo, G., & Loggia, G. L. (2003). Monitoring *Posidonia oceanica* meadows in a Mediterranean coastal lagoon (Stagnone, Italy) by means of neural network and ISODATA classification methods [Article]. *International Journal of Remote Sensing*, 24(13), 2703.
- Carroll, J. (n.d.). *Five ways UAVs are being used by civilians*. Retrieved from <http://www.vision-systems.com/articles/2013/06/five-ways-uavs-are-being-used-by-civilians.html>
- Cho, M. A., Sobhan, I., Skidmore, A. K., & de Leeuw, J. (2008). Discriminating Species Using Hyperspectral Indices at Leaf and Canopy Scales. *Proceedings of the International Society for Photogrammetry and Remote Sensing, XXXVII, Part B7*.
- Civil Aviation Authority of New Zealand. (2007). *Civil Aviation Authority of New Zealand. Issues Paper. Unmanned Aerial Vehicles*. Retrieved from www.caa.govt.nz/ga/uav/uav_issues_paper.pdf
- Civil Aviation Authority of New Zealand. (2013). *Civil Aviation Rules Register Information Leaflet - Edition 4*. Retrieved from www.caa.govt.nz/rules/CARRIL/CARRIL_2013_Edition_04.pdf
- Civil Aviation Authority of New Zealand. (2014). *CAA Consolidation - Transition Rules*. Retrieved from http://www.caa.govt.nz/rules/Rule_Consolidations/Part_019_Consolidation.pdf
- Cochrane, G. R., & Male, A. G. R. (1977). Regional and seasonal patterns of stream sediment discharges along New Zealand coasts from SkyLab and Landsat satellite imagery. *Proceeding of the New Zealand ecological society*, 24, 13-20.
- Cochrane, M. A. (2000). Using vegetation reflectance variability for species level classification of hyperspectral data [Article]. *International Journal of Remote Sensing*, 21(10), 2075-2087. doi:10.1080/01431160050021303
- Colgan, M., Baldeck, C., Féret, J.-B., & Asner, G. (2012). Mapping Savanna Tree Species at Ecosystem Scales Using Support Vector Machine Classification and BRDF Correction on Airborne Hyperspectral and LiDAR Data. *Remote Sensing*, 4(11), 3462-3480.
- Congalton, R. G. (1991). A review of assessing the accuracy of classifications of remotely sensed data. *Remote Sensing of Environment*, 37(1), 35-46.
- Congalton, R. G. (2009). *Assessing the accuracy of remotely sensed data principles and practices*. New York: Lewis Publishers.
- Davis, M., & Meurk, C. (2001). *Protecting and restoring our natural heritage - A practical guide*. Retrieved from <http://www.doc.govt.nz/Documents/conservation/native-plants/motukarara-nursery/restoration-guide-complete.pdf>
- DeFries, & Ruth. (2008). Terrestrial Vegetation in the Coupled Human-Earth System: Contributions of Remote Sensing. *Annual Review of Environment and Resources*, 33, 369-390. doi:10.1146/annurev.enviro.33.020107.113339
- Defries, R. S., & Townshend, J. R. G. (1994). NDVI-derived land cover classifications at a global scale. *International Journal of Remote Sensing*, 15(17), 3567-3586. doi:10.1080/01431169408954345
- Dunford, R., Michel, K., Gagnage, M., PiÉGay, H., & TrÉMelo, M. L. (2009). Potential and constraints of Unmanned Aerial Vehicle technology for the characterization of Mediterranean riparian forest [Article]. *International Journal of Remote Sensing*, 30(19), 4915-4935. doi:10.1080/01431160903023025

- Dymond, J. R., Page, M. J., & Brown, L. J. (1996). Large area vegetation mapping in the Gisborne district, New Zealand, from Landsat TM. *International Journal of Remote Sensing*, 17(2), 263-275. doi:10.1080/01431169608949004
- Everaerts, J. (2008). The Use of Unmanned Aerial Vehicles (UAVS) for Remote Sensing and Mapping. *Proceedings of the Remote Sensing and Spatial Information Sciences, XXXVII, Part B1*.
- ENVI User Guide. (2009).
- Getting Started with ENVI. (2010).
- Exelis Visual Information Solutions. (n.d.). *Calculate Confusion Matrices*. Retrieved from <http://www.exelisvis.com/docs/CalculatingConfusionMatrices.html>
- Förster, M., & Kleinschmit, B. (2009). *Towards an intra annual vegetation analysis the concept of a phenological library*. presented at the meeting of the ISPRS Workshop on High Resolution Earth Imaging for Geospatial Information, Hannover, Germany. Retrieved from http://www.isprs.org/proceedings/XXXVIII/1_4_7-W5/paper/Foerster-173.pdf
- Fahlstrom, P., & Gleason, T. (2012). *Introduction to UAV Systems* (4 ed.). Retrieved from <http://AUT.ebib.com.au/patron/FullRecord.aspx?p=967284>
- Fisher, D. (2013). *Police use drones to catch criminals*. Retrieved from http://www.nzherald.co.nz/nz/news/article.cfm?c_id=1&objectid=10868674
- Frink, S. (n.d.). *The Future of UAV Technology Aims High*. Retrieved from <http://www.militaryaerospace.com/blogs/aerospace-defense-blog/2012/04/the-future-of-uav-technology-aims-high.html>
- Fyfe, S. K. (2003). Spatial and temporal variation in spectral reflectance: Are seagrass species spectrally distinct? *Limnol. Oceanogr.*, 48(1, part 2), 2003, 464-479.
- Gao, J. (1999). A comparative study on spatial and spectral resolutions of satellite data in mapping mangrove forests [Article]. *International Journal of Remote Sensing*, 20(14), 2823-2833. doi:10.1080/014311699211813
- Gay, A. P., Steward, T. P., Angel, R., Easey, M., Eves, A. J., Thomas, N. J., . . . Kemp, A. I. (2009). Developing Unmanned Aerial Vehicles for Local and Flexible Environmental and Agricultural Monitoring Symposium conducted at the meeting of the Proceedings of RSPSoc 2009 Annual Conference, Leicester, UK. Retrieved from http://cadair.aber.ac.uk/dspace/bitstream/handle/2160/4573/RSPSoc2009_209_Gay.pdf?sequence=1.
- Gibbes, C., Adhikari, S., Rostant, L., Southworth, J., & Qiu, Y. (2010). Application of Object Based Classification and High Resolution Satellite Imagery for Savanna Ecosystem Analysis. *Remote Sensing*, 2(12), 2748-2772.
- Government of New Zealand. (n.d.). *CASE STUDY: INCENTIVE MEASURES PROTECTION OF NATURAL HERITAGE ON PRIVATE LAND*. Retrieved from <http://www.cbd.int/doc/case-studies/inc/cs-inc-nz-en.pdf>
- Hamilton, D. (1977). Remote Sensing by Satellite: What Future for an International Regime? *The American Journal of International Law*, 71(4), 707-724. doi:10.2307/2199582
- Hanna, M. M., Steyn-Ross, D. A., & Steyn-Ross, M. (1999). Estimating Biomass for New Zealand Pasture Using Optical Remote Sensing Techniques. *Geocarto International*, 14(3), 89-94. doi:10.1080/10106049908542121
- Harley, G. (2012). *Drone Countdown*. Retrieved from <https://www.cdt.org/blogs/harley-geiger/2703drone-countdown>
- Hartley, J. (2003). Earth Remote Sensing Technologies in the Twenty-First Century. *Proceedings of the Geoscience and Remote Sensing Symposium, 2003, 1*, 627-629
- Hestir, E. L., Khanna, S., Andrew, M. E., Santos, M. J., Viers, J. H., Greenberg, J. A., . . . Ustin, S. L. (2008). Identification of invasive vegetation using hyperspectral remote

- sensing in the California Delta ecosystem. *Remote Sensing of Environment*, 112(11), 4034-4047.
- Hexmoor, H., Rahimi, S., & Little, J. T. (2009). Coordinated UAV Manoeuvring Flight Formation [Article]. *Informatica (03505596)*, 33(3), 375-383.
- Hill, R. A., Wilson, A. K., George, M., & Hinsley, S. A. (2010). Mapping tree species in temperate deciduous woodland using time-series multi-spectral data [Article]. *Applied Vegetation Science*, 13(1), 86-99. doi:10.1111/j.1654-109X.2009.01053.x
- Hunt, E. R., Hively, W. D., Fujikawa, S., Linden, D., Daughtry, C. S., & McCarty, G. (2010). Acquisition of NIR-Green-Blue Digital Photographs from Unmanned Aircraft for Crop Monitoring. *Remote Sensing*, 2(1), 290-305.
- International Association for Vegetation Scientists (IAVS). (n.d.). *What is vegetation classification?* Retrieved from <https://sites.google.com/site/vegclassmethods/about>
- IntraSearch. (n.d.). *Satellite Image Maps - Pricing*. Retrieved from <http://www.mapmart.com/Products/SatelliteImagery/SatelliteImageMaps.aspx>
- Ishihama, F., Watabe, Y., & Oguma, H. (2012). Validation of a high-resolution, remotely operated aerial remote-sensing system for the identification of herbaceous plant species. *Applied Vegetation Science*, 15(3), 383-389. doi:10.1111/j.1654-109X.2012.01184.x
- Israel, S., & Fyfe, J. (1996). *Determining the Sensitivity of SPOT XS Imagery for Monitoring Intertidal and Sublittoral Vegetation of Otago Harbour*. Retrieved from <http://www.doc.govt.nz/documents/science-and-technical/casn131.pdf>.
- Jones, N. (2013). *Drones: Secrets in our skies*. Retrieved from http://www.nzherald.co.nz/nz/news/article.cfm?c_id=1&objectid=10874979
- Kim, J.-h., Lee, D. w., Cho, K.-r., Jo, S.-y., Kim, J.-h., Min, C.-o., . . . Cho, S.-j. (2010). Development of an electro-optical system for small UAV. *Aerospace Science and Technology*, 14(7), 505-511. doi:<http://dx.doi.org/10.1016/j.ast.2010.03.006>
- Kyriakidis, P., & Dungan, J. (2001). A geostatistical approach for mapping thematic classification accuracy and evaluating the impact of inaccurate spatial data on ecological model predictions. *Environmental and Ecological Statistics*, 8(4), 311-330. doi:10.1023/a:1012778302005
- Landcare Research. (n.d.). *Naturally uncommon ecosystems*. Retrieved from <http://www.landcareresearch.co.nz/publications/factsheets/rare-ecosystems>
- Laurent, G. (2012). *Photogramm rie par drone trait e   l'aide de pix4UAV Cloud Pro*. Retrieved from <http://pix4d.com/downloads/mine.pdf>
- LDP LLC. (n.d.-a). Enhanced Normalized Difference Vegetation Index (ENDVI).
- LDP LLC. (n.d.-b). *Vegetation Stress II* Retrieved from http://maxmax.com/vegetation_stress_mkii.htm
- Lewis, D., Phinn, S., & Arroyo, L. (2013). Cost-Effectiveness of Seven Approaches to Map Vegetation Communities — A Case Study from Northern Australia's Tropical Savannas. *Remote Sensing*, 5(1), 377-414.
- Long, J. B., & Giri, C. (2011). Mapping the Philippines' Mangrove Forests Using Landsat Imagery. *Sensors*, 11(3), 2972-2981.
- Longley, R. (2013). *Unmanned Aircraft Used in the United States*. Retrieved from <http://usgovinfo.about.com/od/rightsandfreedoms/a/Unmanned-Aircraft-Used-In-The-United-States.htm>
- Lucieer, A., Robinson, S., Turner, D., Harwin, S., & Keleey, J. (2012). Using A Micro-UAV For Ultra-High Resolution Multi-Sensor Observation of Antarctic Moss Beds. *International Journal of Applied Earth Observation and Geoinformation*, 27(Part A), 53-62.

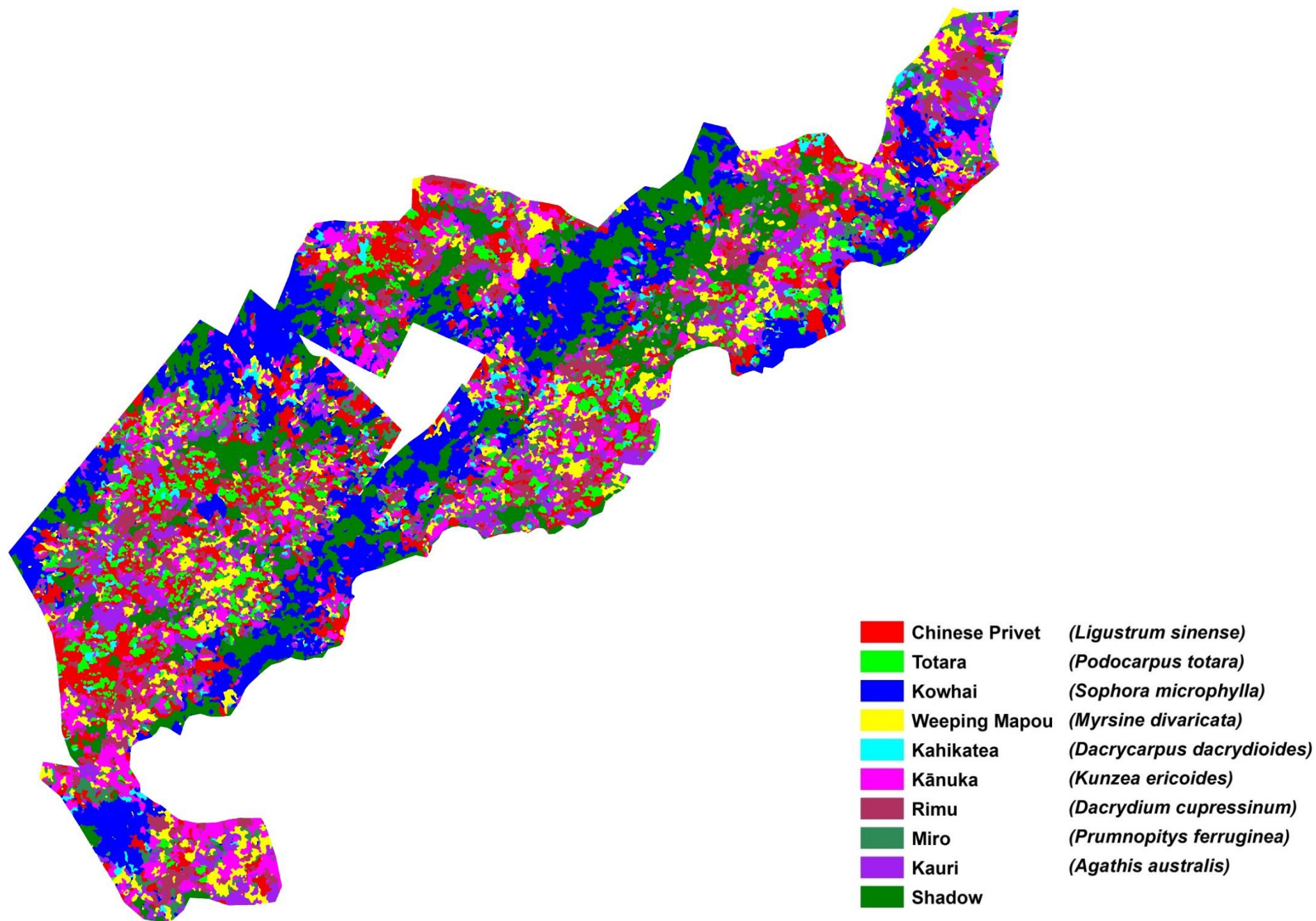
- Mackay, L. (n.d.). *Classifying the Terrestrial Environment using Optical Earth Observed Images*. Retrieved from <http://www.geog.leeds.ac.uk/courses/level2/geog2750/Lecture6.doc>
- Migone, P. (2012). *Drones 'not match ready' Pilots' Association says* Retrieved from <http://www.stuff.co.nz/technology/gadgets/7696350/Drones-not-match-ready-Pilots-Association-says>
- Ministry for the Environment. (2010). *Lagelly protected conservation land in New Zealand*. Retrieved April 18, 2014, from <http://www.mfe.govt.nz/environmental-reporting/land/area-native-land-cover-indicator/legally-protected-conservation-land.html>
- Mitchell, J. J., Glenn, N. F., Anderson, M. O., Hruska, R. C., Halford, A., Baun, C., & Nydegger, N. (2012). *Unmanned Aerial Vehicle (UAV) Hyperspectral Remote Sensing for Dryland Vegetation Monitoring*. Retrieved from http://bcal.geology.isu.edu/docs/UAV_Hyperspectral.pdf.
- Mowrer, H. T. (2000). Quantifying spatial uncertainty in natural resources; theory and applications for GIS and remote sensing. *Scitech Book News*, 24(2).
- Murthy, C. A., Chatterjee, N., Shankar, B. U., & Majumder, D. D. (1992, 30 Aug-3 Sep 1992). IRS image segmentation: minimum distance classifier approach Symposium conducted at the meeting of the Pattern Recognition, 1992. Vol.I. Conference A: Computer Vision and Applications, Proceedings., 11th IAPR International Conference on doi:10.1109/icpr.1992.201676
- National Aeronautics and Space Administration. (2013). *Perspectives on Unmanned Aircraft classification for civil airworthiness standards*. Retrieved from <http://shemesh.larc.nasa.gov/people/jmm/NASA-TM-2013-217969.pdf>
- Nikolos, I., Zografos, E., & Brintaki, A. (2007). UAV Path Planning Using Evolutionary Algorithms. In J. Chahl, L. Jain, A. Mizutani, & M. Sato-Ilic (Eds.), *Innovations in Intelligent Machines - 1* (Vol. 70, pp. 77-111): Springer Berlin Heidelberg. doi:10.1007/978-3-540-72696-8_4
- Oldeland, J., Dorigo, W., Wesuls, D., & Jürgens, N. (2010). Mapping Bush Encroaching Species by Seasonal Differences in Hyperspectral Imagery. *Remote Sensing*, 2(6), 1416-1438.
- Oleire-Oltmanns, S., Marzloff, I., Peter, K., & Ries, J. (2012). Unmanned Aerial Vehicle (UAV) for Monitoring Soil Erosion in Morocco. *Remote Sensing*, 4(11), 3390-3416.
- Oruc, M., Marangoz, A. M., & Buyuksalih, G. (2004). *Comparison of Pixel-Based and Object-Oriented Classification Approaches Using Landsat-7 ETM Spectral Bands*. Retrieved from <http://www.isprs.org/proceedings/XXXV/congress/comm4/papers/510.pdf>
- Penn State University. (n.d.). *Object-Oriented Image Classification Methods*. Retrieved from <https://www.e-education.psu.edu/geog883kls/node/523>
- Pix4UAV User Guide*. (n.d.-a).
- Pix4D. (n.d.-b). *Use Cases*. Retrieved May 28, 2013, from <http://pix4d.com/showcase.html>
- Price, J. C. (1994). How unique are spectral signatures? *Remote Sensing of Environment*, 49(3), 181-186.
- Queen Elizabeth II National Trust. (2013). *Annual Report 2013*. Retrieved from <http://www.openspace.org.nz/includes/download.aspx?ID=130715>
- Queen Elizabeth II National Trust. (n.d.). *About covenanting*. Retrieved from http://www.openspace.org.nz/Site/About_covenanting/default.aspx
- RD Collins & Associates. (n.d.). *UAV Privacy Concerns*. Retrieved from [http://www.rdcollins.com.au/_blog/Unmanned_Aerial_Vehicles_\(UAV\)/post/uav-privacy-concerns/](http://www.rdcollins.com.au/_blog/Unmanned_Aerial_Vehicles_(UAV)/post/uav-privacy-concerns/)

- Richards, J. A., & Jia, X. (2006). *Remote sensing digital image analysis :an introduction*. Retrieved from <http://aut.lconz.ac.nz/vwebv/holdingsInfo?bibId=1010056>
- Ruiliang, P., Peng, G., Yong, T., Xin, M., Carruthers, R. I., & Anderson, G. L. (2008). Using classification and NDVI differencing methods for monitoring sparse vegetation coverage: a case study of saltcedar in Nevada, USA [Article]. *International Journal of Remote Sensing*, 29(14), 3987-4011. doi:10.1080/01431160801908095
- Samad, A. M., Kamarulzaman, N., Hamdani, M. A., Mastor, T. A., & Hashim, K. A. (2013, 19-20 Aug. 2013). The potential of Unmanned Aerial Vehicle (UAV) for civilian and mapping application Symposium conducted at the meeting of the System Engineering and Technology (ICSET), 2013 IEEE 3rd International Conference on doi:10.1109/ICSEngT.2013.6650191
- Saunders, C. (1996). Conservation covenants in New Zealand. *Land Use Policy*, 13(4), 325-329.
- Shen, Y., Li, J., Mantena, V., & Jakkula, S. (2009). Seasonal Adaptation of Vegetation Color in Satellite Images for Flight Simulations. *Journal of Intelligent Learning Systems and Applications*, 1(1), 42-42.
- Skoglar, P., Orguner, U., Törnqvist, D., & Gustafsson, F. (2012). Road Target Search and Tracking with Gimbaled Vision Sensor on an Unmanned Aerial Vehicle. *Remote Sensing*, 4(7), 2076-2111.
- SKYCAM UAV. (n.d.-a). *Ground Control System*. Retrieved from <http://www.kahunet.co.nz/gcs-system.html>
- SKYCAM UAV. (n.d.-b). *KAHU UAV UNMANNED AERIAL SYSTEMS (UAS)*. Retrieved from <http://www.kahunet.co.nz/kahu-uav.html>
- SKYCAM UAV. (n.d.-c). *SWAMPFOX UAV*. Retrieved from <http://www.kahunet.co.nz/swampfox-uav.html>
- Strecha, C. (2011). *The accuracy of automated photogrammetric techniques on ultra-light UAV imagery*. presented at the meeting of the Unmanned Aerial Vehicle in Geomatics, Zürich. Retrieved from www.pix4d.com/downloads/pix4uav_accuracy.pdf
- Strecha, C., Fletcher, A., Lechner, A., Erskine, P., & Fua, P. (2012). DEVELOPING SPECIES SPECIFIC VEGETATION MAPS USING MULTI-SPECTRAL HYPERSPECTRAL IMAGERY FROM UNMANNED AERIAL VEHICLES. *ISPRS Ann. Photogramm. Remote Sens. Spatial Inf. Sci.*, 1-3, 311-316. doi:10.5194/isprsannals-I-3-311-2012
- Titus, J. (2007). Filters improve images. *Test & Measurement World*, 27(4), 19.
- UAVPEOPLE. (n.d.). *Pix4D-Pix4UAV*. Retrieved from <http://www.uavpeople.com/resources/software-reviews/28-pix4d-pix4uav>
- Universiti Kebangsaan Malaysia. (n.d.). *Introduction to Remote Sensing*. Retrieved from <http://www.ukm.my/eoc/e-learning/remote%20sensing/Remote%20Sensing%20Extra%20Notes/classification1.ppt>
- Vassilaros, A. (n.d.). *ISODATA*. Retrieved from http://web.pdx.edu/~jduh/courses/Archive/geog481w07/Students/Vassilaros_ISODATA.pdf
- Vehmas, M., Erik änen, K., Peuhkurinen, J., Packal  n, P., & Maltamo, M. (2011). Airborne Laser Scanning for the Site Type Identification of Mature Boreal Forest Stands. *Remote Sensing*, 3(1), 100-116.
- Verbyla, D., & Hammond, T. (n.d.). *How To Lie With An Error Matrix*. Retrieved from <http://nrm.salrm.uaf.edu/~dverbyla/online/errormatrix.html>
- Verbyla, D. L. (1986). Potential prediction bias in regression and discriminant analysis. *Canadian Journal of Forest Research*, 16(6), 1255-1257. doi:10.1139/x86-222

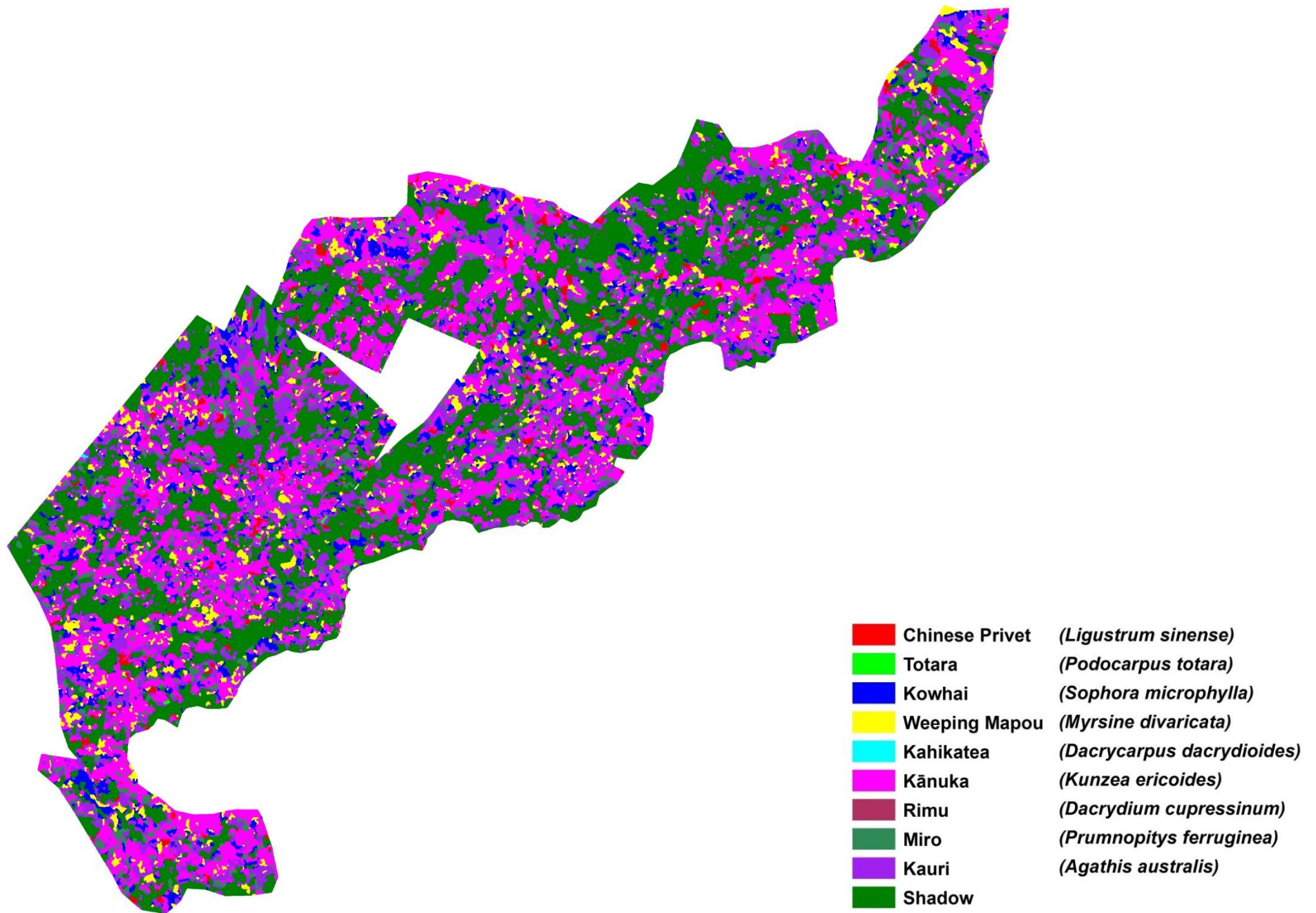
- Verbyla, D. L., & Hammond, T. O. (1995). Conservative bias in classification accuracy assessment due to pixel-by-pixel comparison of classified images with reference grids. *International Journal of Remote Sensing*, 16(3), 581-587. doi:10.1080/01431169508954424
- Weeks, E. S., Ausseil, A.-G. E., Shepherd, J. D., & Dymond, J. R. (2013). Remote sensing methods to detect land-use/cover changes in New Zealand's 'indigenous' grasslands. *New Zealand Geographer*, 69(1), 1-13. doi:10.1111/nzg.12000
- Weibel, R. E., & Hansman, R. J. (2006). *Safety Considerations for Operation of Unmanned Aerial Vehicles in the National Airspace System*. Retrieved from <http://dspace.mit.edu/bitstream/handle/1721.1/34912/Weibel%20-%20ICAT%20Report%20-%20UAV%20Safety.pdf>
- Whiteside, T., & Ahmad, W. (2005). *A Comparison of Object-Oriented and Pixel-Based Classification Methods for Mapping Land Cover in Northern Australia*. presented at the meeting of the Spatial Sciences Conference, Melbourne. Retrieved from http://www.ecognition.com/sites/default/files/273_0168.pdf
- Wildi, & Otto. (2010). *Data Analysis in Vegetation Ecology* (1 ed.). Retrieved from <http://AUT.ebib.com.au/patron/FullRecord.aspx?p=514474>
- Willhauck, G. (2000). Comparison of object oriented classification techniques and standard image analysis for the use of change detection between SPOT multispectral satellite images and aerial photos. *International Archives of Photogrammetry and Remote Sensing, Vol. XXXIII, Part B3*.
- WWF. (2012). *Unmanned Aerial Vehicle to aid Nepal's Conservation Efforts*. Retrieved from <http://wwf.panda.org/?205266/Unmanned-Aerial-Vehicle-to-aid-Nepals-Conservation-Efforts>
- Xiang, H., & Tian, L. (2011). Development of a low-cost agricultural remote sensing system based on an autonomous unmanned aerial vehicle (UAV). *Biosystems Engineering*, 108(2), 174-190.
- Xie, Y., Sha, Z., & Yu, M. (2008). Remote sensing imagery in vegetation mapping: a review. *Journal of Plant Ecology*, 1(1), 9-23. doi:10.1093/jpe/rtm005
- Yu, Q. (2005). *Object-based vegetation classification with high resolution remote sensing imagery* (Ph.D.). University of California, Berkeley, United States -- California. Retrieved from <http://ezproxy.aut.ac.nz/login?url=http://search.proquest.com/docview/305032517?accountid=8440>. Available from ProQuest Dissertations & Theses Full Text database.
- Zhang, S., Lei, Y., Wang, L., Li, H., & Zhao, H. (2011). Crop classification using MODIS NDVI data denoised by wavelet: A case study in Hebei Plain, China. *Chinese Geographical Science*, 21(3), 322-333. doi:10.1007/s11769-011-0472-2
- Zlinszky, A., Mücke, W., Lehner, H., Briese, C., & Pfeifer, N. (2012). Categorizing Wetland Vegetation by Airborne Laser Scanning on Lake Balaton and Kis-Balaton, Hungary. *Remote Sensing*, 4(6), 1617-1650.

Appendix A. Object-based Classification

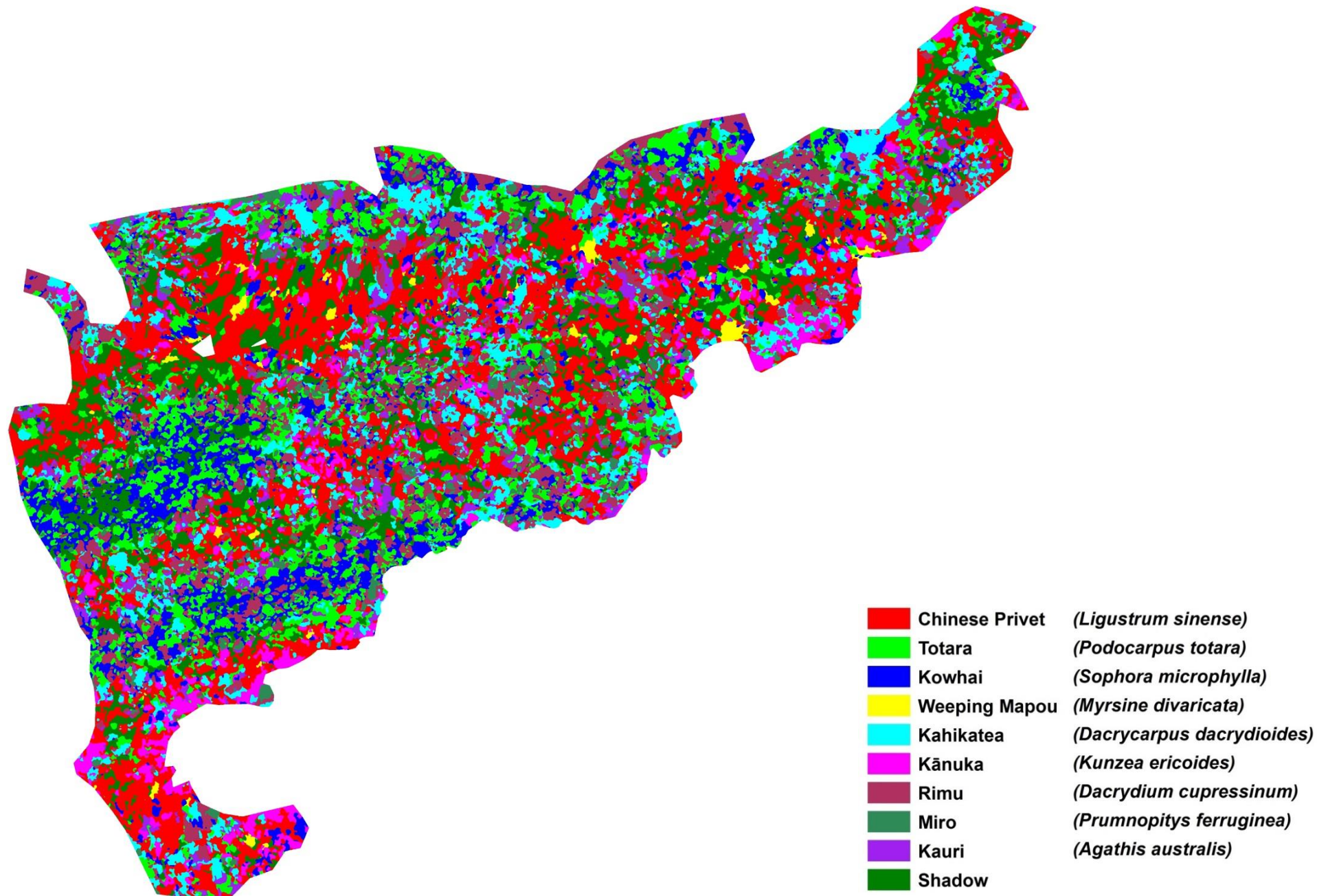
Appendix A.1. (Object-based) Maximum likelihood supervised classification of near-infrared images mosaic acquired on 28 July, 2013



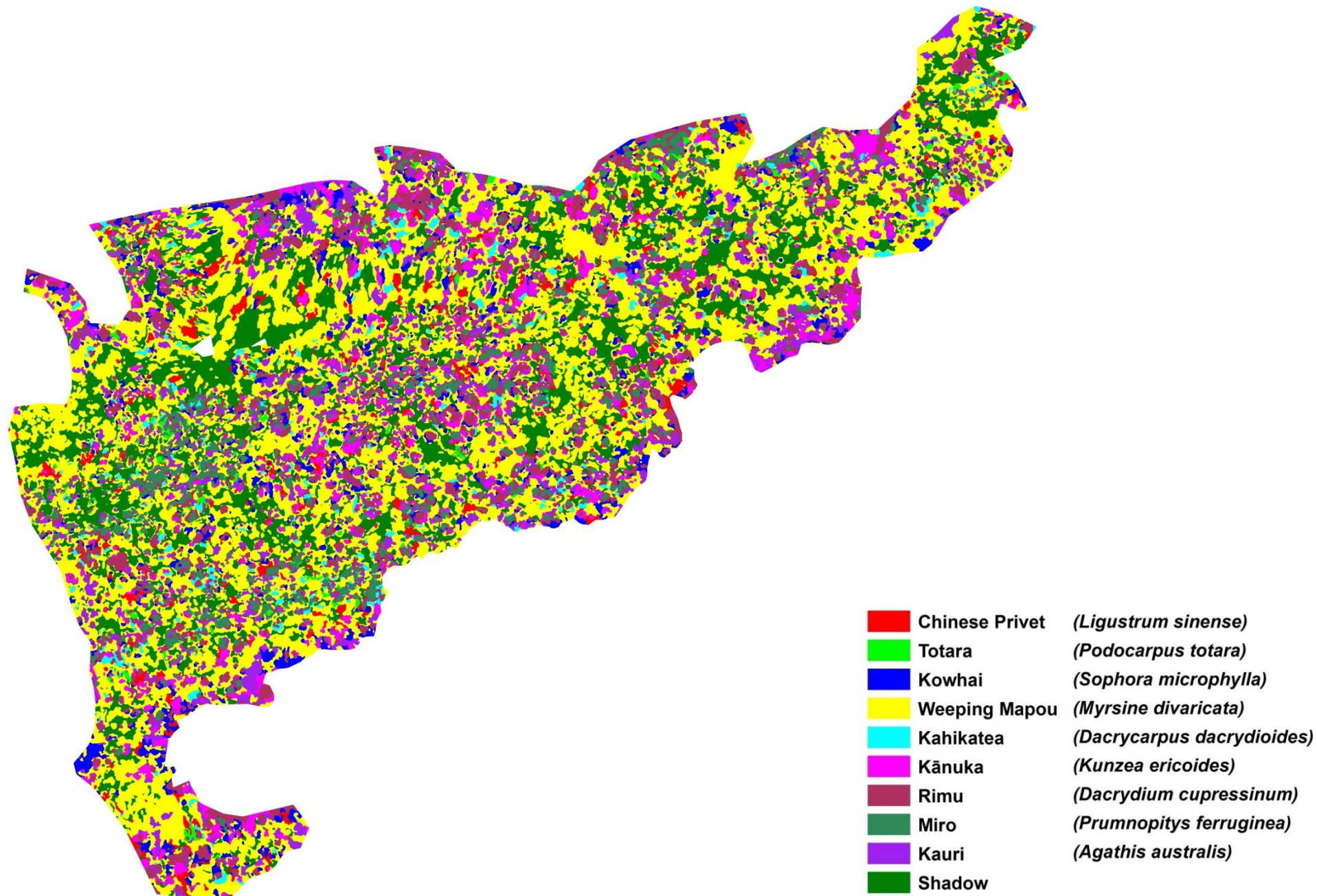
Appendix A.2. (Object-based) Minimum distance supervised classification of near-infrared images mosaic acquired on 28 July, 2013



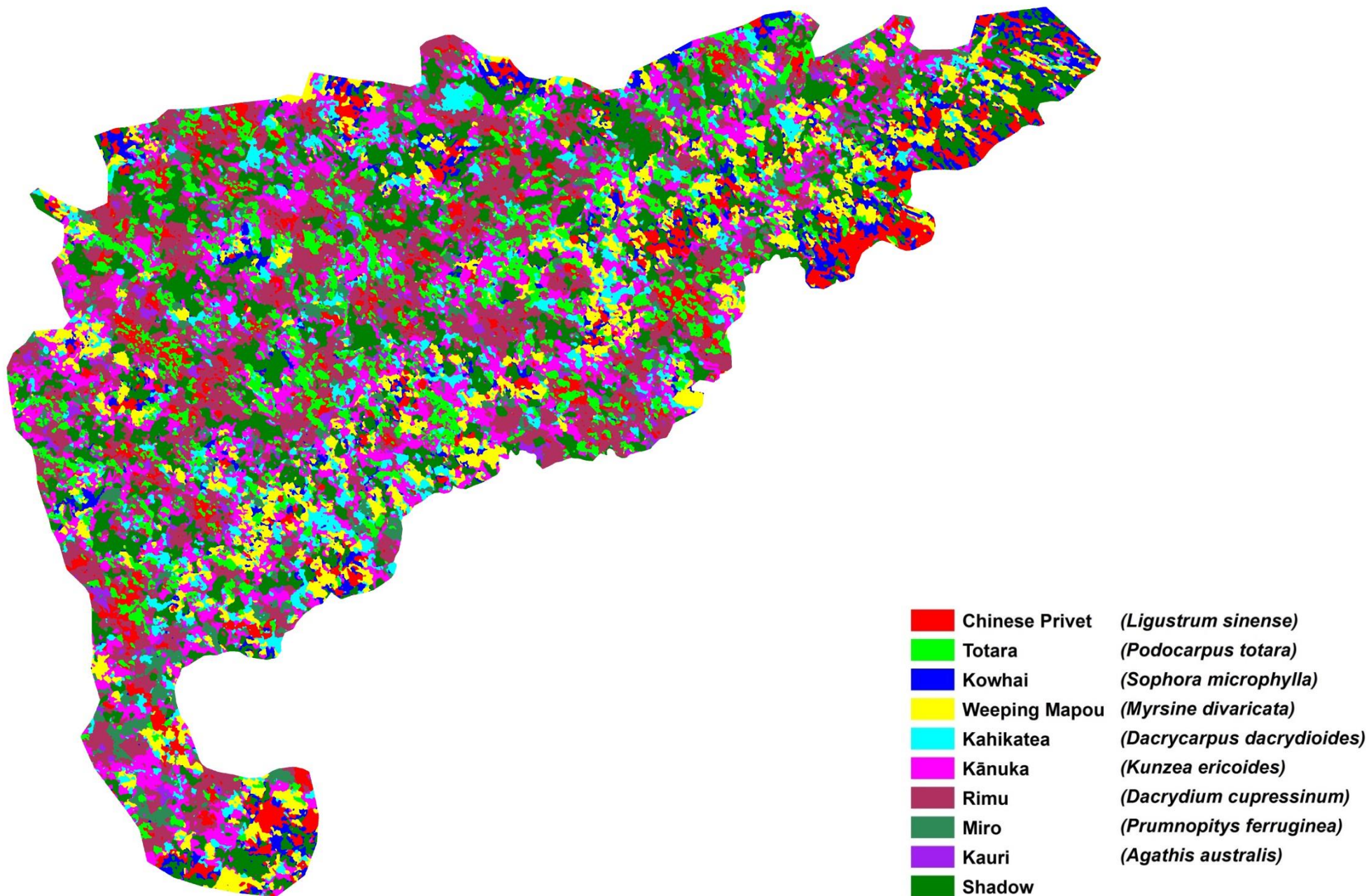
Appendix A.3. (Object-based) Maximum likelihood supervised classification of near-infrared images mosaic acquired on 8 August, 2013



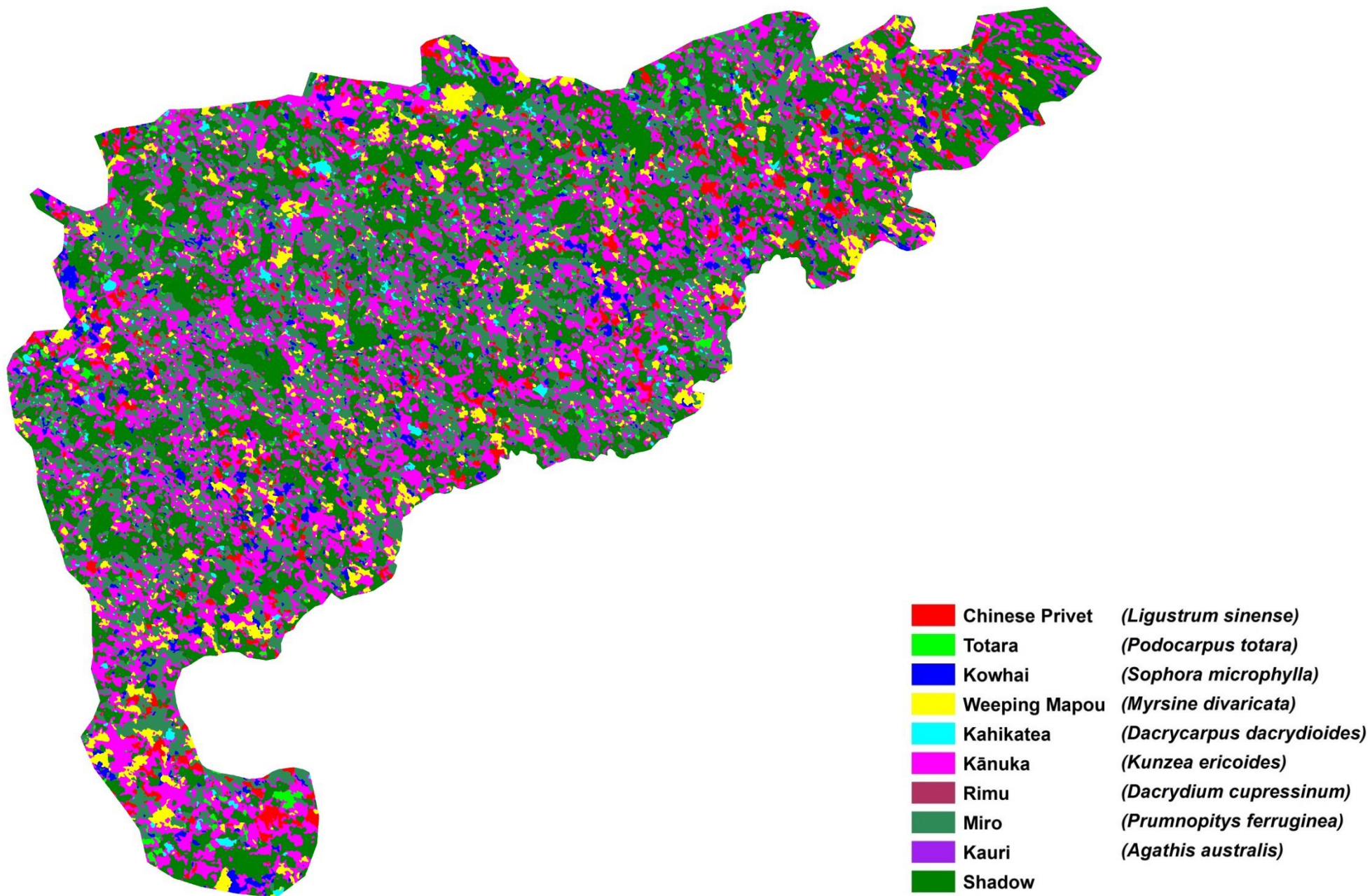
Appendix A.4. (Object-based) Minimum distance supervised classification of near-infrared images mosaic acquired on 8 August, 2013



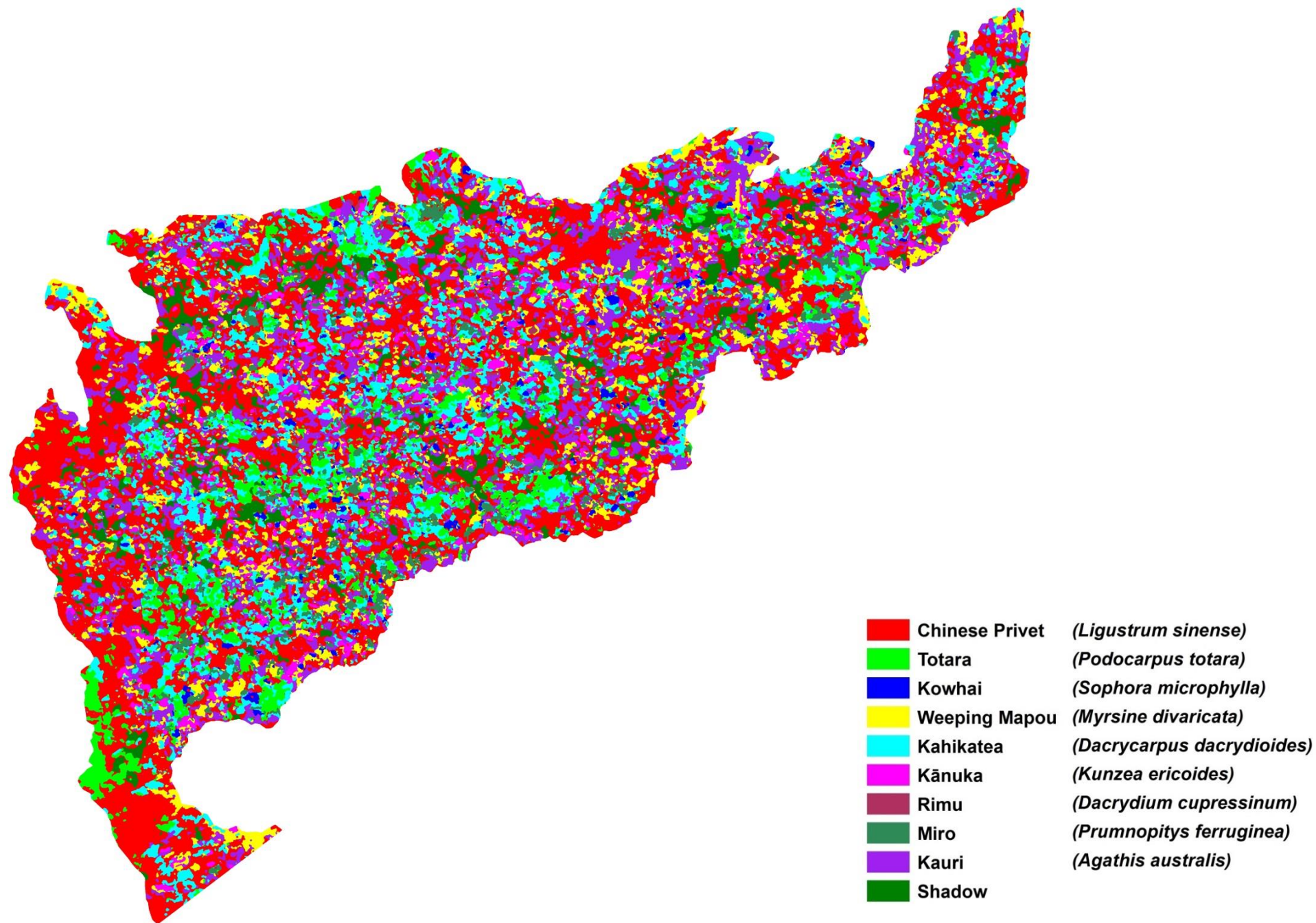
Appendix A.5. (Object-based) Maximum likelihood supervised classification of near-infrared images mosaic acquired on 1 April, 2014 (flight 2)



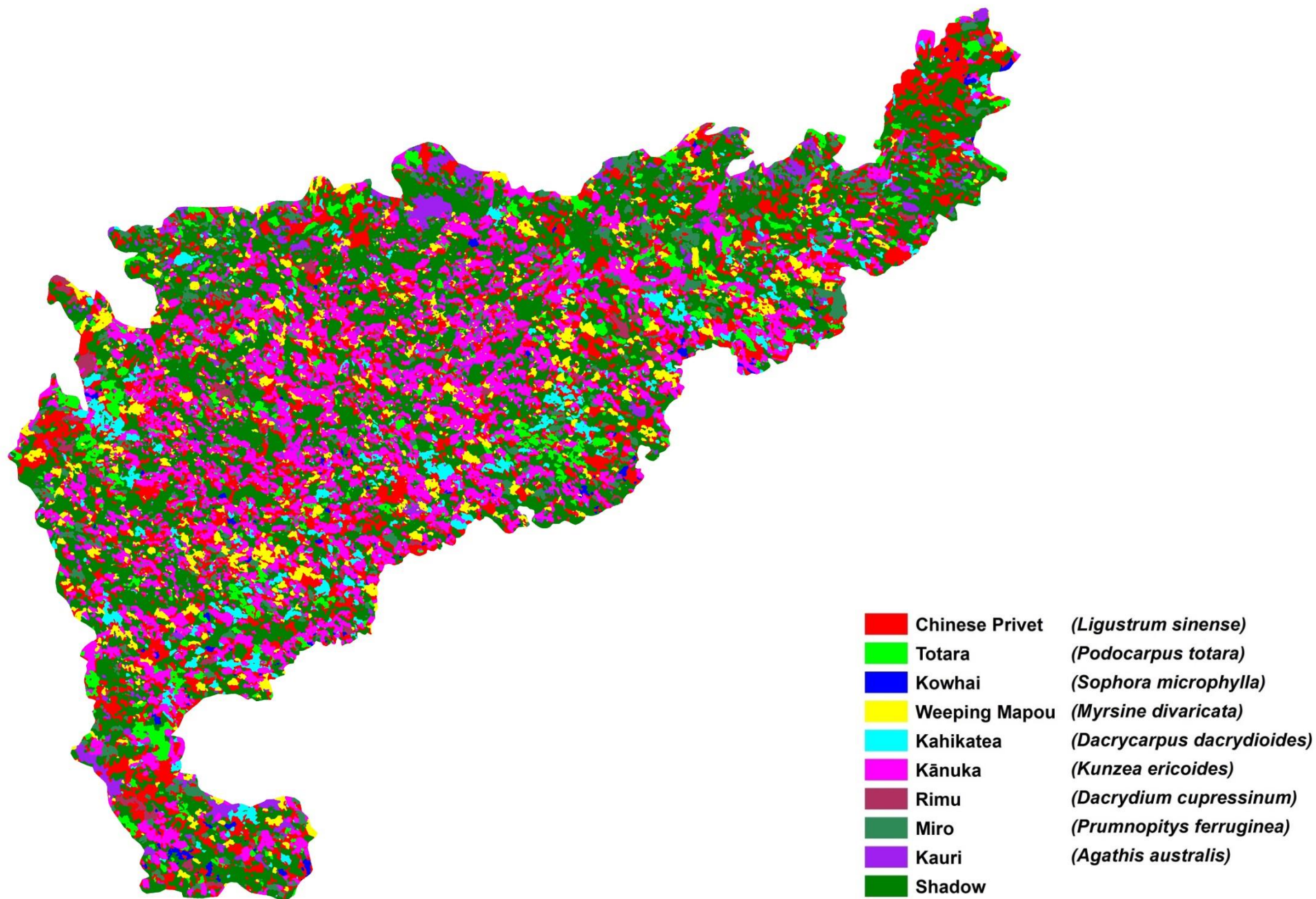
Appendix A.6. (Object-based) Minimum distance supervised classification of near-infrared images mosaic acquired on 1 April, 2014 (flight 2)



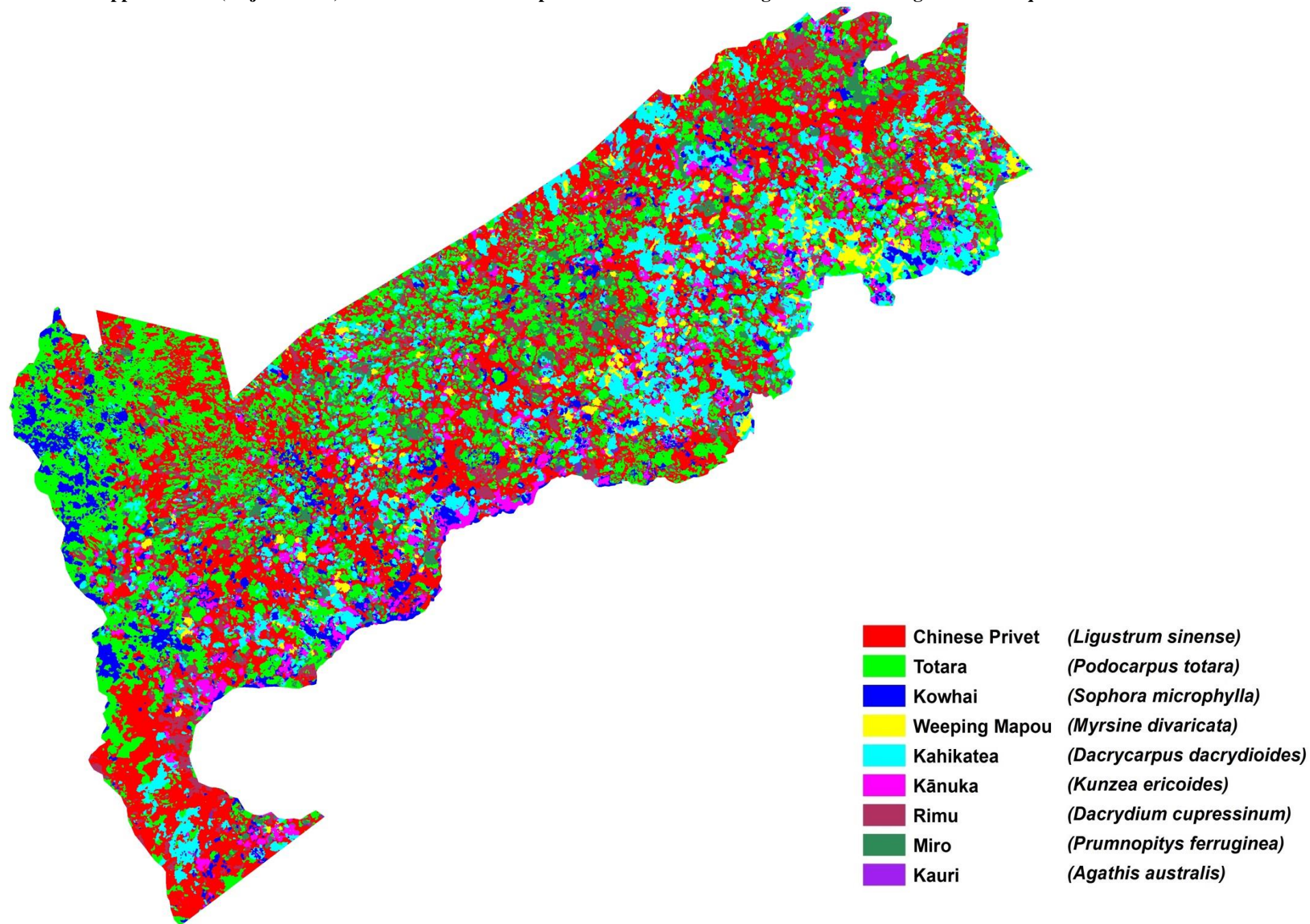
Appendix A.7. (Object-based) Maximum likelihood supervised classification of red edge images mosaic acquired on 8 August, 2013



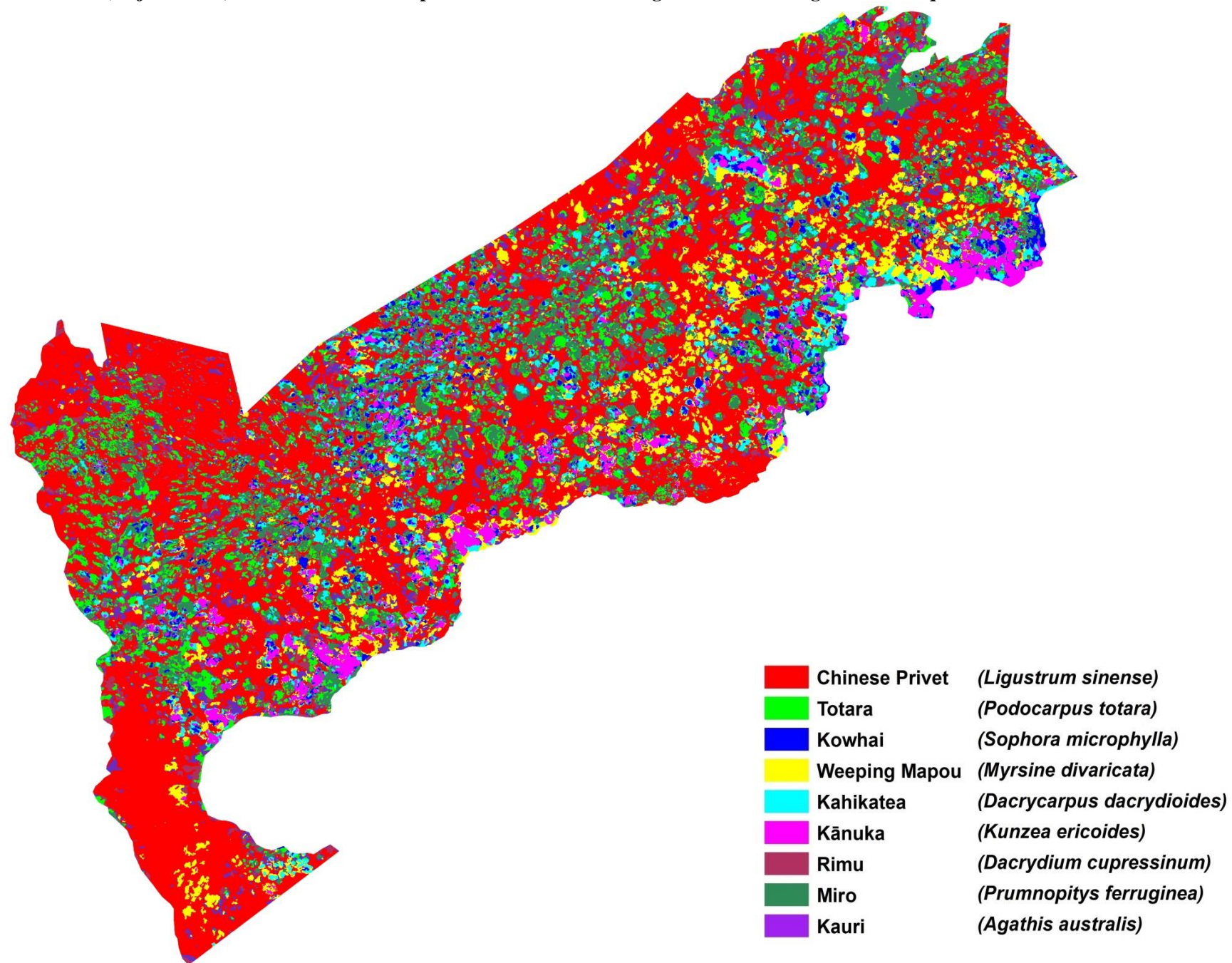
Appendix A.8. (Object-based) Minimum distance supervised classification of red edge images mosaic acquired on 8 August, 2013



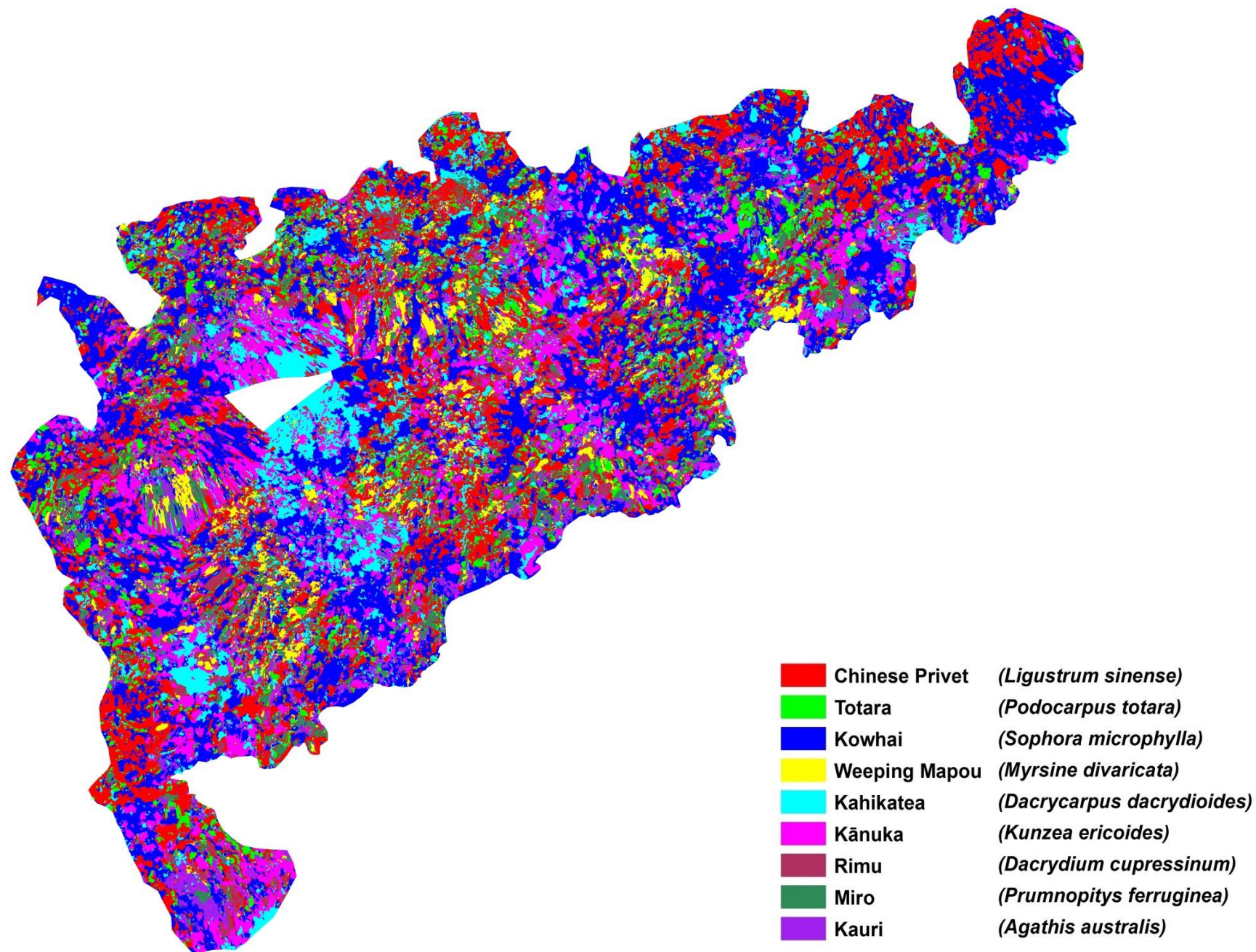
Appendix A.9. (Object-based) Maximum likelihood supervised classification of vegetation stress images mosaic acquired in 2013



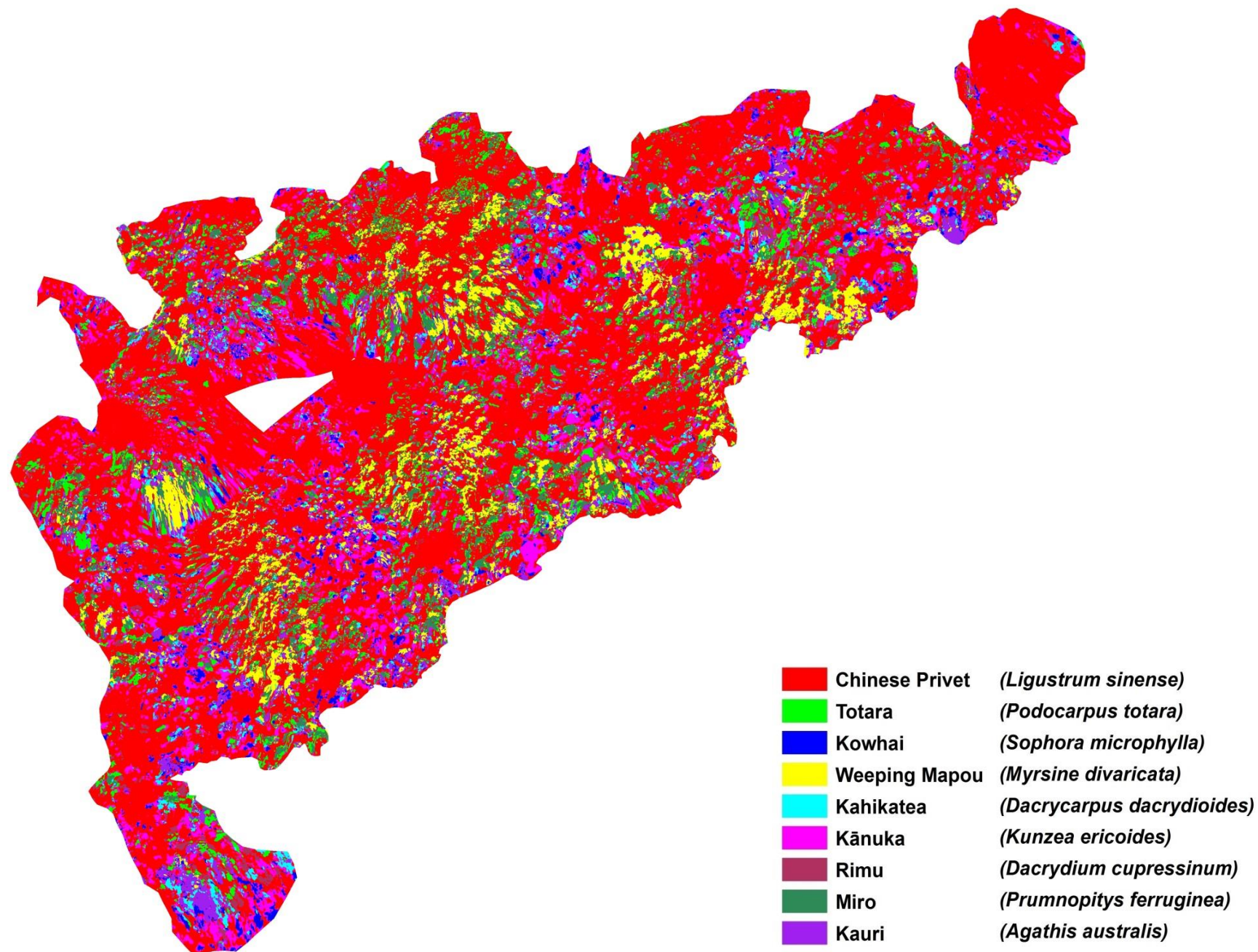
Appendix A.10. (Object-based) Minimum distance supervised classification of vegetation stress images mosaic acquired in 2013



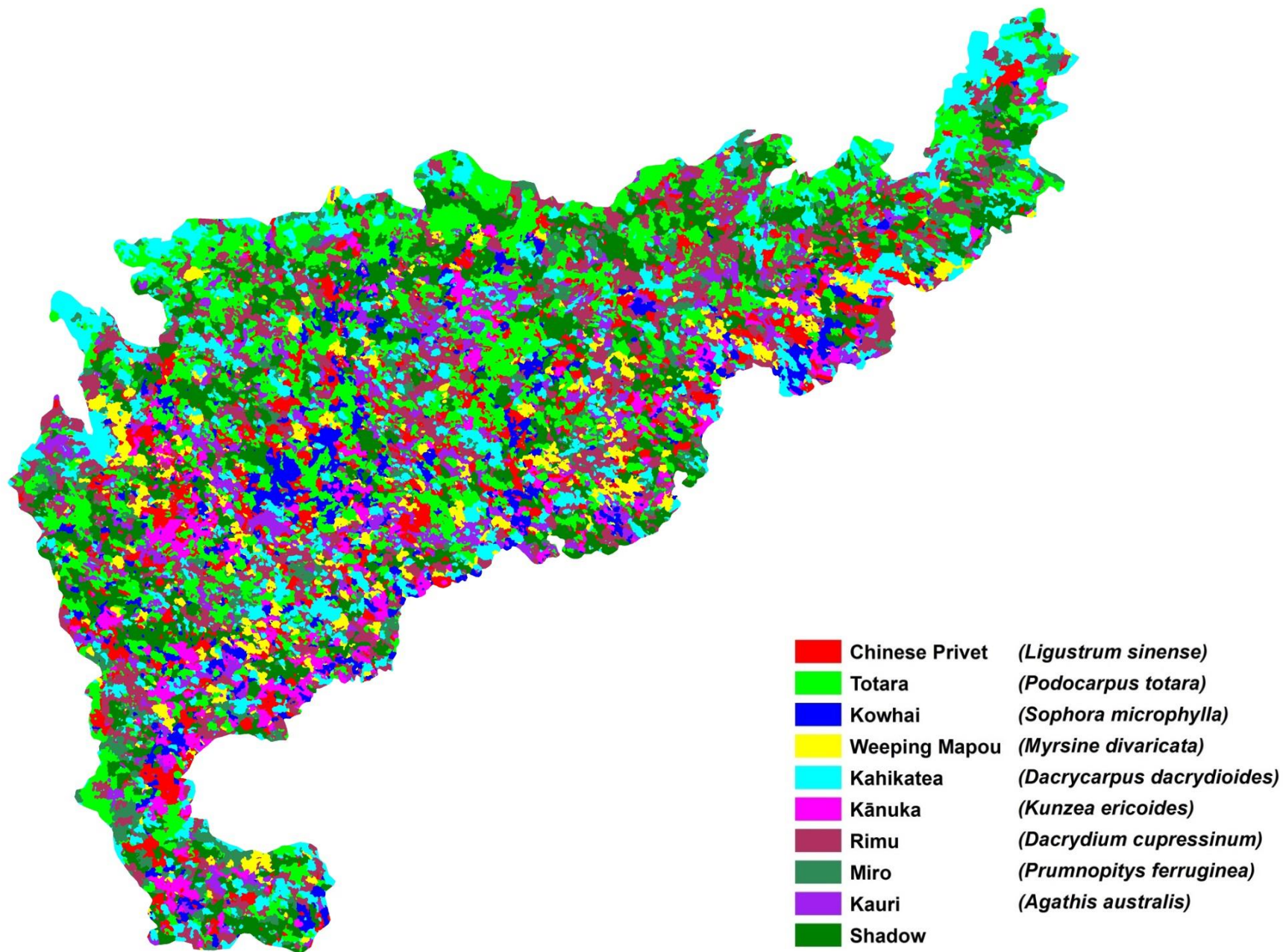
Appendix A.11. (Object-based) Maximum likelihood supervised classification of vegetation stress images mosaic acquired in 2014



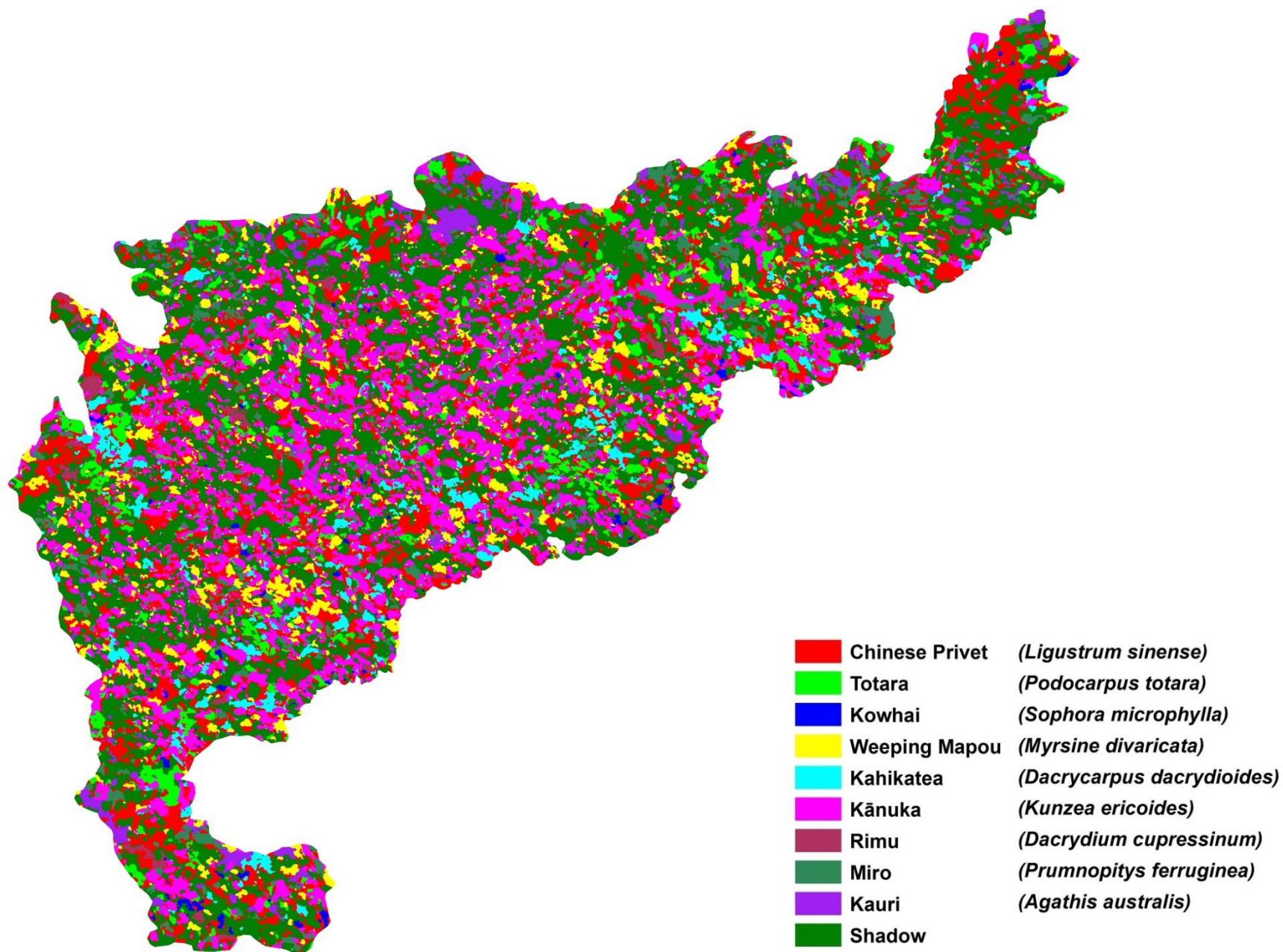
Appendix A.12. (Object-based) Minimum distance supervised classification of vegetation stress images mosaic acquired in 2014



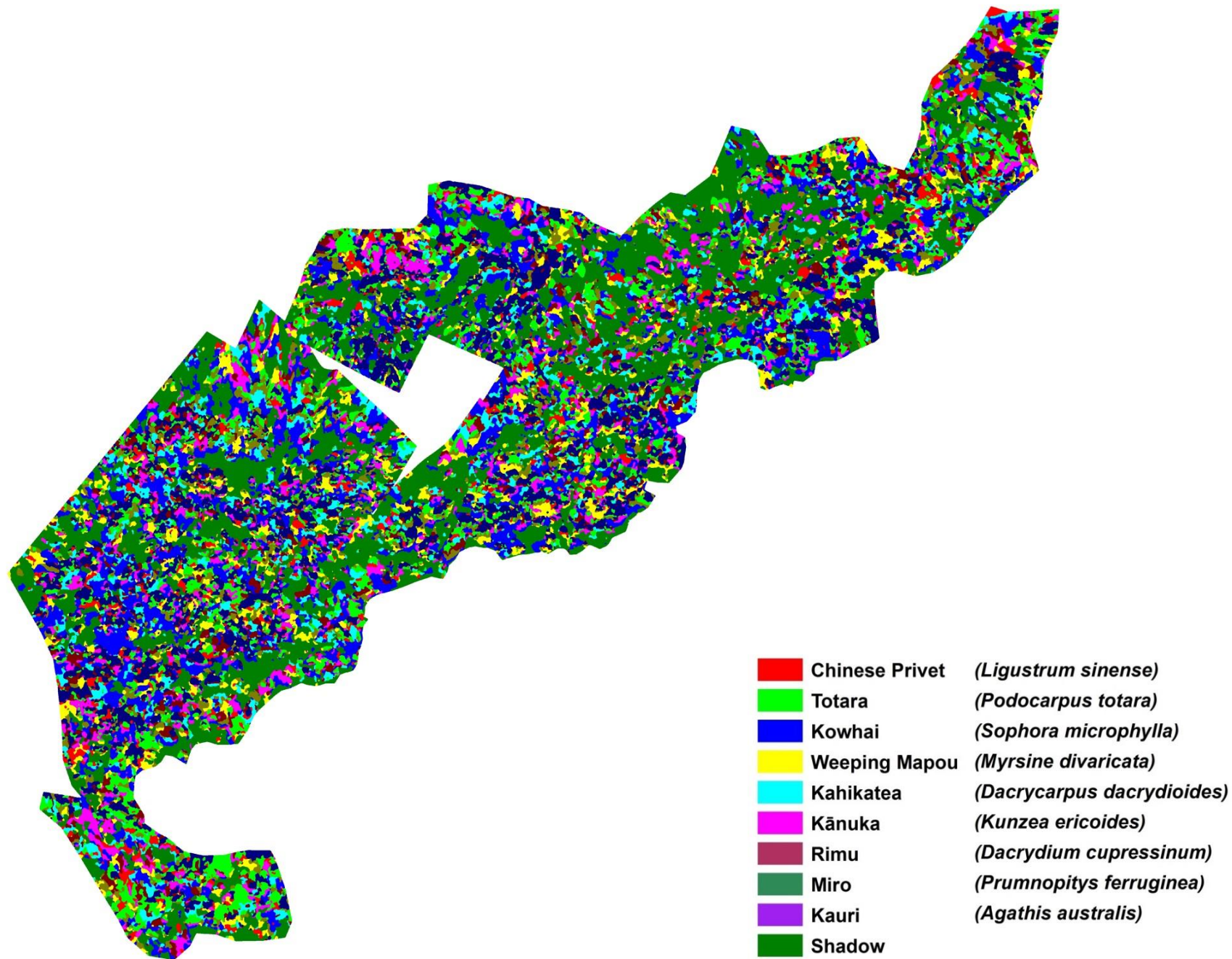
Appendix A.13. (Object-based) Maximum likelihood supervised classification of true colour images mosaic acquired on 1 April, 2014 (merge flight 1 and flight 2)



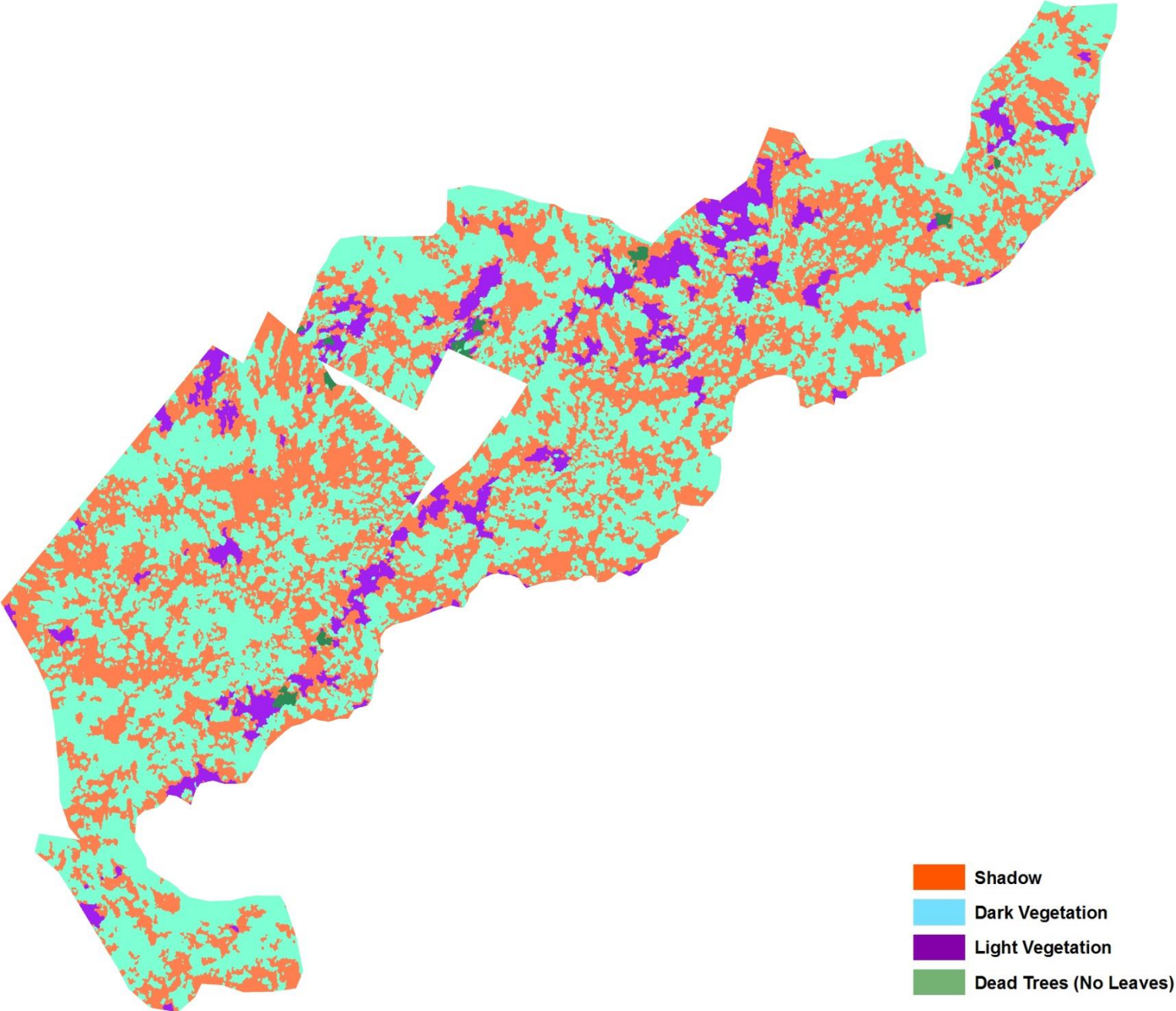
Appendix A.14. (Object-based) Minimum distance supervised classification of true colour images mosaic acquired on 1 April, 2014 (merge flight 1 and flight 2)



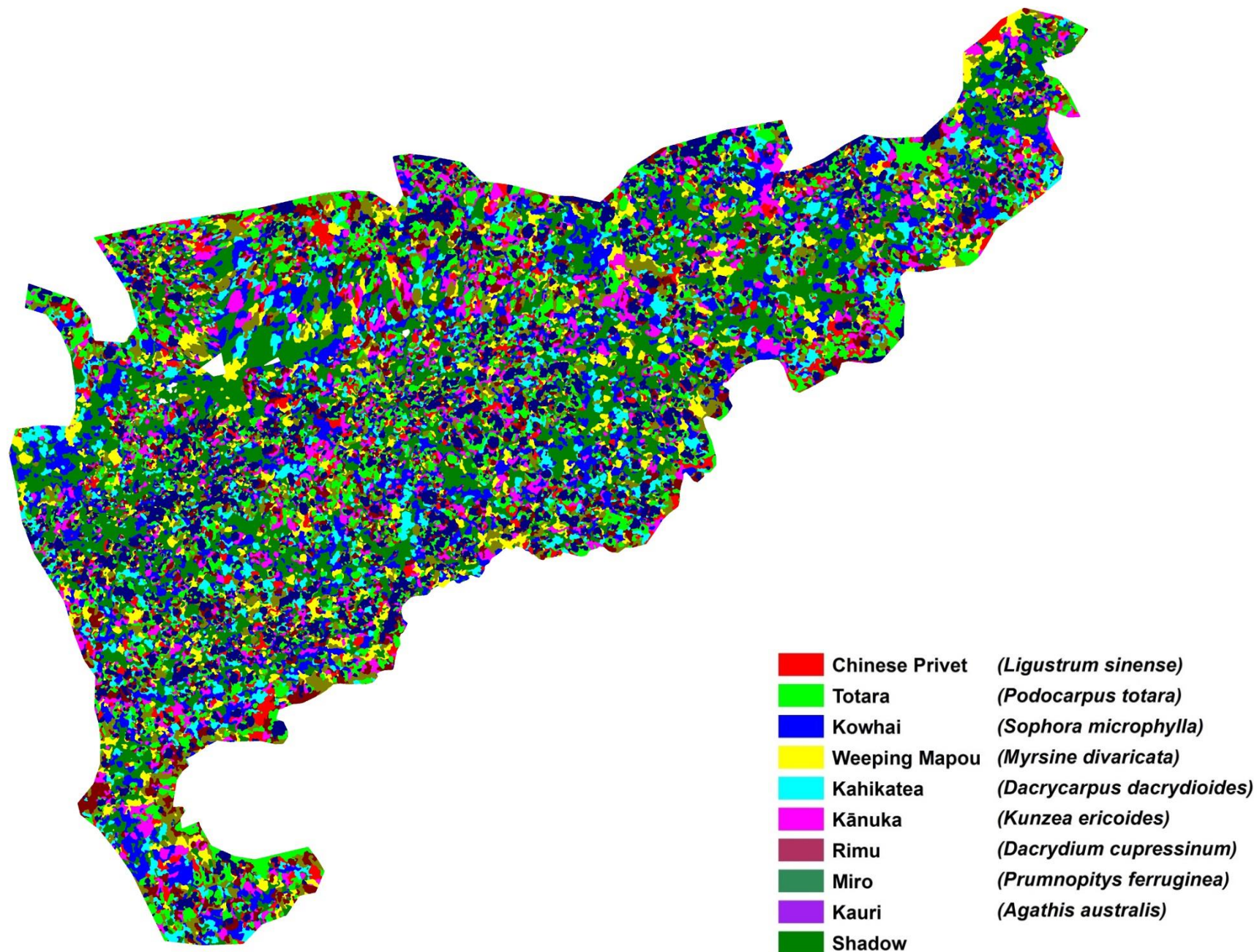
Appendix A.15. (Object-based) ISODATA unsupervised classification of near-infrared images mosaic acquired on 28 July, 2013



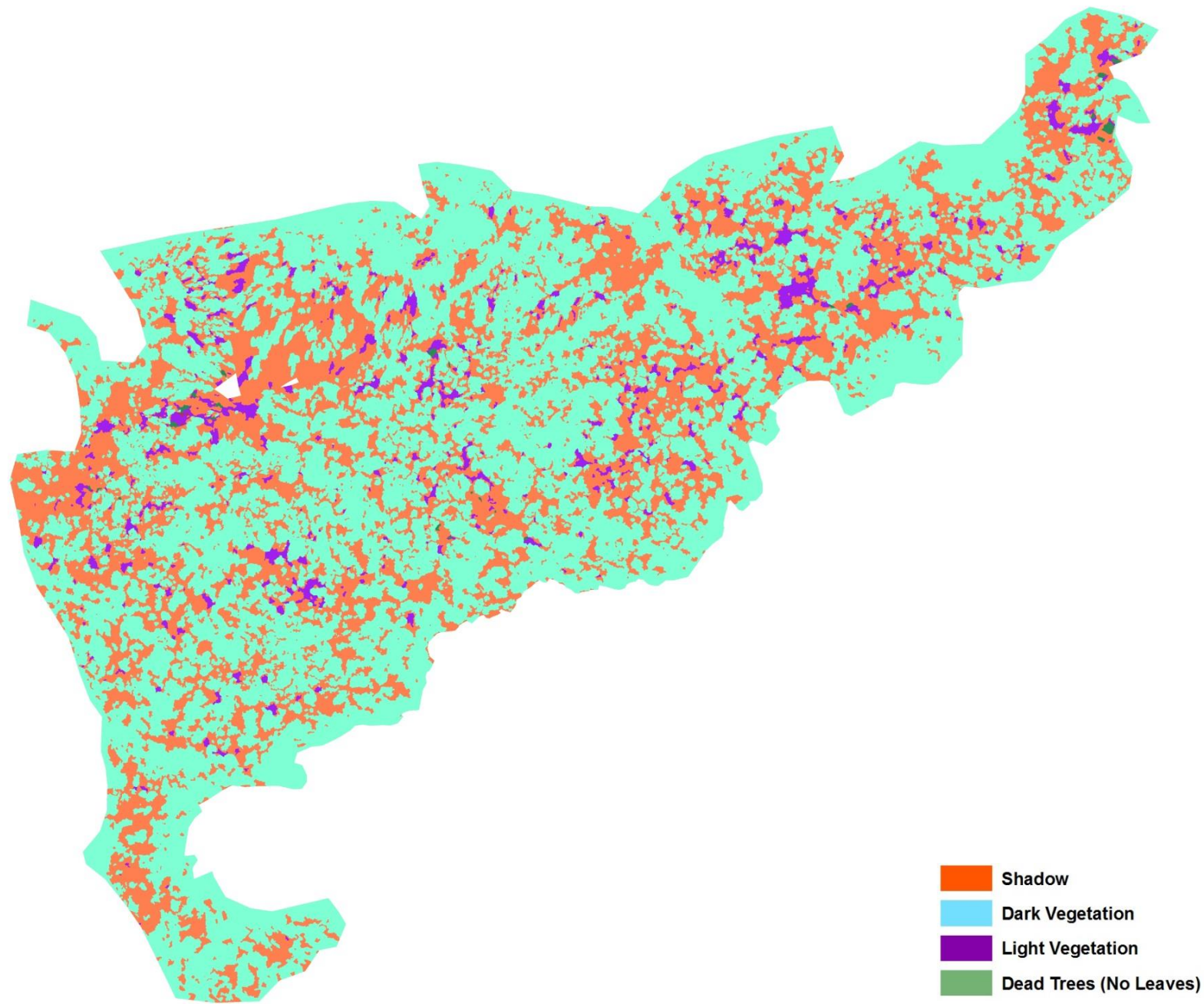
Appendix A.16. (Object-based) K-Mean unsupervised classification of near-infrared images mosaic acquired on 28 July, 2013



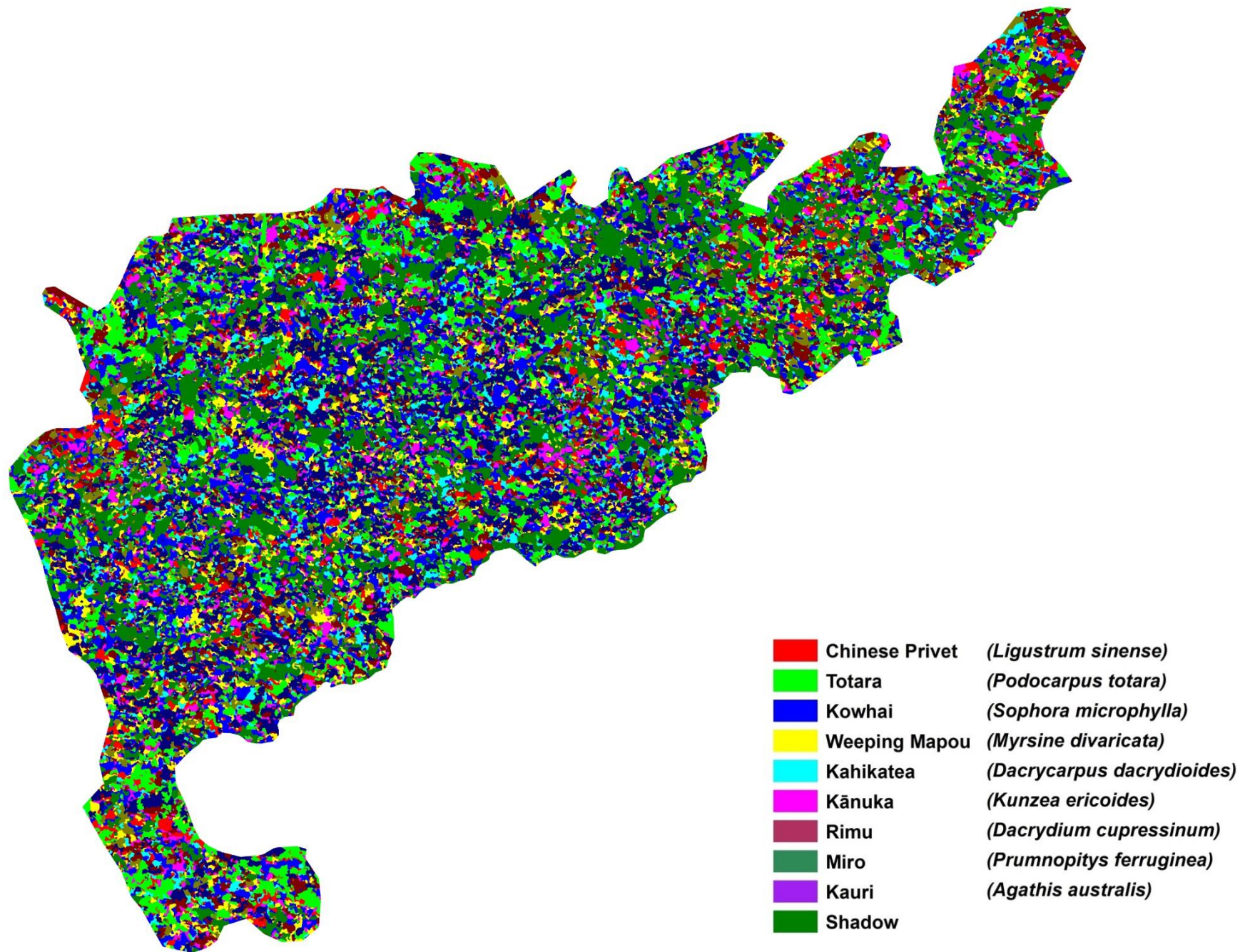
Appendix A.17. (Object-based) ISODATA unsupervised classification of near-infrared images mosaic acquired on 8 August, 2013



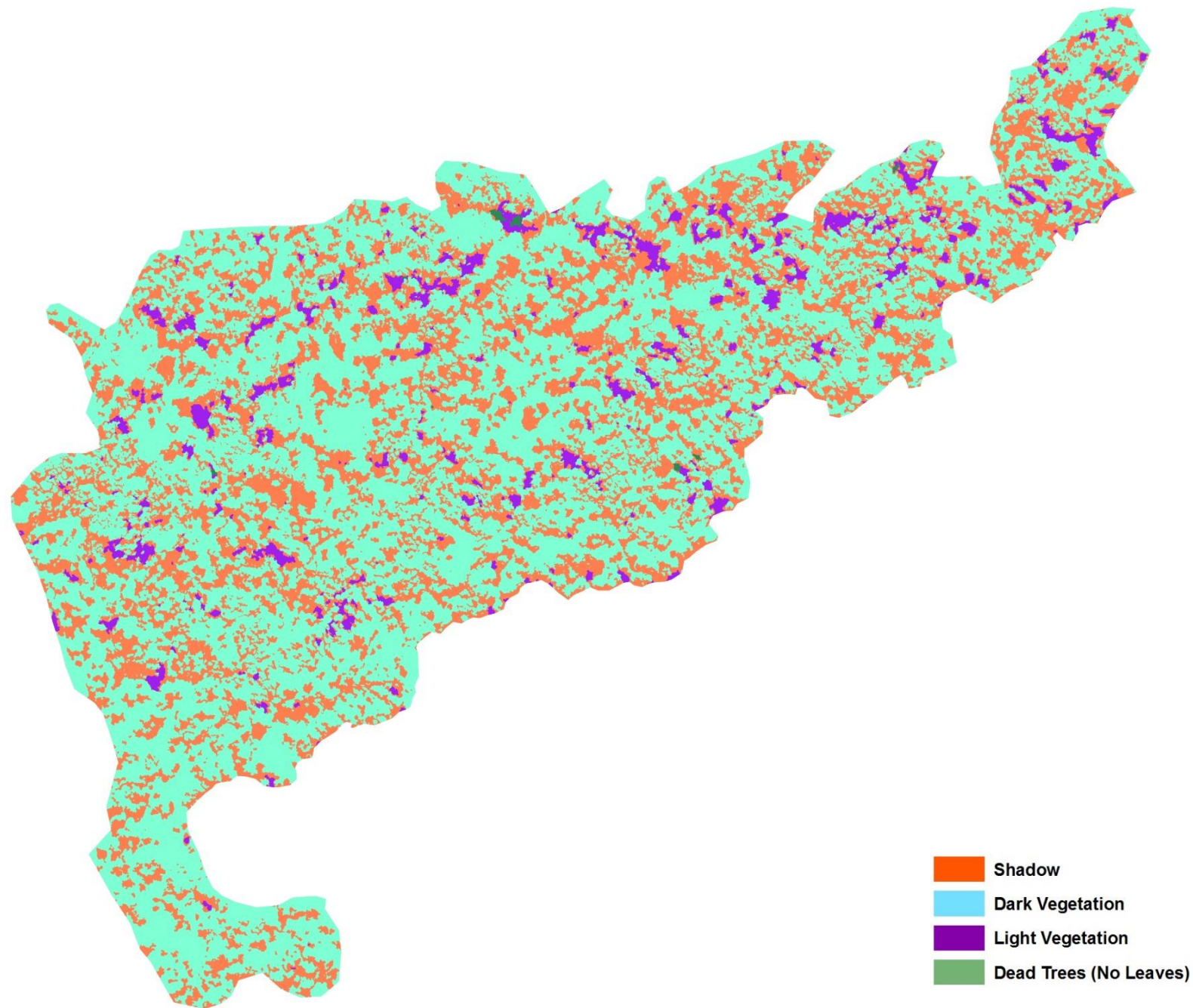
Appendix A.18. (Object-based) K-Mean unsupervised classification of near-infrared images mosaic acquired on 28 July, 2013



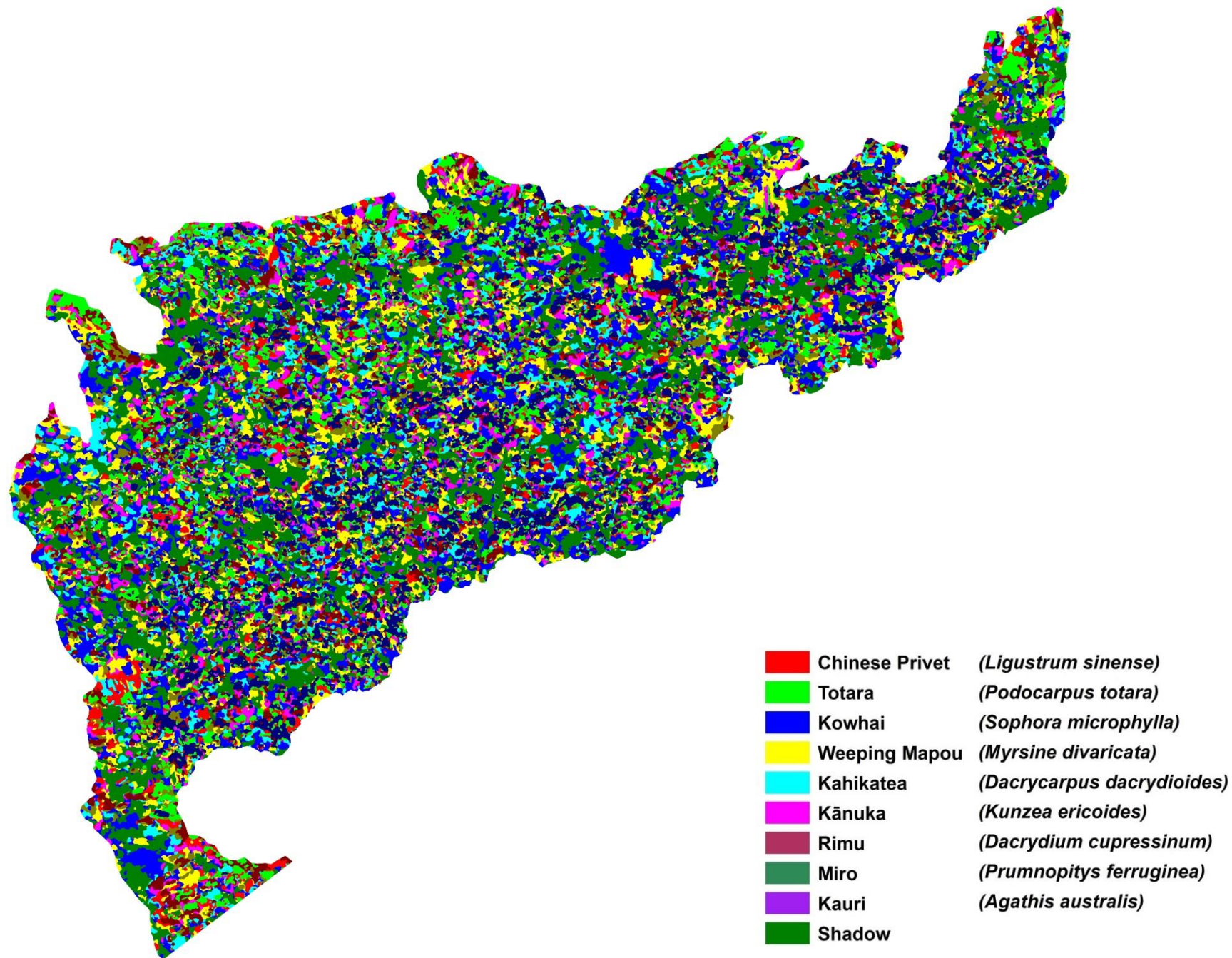
Appendix A.19. (Object-based) ISODATA unsupervised classification of near-infrared images mosaic acquired on 1 April, 2014 (flight 2)



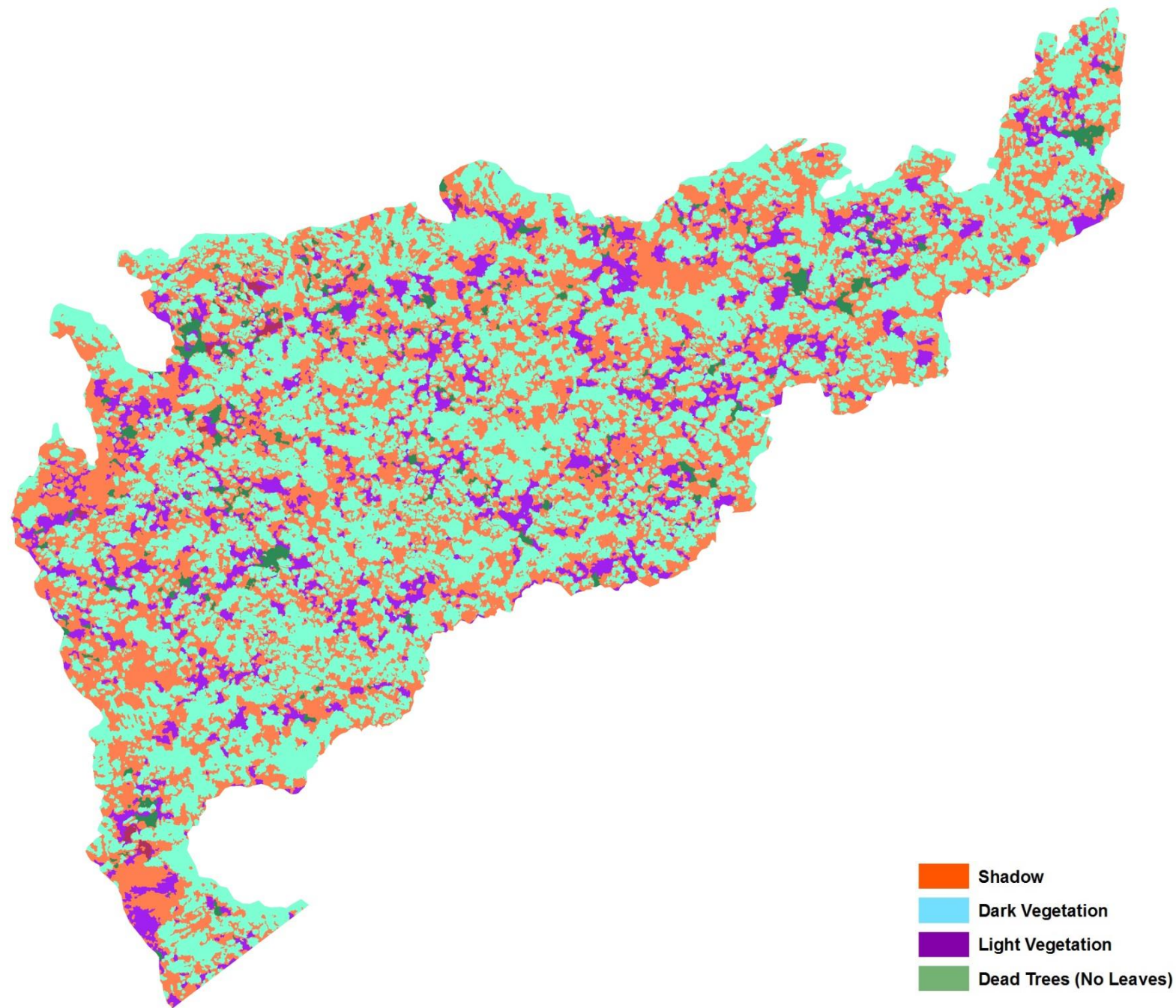
Appendix A.20. (Object-based) K-Mean unsupervised classification of near-infrared images mosaic acquired on 1 April, 2014 (flight 2)



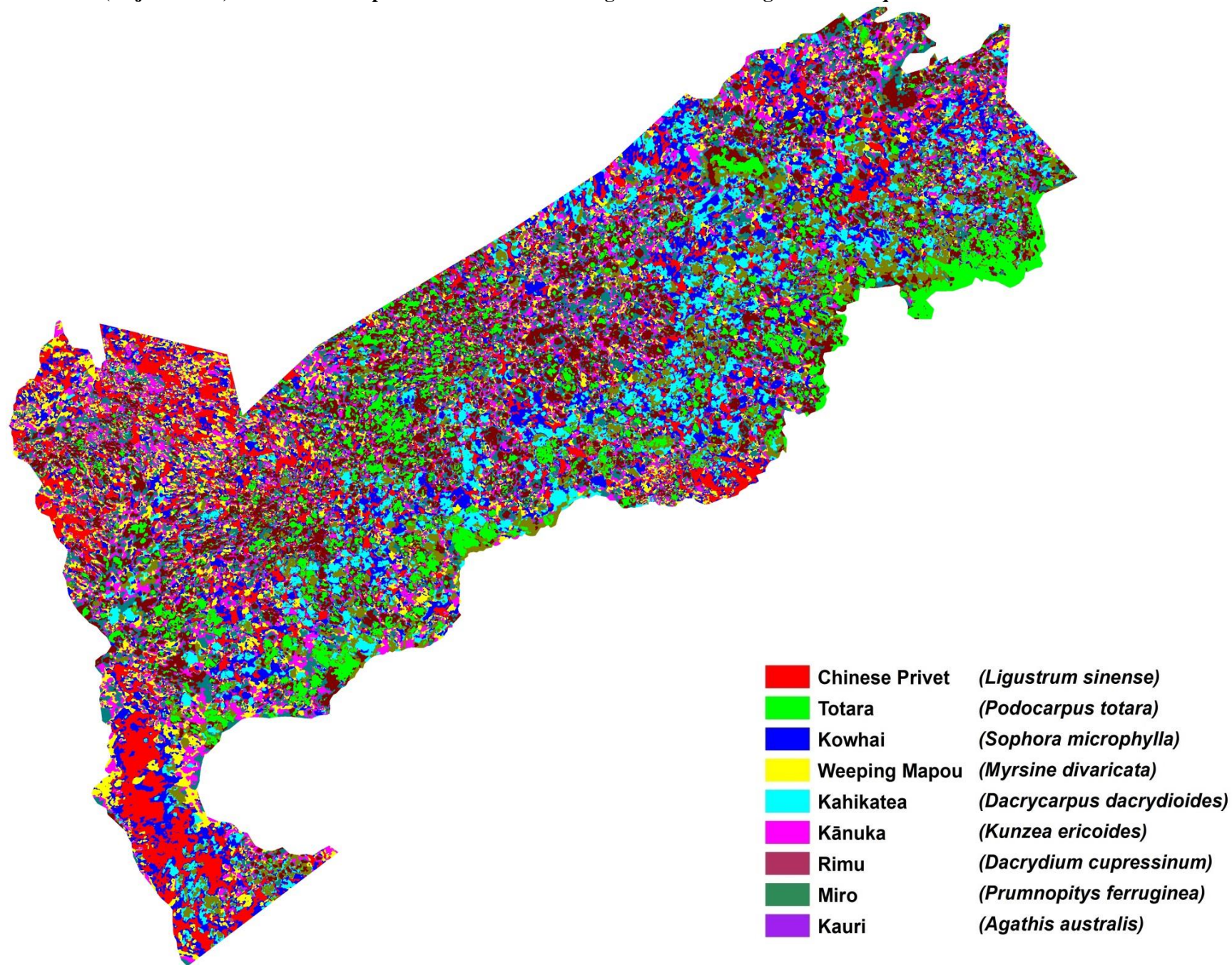
Appendix A.21. (Object-based) ISODATA unsupervised classification of red edge images mosaic acquired on 8 August, 2013



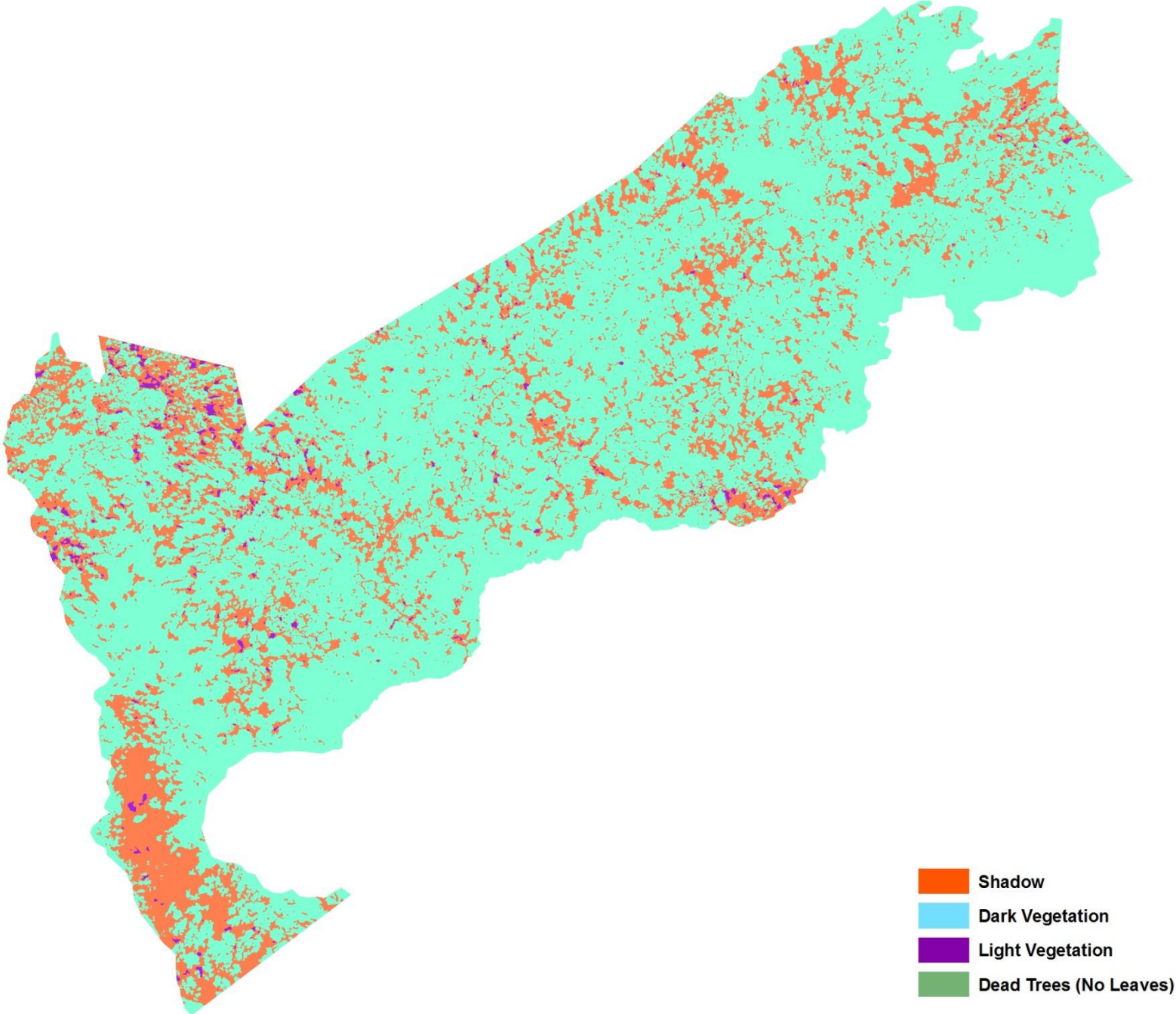
Appendix A.22. (Object-based) K-Mean unsupervised classification of red edge images mosaic acquired on 8 August, 2013



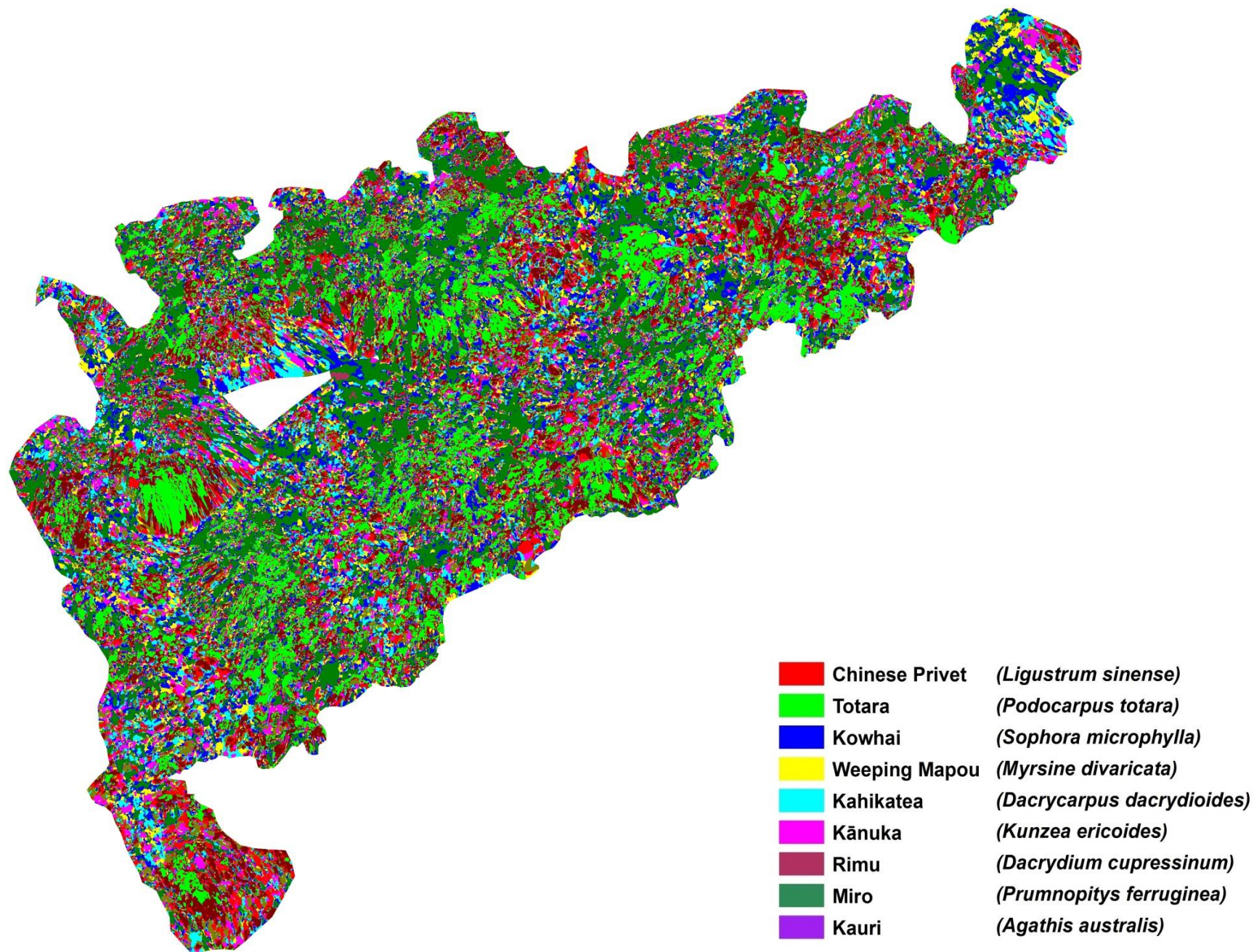
Appendix A.23. (Object-based) ISODATA unsupervised classification of vegetation stress images mosaic acquired in 2013



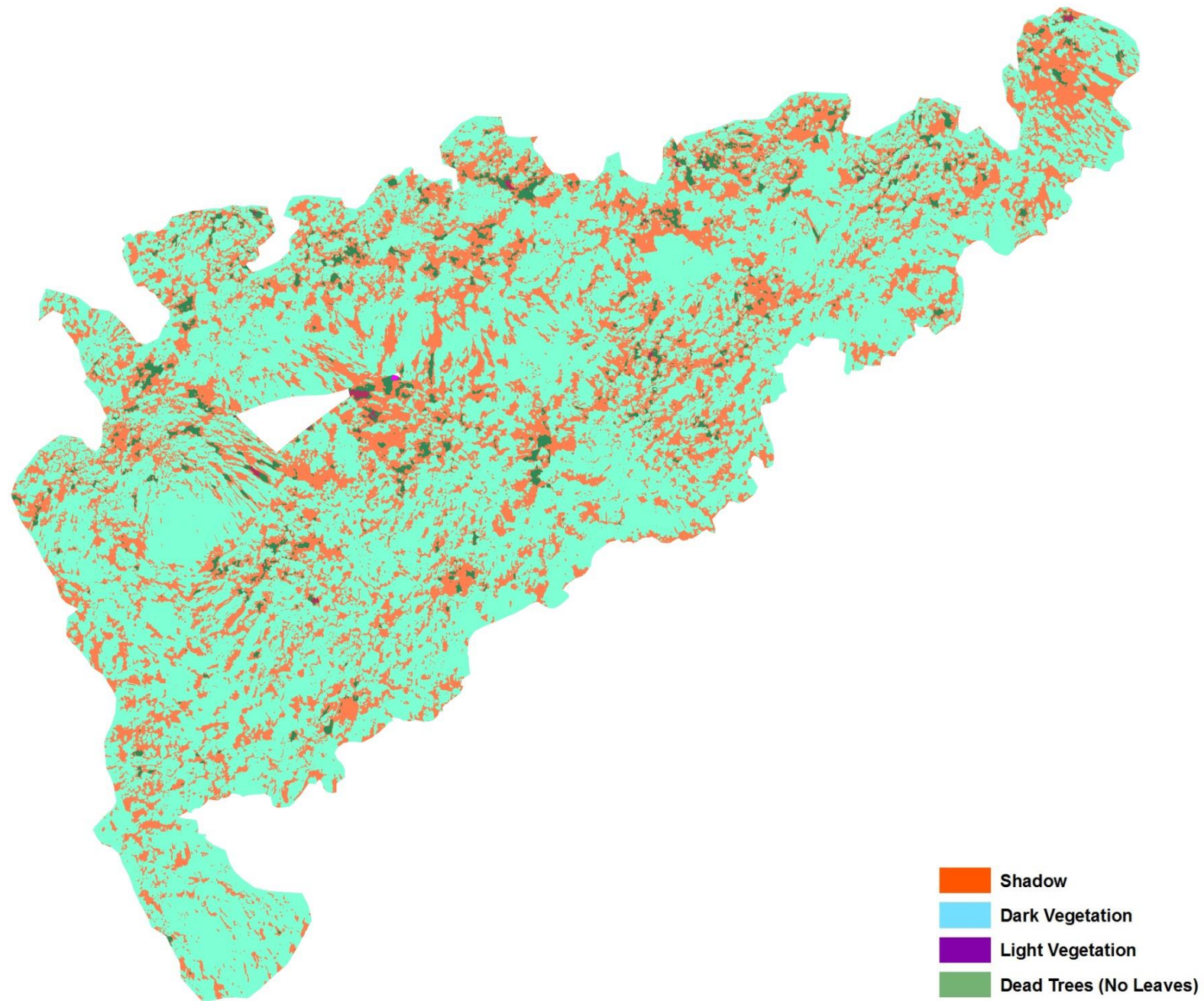
Appendix A.24. (Object-based) K-Mean unsupervised classification of vegetation stress images mosaic acquired in 2013



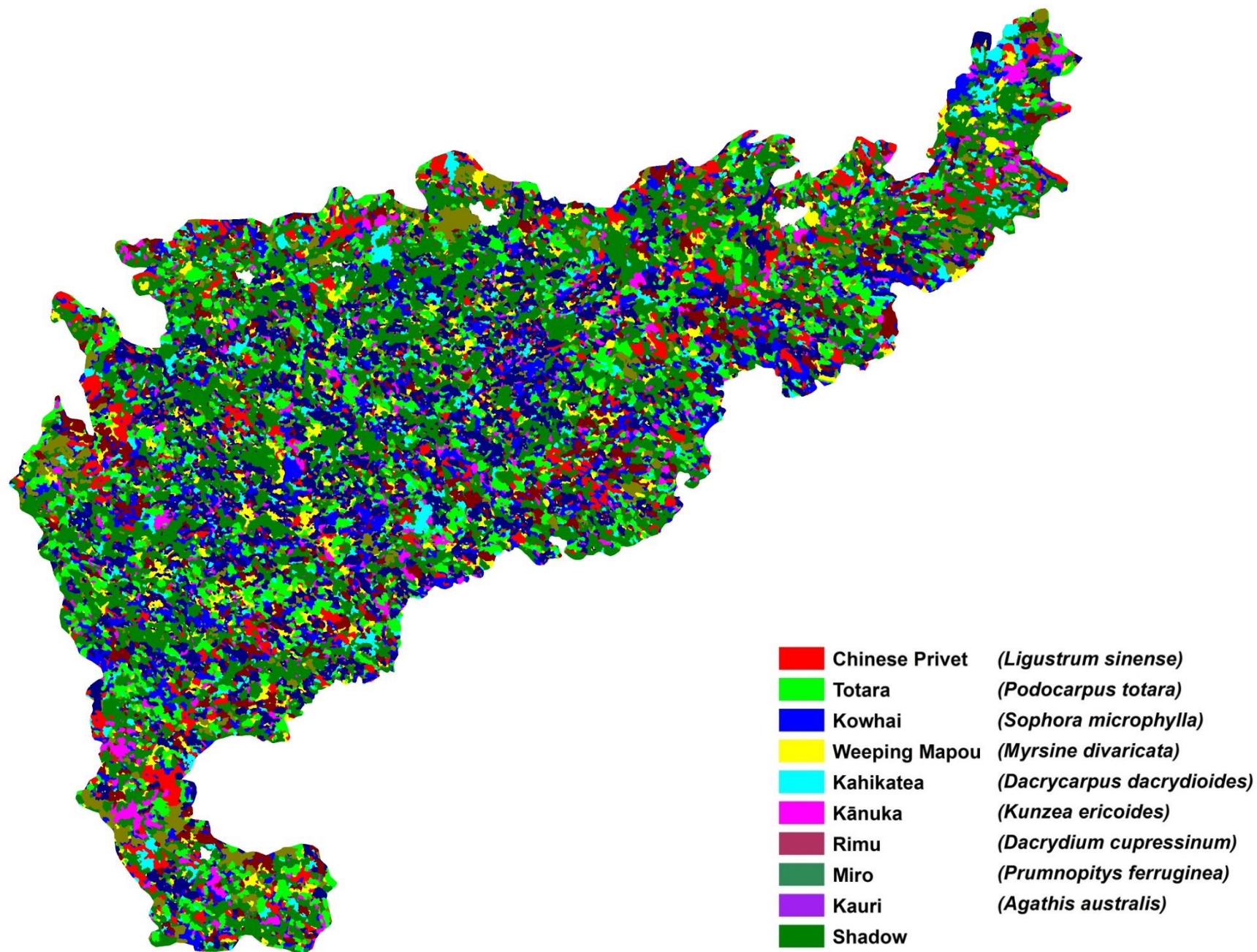
Appendix A.25. (Object-based) ISODATA unsupervised classification of vegetation stress images mosaic acquired in 2014



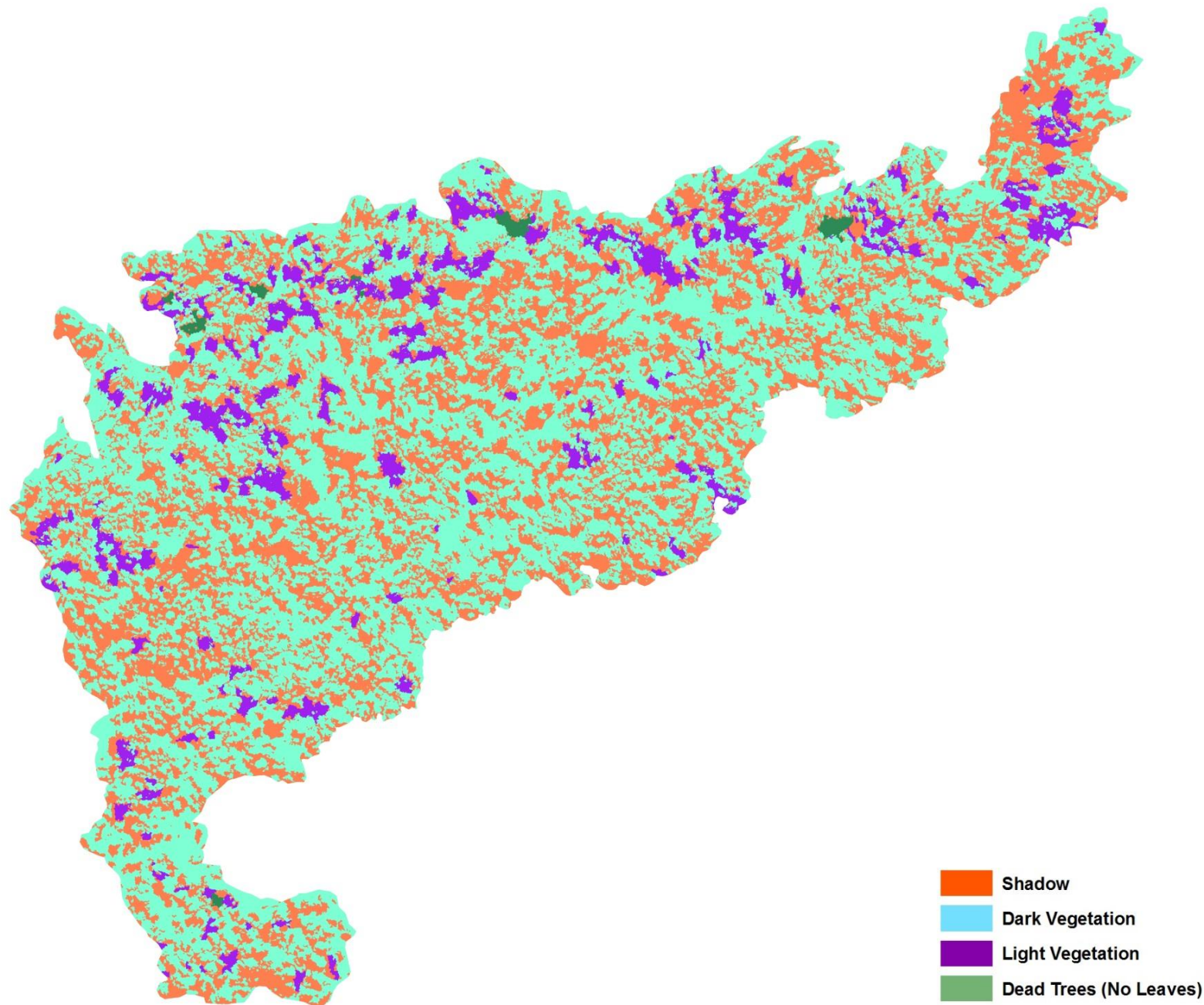
Appendix A.26. (Object-based) K-Mean unsupervised classification of vegetation stress images mosaic acquired in 2014



Appendix A.27. (Object-based) ISODATA unsupervised classification of true colour images mosaic acquired on 1 April, 2014 (merge flight 1 and flight 2)



Appendix A.28. (Object-based) K-Mean unsupervised classification of true colour images mosaic acquired on 1 April, 2014 (merge flight 1 and flight 2)



Appendix B. Mosaic Quality Report

Quality Report



See *Quality Report Help* for detailed explanations. Generated with version 2.2.2 (build 2.2.6)

Summary

Project:	nir
Camera name:	NEX-5N_16.0_1080x1616
Camera name:	NEX-5N_16.0_1616x1080
Average Ground Sampling Distance (GSD):	10.74 cm
Area covered:	0.35 sq. km / 35.33 ha / 0.14 sq. mi.
Image coordinate system:	WGS84
Output coordinate system:	UTM60 / WGS84
Processing type:	full (scale 1)
Time for Initial Processing (without report):	06m:14s:

Quality Check

Images:	median of 4874 keypoints per image	!
Dataset:	151 out of 159 images calibrated (94%) and 2 blocks	!
Camera optimization quality:	95.92% relative difference between initial and final focal length	!
Matching quality:	median of 1159 matches per calibrated image	✓
Georeferencing:	no GCP	!

Preview

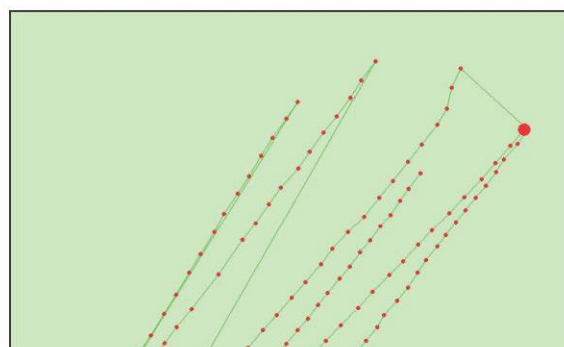


Figure 1: Ortho mosaic and the corresponding sparse digital surface model (DSM) before densification.

Calibration details

Number of calibrated images:	151 out of 159
Number of geotagged images:	157 out of 159

Geotag position



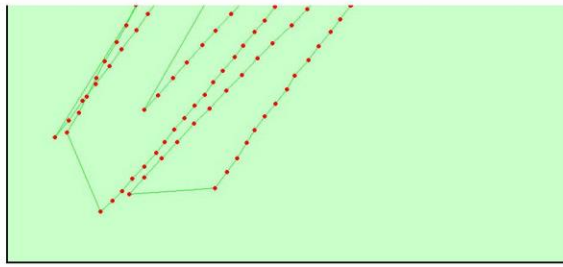


Figure 2: Top view of the geotags. The green line follows the geotag in time starting from the large red dot.

Optimized camera position

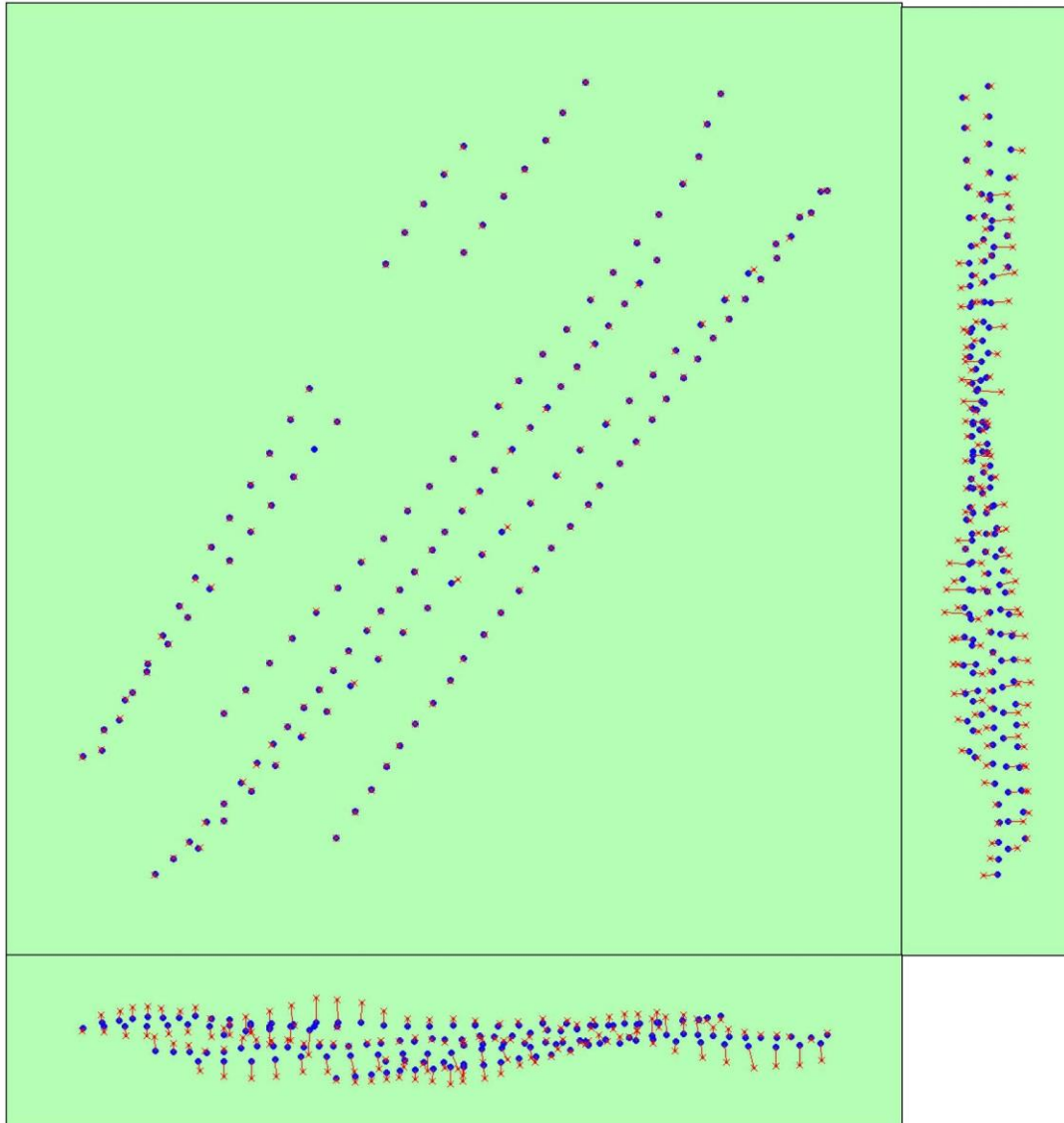


Figure 3: Offset between image geotags (small red crosses) and optimized positions (small blue dots) as well as the offset between the GCPs (large red crosses) and their optimized positions (large green dots) in the top-view (XY plane), front-view (XZ plane) and side-view (YZ plane).

Geotag variance

Geotag localisation variance	sigma [m]
Longitude direction (x)	0.643499
Latitude direction (y)	0.622171
Altitude direction (z)	9.74973

Table 1: Relative camera localisation accuracy of the geotags. Please note that this does not correspond to the accuracy on the ground.

Overlap

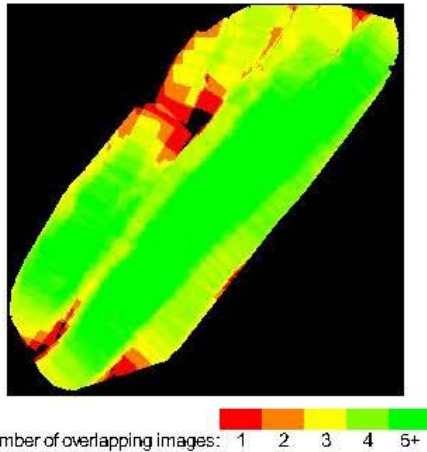


Figure 4: Overlapping score computed for each pixel of the orthomosaic. Red indicates areas where the overlap between the images is too low and could lead to poor results. For good quality results, the overlap should be over 5 images (green) for every pixel of the mosaic.

Bundle Block Adjustment details

number total keypoint observations for bundle block adjustment	180740
number total 3D points for bundle block adjustment	53935
mean reprojection error	0.439036 [pixels]

Internal Camera Parameters NEX-5N_16.0_1080x1616 sensor dimension: 36.24.1 [mm]

	Focal length	Principal point X	Principal point Y	RD 1	RD 2	RD 3	TD 1	TD 2
initial values	718.222 [pix] 16.000 [mm]	808.000 [pix] 18.000 [mm]	540.000 [pix] 12.030 [mm]	0.000	0.000	0.000	0.000	0.000
optimized values	1121.557 [pix] 24.985 [mm]	835.738 [pix] 17.382 [mm]	547.478 [pix] 11.863 [mm]	-0.074	0.104	-0.007	0.001	-0.003

Internal Camera Parameters NEX-5N_16.0_1616x1080 sensor dimension: 36.000 53.867 [mm]

	Focal length	Principal point X	Principal point Y	RD 1	RD 2	RD 3	TD 1	TD 2
initial values	480.000 [pix] 16.000 [mm]	540.000 [pix] 18.000 [mm]	808.000 [pix] 26.933 [mm]	0.000	0.000	0.000	0.000	0.000
optimized values	1131.371 [pix] 37.712 [mm]	547.219 [pix] 17.759 [mm]	798.401 [pix] 27.253 [mm]	-0.068	0.091	0.021	-0.000	0.000

2D Keypoints Table

	Number of 2D keypoints per image	Number of matched 2D keypoints per image
Median	4874.000	1159.000
Mn	378.000	88.000
Max	7881.000	2682.000
Mean	4667.775	1196.954

3D points from 2D keypoints matches

	Number of 3D points observed
In 2 - 3 images	39198
In 4 - 5 images	8142
In 6 - 7 images	2902
In 8 - 9 images	1711

In 10 - 11 images	1197
In 12 - 13 images	443
In 14 - 15 images	194
In 16 - 17 images	103
In 18 - 19 images	35
In 20 - 20 images	10

2D Keypoints Graph

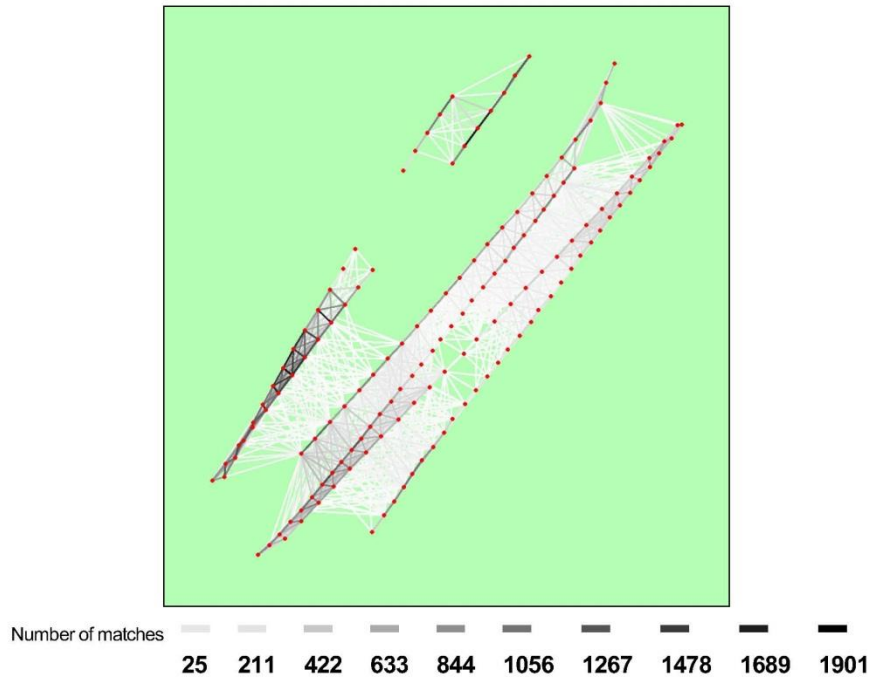


Figure 5: Top view of the geotags with a link between matching images. The darkness of the links indicates the number of matched 2D keypoints between the images. Bright links indicate low confidence and would require more overlap between the images or better quality images.

Most visible 2D keypoints

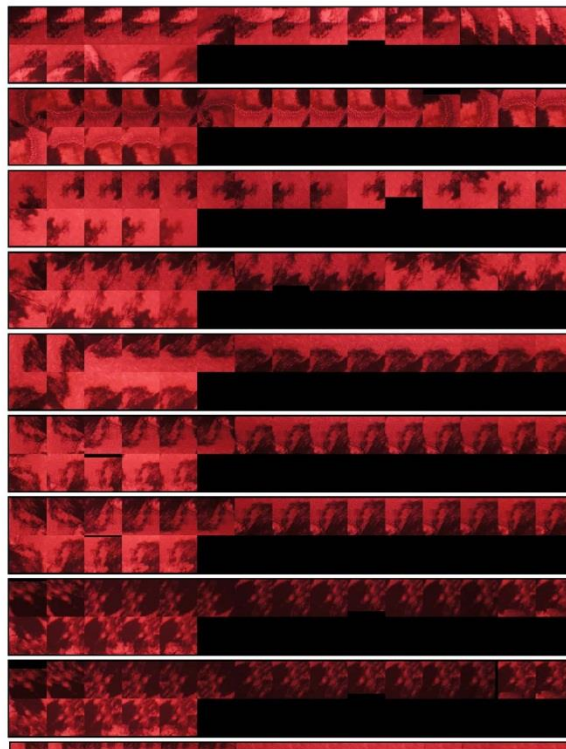




Figure 6: Cropped area of 10 3D points arising from 20 2D keypoints. Each cropped area should represent the same object on the ground.

Quality Report of mosaic map of near-infrared images acquired on 8 August, 2013

Quality Report



See *Quality Report Help* for detailed explanations. Generated with version 2.2.2 (build 2.2.6)

Summary

Project:	nir2
Camera name:	NEX-5N_16.0_1080x1616
Camera name:	NEX-5N_16.0_1616x1080
Average Ground Sampling Distance (GSD):	9.76 cm
Area covered:	0.31 sq. km / 30.75 ha / 0.12 sq. mi.
Image coordinate system:	WGS84
Output coordinate system:	UTM60 / WGS84
Processing type:	full (scale 1)
Time for Initial Processing (without report):	16m:08s:

Quality Check

Images:	median of 1355 keypoints per image	
Dataset:	412 out of 470 images calibrated (87%) and 2 blocks	
Camera optimization quality:	92.6% relative difference between initial and final focal length	
Matching quality:	median of 402 matches per calibrated image	
Georeferencing:	no GCP	

Preview

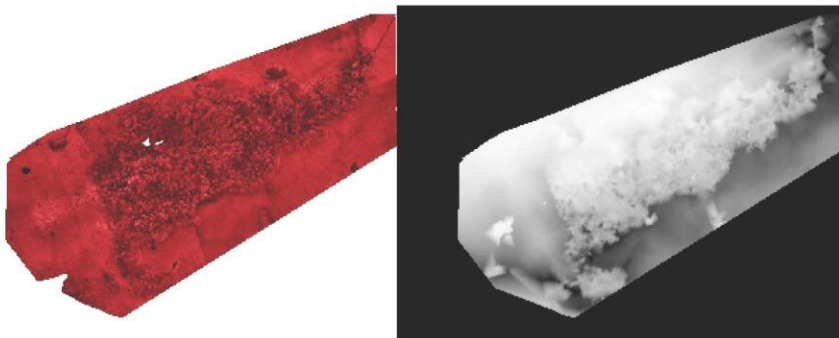


Figure 1: Ortho mosaic and the corresponding sparse digital surface model (DSM) before densification.

Calibration details

Number of calibrated images:	412 out of 470
Number of geotagged images:	470 out of 470

Geotag position

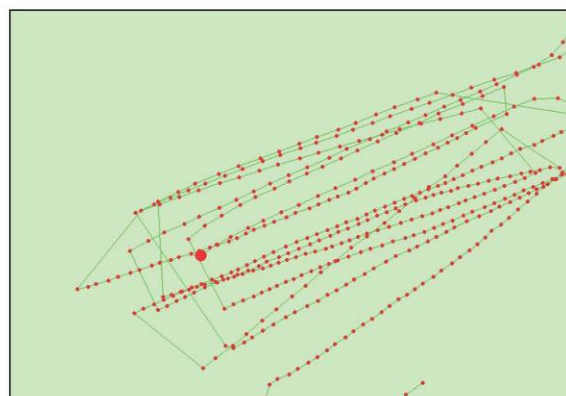




Figure 2: Top view of the geotags. The green line follows the geotag in time starting from the large red dot.

Optimized camera position

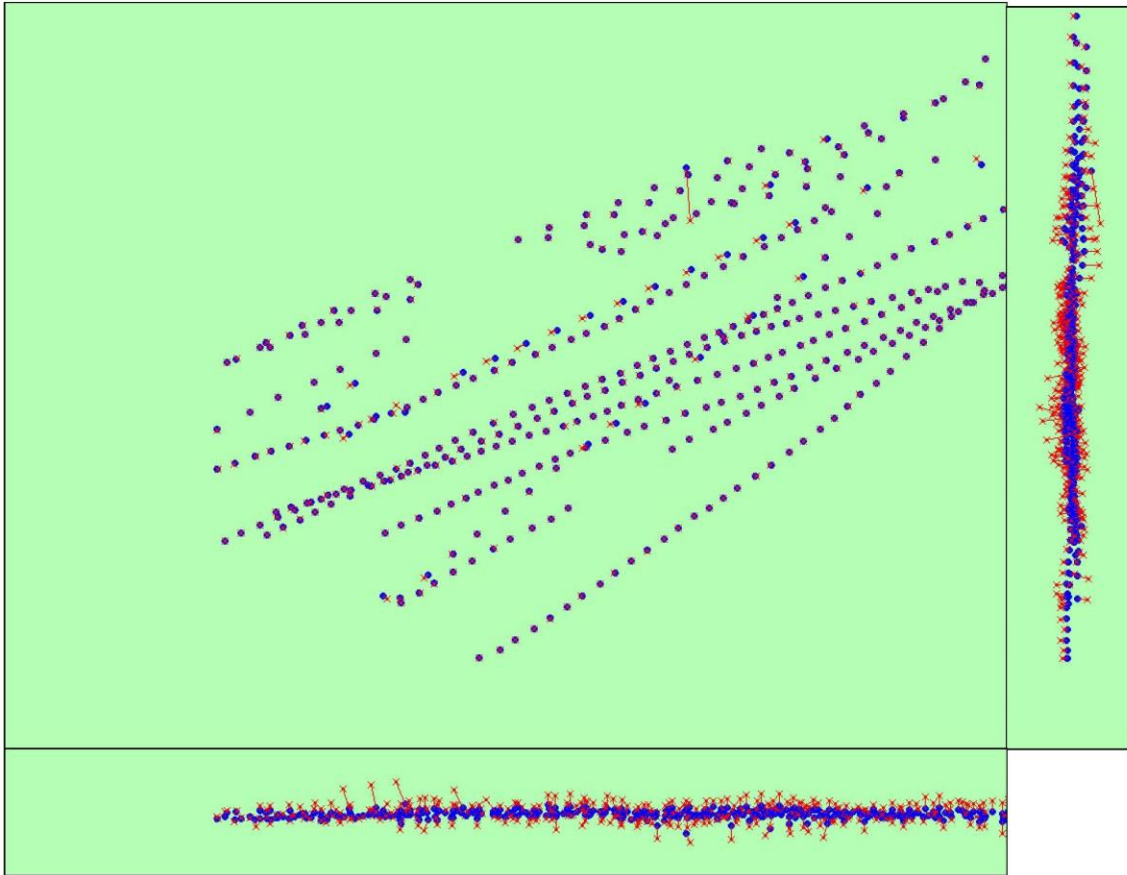


Figure 3: Offset between image geotags (small red crosses) and optimized positions (small blue dots) as well as the offset between the GCPs (large red crosses) and their optimized positions (large green dots) in the top-view (XY plane), front-view (XZ plane) and side-view (YZ plane).

Geotag variance

Geotag localisation variance	sigma [m]
Longitude direction (x)	0.507728
Latitude direction (y)	0.213222
Altitude direction (z)	6.56975

Table 1: Relative camera localisation accuracy of the geotags. Please note that this does not correspond to the accuracy on the ground.

Overlap

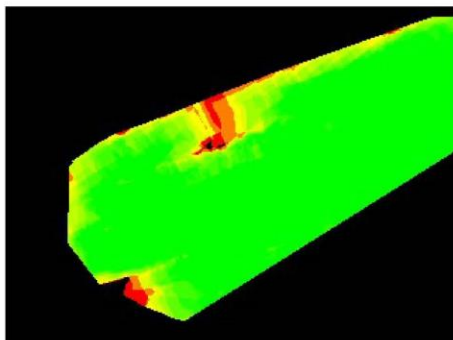




Figure 4: Overlapping score computed for each pixel of the orthomosaic. Red indicates areas where the overlap between the images is too low and could lead to poor results. For good quality results, the overlap should be over 5 images (green) for every pixel of the mosaic.

Bundle Block Adjustment details

number total keypoint observations for bundle block adjustment	262885
number total 3D points for bundle block adjustment	75790
mean reprojection error	0.33673 [pixels]

Internal Camera Parameters NEX-5N_16.0_1080x1616 sensor dimension: 36 24.1 [mm]

	Focal length	Principal point X	Principal point Y	RD 1	RD 2	RD 3	TD 1	TD 2
initial values	718.222 [pix] 16.000 [mm]	808.000 [pix] 18.000 [mm]	540.000 [pix] 12.030 [mm]	0.000	0.000	0.000	0.000	0.000
optimized values	1141.205 [pix] 25.423 [mm]	824.672 [pix] 17.629 [mm]	542.045 [pix] 11.984 [mm]	-0.077	0.104	0.001	0.002	-0.002

Internal Camera Parameters NEX-5N_16.0_1616x1080 sensor dimension: 36.000 53.867 [mm]

	Focal length	Principal point X	Principal point Y	RD 1	RD 2	RD 3	TD 1	TD 2
initial values	480.000 [pix] 16.000 [mm]	540.000 [pix] 18.000 [mm]	808.000 [pix] 26.933 [mm]	0.000	0.000	0.000	0.000	0.000
optimized values	1086.353 [pix] 36.212 [mm]	529.130 [pix] 18.362 [mm]	825.936 [pix] 26.335 [mm]	-0.084	0.064	0.046	-0.001	-0.004

2D Keypoints Table

	Number of 2D keypoints per image	Number of matched 2D keypoints per image
Median	1355.000	402.000
Min	41.000	24.000
Max	7633.000	3753.000
Mean	2197.767	638.070

3D points from 2D keypoints matches

	Number of 3D points observed
In 2 - 3 images	53758
In 4 - 7 images	17414
In 8 - 11 images	2983
In 12 - 15 images	875
In 16 - 19 images	386
In 20 - 23 images	222
In 24 - 27 images	98
In 28 - 31 images	39
In 32 - 34 images	12
In 36 - 36 images	1
In 41 - 43 images	2

2D Keypoints Graph



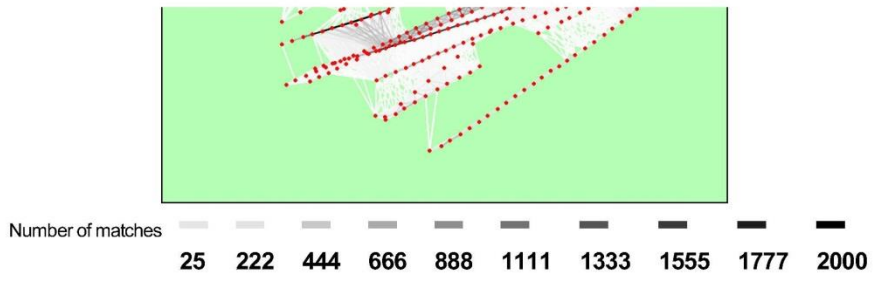


Figure 5: Top view of the geotags with a link between matching images. The darkness of the links indicates the number of matched 2D keypoints between the images. Bright links indicate low confidence and would require more overlap between the images or better quality images.

Most visible 2D keypoints

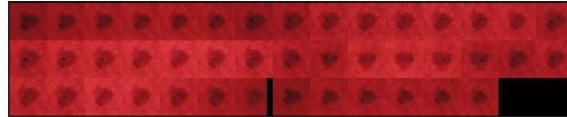


Figure 6: Cropped area of 1 3D points arising from 43 2D keypoints. Each cropped area should represent the same object on the ground.

Quality Report of mosaic map of near-infrared images acquired on 1 April, 2014 (flight 2)

Quality Report



See *Quality Report Help* for detailed explanations. Generated with version 2.2.2 (build 2.2.6)

Summary

Project:	nir_1_apr_run2
Camera name:	NEX-5N_16.0_1080x1616
Camera name:	NEX-5N_16.0_1616x1080
Average Ground Sampling Distance (GSD):	9.09 cm
Area covered:	0.33 sq. km / 32.91 ha / 0.13 sq. mi.
Image coordinate system:	WGS84
Output coordinate system:	UTM60 / WGS84
Processing type:	full (scale 1)
Time for Initial Processing (without report):	37m:03s:

Quality Check

Images:	median of 4152 keypoints per image	!
Dataset:	665 out of 668 images calibrated (99%)	✓
Camera optimization quality:	104.25% relative difference between initial and final focal length	!
Matching quality:	median of 1012 matches per calibrated image	✓
Georeferencing:	no GCP	!

Preview

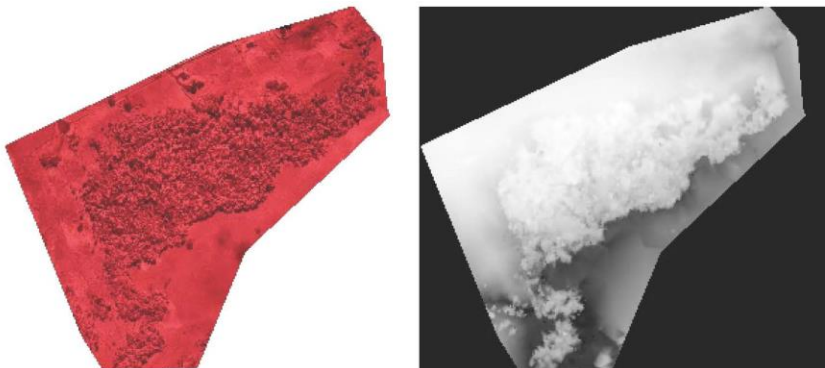
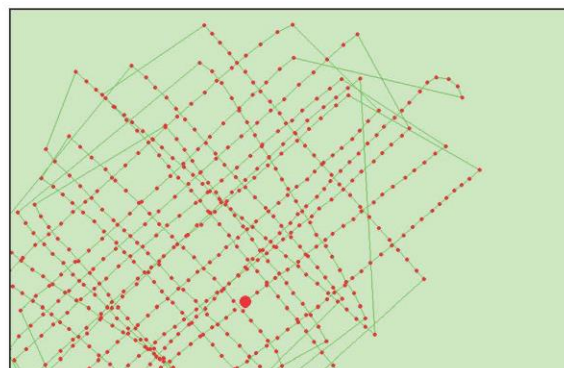


Figure 1: Ortho mosaic and the corresponding sparse digital surface model (DSM) before densification.

Calibration details

Number of calibrated images:	665 out of 668
Number of geotagged images:	668 out of 668

Geotag position



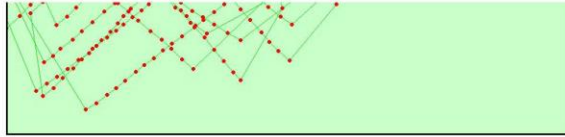


Figure 2: Top view of the geotags. The green line follows the geotag in time starting from the large red dot.

Optimized camera position

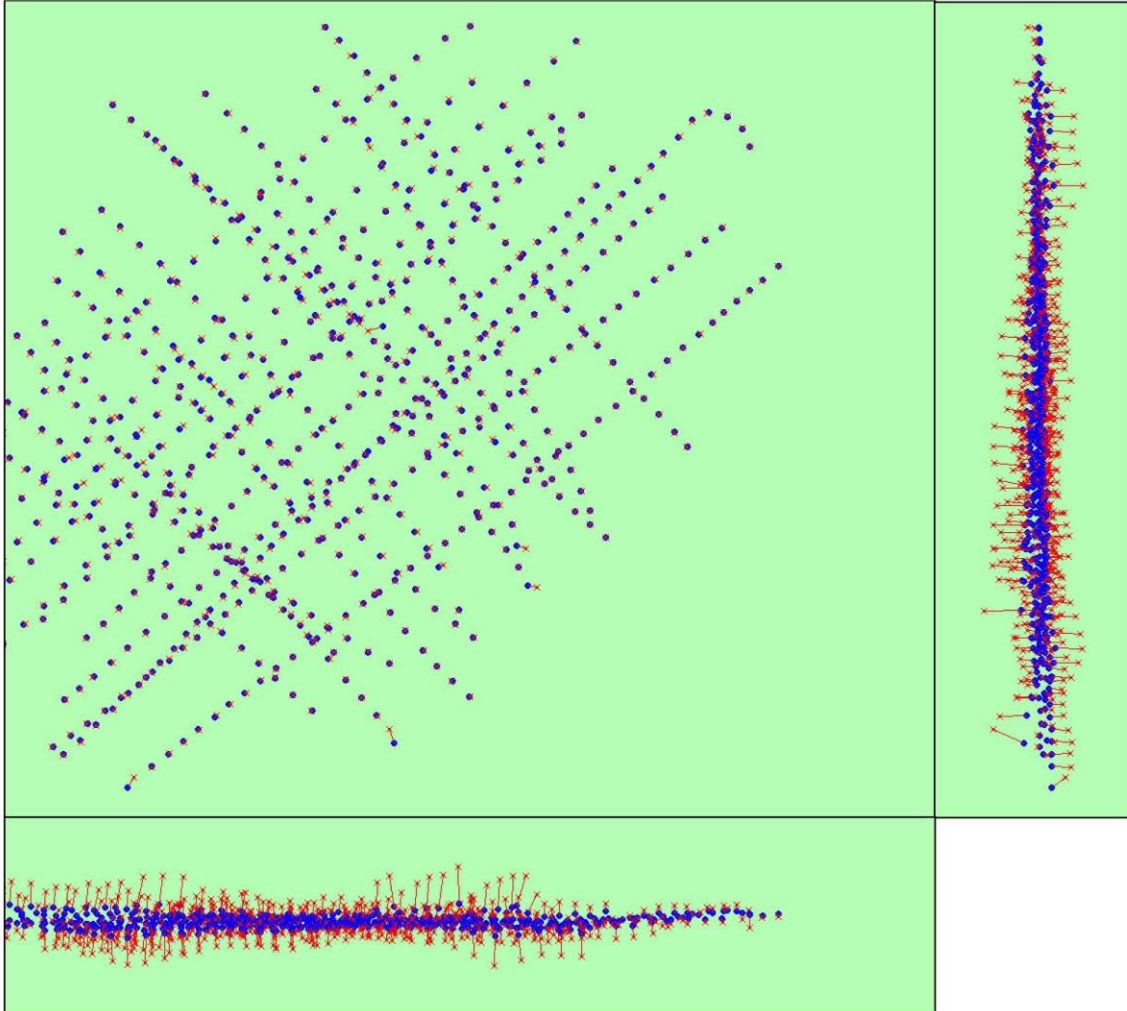


Figure 3: Offset between image geotags (small red crosses) and optimized positions (small blue dots) as well as the offset between the GCPs (large red crosses) and their optimized positions (large green dots) in the top-view (XY plane), front-view (XZ plane) and side-view (YZ plane).

Geotag variance

Geotag localisation variance	sigma [m]
Longitude direction (x)	1.54642
Latitude direction (y)	1.30829
Altitude direction (z)	9.7021

Table 1: Relative camera localisation accuracy of the geotags. Please note that this does not correspond to the accuracy on the ground.

Overlap



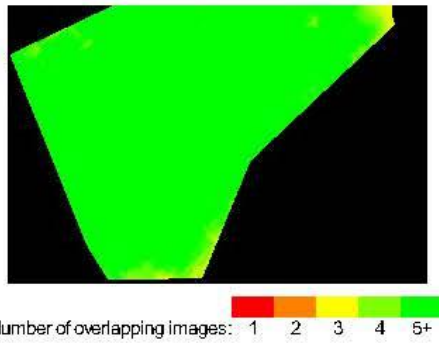


Figure 4: Overlapping score computed for each pixel of the orthomosaic. Red indicates areas where the overlap between the images is too low and could lead to poor results. For good quality results, the overlap should be over 5 images (green) for every pixel of the mosaic.

Bundle Block Adjustment details

number total keypoint observations for bundle block adjustment	712671
number total 3D points for bundle block adjustment	205146
mean reprojection error	0.4631 [pixels]

Internal Camera Parameters NEX-5N_16.0_1080x1616 sensor dimension: 36 24.1 [mm]

	Focal length	Principal point X	Principal point Y	RD 1	RD 2	RD 3	TD 1	TD 2
initial values	718.222 [pix] 16.000 [mm]	808.000 [pix] 18.000 [mm]	540.000 [pix] 12.030 [mm]	0.000	0.000	0.000	0.000	0.000
optimized values	1184.854 [pix] 26.395 [mm]	812.962 [pix] 17.889 [mm]	539.998 [pix] 12.030 [mm]	-0.081	0.096	0.046	-0.000	0.001

Internal Camera Parameters NEX-5N_16.0_1616x1080 sensor dimension: 36.000 53.867 [mm]

	Focal length	Principal point X	Principal point Y	RD 1	RD 2	RD 3	TD 1	TD 2
initial values	480.000 [pix] 16.000 [mm]	540.000 [pix] 18.000 [mm]	808.000 [pix] 26.933 [mm]	0.000	0.000	0.000	0.000	0.000
optimized values	1168.999 [pix] 38.967 [mm]	526.921 [pix] 18.436 [mm]	812.401 [pix] 26.787 [mm]	-0.077	0.084	0.046	0.000	0.001

2D Keypoints Table

	Number of 2D keypoints per image	Number of matched 2D keypoints per image
Median	4152.000	1012.000
Mn	75.000	54.000
Max	9010.000	2771.000
Mean	4507.301	1071.686

3D points from 2D keypoints matches

	Number of 3D points observed
In 2 - 3 images	156840
In 4 - 7 images	34188
In 8 - 11 images	8572
In 12 - 15 images	3310
In 16 - 19 images	1381
In 20 - 23 images	736
In 24 - 27 images	464
In 28 - 31 images	251
In 32 - 35 images	213
In 36 - 39 images	152
In 40 - 43 images	39

2D Keypoints Graph

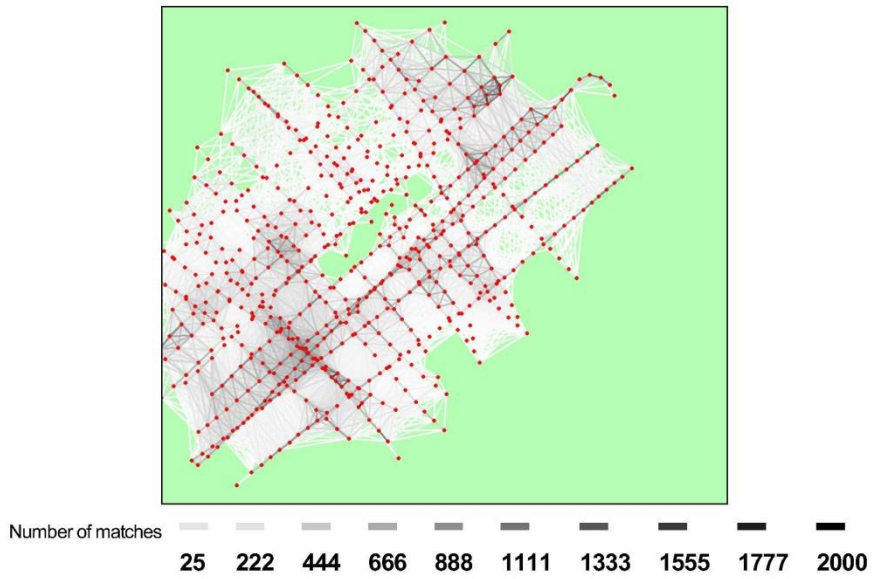


Figure 5: Top view of the geotags with a link between matching images. The darkness of the links indicates the number of matched 2D keypoints between the images. Bright links indicate low confidence and would require more overlap between the images or better quality images.

Most visible 2D keypoints



Figure 6: Cropped area of 1 3D points arising from 43 2D keypoints. Each cropped area should represent the same object on the ground.

Quality Report of mosaic map of vegetation stress images acquired in 2013

Quality Report



See *Quality Report Help* for detailed explanations. Generated with version 2.2.2 (build 2.2.6)

Summary

Project:	combine
Camera name:	CanonPowerShotELPH300HS_4.3_3000x4000
Average Ground Sampling Distance (GSD):	3.9 cm
Area covered:	0.16 sq. km / 15.67 ha / 0.06 sq. mi.
Image coordinate system:	WGS84
Output coordinate system:	UTM 60 / WGS84
Processing type:	rapid
Time for Initial Processing (without report):	07m:06s:

Quality Check

Images:	median of 1347 keypoints per image	✓
Dataset:	224 out of 620 images calibrated (36%)	⚠
Camera optimization quality:	6.73% relative difference between initial and final focal length	⚠
Matching quality:	median of 120 matches per calibrated image	✓
Georeferencing:	no GCP	⚠

Preview

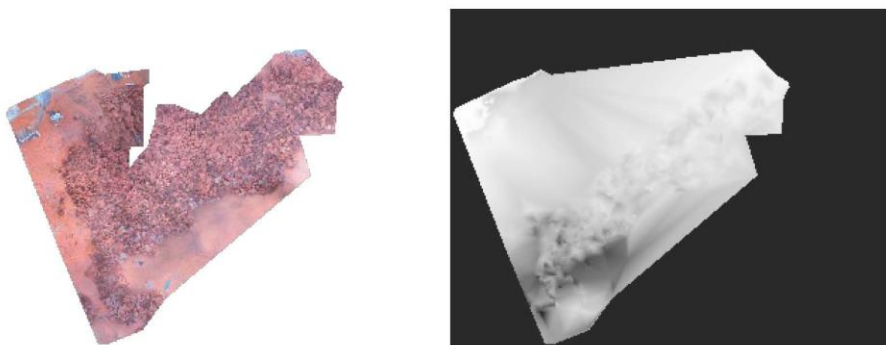


Figure 1: Ortho mosaic and the corresponding sparse digital surface model (DSM) before densification.

Calibration details

Number of calibrated images:	224 out of 620
Number of geotagged images:	619 out of 620

Geotag position

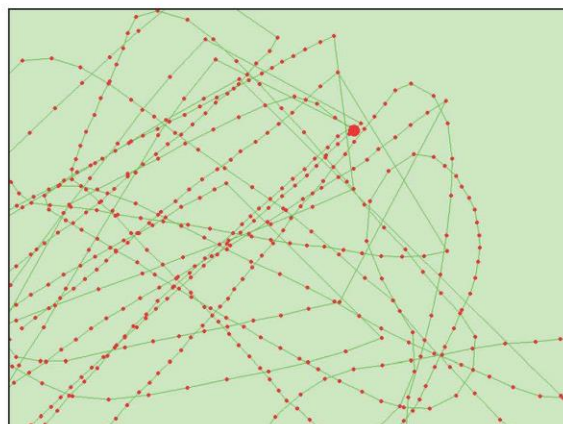




Figure 2: Top view of the geotags. The green line follows the geotag in time starting from the large red dot.

Optimized camera position

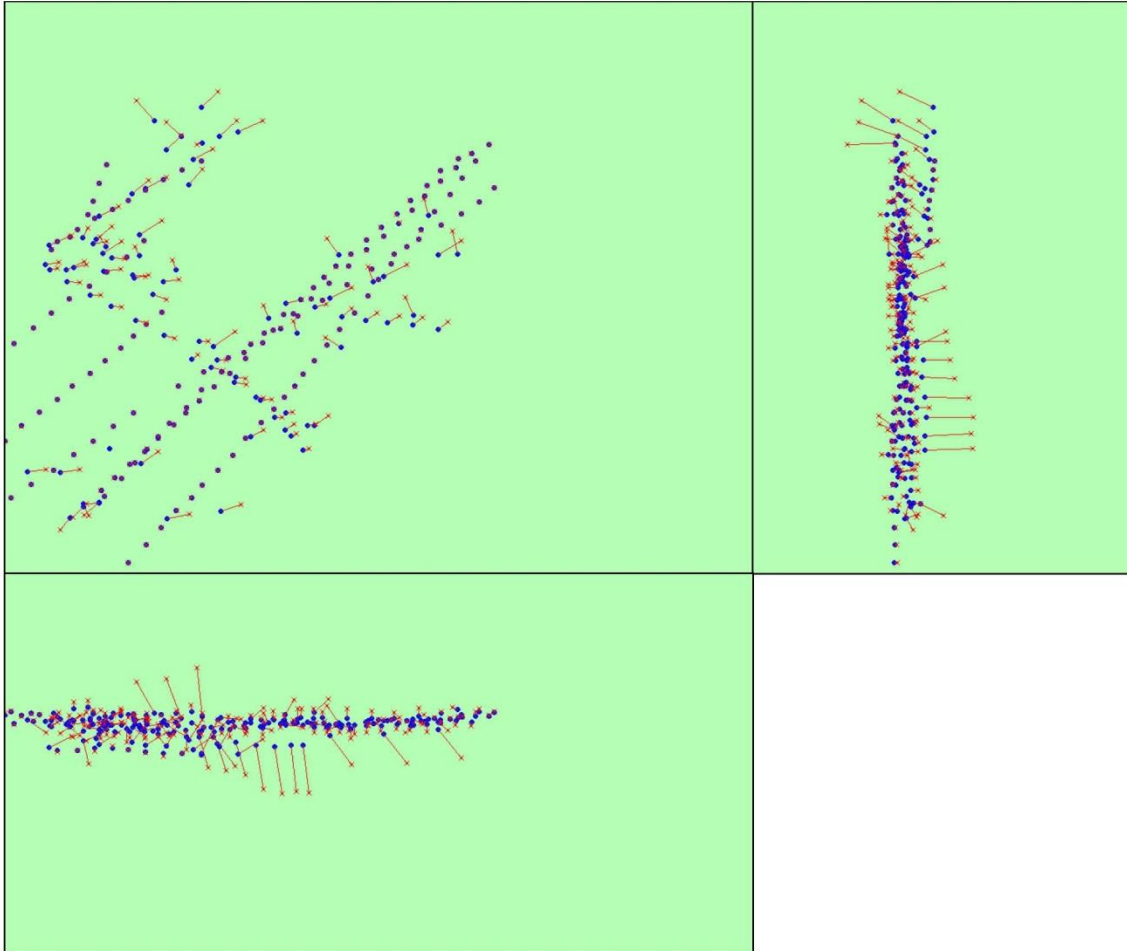


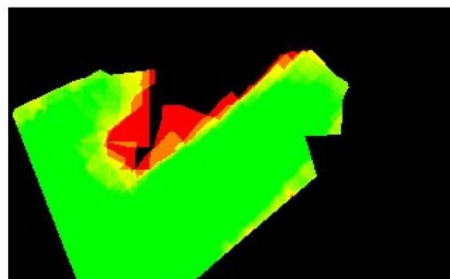
Figure 3: Offset between image geotags (small red crosses) and optimized positions (small blue dots) as well as the offset between the GCPs (large red crosses) and their optimized positions (large green dots) in the top-view (XY plane), front-view (XZ plane) and side-view (YZ plane).

Geotag variance

Geotag localisation variance	sigma [m]
Longitude direction (x)	0.161656
Latitude direction (y)	0.0918379
Altitude direction (z)	5.68624

Table 1: Relative camera localisation accuracy of the geotags. Please note that this does not correspond to the accuracy on the ground.

Overlap



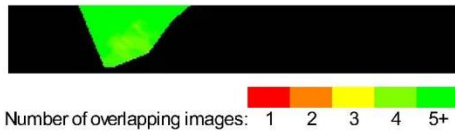


Figure 4: Overlapping score computed for each pixel of the orthomosaic. Red indicates areas where the overlap between the images is too low and could lead to poor results. For good quality results, the overlap should be over 5 images (green) for every pixel of the mosaic.

Bundle Block Adjustment details

number total keypoint observations for bundle block adjustment	37709
number total 3D points for bundle block adjustment	16585
mean reprojection error	0.22033 [pixels]

Internal Camera Parameters CanonPowerShotELPH300HS_4.3_3000x4000 sensor dimension: 6.2 4.65 [mm]

	Focal length	Principal point X	Principal point Y	RD 1	RD 2	RD 3	TD 1	TD 2
initial values	2839.640 [pix] 4.400 [mm]	2019.760 [pix] 3.068 [mm]	1547.000 [pix] 2.251 [mm]	-0.043	0.026	-0.006	0.001	0.002
optimized values	3030.872 [pix] 4.696 [mm]	1937.569 [pix] 3.196 [mm]	1627.347 [pix] 2.127 [mm]	-0.042	0.041	-0.023	0.006	-0.003

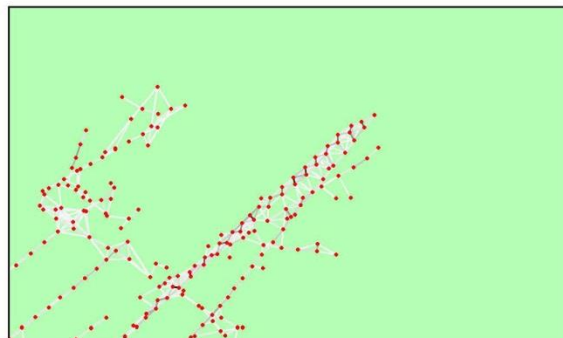
2D Keypoints Table

	Number of 2D keypoints per image	Number of matched 2D keypoints per image
Median	1347.000	120.000
Min	33.000	10.000
Max	5789.000	562.000
Mean	5083.772	168.344

3D points from 2D keypoints matches

	Number of 3D points observed
In 2 images	13687
In 3 images	1970
In 4 images	561
In 5 images	197
In 6 images	92
In 7 images	34
In 8 images	23
In 9 images	8
In 10 images	4
In 11 images	5
In 12 images	2
In 15 images	1
In 16 images	1

2D Keypoints Graph



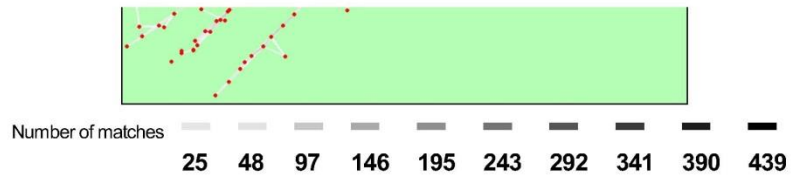


Figure 5: Top view of the geotags with a link between matching images. The darkness of the links indicates the number of matched 2D keypoints between the images. Bright links indicate low confidence and would require more overlap between the images or better quality images.

Most visible 2D keypoints



Figure 6: Cropped area of 1 3D points arising from 16 2D keypoints. Each cropped area should represent the same object on the ground.

Quality Report of mosaic map of vegetation stress images acquired in 2014

Quality Report



See *Quality Report Help* for detailed explanations. Generated with version 2.2.2 (build 2.2.6)

Summary

Project:	ndvi_merge
Camera name:	CanonPowerShotELPH300HS_4.3_3000x4000
Camera name:	CanonPowerShotELPH300HS_4.3_4000x3000
Average Ground Sampling Distance (GSD):	3.61 cm
Area covered:	0.46 sq. km / 46.48 ha / 0.18 sq. mi.
Image coordinate system:	WGS84
Output coordinate system:	UTM60 / WGS84
Processing type:	full (scale 1)
Time for Initial Processing (without report):	01h:15m:03s:

Quality Check

Images:	median of 24574 keypoints per image	✓
Dataset:	358 out of 445 images calibrated (80%) and 3 blocks	⚠
Camera optimization quality:	17.94% relative difference between initial and final focal length	⚠
Matching quality:	median of 1360 matches per calibrated image	✓
Georeferencing:	no GCP	⚠

Preview

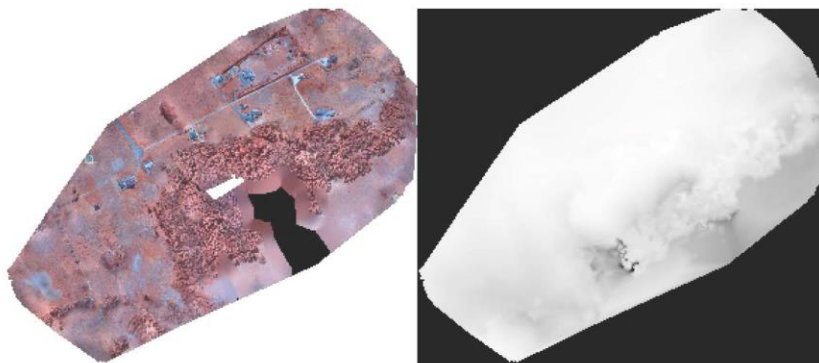
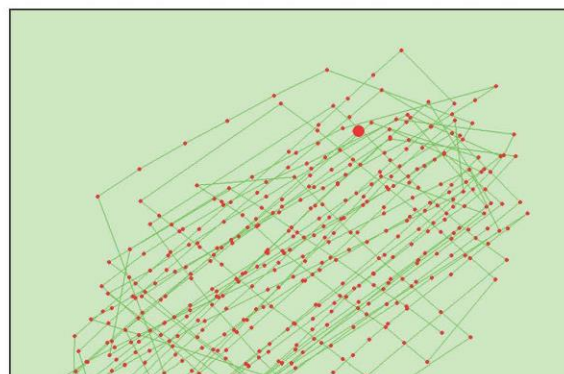


Figure 1: Ortho mosaic and the corresponding sparse digital surface model (DSM) before densification.

Calibration details

Number of calibrated images:	358 out of 445
Number of geotagged images:	445 out of 445

Geotag position



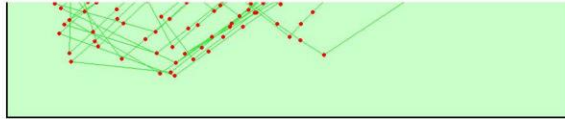


Figure 2: Top view of the geotags. The green line follows the geotag in time starting from the large red dot.

Optimized camera position

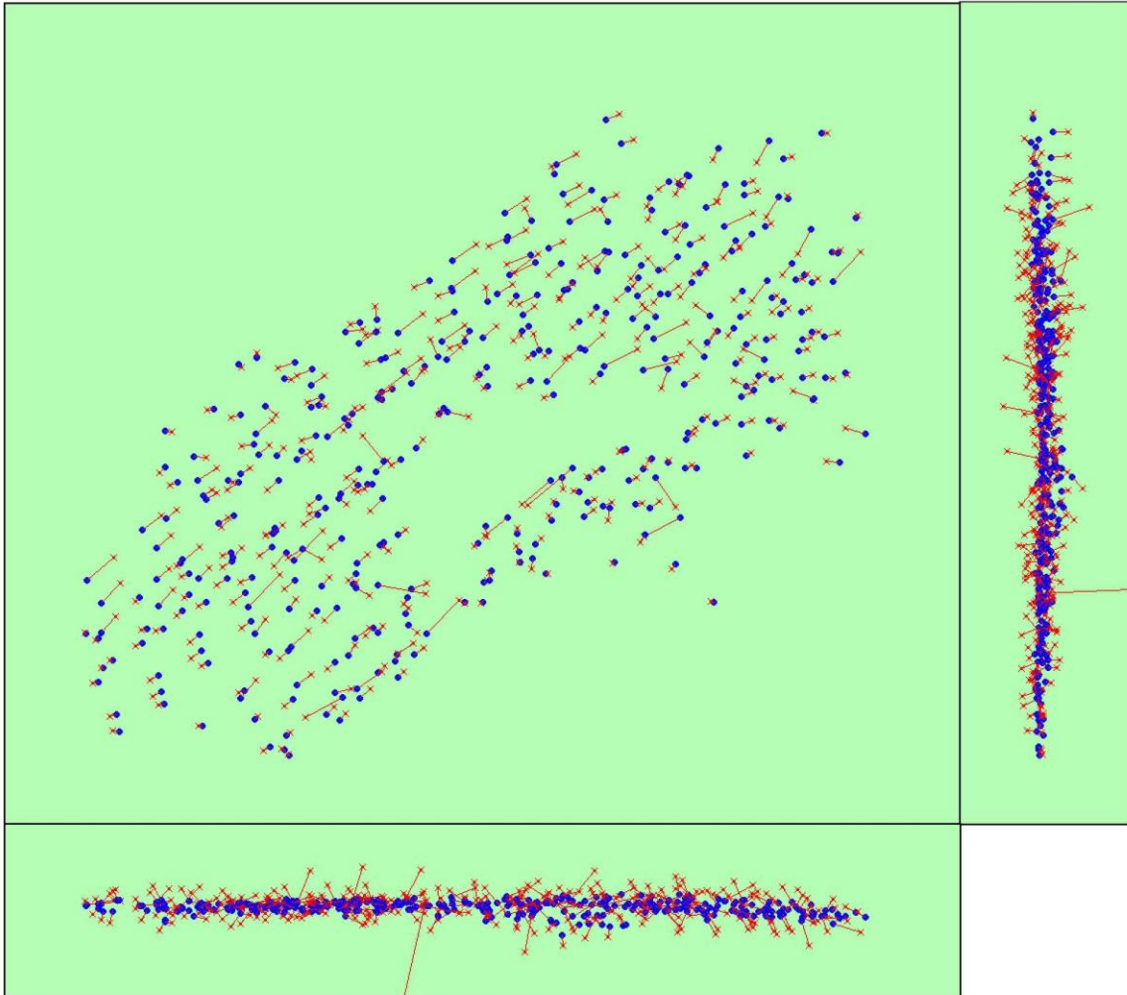


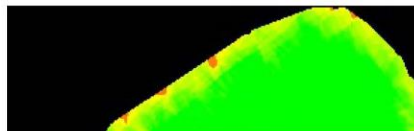
Figure 3: Offset between image geotags (small red crosses) and optimized positions (small blue dots) as well as the offset between the GCPs (large red crosses) and their optimized positions (large green dots) in the top-view (XY plane), front-view (XZ plane) and side-view (YZ plane).

Geotag variance

Geotag localisation variance	sigma [m]
Longitude direction (x)	9.30478
Latitude direction (y)	6.48666
Altitude direction (z)	6.30144

Table 1: Relative camera localisation accuracy of the geotags. Please note that this does not correspond to the accuracy on the ground.

Overlap



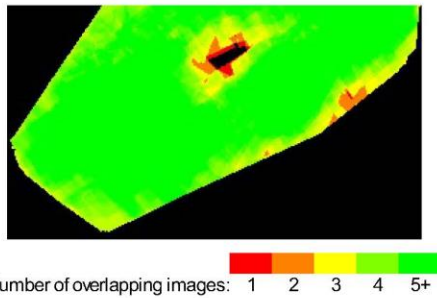


Figure 4: Overlapping score computed for each pixel of the orthomosaic. Red indicates areas where the overlap between the images is too low and could lead to poor results. For good quality results, the overlap should be over 5 images (green) for every pixel of the mosaic.

Bundle Block Adjustment details

number total keypoint observations for bundle block adjustment	752201
number total 3D points for bundle block adjustment	282025
mean reprojection error	0.207132 [pixels]

Internal Camera Parameters CanonPowerShotELPH300HS_4.3_3000x4000 sensor dimension: 6.2 4.65 [mm]

	Focal length	Principal point X	Principal point Y	RD 1	RD 2	RD 3	TD 1	TD 2
initial values	2839.640 [pix] 4.400 [mm]	2019.760 [pix] 3.068 [mm]	1547.000 [pix] 2.251 [mm]	-0.043	0.026	-0.006	0.001	0.002
optimized values	2862.044 [pix] 4.434 [mm]	1986.910 [pix] 3.119 [mm]	1571.326 [pix] 2.214 [mm]	-0.043	0.028	-0.007	0.005	-0.001

Internal Camera Parameters CanonPowerShotELPH300HS_4.3_4000x3000 sensor dimension: 6.198 8.263 [mm]

	Focal length	Principal point X	Principal point Y	RD 1	RD 2	RD 3	TD 1	TD 2
initial values	2081.450 [pix] 4.300 [mm]	1500.000 [pix] 3.099 [mm]	2000.000 [pix] 4.132 [mm]	0.000	0.000	0.000	0.000	0.000
optimized values	2811.922 [pix] 5.809 [mm]	1374.897 [pix] 3.357 [mm]	1977.722 [pix] 4.178 [mm]	-0.028	0.014	-0.011	-0.004	-0.007

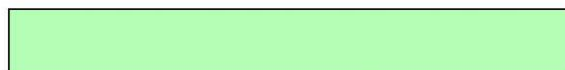
2D Keypoints Table

	Number of 2D keypoints per image	Number of matched 2D keypoints per image
Median	24574.000	1360.000
Mn	1.000	24.000
Max	53303.000	9751.000
Mean	32158.712	2101.120

3D points from 2D keypoints matches

	Number of 3D points observed
In 2 - 3 images	239722
In 4 - 5 images	28947
In 6 - 7 images	8610
In 8 - 9 images	3168
In 10 - 11 images	1124
In 12 - 13 images	390
In 14 - 15 images	57
In 16 - 17 images	7

2D Keypoints Graph



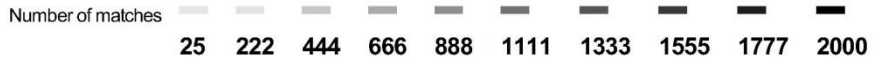
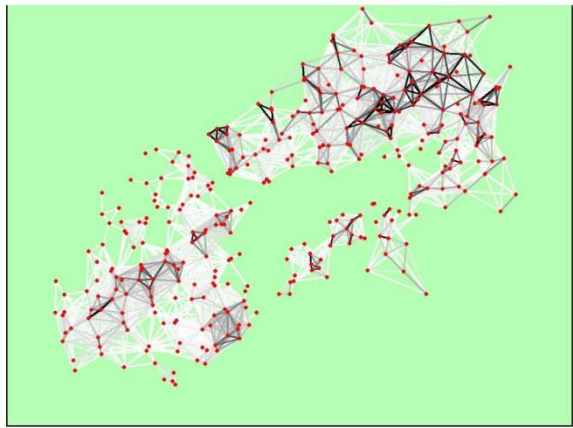


Figure 5: Top view of the geotags with a link between matching images. The darkness of the links indicates the number of matched 2D keypoints between the images. Bright links indicate low confidence and would require more overlap between the images or better quality images.

Most visible 2D keypoints



Figure 6: Cropped area of 1 3D points arising from 17 2D keypoints. Each cropped area should represent the same object on the ground.

Quality Report of mosaic map of red edge images acquired on 8 August, 2013

Quality Report



See *Quality Report Help* for detailed explanations. Generated with version 2.2.2 (build 2.2.6)

Summary

Project:	nirrgb
Camera name:	NEX-5N_16.0_1080x1616
Camera name:	NEX-5N_16.0_1616x1080
Average Ground Sampling Distance (GSD):	9.59 cm
Area covered:	0.23 sq. km / 23.24 ha / 0.09 sq. mi.
Image coordinate system:	WGS84
Output coordinate system:	UTM60 / WGS84
Processing type:	full (scale 1)
Time for Initial Processing (without report):	49m:09s:

Quality Check

Images:	median of 5149 keypoints per image	!
Dataset:	499 out of 535 images calibrated (93%) and 2 blocks	!
Camera optimization quality:	93.44% relative difference between initial and final focal length	!
Matching quality:	median of 1331 matches per calibrated image	✓
Georeferencing:	no GCP	!

Preview

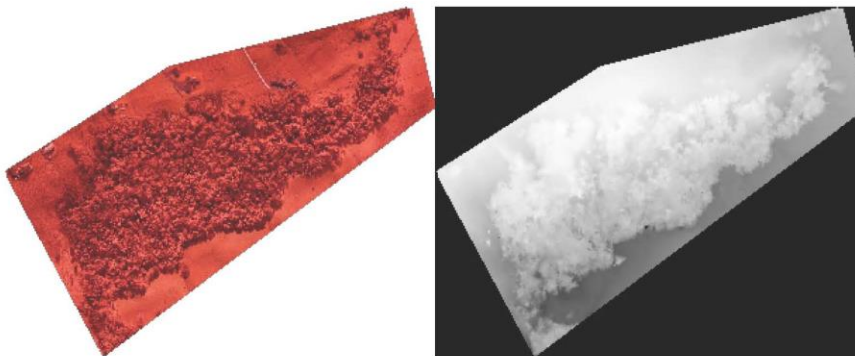


Figure 1: Ortho mosaic and the corresponding sparse digital surface model (DSM) before densification.

Calibration details

Number of calibrated images:	499 out of 535
Number of geotagged images:	535 out of 535

Geotag position

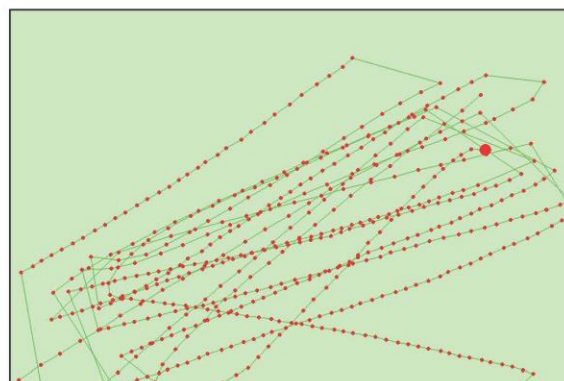




Figure 2: Top view of the geotags. The green line follows the geotag in time starting from the large red dot.

Optimized camera position

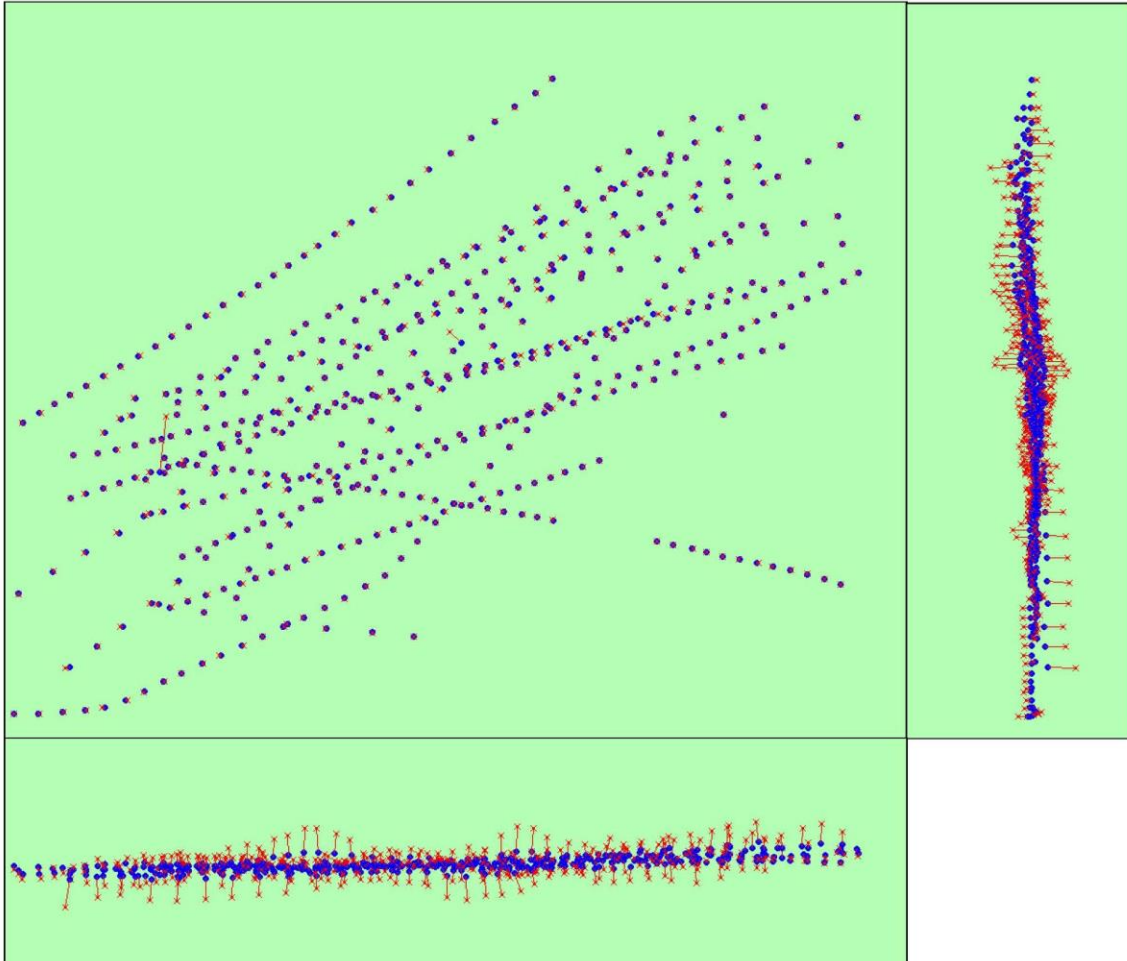


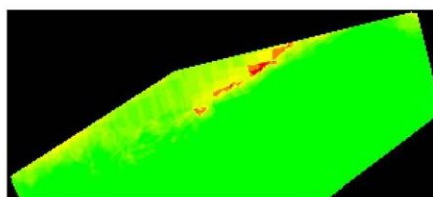
Figure 3: Offset between image geotags (small red crosses) and optimized positions (small blue dots) as well as the offset between the GCPs (large red crosses) and their optimized positions (large green dots) in the top-view (XY plane), front-view (XZ plane) and side-view (YZ plane).

Geotag variance

Geotag localisation variance	sigma [m]
Longitude direction (x)	1.21163
Latitude direction (y)	0.365463
Altitude direction (z)	6.76016

Table 1: Relative camera localisation accuracy of the geotags. Please note that this does not correspond to the accuracy on the ground.

Overlap





Number of overlapping images: 1 2 3 4 5+

Figure 4: Overlapping score computed for each pixel of the orthomosaic. Red indicates areas where the overlap between the images is too low and could lead to poor results. For good quality results, the overlap should be over 5 images (green) for every pixel of the mosaic.

Bundle Block Adjustment details

number total keypoint observations for bundle block adjustment	665528
number total 3D points for bundle block adjustment	196729
mean reprojection error	0.397533 [pixels]

Internal Camera Parameters NEX-5N_16.0_1080x1616 sensor dimension: 36 24.1 [mm]

	Focal length	Principal point X	Principal point Y	RD 1	RD 2	RD 3	TD 1	TD 2
initial values	718.222 [pix] 16.000 [mm]	808.000 [pix] 18.000 [mm]	540.000 [pix] 12.030 [mm]	0.000	0.000	0.000	0.000	0.000
optimized values	1118.367 [pix] 24.914 [mm]	835.293 [pix] 17.392 [mm]	544.498 [pix] 11.929 [mm]	-0.078	0.102	-0.006	0.001	-0.002

Internal Camera Parameters NEX-5N_16.0_1616x1080 sensor dimension: 36.000 53.867 [mm]

	Focal length	Principal point X	Principal point Y	RD 1	RD 2	RD 3	TD 1	TD 2
initial values	480.000 [pix] 16.000 [mm]	540.000 [pix] 18.000 [mm]	808.000 [pix] 26.933 [mm]	0.000	0.000	0.000	0.000	0.000
optimized values	1109.663 [pix] 36.989 [mm]	532.403 [pix] 18.253 [mm]	831.194 [pix] 26.160 [mm]	-0.076	0.101	-0.006	-0.002	-0.001

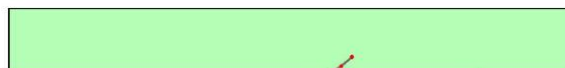
2D Keypoints Table

	Number of 2D keypoints per image	Number of matched 2D keypoints per image
Median	5149.000	1331.000
Mn	14.000	37.000
Max	8696.000	4119.000
Mean	5047.739	1333.723

3D points from 2D keypoints matches

	Number of 3D points observed
In 2 - 3 images	150646
In 4 - 7 images	33550
In 8 - 11 images	6686
In 12 - 15 images	2827
In 16 - 19 images	1387
In 20 - 23 images	763
In 24 - 27 images	430
In 28 - 31 images	292
In 32 - 35 images	101
In 36 - 39 images	45
In 40 - 43 images	2

2D Keypoints Graph



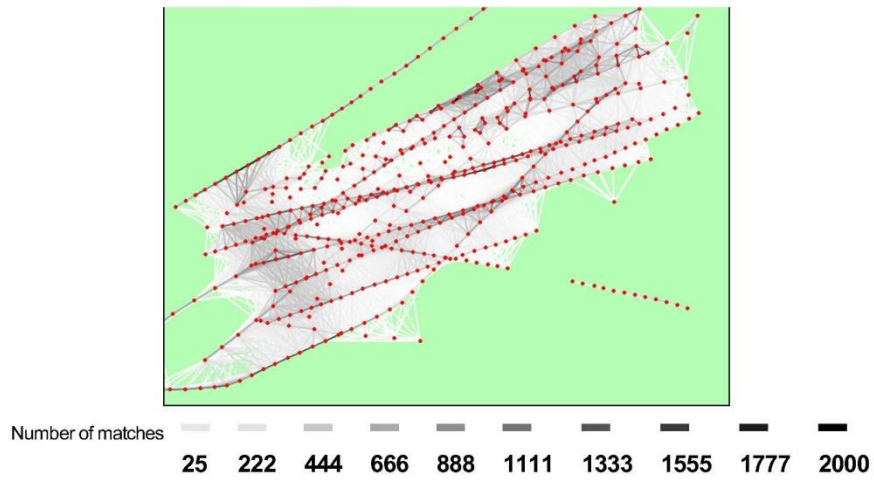


Figure 5: Top view of the geotags with a link between matching images. The darkness of the links indicates the number of matched 2D keypoints between the images. Bright links indicate low confidence and would require more overlap between the images or better quality images.

Most visible 2D keypoints

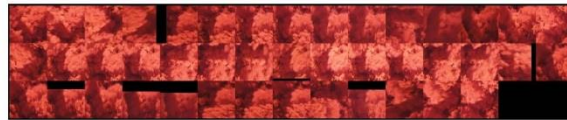


Figure 6: Cropped area of 1 3D points arising from 43 2D keypoints. Each cropped area should represent the same object on the ground.

Quality Report of mosaic map of true colour images acquired on 1 April, 2014 (merge Flight 1 and Flight 2)

Quality Report



See *Quality Report Help* for detailed explanations. Generated with version 2.2.2 (build 2.2.6)

Summary

Project:	4_1_rgb_merge
Camera name:	NEX-5N_16.0_1080x1616
Camera name:	NEX-5N_16.0_1616x1080
Average Ground Sampling Distance (GSD):	9.58 cm
Area covered:	0.73 sq. km / 73.03 ha / 0.28 sq. mi.
Image coordinate system:	WGS84
Output coordinate system:	UTM60 / WGS84
Processing type:	full (scale 1)
Time for Initial Processing (without report):	04h:24m:52s:

Quality Check

Images:	median of 6092 keypoints per image	!
Dataset:	1195 out of 1196 images calibrated (99%)	✓
Camera optimization quality:	108.87% relative difference between initial and final focal length	!
Matching quality:	median of 1797 matches per calibrated image	✓
Georeferencing:	no GCP	!

Preview

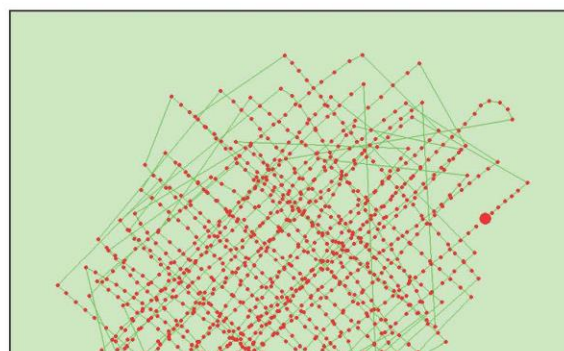


Figure 1: Ortho mosaic and the corresponding sparse digital surface model (DSM) before densification.

Calibration details

Number of calibrated images:	1195 out of 1196
Number of geotagged images:	1196 out of 1196

Geotag position



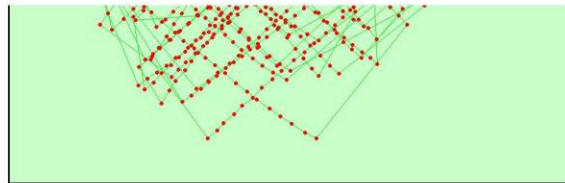


Figure 2: Top view of the geotags. The green line follows the geotag in time starting from the large red dot.

Optimized camera position

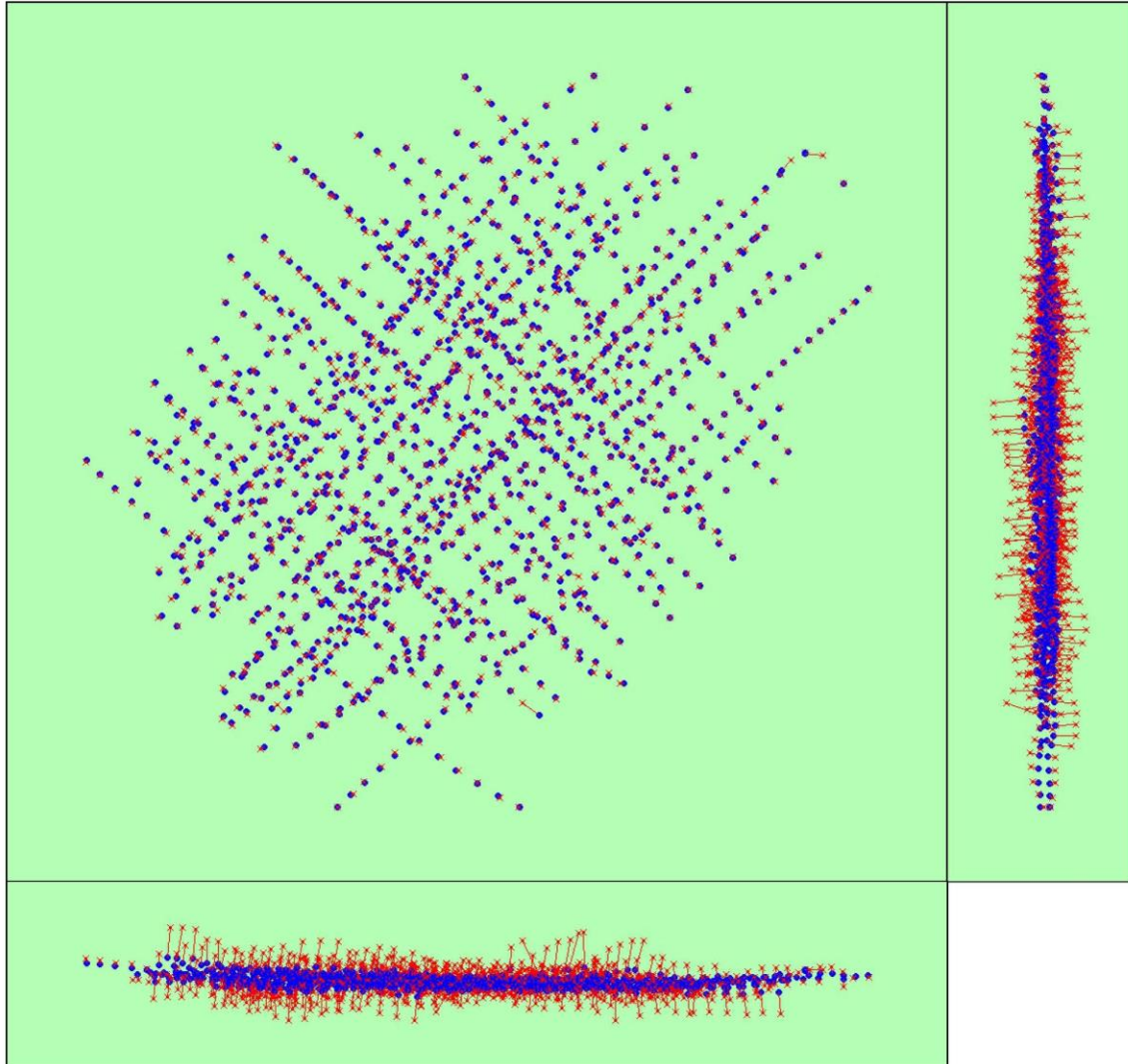


Figure 3: Offset between image geotags (small red crosses) and optimized positions (small blue dots) as well as the offset between the GCPs (large red crosses) and their optimized positions (large green dots) in the top-view (XY plane), front-view (XZ plane) and side-view (YZ plane).

Geotag variance

Geotag localisation variance	sigma [m]
Longitude direction (x)	2.50196
Latitude direction (y)	2.55234
Altitude direction (z)	8.98668

Table 1: Relative camera localisation accuracy of the geotags. Please note that this does not correspond to the accuracy on the ground.

Overlap

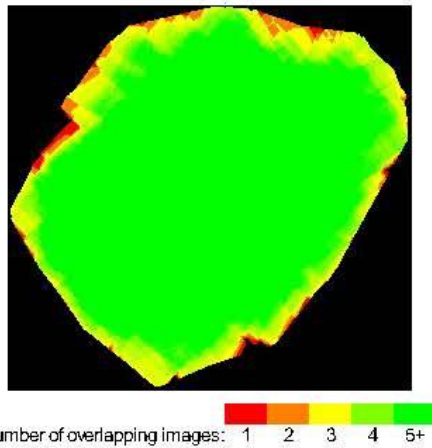


Figure 4: Overlapping score computed for each pixel of the orthomosaic. Red indicates areas where the overlap between the images is too low and could lead to poor results. For good quality results, the overlap should be over 5 images (green) for every pixel of the mosaic.

Bundle Block Adjustment details

number total keypoint observations for bundle block adjustment	1982319
number total 3D points for bundle block adjustment	502059
mean reprojection error	0.362318 [pixels]

Internal Camera Parameters NEX-5N_16.0_1080x1616 sensor dimension: 36 24.1 [mm]

	Focal length	Principal point X	Principal point Y	RD 1	RD 2	RD 3	TD 1	TD 2
initial values	718.222 [pix] 16.000 [mm]	808.000 [pix] 18.000 [mm]	540.000 [pix] 12.030 [mm]	0.000	0.000	0.000	0.000	0.000
optimized values	1207.700 [pix] 26.904 [mm]	819.830 [pix] 17.736 [mm]	530.273 [pix] 12.246 [mm]	-0.083	0.120	0.029	0.002	0.001

Internal Camera Parameters NEX-5N_16.0_1616x1080 sensor dimension: 36.000 53.867 [mm]

	Focal length	Principal point X	Principal point Y	RD 1	RD 2	RD 3	TD 1	TD 2
initial values	480.000 [pix] 16.000 [mm]	540.000 [pix] 18.000 [mm]	808.000 [pix] 26.933 [mm]	0.000	0.000	0.000	0.000	0.000
optimized values	1198.093 [pix] 39.936 [mm]	533.646 [pix] 18.212 [mm]	797.537 [pix] 27.282 [mm]	-0.076	0.082	0.065	-0.004	0.000

2D Keypoints Table

	Number of 2D keypoints per image	Number of matched 2D keypoints per image
Median	6092.000	1797.000
Mn	329.000	25.000
Max	11392.000	3338.000
Mean	6188.865	1658.844

3D points from 2D keypoints matches

	Number of 3D points observed
In 2 - 7 images	454868
In 8 - 15 images	31193
In 16 - 23 images	9277
In 24 - 31 images	3936
In 32 - 39 images	1488
In 40 - 47 images	684
In 48 - 55 images	324
In 56 - 63 images	181
In 64 - 71 images	84

In 64 - 71 images	84
In 72 - 79 images	24

2D Keypoints Graph

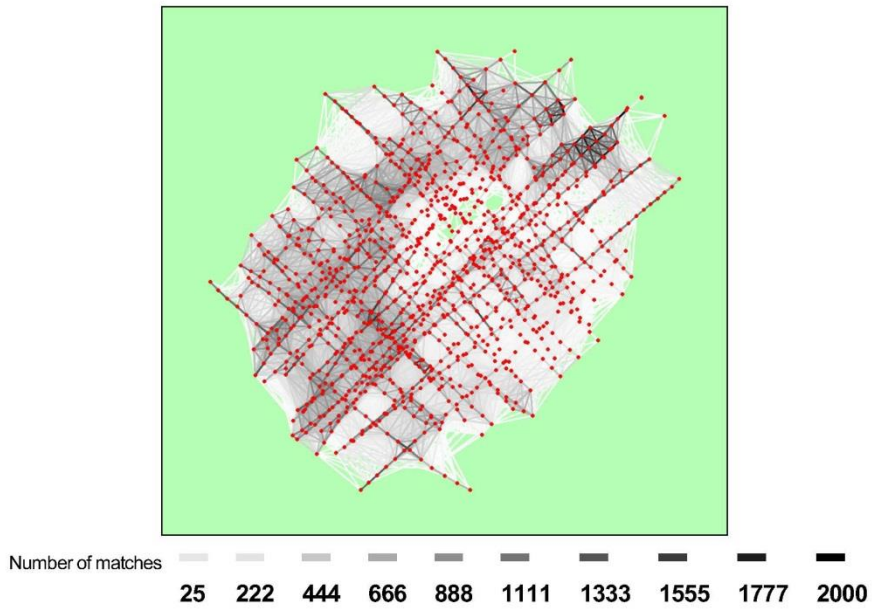


Figure 5: Top view of the geotags with a link between matching images. The darkness of the links indicates the number of matched 2D keypoints between the images. Bright links indicate low confidence and would require more overlap between the images or better quality images.

Most visible 2D keypoints

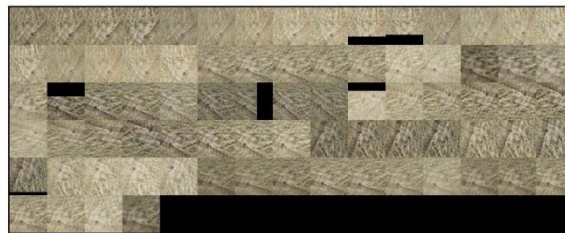


Figure 6: Cropped area of 1 3D points arising from 79 2D keypoints. Each cropped area should represent the same object on the ground.